N° :

THESE DE DOCTORAT

Synthesis of novel phosphinate salts and development of formulations for the flame retardancy of glass fiber reinforced PolyButylene Terephthalate (PBT)

Présentée et soutenue publiquement à

L'UNIVERSITE DE LILLE 1 – SCIENCES ET TECHNOLOGIES

Pour obtenir le grade de

Docteur

Spécialité : Molécules et Matière condensée

Par

Jérémie LOUISY

Ingénieur diplomé de l'Ecole Nationale Supérieure de Chimie de Lille

Thèse Dirigée par

Prof. Serge BOURBIGOT et Prof. Sophie DUQUESNE

Soutenue le 12 octobre 2012 devant la Commission d'Examen composée de :

Dr. Jean-Marc LEFEBVRE, Université Lille 1	Président du jury
Prof. Richard HULL, University of Central Lancashire	Rapporteur
Prof. Manfred DÖRING, Fraunhofer Institute	Rapporteur
Prof. Serge BOURBIGOT, Université Lille 1	Directeur de thèse
Prof. Sophie DUQUESNE, Université Lille 1	Co-directeur de thèse
Dr. Alexander KÖNIG, BASF SE	Examinateur
Dr. Martin KLATT, BASF SE	Examinateur

Acknowledgements

The work presented in this manuscript has been carried out for the most part in the UMET headed by Alexandre Legris in the “Ingénierie des Systèmes Polymères (ISP)” team led by Prof. Serge Bourbigot. I would like to express my sincere thanks to them for having welcomed me in the laboratory and in the team and for having given me the opportunity to work on this interesting project.

I would particularly like to express my gratitude to Prof. Serge Bourbigot and Prof. Sophie Duquesne, who supervised me during these three years. Their expertise and excellent advices have contributed to enrich this experience, both in human and scientific terms. I thank Prof. Bourbigot and Prof. Duquesne for their valuable support which allowed me to perform this work properly and in the best conditions.

I would like to express my thanks to the BASF company, more particularly to Dr. Philippe Desbois, Dr. Alexander König and Dr. Martin Klatt for having supervised me in this project and for the trust they have placed in me to lead this research.

I would like to acknowledge Mr. Jean-Marc Lefebvre who has agreed to chair this jury as well as Prof. Richard Hull and Prof. Manfred Döring for having accepted to take on their time and to bring their expertise as examiners to assess this manuscript.

I extend these thanks to the team of the NMR research centre of Lille 1, especially to Bertrand Revel, Xavier Trivelli and Bertrand Doumert for their time and patience training me on the NMR techniques and for their kindness.

I thank all members of the ISP team for all these moments shared in the joyous and easy-going atmosphere. A very special thanks to Oriane, Mathilde, Louis, Pierre and Bastien with whom I have become friendly, not forgetting all other members of the team, Antoine, Brigitte, Mathieu, Maryska, Clemence, Carmen, Aurore, Fabienne, Gaëlle, Charaffedine, Michel, Severine, Mathilde, Maude, Ghassan, Fouad, Marion, Nicolas, Mariane, Franck, Gwenaëlle as well as some persons that used to work in the lab, including Damien, Thomas, Jérémy, Caroline, Christelle, Nadine and Helene.

Finally, I would like to thank my family, my mother, my father, my two brothers and my grandmother for their invaluable support as well as my friends, especially Andrea.

I dedicate this manuscript to my grandfather…

TABLE OF CONTENTS

ABBREVIATIONS 9
INTRODUCTION 11
CHAPTER 1 – STATE OF THE ART 17
1. Poly (Butylene Terephthalate) (PBT) 19
1.1 Synthesis processes 19
1.1.1 General aspects 19
1.1.2 PTA continuous process 20
1.1.3 DMT continuous process 21
1.1.4 Comparison between DMT and PTA processes 22
1.2 Structure and properties 23
1.2.1 Structure 23
1.2.2 Mechanical properties 26
1.2.3 Electrical properties 26
1.2.4 Resistance to moisture and chemical agents 26
1.2.5 Thermal degradation and burning behavior 26
1.3 Additives and blends 29
1.3.1 Glass fibers 29
1.3.2 Flame retardants 29
1.3.3 Other conventional additives and PBT blends 29
1.4 Applications 30
1.5 Conclusion 31
2. Flame retardancy of PBT 32
2.1 Flame retardant classes and their modes of action 34
2.1.1 Halogenated flame retardants 34
2.1.2 Melamine and its derivatives 35
2.1.3 Metal hydroxides and hydrocarbonates 36
2.1.4 Phosphorus-based compounds 37
2.2 Flame retardants in PBT 37
2.2.1 Halogenated based compounds 37
2.2.2 Melamine and its salt derivatives 39
2.2.3 Metal hydroxides and hydrocarbonates 40
2.2.4 Phosphorus-based compounds 40

2.3 The oxaphospholane oxide Exolit PE110 in flame retardancy of PBT 47
2.4 Nanocomposites and nano-additives 51
2.4.1 Nanocomposites..... 51
2.4.2 Nanocomposites with conventional flame retardants 54
2.5 Conclusion 55
3. Conclusion..... 56
CHAPTER 2 – MATERIALS COMPOUNDING AND EXPERIMENTAL TECHNIQUES 57
1. Materials, compounding and experimental techniques 59
1.1 Materials 59
1.2 Material compounding 60
1.3 Fire Testing Methods 60
1.3.1 UL94 vertical burning test 61
1.3.2 Limiting Oxygen Index (LOI) 62
1.3.3 Mass Loss Calorimeter (MLC)..... 63
1.4 Characterization of the materials degradation..... 63
1.4.1 ThermoGravimetric Analysis (TGA) 64
1.4.2 Condensed phase analysis..... 65
1.4.3 Gas phase analysis..... 68
2. Experimental procedures for the synthesis of novel phosphinate salts 69
2.1 Materials and Techniques..... 70
2.2 Experimental procedures for the synthesis of the (di)phosphinic acids 72
2.3 Experimental procedures for the synthesis of the (di)phosphinate salts 76
3. Conclusion..... 81
CHAPTER 3 – DEVELOPMENT OF A NOVEL FLAME RETARDED PBT/GF FORMULATION BASED ON COMMERCIAL PHOSPHINATE SYSTEMS 83
1. Flame retardant screening..... 85
1.1 Flame retardant additives selected 85
1.2 Fire test results..... 88
1.2.1 Exolit OP1240 based combinations..... 88
1.2.2 Exolit OP1200 based combination 91
1.2.3 Conclusion 93
2. Optimization and comparative study: Exolit OP1240/RDP bentonite flame retardant combination..... 93
2.2 Optimization of the Exolit OP1240/RDP bentonite combination..... 94

2.3 Comparative study: influence of RDP and non-modified bentonite on the fire properties of PBT/GF 95
2.4 Conclusion 96
3. Investigation of the fire properties of the Exolit OP1240/RDP bentonite containing formulation (optimized) through the Limiting Oxygen Index (LOI) and Mass Loss Calorimeter (MLC) tests 96
4. Conclusion 99
CHAPTER 4 – DEVELOPMENT OF A NOVEL FLAME RETARDED PBT/GF FORMULATION BASED ON SELF-SYNTHESIZED PHOSPHINATE SALTS 101
1. Synthesis and characterization of novel phosphinate salts 104
1.1 Survey: selection of the raw materials 104
1.2 Synthesis and characterization of phosphinic acids 106
1.2.1 Syntheses involving amine reagents 106
1.2.2 Synthesis involving PEPA 110
1.2.3 Conclusion 113
1.3 Conversion of phosphinic acids into salts 114
1.3.1 Preparation and characterization of aluminum salts 114
1.3.2 Preparation and characterization of zinc and calcium salts of the aniline based phosphinic acid 124
1.3.3 Conclusion 127
1.4 Thermal behavior of the phosphinate salts 128
1.5 Conclusion 131
2. Flame retardant properties of the novel phosphinate salts 132
2.1 Fire testing of the aluminum phosphinates containing formulations 132
2.2 Fire performances of the zinc and calcium salts of the aniline based phosphinic acid 136
2.3 Fireproofing combinations: combination of the aluminum salts of the aniline and benzyl amine based phosphinates with commercial flame retardants and synergistic agents 137
2.3.1 Selection of the co-additives 137
2.3.2 Fire performances of the fireproofing combinations 138
2.4 Conclusion 141
3. Conclusion 141
CHAPTER 5 – FLAME RETARDANCY MECHANISM OF PHOSPHINATE SALTS IN REINFORCED PBT: COMPARISON BETWEEN COMMERCIAL AND SELF-SYNTHESIZED FLAME RETARDANT MODES OF ACTION 143

1. Thermal degradation behavior of glass fiber reinforced PBT 146
1.1 Thermal degradation 146
1.2 Evolved gases 147
1.3 Analysis of the PBT/GF residue 150
1.4 Degradation mechanism 152
2. Thermal degradation behavior of glass fiber reinforced PBT flame retarded with aluminum phosphinate salts 153
2.1 PBT/GF flame retarded with the aniline based phosphinate aluminum C9 153
2.1.1 Thermal decomposition behavior of C9 153
2.1.2 Thermal decomposition of PBT/GF flame retarded with C9 162
2.2 PBT/GF flame retarded with the aluminum phosphinate salt Exolit OP1240 172
2.2.1 Thermal decomposition of Exolit OP1240 172
2.2.2 Thermal decomposition of PBT/GF flame retarded with Exolit OP1240 179
3. Conclusion 188
GENERAL CONCLUSION - OUTLOOK 189
REFERENCES 197
APPENDICES 211

ABBREVIATIONS

ABS	Acrylonitrile Butadiène Styrène
AHP	Aluminum HypoPhosphite
ATH	Aluminum Tri-Hydroxide
BDO	1,4-Butanediol
BDP	Bisphenol A bis-Diphenyl Phosphate
CP	Cross-Polarization
DD	Dipolar Decoupling
DMT	DiMethyl Terephthalate
DP	DiPhenyl
DSC	Differential Scanning Calorimetry
DTG	Derivative ThermoGravimetric
EEE	Electrical and Electronic Equipments
Exolit OP1200	Aluminum diethylphosphinate + Melamine cyanurate
Exolit OP1240	Aluminum diethylphosphinate
Exolit PE110	2-methyl-2,5-dioxo-1,2-oxaphospholane
FTIR	Fourier Transformed Infra-Red spectroscopy
FR	Flame Retardant
GCMS	Gas Chromatography – Mass Spectrometry
HIPS	High Impact PolyStyrene
HRR	Heat Release Rate
HMQC	Heteronuclear Multiple Quantum Coherence
LOI	Limiting Oxygen Index
MAS	Magic Angle Spinning
MDH	Magnesium Di-Hydroxide
MLC	Mass Loss Calorimeter
MMT	MontMorilloniTe
MQ	Multi-Quantum
MWNT	Multi-Walled Carbon Nanotube
NMR	Nuclear Magnetic Resonance
OMMT	Organo-Modified Montmorillonite
OP	2-methyl-2,5-dioxo-1,2-oxaphospholane (Exolit PE110)
PA	PolyAmide
PBT	PolyButylene Terephthalate

PC	PolyCarbonate
PE	PolyEthylene
PEPA	2,4,6-trioxa-1-phosphabicyclo[2,2,2]octane-4-methanol
PET	PolyEthylene Terephthalate
pHRR	peak Heat Release Rate
PP	PolyPropylene
PPO	PolyPhenylene Oxide
PTA	Pure Terephthalic Acid
PTT	PolyTrimethylene Terephthalate
RDP	Resorcinol bis-Diphenyl Phosphate
RFDR	RadioFrequency Driven Recoupling
SWNT	Single-Walled Carbon Nanotube
TGA	Thermo-Gravimetric Analysis
THF	TetraHydroFurane
THR	Total Heat Release
TTI	Time To Ignition
XRD	X-Ray Diffraction

INTRODUCTION

The use of plastic materials has substantially increased since the end of the Second World War. With an average growth rate of 9% per year, the total world production of plastics increased from 1.5 million tonnes in 1950 to 260 million tonnes in 2007[1]. The consumption of plastic saw its rate slightly decline during the last economic crisis (2008) but the demand is still rising today. 265 million tonnes of plastics have been produced in 2011, namely more than 8400 kilos plastics each second, representing about 8% of the global consumption of oil[2].

Applications of plastic materials are as varied as their range of accessible properties. Their ease of manufacture as well as their low cost also constitutes factors favoring their industrial development. Plastic materials are utilized in a plethora of domains (packaging, construction, transportation, electric/electronic industry, agriculture, health, sport…) where they can advantageously replace other materials, especially metal and ceramic parts that often necessitate burdensome and costly manufacturing. Nevertheless, plastics in general have serious drawbacks from a weathering, chemical resistance and electrostatic point of view. Moreover, their major drawbacks concern their poor resistance to heat and their flammability which can be horrendous in both human and economic terms. Fire still causes significant damage and public health problems in recent years. The National Fire Protection Association (NFPA) has conducted national surveys of human and economic losses due to fire in United State. The numbers in this area are impressive: On average, in 2010, someone died in fire every 169 minutes, and someone was injured every 30 minutes[3]. In 2009, the total cost of fire was estimated to $331 billion (2.3% of U.S. gross domestic product), including lives lost, medical treatment of injuries, pain and suffering, property damage, business interruption as well as cost of provisions to prevent or diminish the cost of fire (i.e. fire department, insurance, fire protection equipment and construction)[4]. As an illustration, Figure 1 depicts the breakdown by segment of the cost of fire in United States in 2009.

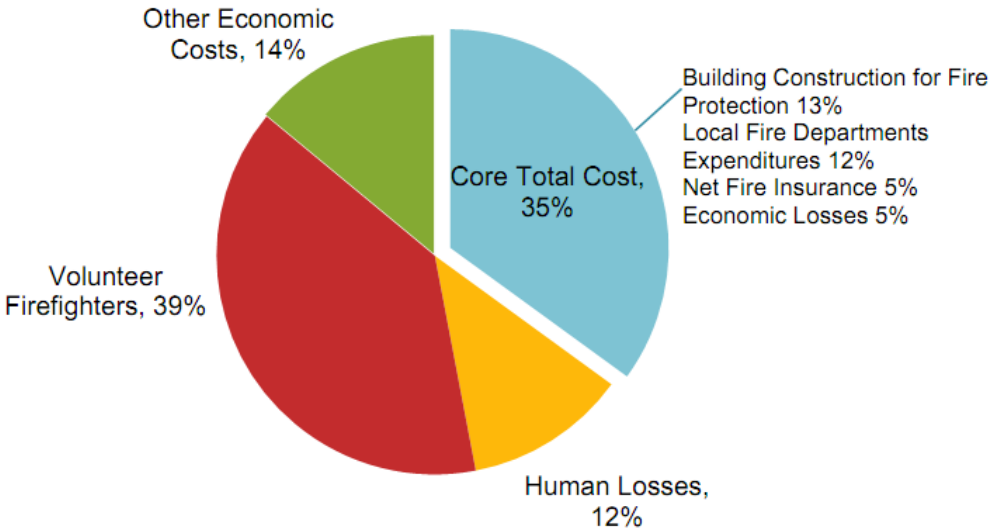

Figure 1 : Total cost of fire in United States in 2009[4]

Fire is therefore a challenging issue the world facing today, with both economic and security stakes. Looking for solutions adapted to improve the fire behavior of polymers is thus of special importance. It is in that context that the research program carried out in collaboration with the UMET-ISP laboratory (Unité Matériaux Et Transformations – Ingénierie des Systèmes Polymères) and the BASF company has been elaborated. This project deals with the flame retardancy of glass fiber (GF) reinforced polybutylene terephthalate (PBT) for electronic/electrical applications. Indeed, PBT exhibits excellent insulating and heat resistance properties as well as outstanding resistance to chemicals and solvents. Furthermore, the polymer is easy to handle during processing as it achieves fast crystallization and low shrinkage during forming. These properties make the PBT particularly valuable for a number of applications (especially for electrical and electronic equipments) which is why the consumption of PBT currently shows one of the highest growth rates among polymers (Figure 2)[5]. As for a majority of polymers, though, the use of PBT is limited because of its low resistance to fire.

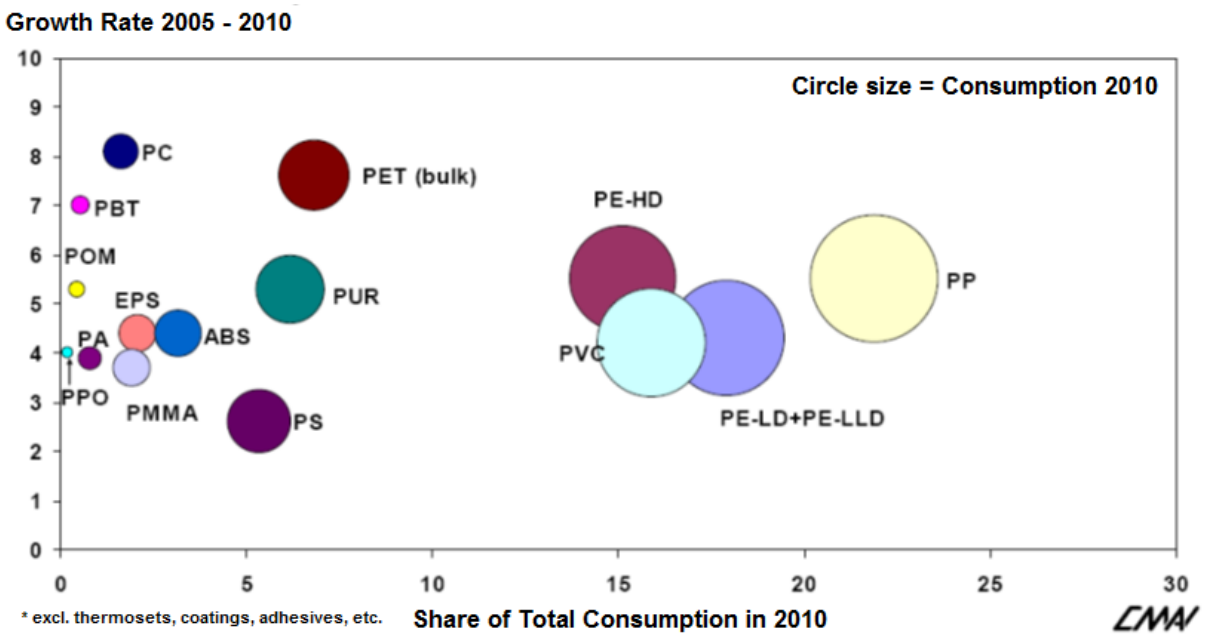

Figure 2 : Global consumtion of plastic materials[5]

The objective of the project is to bring novel flame retardant solutions for PBT/GF by exploring the additive route (incorporation of flame retardant additives in the PBT melt). To this aim, two approaches have been chosen: The first approach consists in determining novel flame retardant (FR) combinations susceptible to provide improved FR performances. It is intended to combine commercial products (having proven FR properties in PBT/GF) with various additives acting as synergistic agents. The second approach aimed at synthesizing novel flame retardants which exhibit better (or at least comparable) effectiveness than the solutions currently available on the market. The conception of novel flame retardants relates to the willingness of BASF to develop and commercialize its own FR products.

Having a good knowledge of the material is a basis to investigate potential solutions for flame retarding PBT. The first chapter of this project discloses the general properties of PBT. The synthesis and industrial production of PBT, its physico-chemical, mechanical, and fire performances are presented. The properties of PBT are reviewed to enlighten the reader on the reasons that led the polymer to be developed and used for specific - not to say major - applications. The latter will also be detailed. To allow the selection of potential flame retardant additives, the second section of the first chapter reports the fundamentals of flame retardancy and the diverse mode of actions which can be involved. The flame retardant available on the market and/or described in the academic or patent literature and used in PBT will also be discussed

The second chapter describes the investigated materials, namely the glass fiber reinforced PBT, and the experimental techniques used in this project. The methods implemented to evaluate the flame retardant behavior of formulations and the analysis techniques employed to perform the comprehensive study of flame retardant mechanisms are presented. This chapter further outlines the experimental procedures used for the synthesis of various FR additives (phosphinate salts).

The third chapter deals with the first approach of this project. It is devoted to the development of high-performing FR systems using the commercial phosphinate salts Exolit OP1240 and Exolit OP1200 marketed by Clariant (respectively aluminum diethylphosphinate and aluminum diethylphosphinate + melamine cyanurate). These commercial flame retardants were accordingly combined with several nano-particles since the latter were expected to act as synergists. The screening of the FR systems is first discussed. The optimization of the formulation containing the best flame retardant combinations, that is to say Exolit OP1240 and the organo-clay RDP bentonite (bentonite clay modified with resorcinol bis-diphenyl phosphate) is then detailed.

The fourth chapter covers the second approach of this project. A variety of novel phosphinate salts modeled on the structure of the Clariant's OP systems are synthesized from the reactive flame retardant Exolit PE110 (2-methyl-2,5-dioxo-1,2-oxaphospholane). FR performances of these new phosphinate salts are assessed in PBT/GF, as single constituents first and then in combination with traditional flame retardants or synergists.

The last chapter of this manuscript aims at investigating the flame retardant mechanisms of the FR systems explored in this project. In particular, it is intended to compare the FR mechanism of the most effective phosphinate systems from Clariant, namely aluminum dethylphosphinate (Exolit OP1240), with that the most promising phosphinate salt hereby synthesized.

CHAPTER 1 – STATE OF THE ART

This chapter aims first at giving an overview of the mode of production, the raw material properties and the applications of Poly(Butylene Terephthalate) (PBT). Second the strategies to improve the flame retardant properties of polymers and most particularly those of PBT will be reviewed. The additive route (incorporation of flame retardant additives into polymer melt) is most largely described since this method will thereafter be employed. Further, a special section is dedicated to the description of the reactive flame retardant Exolit PE110 (2-methyl-2,5-dioxo-1,2-oxaphospholane) that has been used - within the framework of this project - for the synthesis of a variety of flame retardant additives. The nanocomposite approach for enhancing the fire behavior of polymers will also be discussed.

1. Poly (Butylene Terephthalate) (PBT)

Poly(Butylene Terephthalate), hereafter called PBT, is a semicrystalline polyester of the class of engineering thermoplastics that was first brought to the market in the late 1960s by Hoechst Celanese[6] (currently Ticona). The polyester is nowadays produced from the melt phase polycondensation of pure terephthalic acid (PTA) or its dimethyl ester (DMT) on 1,4-butanediol (Figure 3).

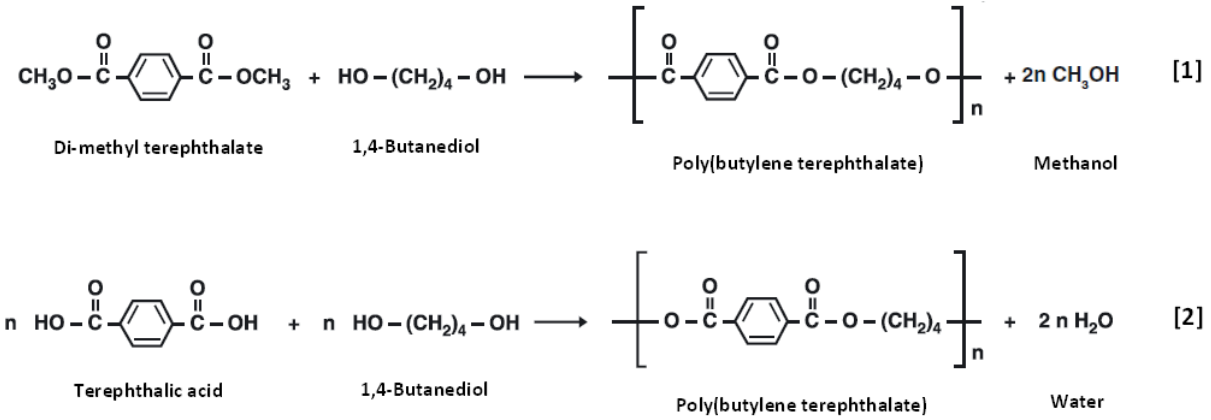

Figure 3 : Synthesis routes of PBT; [1] DMT route; [2] PTA route

1.1 Synthesis processes

1.1.1 General aspects

Several reactions can be used to prepare PBT but only two of them are of importance industrially[7,8,9,10,11]. The first reaction - DMT route or transesterification - involves the use of 1,4-butanediol together with dimethyl terephethalate. The second reaction - PTA route or direct esterification - consists in the condensation of 1,4-butanediol with pure terephthalic acid (Figure 3). Since these reactions are slow and balanced, an excess of 1,4-butanediol and very low amounts of a catalyst (i.e. $Ti(OBu)_4$) are incorporated in the bulk synthesis so as to accelerate the conversion of the reactants[12].

Several side reactions may occur besides the main reaction. It is thus necessary to control them so that the final product reaches the quality required for the market. Tetrahydrofuran (THF) is the most important byproduct obtained in both routes. It is formed by a cyclisation reaction of butadiol (with release of water) at temperature above 180°C, especially in the presence of acidic groups such as the PTA carboxylic acids. The PTA route accordingly generates higher amount of THF as compared to the DMT route.

The industrial production process of PBT exhibits two general steps. The first step corresponds to the proper reactions of transesterification (for DMT) or direct esterification (for PTA) which mostly result in the formation of Bis(4-hydroxybutyl) terephthalate[6]. 4-hydroxybutyl-terminated oligomers, whose proportion decreases with the molecular weight, are also produced in lower rates. The polycondensation constitutes the second step which leads to the formation of PBT linear chain of high molecular weight containing a relatively low amount of oligomers (~1%)[12]. For special applications which necessitate PBT with ultra-high molecular weight, a further Solid State Polycondensation (SSP) stage is required. This stage consists in heating the polymer in a reactor at temperature closed to its melting point under an inert gas flow.

The main technologies for the PBT manufacturing were developed by Zimmer and Ems-Inventa-Fischer[12]. Depending on the market demand, a PBT plant can either be continuous or discontinuous (batch). The following descriptions of the DMT and PTA routes will only focus on the Zimmer continuous processes.

1.1.2 PTA continuous process

The schematic diagram of the Zimmer PTA continuous process is shown in Figure 4. An exhaustive description of this process can be found in a patent assigned to Davy McKee A.G.[14].

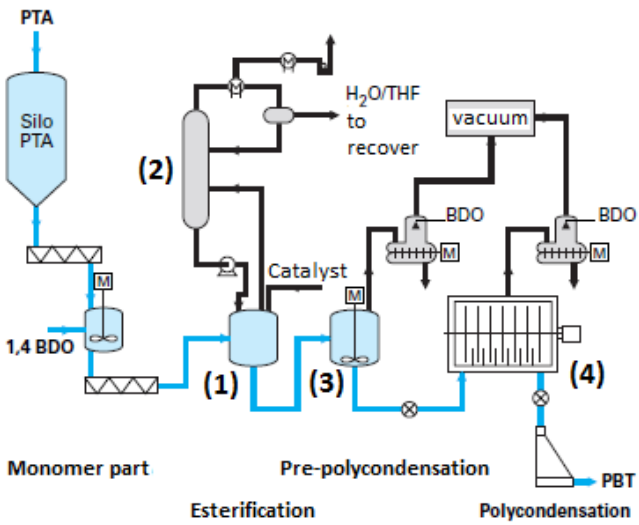

Figure 4 : Zimmer PTA continuous process[12]

In the first step, PTA, 1,4-butanediol and the catalyst are continuously introduced in an esterification reactor (1). The esterification is performed at temperatures between 220 to 260°C and under reduced pressures of 0.1 bar up to a maximum of 1 bar. During this stage, water, THF and 1,4-butanediol are evaporated. 1,4-butanediol is cycled back to the esterification reactor after the separation from water and THF in a distillation column (2). The esterification product is transferred to a second reactor (3) for the pre-polycondensation stage. This second stage is performed at temperatures between 230°C to 260°C, under further reduced pressures (10 to 200 mbar). Transesterification reactions take place which leads to the formation of low molecular weight PBT and 1,4-butanediol. The latter is split off together with THF. The pre-condensate obtained is finally transferred in a Disc Ring Reactor (DRR) (4) where the polycondensation takes place at temperatures of 240°C to 265°C and at pressures of 0,3 to 25 mbar.

1.1.3 DMT continuous process

The schematic diagram of the Zimmer DMT continuous process is presented in Figure 5. The description of the process can be found in a patent likewise assigned to Davy McKee A.G.[15].

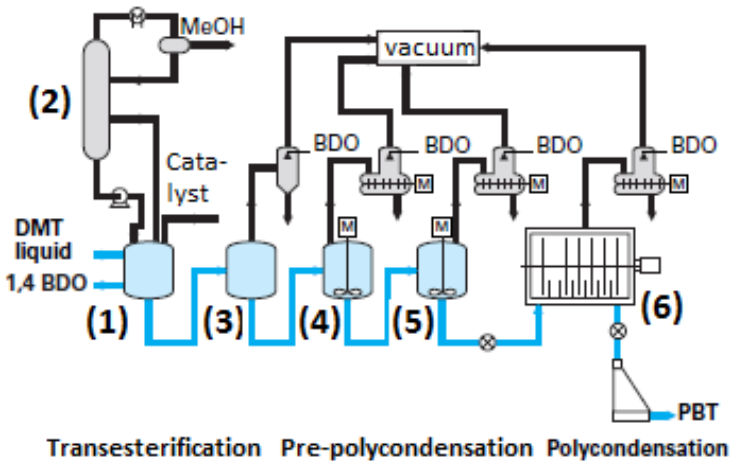

Figure 5 : Zimmer DMT continuous process[12]

For the DMT route, Zimmer developed a 5-reactor continuous process (Figure 5) which can be divided in three sections: transesterification, pre-polycondensation and polycondensation. DMT, 1,4-butandiol and the catalyst are fed into a first transesterification reactor (1) where an intermediate polymer is formed. The reaction is performed at temperatures of 160°C to 180°C and at pressures of 1.2 to 1.6 bars. During this stage, mainly DMT, methanol and BDO are vaporized from the reactor chamber to a distillation column (2). Methanol is recovered at the top of the distillation column while DMT and BDO are condensed and cycled back to the reactor. The reaction mixture is transferred to a second transesterification reactor (3) where it is submitted to higher temperatures (180°C to 210°C) and lower pressures (0.5 to 0.9 bar). As a result, a further conversion of DMT takes place and THF is formed. The latter is taken off from the reactor together with methanol and water.

BDO which is also collected can either be recovered or recycled into the first transesterification reactor. The reaction mixture from the second reactor is then fed successively into two pre-polycondensation reactors (4) (5) with increasing temperatures (210°C to 255°C) and reduced pressures (5 to 500 mbar). During this precondensation stage, DMT is almost completely transesterified and low molecular weight PBT is produced, while THF and BDO are evaporated and recovered. The molten product from the second pre-polycondensation reactor (5) is finally sent into a polycondensation Disc Ring Reactor (6) where the desired PBT is produced.

1.1.4 Comparison between DMT and PTA processes

Both DMT and PTA routes constitute the basis of the current polycondensation processes, whatever continuous or discontinuous, but since it is easier to access to a terephthalic acid of high purity, the PTA route gets more and more developed in the new facilities[12]. The PTA process also exhibits other notable advantages compared to the DMT process as depicted in Table 1. It exhibits less process stages and higher polycondensation speed; it consumes fewer raw materials and does not necessitate a methanol handling. THF is moreover a commercially valuable product which can be obtained with relatively high purity (>99.5%) through the PTA process. THF produced throughout the DMT process is mainly polluted by methanol and it cannot be easily purify due to the azeotropic character of the THF/methanol mixture.

Table 1 : Characteristic aspects of the DMT and PTA processes[8]

		DMT process	PTA process
Number of reactors	**-**	5	3(2)
Throughput (per line) **- discontinuous** **- continuous**	 **tons/day** **tons/day**	 15-50 60-300	 15-50 60-360
Raw material consumption	**kg/ton PBT** **kg/ton PBT**	DMT: 885 BDO : 439	PTA : 759 BDO : 496
Byproducts	**kg/ton PBT** **kg/ton PBT**	MeOH : 290 THF : 20	H2O : 180 THF : 61
Purity	**wt%**	MePH : >95%	THF : >99.5%
Utility consumption **- Current/Power** **- Heating oil**	 **kWh/ton PBT** **kWh/ton PBT**	 125 98	 105 85

1.2 Structure and properties

1.2.1 Structure

PBT is a semicrystalline polymer which exhibits a degree of crystallinity of about 35-40% when produced under moderate conditions[6]. The PBT crystals present two possible phases, the α-form and the β-form, which are both characterized by an elementary triclinic structure (Figure 6).

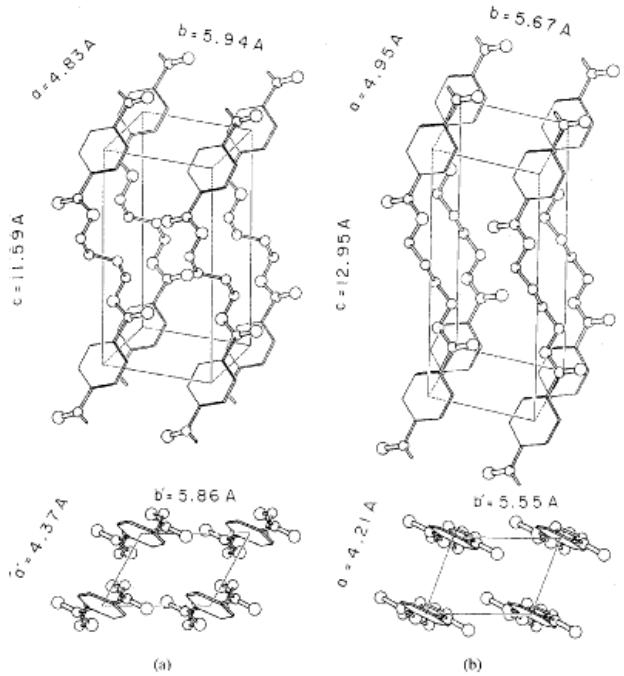

Figure 6 : Crystal structure of PBT; (a) α-form, (b) β-form[16]

The α-form corresponds to a relaxed crystalline state which is predominantly obtained upon cooling PBT from the melt[17]. It can reversibly converts into the β-form by uniaxial stretching (i.e. fiber drawing) of the material[16,18-20]. Up to a 12% strain, removal of the stretching will lead to a complete recovering of the α-form. Above 12% strain, the β-form will persist or it will partially transform into the α-form.

At higher morphological scale, PBT is constituted of two different types of spherolitic structures as observed between crossed polarizers[21,22]. One structure exhibits an usual maltese cross-like pattern (i.e. PA and PP) while the characteristic rapidity of the PBT crystal growth gives rise to a spherolitic structure with an unusual maltese pattern. Spherolites consisting in a combination of the two patterns may also be observed.

One major particularity of PBT is its rapid crystallization[23]. It is faster than most of the engineering polymers with comparable application property profiles Table 2.

Table 2: Relative speed of crystallization for various engineering polymers[8]

	PBT	PTT	PET	PA 6	PA 66
Crystallization speed index*	15	10	1	5	12

*Reciprocal of time from starting point of cooling crystallization temperature to its maximum peak

This rapid crystallization of PBT is a great benefit for the production of parts by injection molding. Comparatively to polymers with lower crystallization kinetics (i.e. PET, Table 2), it is possible to use lower mould temperatures and shorter cycle times. Therefore, this lead to economical processing. Isothermal crystallization experiments performed from the PBT melt state (225°C) to 180°C have shown that crystallization speed of the polymer tended to drastically increase with decreasing of the temperature (Figure 7)[23]. When further reducing the temperature, the crystallization of the polymer slows down but it is still sufficient at 80°C, temperature of the mould which is generally used for injection processes.

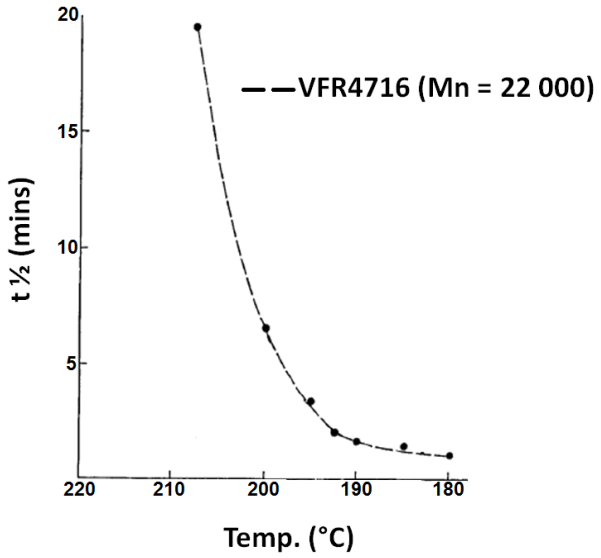

Figure 7 : Half time of crystallization (t½) of PBT as a function of isothermal crystallization temperatures[23]

On the other hand, PBT exhibits a glass transition temperature (Tg) in a range between 30°C to 50°C depending on the thermal history of the polymer. Specimens with higher degree of crystallinity presents higher Tg value[24].

The melting behavior of PBT has been extensively studied by DSC [17,20,24-30]. PBT thermograms, obtained by scanning the polymer from below the Tg up to the melting temperature, often display a "multiple melting peak" which supposes the existence of several crystal structures with proper thermal stabilities (Figure 8).

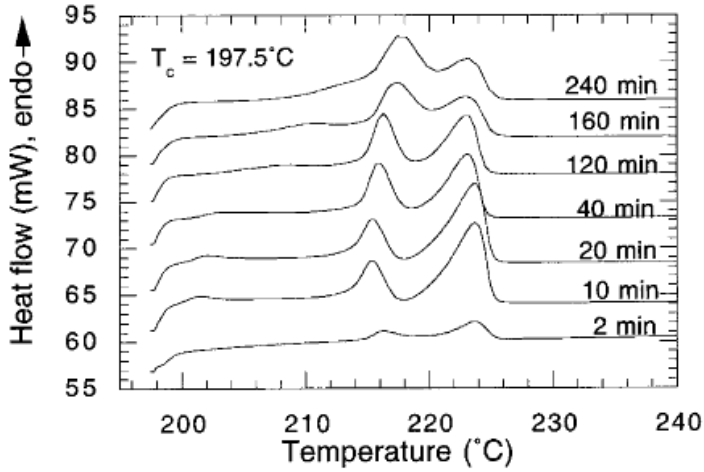

Figure 8 : Melting endotherms obtained for PBT after different isothermal crystallization times at 197.5°C. The scan rate was 10K/min[29]

This multiplicity was first ascribed to the presence of different spherolitic structures in the material; however it has been showed that the various spherolitic forms could all contribute into the same melting peaks[22]. Most of the researchers now attribute this "multiple melting peak" to simultaneous melting, recrystallization and crystal perfection of the polymer [25,27-30].

On the other hand, annealing of PBT at given temperatures, in a range from the Tg to the melting point, usually results in the appearance of a supplementary melting endotherm on the thermograms (Figure 9). This new melting event, which occurs at a temperature close to that of the annealing temperature and whose intensity increases with this latter, was assigned to new crystallites formed during the thermal treatment and having lower degree of perfection[17].

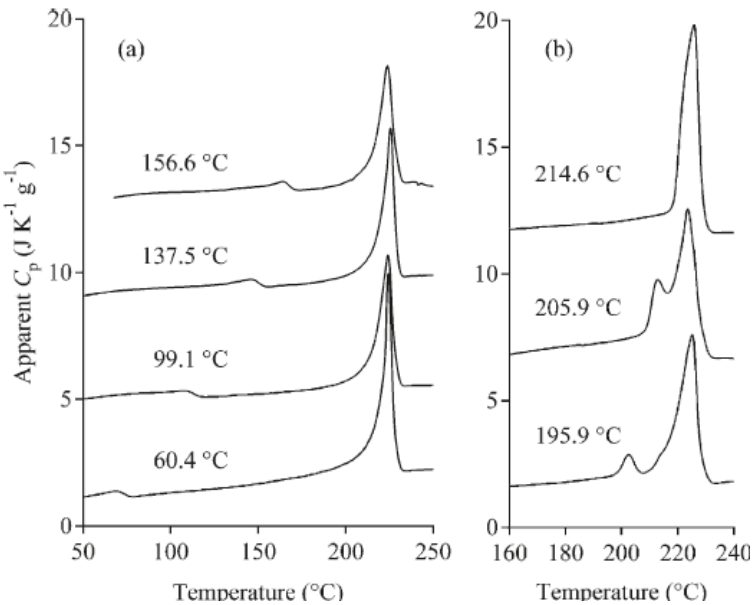

Figure 9 : DSC curves of PBT after different annealing temperatures of 10 min from the quenched state. The scan rate was 10K/min[17]

1.2.2 Mechanical properties

One of the main reasons for the use of PBT (common to that of the different types of engineering plastics) is its relative high strength, stiffness and heat deflection stability. Unreinforced PBT exhibits a tensile strength of 55 MPa. With a 30 wt% glass fiber reinforcement, the latter can be increased to about 140 MPa[31]. In addition to the enhancement of the tensile strength, glass fibers also improve many of the other mechanical properties of the polymer. For instance, unreinforced PBT has a flexural modulus of about 2500 MPa and a heat-deflection temperature of 170°C at 0,46 MPa while the same properties are respectively of 9000 MPa and 215°C for a 30 wt% glass fiber reinforced PBT.

1.2.3 Electrical properties

PBT has excellent electrical and dielectrical properties which is the reason why it is an insulating material of choice for electrical and electronic applications. As a foremost point, the environmental moisture has a low impact on the electrical properties of PBT. The polymer has outstanding creep current and arc-tracking resistance and it exhibits a high dielectric strength even for thinner wall sections[6,31].

1.2.4 Resistance to moisture and chemical agents

The water uptake of PBT, determined after immersion of specimens in water at 100°C, is approximately of 0,8% in the saturated state[32]. This low moisture absorption of PBT constitutes a key advantage since it results in a particularly good dimensional stability of the material. However, due the relative sensitivity of polyesters to hydrolysis, PBT is not recommended for long-term uses in water above its glass transition temperature[6]. Below 60°C, PBT has a good resistance to a variety of chemical agents such as organic solvents (esters, alcohols, ether, aliphatic hydro-carbons and petroleum products) as well as oils, brake fluids, aromatic products, diluted acid or basic solutions and water[6,31]. Above 60°C, PBT is particularly sensible to ketones, aromatics and chlorinated substances as well as weak acids and bases.

1.2.5 Thermal degradation and burning behavior

The high thermal stability of PBT mainly results from its semicrystalline feature which allow it to be maintained for short time at temperature close to its melting temperature without significant degradation[31].

In TGA analysis performed in inert atmosphere, the thermal decomposition of the polymer starts at about 350°C and it is characterized by one single apparent step. PBT is a low charring polymer which decomposes almost completely into volatile products.

The degradation pattern of PBT, depicted in Figure 10, has mainly been elucidated by pyrolysis coupled to gas chromatography/mass spectrometry (pyrolysis-GCMS)[33-35]. The

scission products recovered from the analyses and their relative proportion usually differ depending on the experimental conditions (i.e. pyrolysis temperature and type of the chromatographic column). However, a number of these scissions products, most particularly high-boiling point fragments with vinyl and/or phenyl end groups, terephthalic acid ester (A2), terephthalic ester (B2), benzoic acid (A1) and benzoic ester (B1), are unambiguously detected as well as THF, butadiene (C4), benzene (B) and diphenyl (DP). Terephthalic acid (TA), as one of the main volatile products which would be expected from the pyrolysis of PBT, is often not recognized on the pyrograms since the compound is not effectively separated in the columns[33].

The chain scission mechanism of PBT during pyrolysis has been subjected to several assumptions either involving heterolytic or homolytic cleaveages. According to some researchers[35], the vinyl end groups are likely to be obtained through an heterolytic elimination process implying a six member cyclic transition state (Figure 11). On the contrary, several authors while studying the nature of some minor scission products of PBT [36,37] and also to explain the formation of THF[38], have suggested that homolytic cleavages could be the prevailing scission mechanisms.

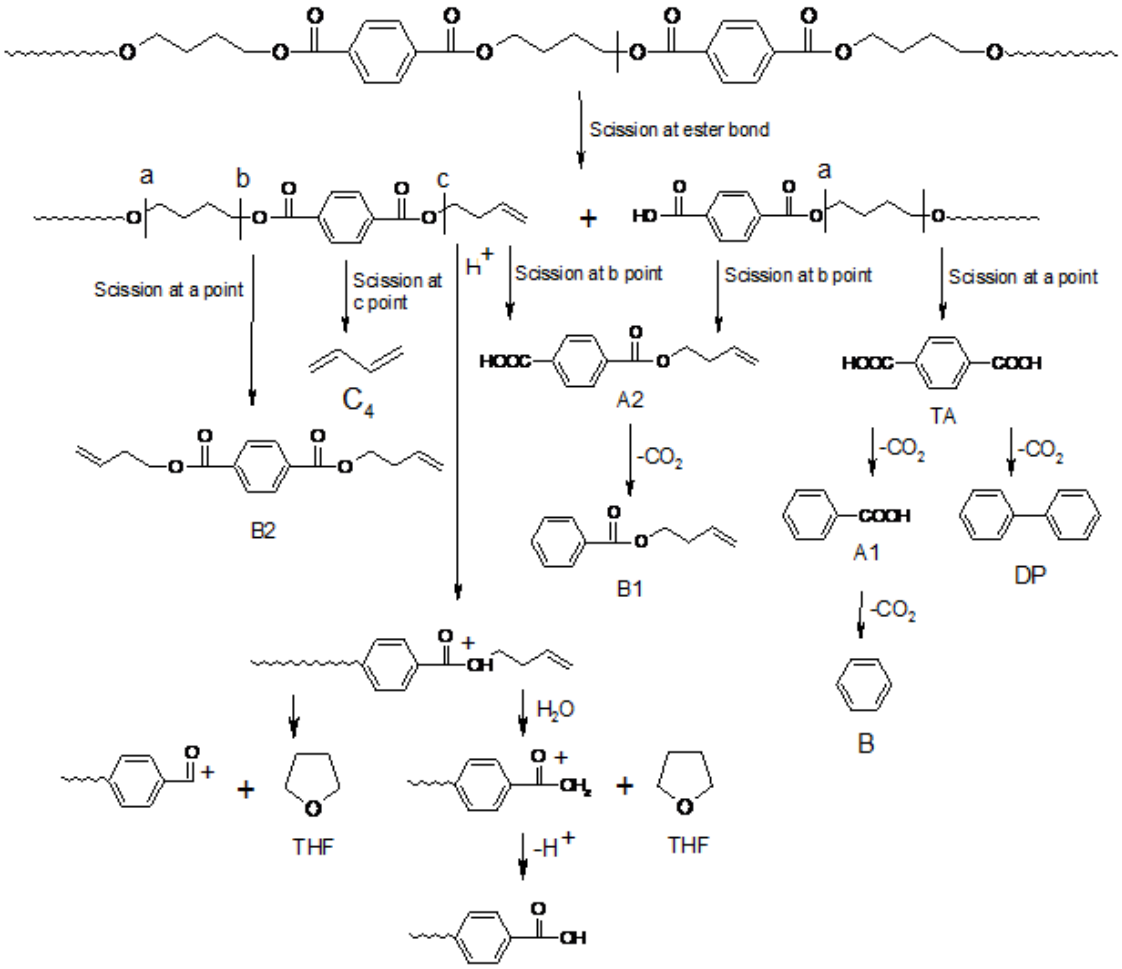

Figure 10 : Degradation pattern of PBT[33]

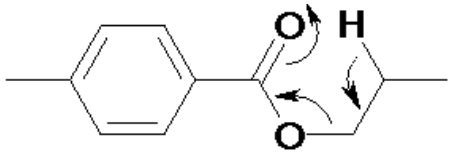

Figure 11 : Cyclic transition state of the ester bond of PBT resulting in the formation of carboxylic acid and vinyl end groups

On the other hand, PBT is intrinsically flammable due to its organic nature. Whatever pure or reinforced with glass fiber, the polymer is not classified at the UL94 vertical test[39,40].

At the LOI test, pure PBT achieves 22 Vol% while incorporating glass fibers in the polymer tends to decrease the LOI value to about 19-20 Vol%[39-41]. Casu et al[41] have investigated the effect of glass fibers on the flammability of PBT. The authors have come to the conclusion that glass fibers, because of their alignment in the polymer matrix and due to a higher heat conduction coefficient of glass compared to the plastic material, bring about a "wick effect" that is likely to increase the propagation of the flame on the burning specimens during LOI experiments.

Through the cone calorimeter test, glass fibers on the contrary help to improve the PBT flame retardancy[41]. During the test, while the PBT plate is burning, glass fibers accumulate at the surface of the sample and act like an insulating shield which restricts the heat and mass transfers between the surface and the bulk of the polymer. This results in a drastic reduction of the peak of Heat Release Rate (pHRR) of the sample as depicted in Figure 12. The Total Heat Release (THR) was nonetheless found to be comparable for the reinforced and the non-reinforced polymer, result from which it was deduced that glass fibers tended to change the degradation pattern of PBT and to favor the release of more combustible volatiles.

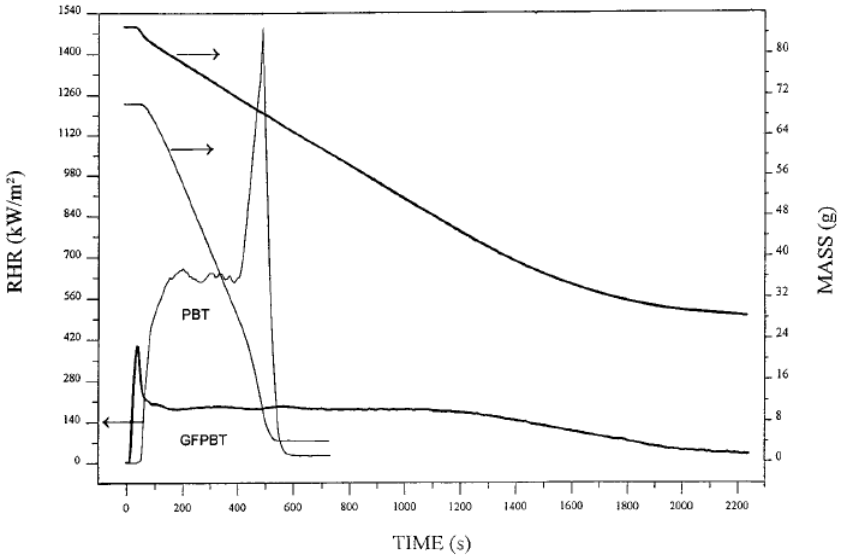

Figure 12 : Cone calorimeter results (HRR and mass loss) of PBT and 30 wt% PBT/GF. Irradiance of 50kW/m^2 [41]

1.3 Additives and blends

Right after the polycondensation process when the desired molecular weight is obtained, PBT is extracted from the reactor under the form of strand or band to finally be cut up into pellets or disc[31]. PBT is rarely used in the pure form[31]. It is generally compounded with processing aids and additives or blended with other polymers to endow the final material with specific properties which will depend on the type of application.

1.3.1 Glass fibers

Glass fibers are added to PBT in order to improve properties such as stiffness, strength, creep and to increase the dimensional stability of the polymer under heat[42]. The amount (20-50 wt%) and length of fibers,[43] as well as their orientation[42-44] in the polymer matrix constitute chief factors that may drastically affect the mechanical properties of the composite material. During the production process, glass fibers undergo a sizing treatment which consists of applying a silane-based coupling agent to their surface[45-47]. This treatment aims at improving the PBT/fibers adhesion so as to obtain more efficient transfers of mechanical stresses to within the material.

Glass fiber reinforced PBT has largely penetrated the market and it represents nowadays about 70% to 80% of the global consumption of PBT[48].

1.3.2 Flame retardants

Flame retardants are used to enhance the fire properties of materials. These additives are particularly important for PBT since the polymer is flammable and because it is extensively used in electrical/electronic facilities which are a major source of accidental fires. The different types of flame retardants, their modes of action and their performances in PBT will be detailed in the next sections of this chapter.

1.3.3 Other conventional additives and PBT blends

As most of the polymers, PBT can be compounded with various fillers and additives in order to fulfill some required properties. Fillers such as talc, chalk and glass beads can be used to increase the hardness, thermal stability and/or to decrease the price of the polymer. Antioxidants, UV stabilizers, pigments, processing aids, mold releasing agents are also common additives that are often required. Table 3 depicts usual amounts of these additives to be introduced in PBT.

Polymer alloys and blends of PBT have gained from the last decade great deal of attention. Combining materials indeed allows to conciliate advantages of the different components and to bring about attractive properties. PBT/PC alloys have for instance found large scale

applications in automotive industry (i.e. car bumpers). The material gathers high toughness and dimensional stability of PC with good flow and high solvent resistance of PBT[49].

Table 3 : Amount of the various additives to be introduced in PBT

Additive	Amount to be added (wt%)
Fillers	20 - 50
Pigments	1 - 4
Carbon black (colouring, UV stabilization)	0.3 - 0.5
Processing aids, slip agents	0.3 - 0.5
Molybdenum sulfide or graphite (increase processibility, decrease friction)	1 - 4
Antioxidants and heat stabilizers	Depend on the nature of the agents
UV stabilizers	0.1 - 0.5

On the other hand, the impact strength (reciprocal to toughness) of PBT can be improved by blending it with elastomers (typically ABS[50]). Polytetramethyleneglycol (PTMG) is also compounded with PBT to provide the latter with flexibility, softness and higher toughness. PBT/PET blend provides better processibility, heat deflection stability and it has lower cost[51].

1.4 Applications

The worldwide market of PBT exhibits one of the highest growth rates among engineering plastics. The global demand by 2005-2006 was of about 700kt[5] and it is predicted to reach 1300 kt by 2017[52]. The polymer finds its largest consumption in Europe, United States and Japan particularly for applications in automotive and electrical and electronic equipments (EEE). It is also largely use in Asia (especially China) where the demand has lately known the highest growth thanks to the strong and fast development of the automotive industry, in addition to the already extensive use of the polymer in EEE.

Most part of the consumption of PBT is dedicated to the automotive and the electrical/electronic industries (Figure 13) for applications that mainly require high stiffness, high thermal and dimensional stability, low moisture absorption, high resistance to chemical agents, light and weathering and excellent dielectric properties.

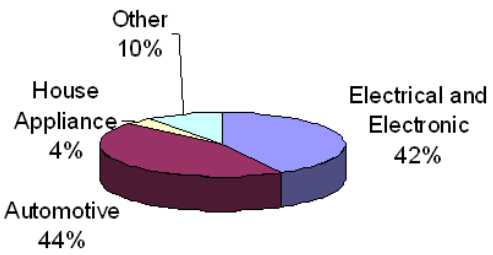

Figure 13 : Worldwide use and demand for PBT[5]

In cars, the PBT is notably used as air-conditioning valves, gas cap, rear and side view mirror panels, lamp socket inserts, structural brackets, brake system and hydraulic transmission parts as well as door handles, wiper systems, cowl vents, bumpers, fender extension, and different other motor, gear and electronic housings (Figure 14)[5,6,31].

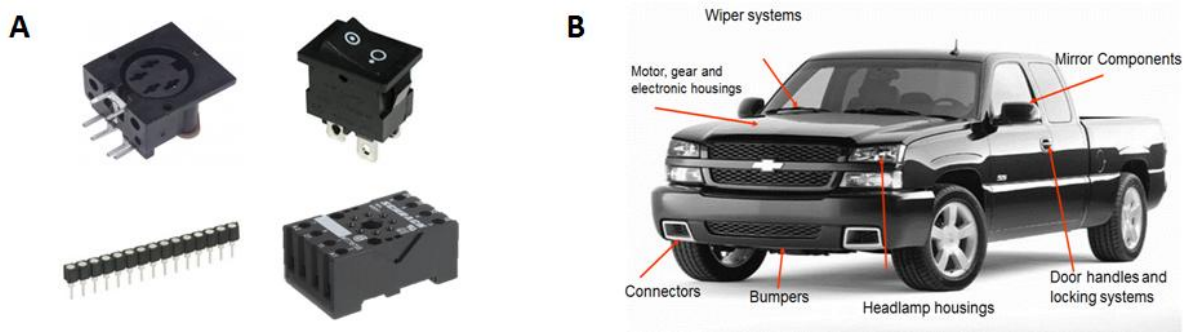

Figure 14 : (A) Plug, switch, relay, connector; (B) Automobive parts using PBT

In the electronic/electrical industry (Figure 14), PBT is used for connectors, relays, bobbins, contactors, capacitors, switches, plugs, lamp sockets, terminal boards, integrated circuit carriers, etc.

PBT has also a number of applications in domestic and industry appliances. Typical examples for consumer goods include handles for hair dryers, irons, oven doors, cookers and fryers as well as hair dryer nozzles, iron bases, toaster housings. In industry, PBT is used for pump housings and impellers, gears, valves, tool housings, filter media, pushbutton, etc.

PBT can be found in many other applications. For instance, PBT fibers can be used to produce apparel. They are particularly adapted for the production of swimwear thanks to their good resistance to chemical agents such as chloride and their good stability in water. Other applications will not be further detailed as they do not fall within the framework of this project.

1.5 Conclusion

This chapter has given an overview on the synthesis, properties and uses of PBT. Owing to its good processability, high stiffness and thermal stability associated to outstanding dielectric properties and good resistance to water and chemical agents, the material has found reliable utility in important domains, most particularly in the automotive and in the electrical and electronic industries.

The organic nature of PBT however constitutes a key concern in terms of flammability risk, as for a majority of polymers. That is the reason why the material has to comply with severe fire safety requirements. The next part of this chapter will thus focus on the strategies employed to improve the flame retardancy properties PBT.

2. Flame retardancy of PBT

Polymers, despite their widespread use, often lie at the origin of fire outbreak and propagation. Since they are organic materials, indeed, they decompose into combustible gases when exposed to heat. That is why they have to be treated so as to reduce their combustion, to reduce the release of fumes and to prevent the fall of inflamed drops during the combustion.

In order to understand how to prevent the burning of a material, it is necessary first to understand how it burns. The combustion process occurring at the surface of a polymer is the ultimate stage of a sequence of events which is originally induced by a heat source. As the latter brings about an increase of the temperature of the polymer surface, chain scissions occur into the material and volatile species are released into the air. A flammable gaseous mixture is therefore produced which is composed of the combustible gases evolved from the material (degradation products) and of the oxygen from air. This gaseous mixture may ultimately ignite if the heat source conveys enough energy and if the concentration of gaseous products is sufficient to activate the combustion reaction. Throughout combustion, very reactive radical species (i.e. H° and OH°) are produced which allows to maintain the process alive via cascade-chain reactions and to continuously produce heat and further polymer degradation.

The thermal degradation of polymers usually implies oxidizing and/or non-oxidizing processes. The non-oxidizing process, or pyrolysis, consists in the direct scission of polymer chains (heterolytic or homolytic) under the effect of heat. The oxidizing process involves radical interactions between the organic material and O_2. This leads to the formation of a variety of functional groups such as alcohols, ketones, aldehydes, carboxylic acids as well as production of reactive species such as H° and OH°.

Flame retardants are substances whose role is to interact with a polymer and/or with the volatile species which are released subsequently to degradation and burning of the polymer in order to prevent or inhibit the combustion processes. Flame retardants may act in the different stages involved in the combustion processes of polymers. They act either in the gas and/or the condensed phase according to physical or chemical mechanisms:

• In the gas phase, FRs act

- *by flame inhibition*. The fire retardant releases active species whose role are to interrupt the combustion reactions that take place into the flame. A large variety of halogenated and phosphorus based compounds act through this mechanism.

- *by dilution of combustible species*. Flammable gaseous species arising from decomposition of the polymer are released into the flame together with non-flammable species (such as for example H_2O) evolving from the fire retardant. This results in lowering the concentration of

combustibles in the gas phase. Metal hydroxide, carbonates and nitrogen-based compounds are examples of FR additives that may act as fuel diluting agents.

• In the condensed phase, FRs act

- *by formation of a protective shield at the surface of the polymer*. The flame retardant favors the production of a superficial carbonaceous (char) or ceramized layer which limits the diffusion of degradation products into the gas phase and lowers the heat transfer into the bulk polymer. Intumescent systems are FR combinations that typically work according to this mechanism. There are classically composed of three elements, namely a charring agent (i.e. pentaerythritol), an acid source that promotes crosslinking of the charring agent (i.e. ammonium polyphosphate) and a blowing agent (i.e. melamine) that expends the char through volatilizing.

- *by cooling of the polymer environment.* The evolution of some flame retarding agents involves endothermic processes that act like heat sink, therefore reducing the warming of the polymer matrix. Metal hydroxides present such an action.

The flame retardant mode of action often implies at the same time several of those mechanisms above-mentioned, though one is usually prevailing upon the others. On the other hand, the combination of different flame retardants may be an attractive means to induce synergistic effects during FR processes, hence to further decrease flammability of polymers.

On the other hand, various methods for flame retarding polymers exists. The fireproofing agent can indeed be directly incorporated as co-monomer into the polymer chain during the polymerization reaction (or afterward grafted to the chain) or it can be introduced as additive into the melted polymer during its processing. The first method, also called reactive route, may have valuable advantages since it may prevent the flame retardant from blooming out and because the random dispersion of the FR moieties into the material does not impair mechanical properties of the polymer[53,54]. However, the second method is usually preferred for the main reason that handling and processing in that case are easier and therefore more cost-effective[54,55]. Hereinafter, the state of the art will mostly focus on the additive route. The main question is what are the common flame retardant additives and what is their influence on the flame retardancy of PBT? We propose to answer those questions in the following part. The different flame retardant classes and their modes of action will be first presented from a general point of view. Their performance in PBT will then be reviewed. Yet it will be put a special emphasis on describing Exolit PE110 as the latter was used in this project to synthesize a variety of phosphinate salts for applications as FR additives in PBT. Finally, the flame retarding properties of nano-additives will be discussed.

2.1 Flame retardant classes and their modes of action

2.1.1 Halogenated flame retardants

Halogenated compounds, especially the brominated ones, have been widely used as flame retardants in various polymers thanks to their high performances. Chlorinated FRs have lower commercial diffusion as they usually exhibit lower efficiency as compared to brominated FRs[56-58], while ionidated and fluorinated compounds often present no significant activity in the decomposition temperature range of polymers[54].

● Mode of action

Halogenated flame retardants mainly act by flame inhibition (Figure 15). During the thermal decomposition process, hydrogen halide species - namely hydrogen bromide and chloride - are released in the gas phase and scavenge the radical intermediates in the combustion reactions[54]. Halogenated FRs may also have a condensed phase mode of action[54]. Hydrogen halides are indeed formed from reaction between the free radical halogens (resulting from the decomposition of the flame retardant) and hydrogen from the polymer. The latter, itself transformed into radical species, has the possibility to cross-links to other macromolecular parts which may lead to the creation of a carbonaceous protective shield at the surface of the material.

$$RX \rightarrow R^{\bullet} + X^{\bullet} \qquad \text{X may be Br or Cl}$$

$$X^{\bullet} + R'H \rightarrow R'^{\bullet} + HX$$

$$HX + H^{\bullet} \rightarrow H_2 + X^{\bullet}$$

$$HX + OH^{\bullet} \rightarrow H_2O + X^{\bullet}$$

Figure 15 : Quenching mode of halogen-based species released in the gas phase

Antimony oxide (Sb_2O_3) is one of the major synergistic agents used with halogenated FRs. The oxide interacts with halogenated species during the combustion processes which results in the formation of antimony trihalides (i.e. Sb_2Cl_3 and Sb_2Br_3) or oxyhalides. Those were found to be more effective free-radical trapping agents in the gas phase than the single halogen halides[57,58].

● Environmental and health issues

Since the late 1980s, numerous studies have pointed out that some of the halogenated FRs involved environmental and health risks at every compartments of their lifecycle, including production, distribution, use and disposal. In particularly, some brominated FRs have been found to be persistent in the environment, including far-off areas (i.e. Arctic, deep oceans…), to accumulate in biota and to cause toxic effects on humans health and development (i.e. thyroidogenic, estrogenic…)[59,60]. Another key concern is that some of the brominated FRs,

most particularly polybromodiphenyl ethers (PBDEs) and polybrominated diphenyls (PBBs), were proved to form highly toxic dioxin and furan derivatives during manufacturing, waste incineration or accidental fires[61]. As a consequence of it, a certain number of halogenated FRs have been withdrawn from the market (i.e. RoHS directives from the European commission) and there are currently new trends for the commercialization and use of more friendly flame retardants.

2.1.2 Melamine and its derivatives

Melamine is a non-halogenated compound which is widely used in intumescent systems (i.e. blowing agent). It can also be used in its pure form or as salt derivative (melamine cyanurate, melamine phosphates) to flame retard thermoplastics. Besides, condensed homologues of melamine such as melam, melem and melon, have also been exploited in some experimental formulations. The structure of melamine and its derivatives are depicted in Figure 16.

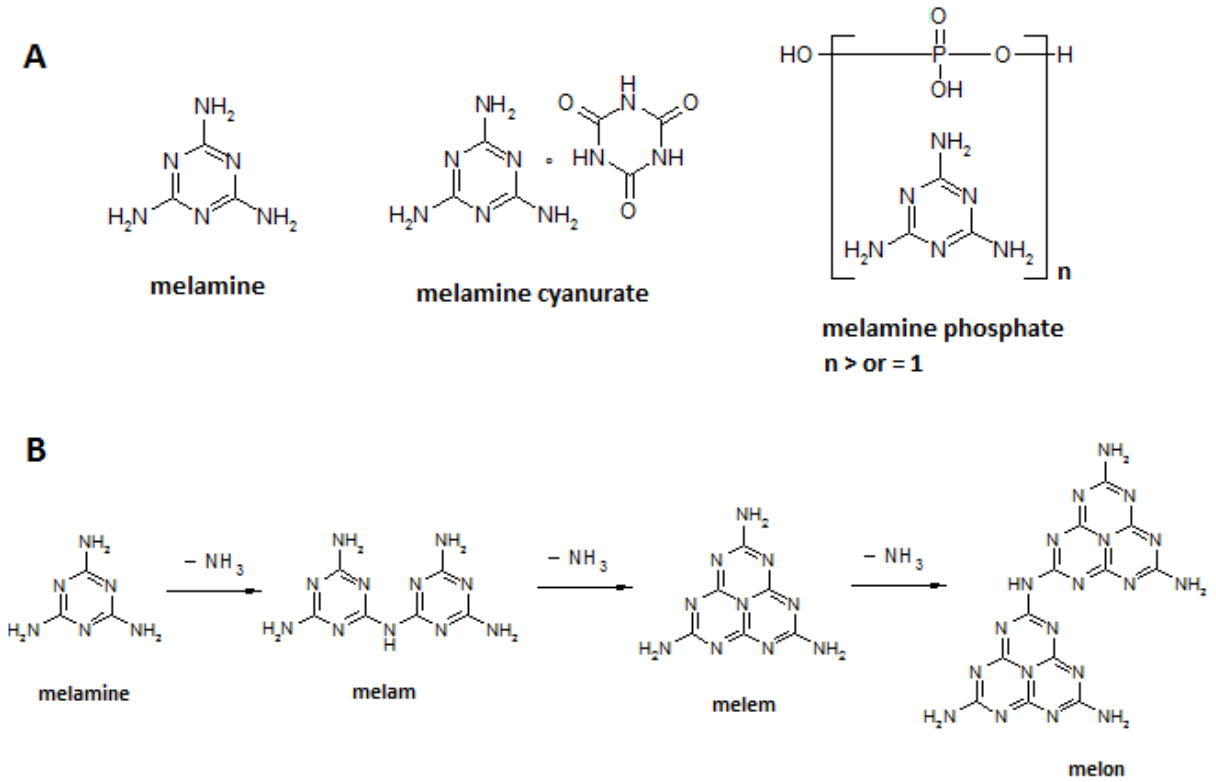

Figure 16 : Chemical structure of melamine, of its salt derivatives (A) and of its condensed homologues (B)

● **Mode of action**

Melamine is a high thermally stable compound that sublimates around 300°C. Endothermal feature of the sublimation brings about cooling of the polymer matrix while volatilization of the compound in the gas phase results in the dilution of combustible species[54]. By increasing

the temperature, melamine condenses into non-volatile congeners (i.e. melam, melem and melon), releasing ammonia that further dilutes flammables gases.

The salt derivatives of melamine, namely melamine cyanurate, melamine phosphate, melamine pyrophosphate and melamine polyphosphate exhibit superior thermal stabilities as compared to the pure melamine. Besides releasing melamine in the gas phase, they provide supplementary condensed phase mode of action (more particularly phosphate based salts), for instance favoring the formation of an insulating barrier.

2.1.3 Metal hydroxides and hydrocarbonates

Metal hydroxides and hydrocarbonates represent the largest proportion of the worldwide consumption of flame retardants. Among them, Aluminum Tri-Hydroxide (ATH) and Magnesium Di-Hydroxide (MDH) are by far the most widely used especially for applications in the wire and cable industry (i.e. EVA)[62,63]. Key advantages of those flame retardants include a relative low cost, a low impact on environment and human health, a low corrosiveness and outstanding smoke suppressant properties[62,64]. Adversely, they suffer from being moderately efficient to improve fire performances of polymers and therefore should be employed at elevated amounts (higher than 50 wt%).

● Mode of action

Upon heating, Aluminum Tri-Hydroxide $Al(OH)_3$ and Magnesium Di-Hydroxide $Mg(OH)_2$ decompose endothermally through releasing water. This cools down the polymer bulk while the evolved water acts as fuel diluting agent. A third effect comes when complete dehydration of metal hydroxides ends up creating a metal oxide residue (Al_2O_2, MgO) that act like a protective layer (Figure 17).

Thermal decomposition of ATH and MDH respectively takes place between 190-350°C (depending on the particle size and treatments) and 340-450°C[65,66]. Besides having superior thermal stability, MDH exhibits a more elevated dehydration enthalpy than that of ATH (see Figure 17) which endows the former with better heat sink properties.

$$2Al(OH)_3 \longrightarrow Al_2O_3 + 3H_2O \ (1050kJ/kg) \qquad eq.1$$

$$2Mg(OH)_2 \longrightarrow 2MgO + 2H_2O \ (1300kJ/kg) \qquad eq.2$$

Figure 17 : Thermal decomposition products of ATH (eq.1) and MDH (eq.2)

Among the different hydrocarbonates, hydromagnesite $Mg_5(CO_3)_4(OH)_2.4H_2O$ and the mixture of hydromagnesite and huntite $Mg_3Ca(CO_3)_4$ are the most largely reported in the literature[54,65,66]. Both fillers endothermally release water and CO_2 on an extended range of

temperatures, starting with water between 200 and 450°C, then CO_2 (also fuel diluting agent) to about 510°C[65].

2.1.4 Phosphorus-based compounds

Phosphorus-based compounds have known a great deal of attention as they represent the closest alternative to halogenated FRs. A large variety of these compounds, including phosphates, phosphonates, phosphinates, phosphine oxides (Figure 18) and elemental phosphorus (i.e. red phosphorus), has been investigated for flame retardancy applications in polymers.

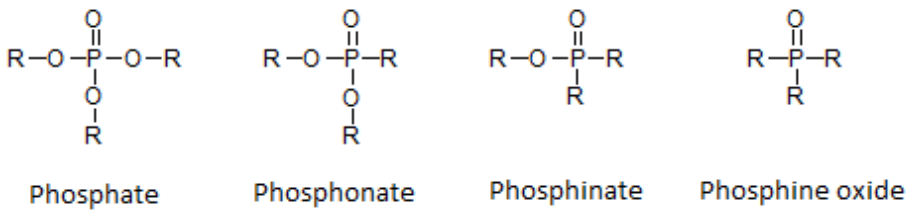

Figure 18 : Chemical structure of phosphorus compounds

● Mode of action

Phosphorus-based FRs can be active in both condensed and gas phase. In the condensed phase, they may promote the char formation (i.e. phosphoric acid in intumescent systems) and they also act as crosslinking precursors that take part to the constitution of an insulating shield at the surface of polymers and contribute to its consolidation[54]. They may also be active in the gas phase through releasing radical capturing species (i.e. PO•, PO_2•, HPO•…) that scavenge exothermic combustion reactions.

2.2 Flame retardants in PBT

2.2.1 Halogenated based compounds

Halogenated FRs have been extensively used in the electrical/electronic field where requirements in terms of fire reaction are severe. Tetrabromobisphenol A (TBBPA) and polybromodiphenyl ether (PBDE) are the most widely commercialized family of halogenated FRs on the worldwide market[54] (Figure 19).

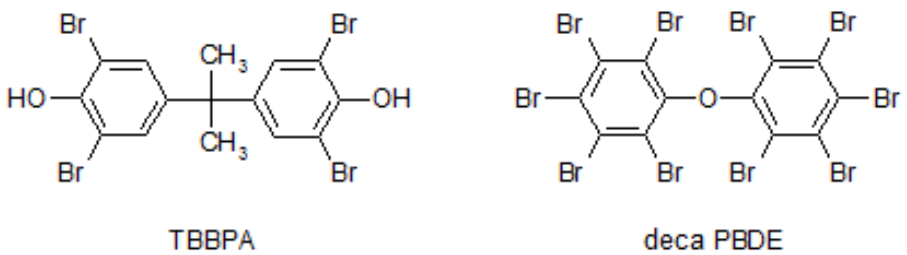

Figure 19 : Chemical structure of TBBPA and deca PBDE

TBBPA is a reactive fireproofing agent that is mainly used for epoxy and polycarbonate resins in printed circuit boards and electronic equipment[67,68]. A brominated polycarbonate oligomer, synthesized from the TBBPA monomer, has besides been marketed as high-performance FR additive. The latter has been successfully used in glass fiber reinforced PET/PBT blends in combination with antimony oxide[56,69].

PBDE are cost-effective flame retardants which are marketed under three major commercial forms, namely penta, octa and deca bromodiphenyl ether. Decabromodiphenyl ether is used for injection-molded polyesters, including glass fiber reinforced PBT for which V-0 rating (0.8 mm) is achieved at content of about 10 wt% plus 5 wt% antimony oxide[70].

Superior FR performances were obtained in glass fiber reinforced PBT with ethylene bis(tetrabromophthalimide), commercialized under the trademark SAYTEX BT-93 (Figure 20). 9 wt% of the flame retardant combined to 3 wt% antimony oxide allows to achieve V-0 rating (0.8 mm) with a LOI value of 35 Vol%[56,70]. As compared to other halogenated FRs, ethylene bis(tetrabromophtalimide) brings better color stability as well as better thermal and mechanical properties for the material.

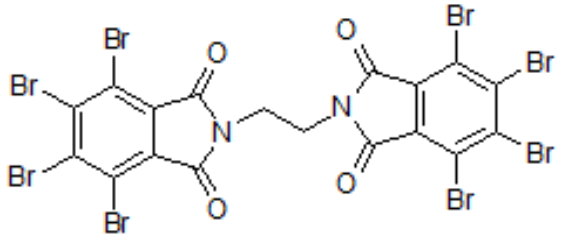

Figure 20 : Chemical structure of ethylene bis(tetrabromophtalimide)

A number of other halogenated FRs reviewed by Levchik et al[56] (Figure 21) have found commercial applications in PBT. Glass fiber reinforced formulations containing 10 to 12 wt% of these FRs, combined to 2 – 5 wt% antimony oxide, reach V-0 rating (0.8 mm) at the UL94 test.

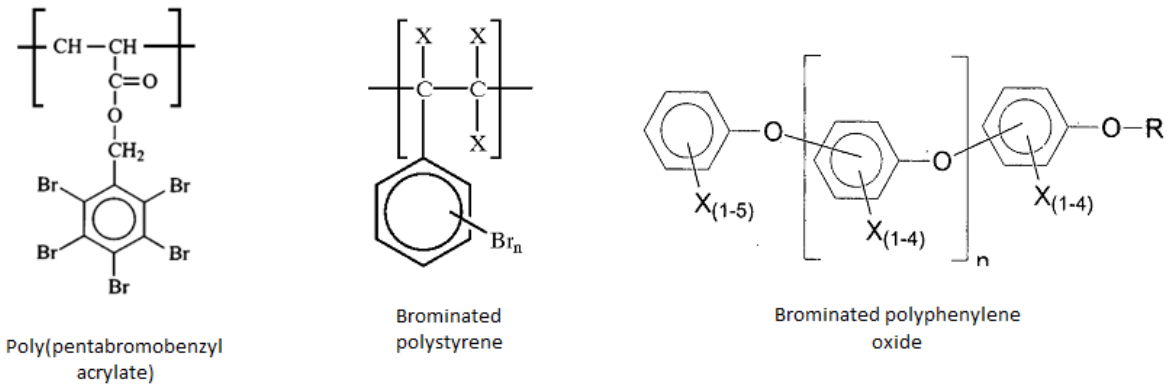

Figure 21 : Chemical structure of various halogenated flame retardants used in PBT

Halogenated flame retardants provide high fireproofing properties to PBT since, at relatively low loading, they allow achieving the best results in fire tests (i.e. UL94). However, their adverse effects on the environment and human health lead them to be progressively withdrawn from the market, replaced by more environmentally friendly products.

2.2.2 Melamine and its salt derivatives

Melamine alone in PBT shows limited FR efficiency. A 40 wt% loading in the unreinforced material is required so as to obtain a V-0 rating (2 mm)[71]. At this content, the LOI value slightly increases from 22 to 26 Vol%. Balabanovich[71] investigated the effect of melamine on the combustion of PBT. The author has established that melamine condenses into high thermally stable products (i.e melem, melon) that may eventually promote the formation of a protective char at high FR contents. The ammonia resulting from the condensation reactions modifies the degradation pathway of PBT through aminolysis of ester bonds with subsequent formation of aromatic amides and nitriles (Figure 22). Those latter volatilize and are assumed to act as fuel diluting and flame cooling agents. Melamine would additionally capture butadiene delaying the volatilization of flammable gases.

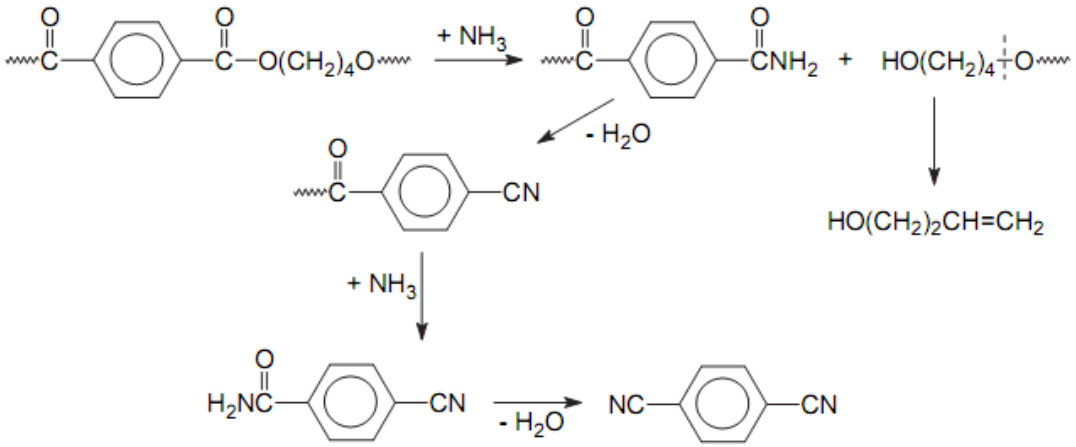

Figure 22 : Ammonolysis of PBT and formation of aromatic amides and nitriles[71]

Melamine cyanurate, at content of 20-30 wt% in the unreinforced PBT, also moderately increases the LOI value to about 26 Vol%[72,73]. Such loadings are not sufficient to obtain a V-0 classification. Upon heating (> 320°C), melamine and cyanuric acid dissociate via an endothermal process which cools down the polymeric matrix. Furthermore, the melamine salt provides a gas phase mode of action through releasing fuel dilution products, namely isocyanic acid (HOCN) and CO_2 as well as melamine and cyanuric acid [39,72].

On the other hand, PBT including 38 wt% melamine pyrophosphate achieves V-0 and V-1 rating at the UL94 test with bar specimens of respectively 1.6 mm and 0.8 mm thick[74].

In conclusion, melamine or its salt derivatives alone are not suitable for flame retarding PBT. So as to meet fire requirements, the polymer shall contain large amount of these substances

leading to poor mechanical properties. However, their combination with other flame retardants such as for example phosphorus based FR could be beneficial and will be discussed below.

2.2.3 Metal hydroxides and hydrocarbonates

Owing to its low thermal stability, ATH is normally not appropriated for compounding with PBT. However specific surface treatments (i.e. coating of ATH with stearic acids, silanes or titanes)[75] can be employed so that the filler may resist high to processing temperature. Boehmite (AlOOH), resulting from thermal treatment of ATH, may also be employed for flame retarding PBT[76].

$Mg(OH)_2$ and the basic hydromagnesite/huntite mixture have to be introduced at relatively high loadings (45-50 wt%) in unreinforced PBT so that the material achieves V-0 rating on UL94 specimens of 1.6 mm[56].

Metal hydroxides and hydrocarbonates have the advantage to be environmentally friendly flame retardants. As for melamine based products, though, they present relatively limited FR performances in PBT and therefore shall be rather employed as synergists with more effective products such as for example phosphorus based flame retardants.

2.2.4 Phosphorus-based compounds

● Phosphinate salts

There are known dialkylphosphinate salts, especially the aluminum based ones, that have proven high level of flame retardant efficiency in polyesters (Figure 23). At content of 20 wt% in the reinforced PBT, these organophosphates provide V-0 rating (1.6 mm)[77-79] and they furthermore show beneficial effects on the tracking resistance of the material.

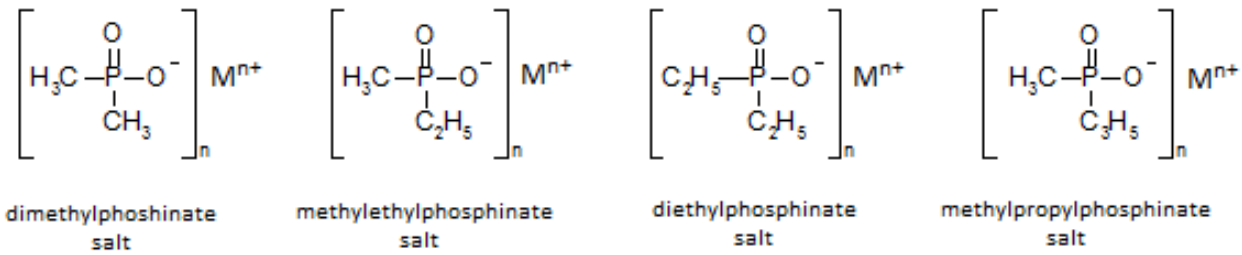

Figure 23 : Chemical structure of dialkylphosphinate salts used in PBT

The aluminum and zinc salts of the diethylphosphinic acid have known further industrial developments. They are nowadays commercialized by Clariant, under the brand name respectively Exolit OP1240 and Exolit OP950. 20 wt% of Exolit OP1240 enable glass fiber reinforced PBT to achieve V-0 rating (0,8 mm) together with a LOI of 44 Vol%[39]. Exolit OP950 has a melting point of 240°C and can then melt during the polymer processing which makes

it more suitable for the production of thin-walled items or fibers. However, at content of 20 wt%, the zinc salt has no satisfactory FR properties in PBT/GF since it does only provide a LOI of 27 Vol%. The material is furthermore not classified at the UL94 test (0,8 mm)[80].

Braun et al[39,80] have investigated the mode of action of the aluminum and zinc salts of diethylphosphinic acid in glass fiber reinforced PBT. The authors have reported that the aluminum phosphinate salts evolved during the main decomposition step through releasing two diethyl phosphinic acids in the gas phase (see Figure 24). This is accompanied by formation of aluminum phosphinate-terephthalate complexes in the condensed phase. The diethylphosphinic acid released acts in the gas phase by inhibition of the combustion reactions. A further minor decomposition step occurs at higher temperature which is characterized by release of benzene and CO_2 from the metal complexed terephthalates as well as ethene from cleavage of the ethylenic groups attached to the diethylphosphinates remained in the condensed phase. As a result, aluminum phosphates and relatively small amount of carbonaceous char are obtained in the final decomposition residue. The char apparently acts as an adhesive for glass fibers and increases the mechanical stability of the residue. The latter would consequently provide an additional protection against transfer of flammable volatiles in the gas phase during the burning process.

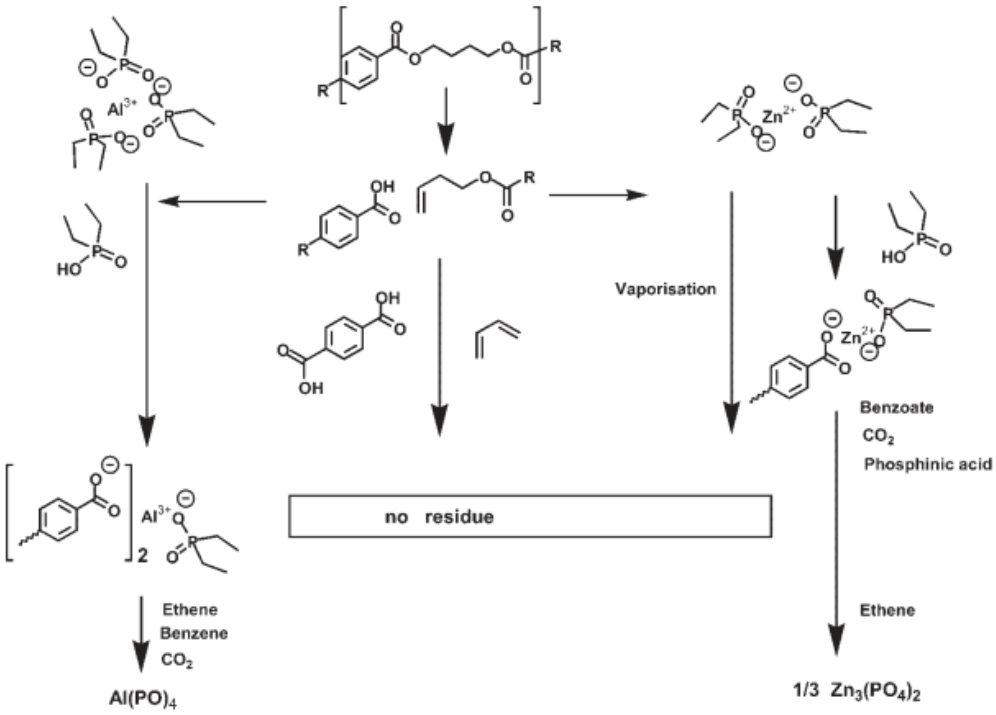

Figure 24 : Decomposition pathway of PBT in the presence of aluminum (left) and zinc (right) diethyphosphinate[80]

The zinc salt evolves in the same way than its aluminum analogous but part of the salt was found to volatilize in the gas phase and lower carbonaceous char is obtained in the residue (Figure 24). Because of its poorer mechanical stability, the charred residue would not act as

an effective barrier to mass transfers. This would partly explain the lower efficiency of the zinc salt as compared to the aluminum salt.

The combination of diethylphosphinate salts with other flame retardants (particularly melamine-based compounds) has been the subject of numerous researches. Usually, these combinations do not provide better flame retardant properties to the polymer but they do have the advantage of being more cost-effective than the pure phosphinates since the latter are particularly expensive to produce. Lately, the combination of aluminum diethylphosphinate and melamine cyanurate (2 and 1 parts by weight respectively) has been marketed by Clariant under the trade name of Exolit OP1200. It brings about similar flame retardant efficiency than the pure phosphinate salt in reinforced PBT. Melamine cyanurate decomposes without significant interactions with the polymer matrix and the phosphinate salt, releasing fuel diluting agents such as isocyanic acid, carbon dioxide, cyanurate and melamine[39,80]. A few patents assigned to Clariant further relate to the combination of aluminum diethylphosphinate with melamine polyphosphate[81] as well as aluminum phosphate, melamine, aluminum hydroxide, dihydrotalcite, natural huntite/hydromagnesite mixture, zinc stannate or zinc borate[79].

Hypophosphite salts (based on calcium and aluminum) have recently been introduced on the market by Italmach as cost effective phosphinates for use in thermoplastics. Despite their high phosphorus content (36 and 42 wt% for the calcium salt and the aluminum salt respectively), these compounds do not exhibit higher efficiency in PBT than that of organophosphinate salts and they furthermore tend to release very toxic phosphine (PH_3) upon decomposition[82,83]. Aluminum hypophosphite (AHP) alone, at content of 20 wt% in reinforced PBT, gives a LOI of 31 Vol% along with V-0 and V-2 rating on specimens of respectively 1.6 mm and 0.8 mm depth.

Yang and co-workers[82,83] have reported that aluminum hypophosphite (Figure 25), besides some gas phase activities (i.e. release of PH_3), exhibited notable condensed phase mode of action by strongly enhancing the carbonization of PBT during the burning process. TGA measurements indeed clearly highlighted the occurrence of an interaction between the hypophosphite salt and the polymeric matrix from which results a drastic increase of the residue yield of the material at 700°C (+ 19 wt% as compared to neat PBT). The authors have further exploited the char promoting potentiality of AHP to within a novel intumescent system composed of portions of high charring polycarbonate (PC) and melamine cyanurate (MC)[83]. 10 wt% AHP, 10 wt% MC and 7.5 wt% PC were capable of providing a V-0 rating (0.8 mm) to reinforced PBT but no significant improvement of the LOI as well as no extensive reduction of the heat release rate in cone calorimetry as compared to the formulation containing AHP alone were observed. For this latter formulation, the final residue yield in TGA was still slightly superior compared to PBT/AHP formulation.

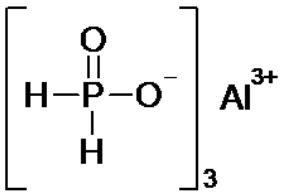

Figure 25 : Chemical structure of aluminum hypophosphite

● **Phosphonates**

Phosphonates have generally proven lower performances compared to phosphinates. For instance, the aluminum salt of O-methyl P-methylphosphonic acid (Figure 26), a product patented in the late 80s by Ciba-Ceigy, showed no satisfactory FR properties in PBT[84]. 6 wt% of this phosphonate salt in reinforced PBT shows however synergism with 14 wt% aluminum ethylmethylphosphinate providing a V-0 rating at 0.8 mm[85].

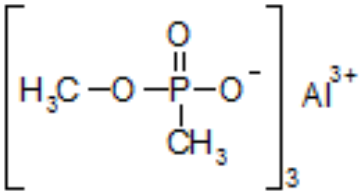

Figure 26 : Chemical structure of aluminum O-methyl P-methylphosphinic acid

A mixture of the cyclic diphosphonate ester Antiblaze 1045 (from Rhodia) and melamine has earlier found commercial applications in injection molded resins of PBT[86]. Antiblaze 1045 (Figure 27) is mentioned as a highly viscous liquid which on account of its plasticizing feature increases the elongation at break and impact strength of the polyester. Alone in PBT, the cyclic diphosphonate ester has moderate flame retardancy effects providing a LOI of about 27 Vol% and a V-2 rating (1.6 mm) at loading of 20 wt%[87]. 2 parts of the phosphonate combined to 3 parts of melamine, in an overall content of 20 w%, increase the LOI to 38 Vol% while the material meets the V-0 rating (1.6 mm).

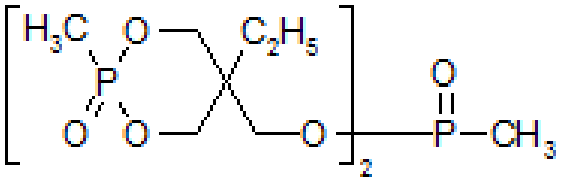

Figure 27 : Chemical structure of Antiblaze 1045

The synergistic effect between Antiblaze 1045 and melamine has been investigated by Balabanovich et al[87]. Part of the melamine was reported to behave in the same way than when it is alone in PBT, influencing the degradation pathway of the polymer towards the

formation of aromatics amides and nitriles. A flame retardancy effect therefore arises from the endothermic dehydration of the aromatic amides and the dilution effect of nitriles which are less flammable volatiles. A supplementary condensed phase mechanism was recognized since melamine proved to interact with the phosphonate during the thermal decomposition process. From this interaction results the creation of a glassy phosphorus and nitrogen containing residue at the surface of the material which act as an effective insulator.

Some patents relate to synergistic combinations between Antiblaze 1045 and metal hydroxide, carbonate or melamine based flame retardants in reinforced PBT. A V-0 classification on specimens of 1.6 mm thick can for instance be achieved by mixing 10 wt% of the phosphonate with 10 wt% $Mg(OH)_2$ or natural huntite/hydromagnesite[88]. Similar performances would be achieved by combining 12 wt% of the phosphonate with 8 wt% melamine cyanurate[56].

● **Phosphine oxides**

Among phosphine oxides, triphenylphosphine oxide (TPPO) and 1,4-diisobutylene-2,3,5,6-tetraxydroxy-1,4-diphosphine oxide (Cyagard RF 1204 from Cytec Industries) have earlier been under consideration for the flame retardancy of PBT. The chemical structure of the flame retardants is depicted in Figure 28. In PET, TPPO was found to completely vaporize during the decomposition process imparting to the polyester a vapor flame inhibition[89]. The same mode of action would be assumed for PBT. Glass fiber reinforced PBT achieves V-2 rating (1.6 mm) when compounded with 25 wt% TPPO[90] and V-0 rating when 20 wt% of the phosphine oxide is combined with 15 wt% melamine cyanurate[91]. On the other side, Cyagard was reported to destabilize PBT and to modify its decomposition pathway without promoting any char layer[92]. The addition of Cyagard in neat PBT, at content of 15 wt%, only slightly increases the LOI to about 23 Vol% and the material achieves a marginal V-2/V-0 classification. By increasing the flame retardant loading to 20 wt%, the LOI value of the material levels off at 23 Vol% and its UL94 ranking stands at V-2.

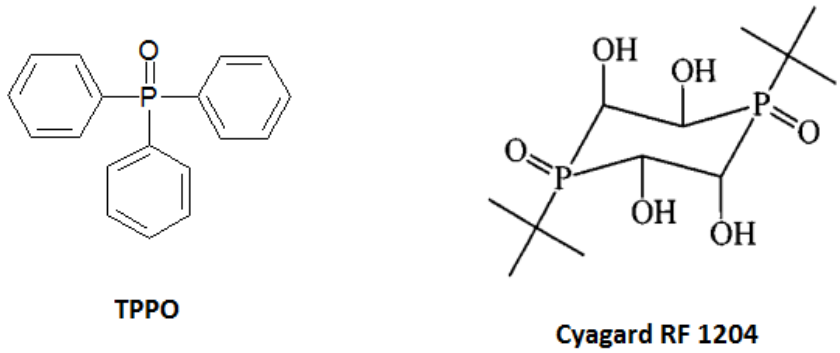

Figure 28 : Chemical structure of TPPO and Cyagard RF 1204

● **Aromatic phosphates**

Aromatic phosphates Resorcinol bis(Diphenyl Phosphate) (RDP) and Bisphenol A bis (Diphenyl Phosphate) (BDP) are low volatile flame retardant plasticizers that found commercial applications to flame retard polycarbonate and its alloys, namely PC/ABS and PPO/HIPS[62]. For those polymers which have an already high propensity to char, RDP and BDP (Figure 29) are convenient flame retardants since they may easily crosslink with phenolic functionalities and therefore supply an important condensed phase mode of action during the thermal decomposition process[54,93].

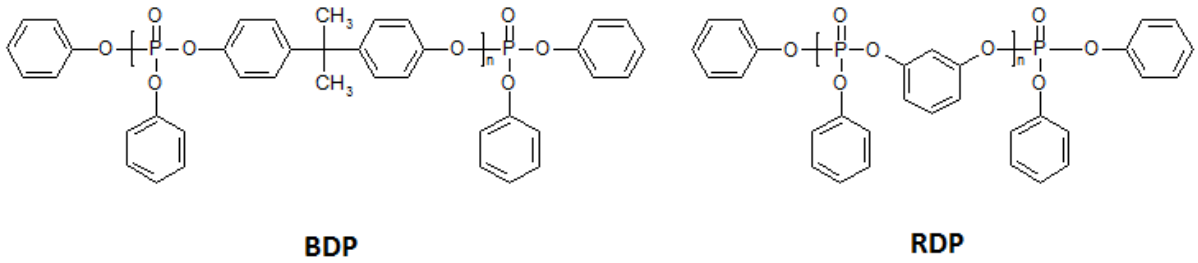

Figure 29 : Structure of the aromatic phosphate oligomers RDP and BDP

RDP and BDP alone have limited FR performances in PBT. Indeed, these flame retardants can hardly promote charring (so favor the formation of a protective shield) in such a polymer since the latter has itself low charring properties. A major drawback of those aromatic phosphates is that they migrate to the surface of the polymer beyond a certain concentration (i.e. 8 wt% and 10 wt% for RDP and BDP respectively)[94]. Some strategies to flame retard PBT were used which consisted in combining those aryl phosphates with high charring polymers such as the phenol-formaldehyde resin Novolac[94]. Upon decomposition, significant carbonization of the polyester was obtained with mixtures of BDP/novolac (12,5 wt% each) and RDP/Novolac respectively incorporated at 15 wt% and 10 wt%. These two FR systems give a V-0 rating (1.6 mm) in neat PBT. They are less efficient in reinforced PBT. It is due to the fact that glass fibers prevent swelling of the char and therefore reduce the effectiveness of the protective carbonaceous shield. Another positive effect of Novolac relies upon its capability to decrease blooming of the aryl phosphates in the material.

A few patents relate to flame retardant combinations involving RDP or BDP with melamine cyanurate and melamine pyrophosphates[74,95]. These combined systems should be incorporated in reinforced PBT at loadings as high as 35-40 wt% so the material may reach the V-0 ranking (1.6 mm).

● **Cyclophosphazene, polyphosphoramide and phosphorus oxinitride**

Special nitrogen-phosphorus based substances such as cyclophosphazenes have been perceived as promising flame retardants due to their relatively high nitrogen and phosphorus content. A major drawback of these compounds lies in their expensive cost. A

series of cyclophosphazenes, obtained by reaction of hexachlorotricyclophosphazene with (di)amino benzenes, (di)hydroxy benzenes and amino-hydroxy benzene (Figure 30), have been investigated in unreinforced PBT as flame retardant by Levchik et al[96].

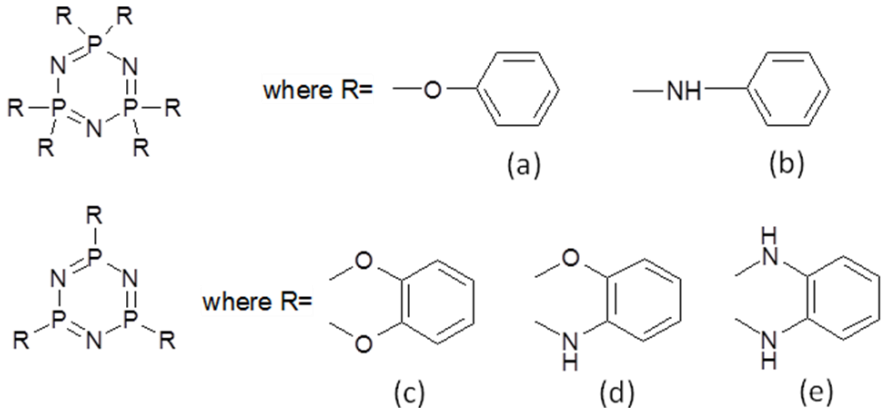

Figure 30 : Chemical structure of the different cyclophosphazenes investigated by Levchik et al[96]

Best performances were achieved with the amino-hydroxy benzene based cyclophosphazene (Figure 30, d) which provides a LOI of 29 Vol% and V-2 rating (1.6 mm) at content of 20 wt%. The cyclophosphazenes exhibited a large variety of thermal stabilities. However, the authors found no correlation between tendency to produce a solid residue and the combustion performance of the products[96].

Polyphosphoramide $(PN_2H)_n$ and phosphorus oxinitride $(PON)_m$ are other variety of nitrogen-phosphorus based compounds which have been investigated by Levchik and co-workers[96,97]. The former substance was prepared by heating hexa-aminotricyclophosphazene (Figure 30, b) in vacuum at 300°C and the second was prepared by heating urea, melamine and phosphoric acid at 350°C (about 2-3h), then at 750°C (2h). Both $(PN_2H)_n$ and $(PON)_m$ were characterized by exceptional thermal stabilities and exhibited very high residue yield in TGA (83% and 90% at 600°C respectively). The study reports that $(PN_2H)_n$ exhibits low FR performances and does almost not interact with PBT. Comparable performances were obtained with $(PON)_m$ but the latter was surprisingly found to trigger the char formation. On account of its low insulating efficacy, the char was assumed to be penetrable to flammables gases.

● **Red phosphorus**

Red phosphorus is one of the allotropic forms of elemental phosphorus which proved to be an efficient flame retardant additive in oxygen and/or nitrogen containing polymers (i.e. polyamides, polyesters, polyurethanes, epoxy resins…)[54]. The compound however presents some major disadvantages such as its red color which limits its use in applications requiring colorless items. Another key concern is that it may ignite when submitted to high temperatures or mechanical shocks and it furthermore releases phosphine and corrosive

phosphoric acids upon exposure to moisture[98-100]. There are now well established methods that consist in encapsulating red phosphorus, for instance with thermosetting resins (i.e phenolic resin, urea resin, melamine resin…), in order to increase its stability and most particularly to reduce the release phosphine[98,101].

Alone in unreinforced PBT, a coated grade of red phosphorus was claimed to provide V-0 rating (0.8 mm) at content of only 5-6 wt%[102]. In glass fiber reinforced PBT, the combination of 5.5 wt% red phosphorus (untreated) and 5.5 wt% of the phenol formaldehyde Novolac gives a V-0 rating (0.8 mm) and a LOI of 35 Vol%[101]. When doubling the amount of both additives, the LOI of the material increases to 38 Vol%.

The mode of action of red phosphorus has not been established in PBT. On the basis of studies performed with PET and some oxygen containing polymers[54,103], it is assumed that the elemental phosphorus mainly decomposes into orthophosphoric and polyphosphoric acids. The latter would promote the formation of a protective char layer. The synergistic action between red phosphorus and high charring Novolac seems to be consistent with this assumption.

● **Overview on phosphorus based compounds in flame retardancy of PBT**

A large variety of phosphorus based compounds have been investigated as flame retardants for PBT. So far, the phosphinate salts and red phosphorus represent the most effective ones. While the first exhibits a prevailing gas phase mode through releasing active phosphorus species, the second would appear to favor the production of a protective char layer at the surface of PBT. It provides evidence that both gas and condensed phase mechanisms may be adapted to improve the fire behavior of the polymer. In spite of its outstanding FR performances, red phosphorus still raises some concerns as it may release environmentally damaging and corrosive products. On the other hand, the beneficial combination of phosphorus based compounds with other FR additives (especially melamine and its derivatives) was largely reported in the literature. Developping FR combinations appears to be a strategy of choice for designing novel and high-performing flame retarded materials.

2.3 The oxaphospholane oxide Exolit PE110 in flame retardancy of PBT

2-methyl-1,2-oxaphospholan-5-one 2-oxide (OP) is a reactive flame retardant which is basically used for the production of an inherently flame retardant PET fiber. The latter has been developed by Hoechst in the 1970s as Trevira CS® (currently Trevira)[104,105]. Oxaphospholane is directly incorporated into the macromolecular chain of PET during the co-polymerization process (Figure 31).

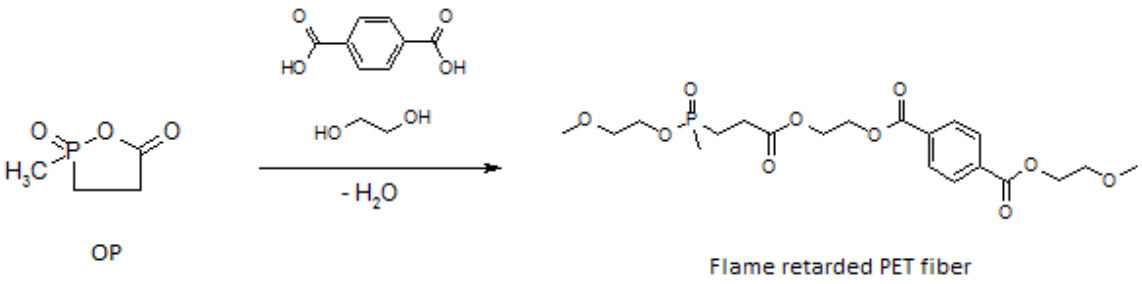

Figure 31 : Schematization of the copolymerization of OP with PET monomers

OP is nowadays commercialized by Clariant under the trade name Exolit PE110. It is synthesized from methyldichlorophosphine, in a two-step process which was originally described by Chajrullin et al[106] (Figure 32). In the first step, the methyldichlorophosphine is reacted with an equimolar ratio of acrylic acid to yield chloroformylphosphonic acid chloride. The latter is then cyclized into OP in the presence of acetic anhydride.

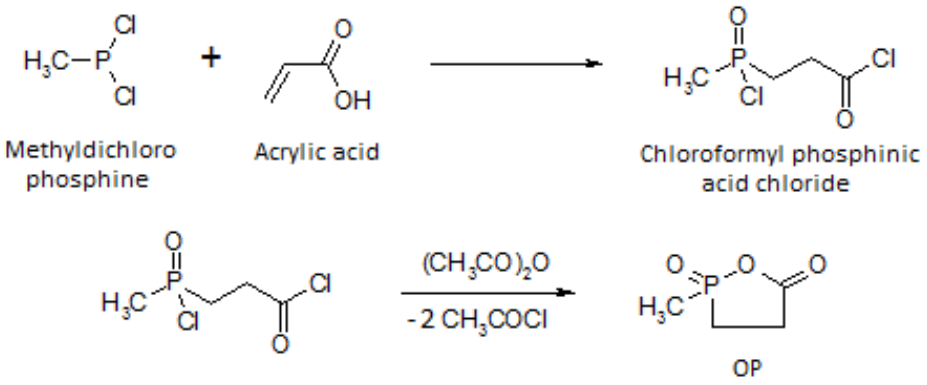

Figure 32 : Reaction scheme of the oxaphospholane synthesis

Balabanovich et al[38,107] have investigated OP as single flame retardant additive in PBT. The authors reported that unreinforced PBT could achieve V-0 rating (2 mm) together with a LOI of 28 Vol% by incorporating 10 wt% of the Clariant's phospholane with 10 wt% poly(sulfonyldiphenylene phenylphosphonate) (PSPPP) and 10 wt% polyphenylene oxide (PPO). PSPPP is a condensed-phase active flame retardant that induces the char formation in PBT through favoring the formation of polyarylates and phenolic functionalities. PPO, in its capacity as high charring polymer, brings a supplementary reinforcement of the char residue while OP was assumed to provide a flame inhibition activity by mostly vaporizing in the gas phase.

A few patents refer to OP as an electrophilic reagent for the synthesis of flame retardant additives. From a kinetic point of view, the reactivity of OP differs depending on the nature of the nucleophilic reagent[108]. As pictured in Figure 33, hydroxyl containing substances preferentially attack the oxaphospholane on its phosphonyl functional group which, after ring opening and proton-transfer, gives the phosphinic ester derivative. On the contrary,

amine containing substances react on the carbonyl group which leads to the formation of the phosphinic acid derivative.

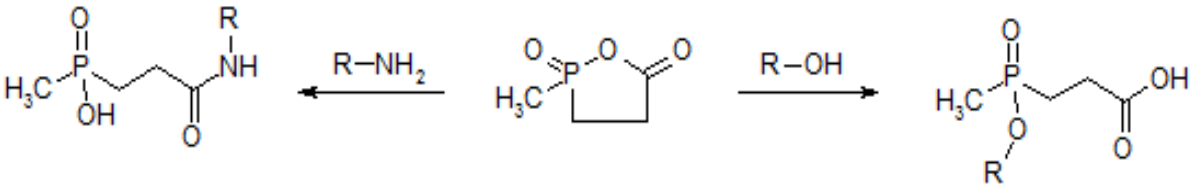

Figure 33 : Reactivity of OP toward amines (left) and alcohols (right)

The use of OP as a raw material for the conception of a variety of phosphinate flame retardant additives (Figure 34) has been disclosed in Hoechst patents[109,110]. The latter most particularly relate to the generic synthesis of monofunctional, difunctional and trifunctional phosphinic acids, as well as their corresponding salts, from the condensation of OP with amine based substances.

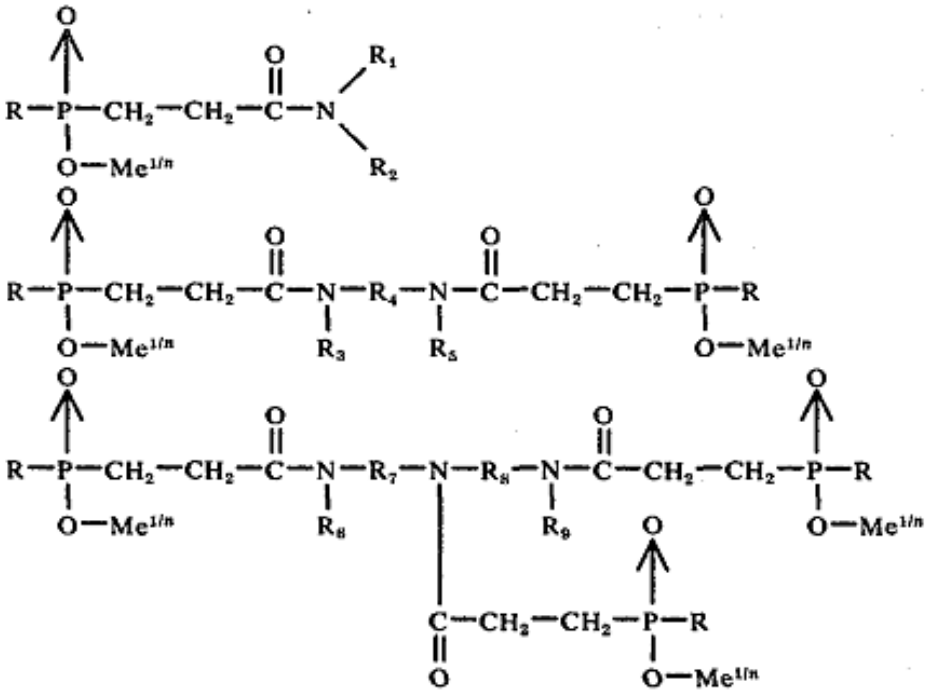

Figure 34 : Generic structure of the nitrogen containing phosphinates patented by Hoechst[110]

The examples listed in these patents only refer to one type of nitrogen-containing phosphinic acid obtained from the reaction between OP and 2,4,6-tri-bromoaniline (Figure 35). This phosphinic acid and its corresponding sodium and zinc salts were claimed to ensure excellent flame retarding properties in polyethylene, polypropylene and polyamide according to the fire test UL94 HB (ASTM D 635-68).

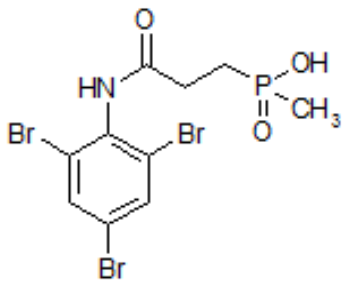

Figure 35 : Chemical structure of the tri-bromoaniline based phosphinic acid

Another Hoechst patent[111] relates to the synthesis of high boiling point nitrogen containing diphosphinic acids (Figure 36). These were prepared by reaction of aromatic or aliphatic diamines with two equivalents of OP in dimethylformamide medium, at temperature of 100-130°C. Glass fiber reinforced PBT formulations containing 12 to 15 wt% of these diphosphinic acids and 2 to 9 wt% of melamine or benzoguanamine as synergistic agents show V-0 rating (1,6 mm) at the UL94 test. It is further reported that the melamine salts derived from these diphosphinic acids exhibit equivalent FR properties as compared to the separated components.

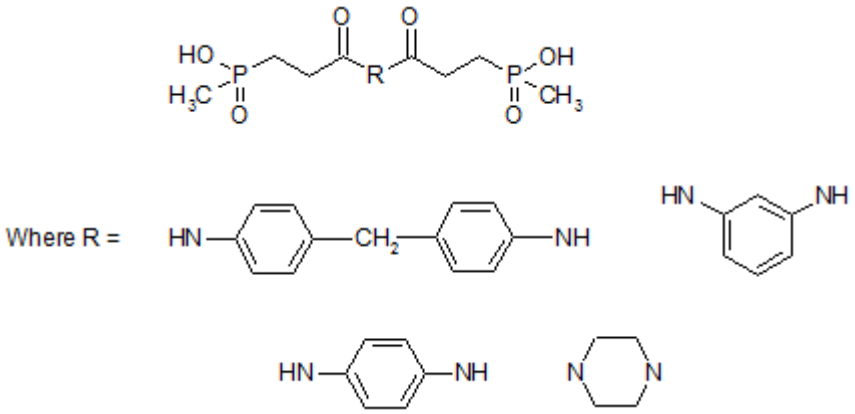

Figure 36 : Chemical structure of the nitrogen containing diphosphinic acids synthesized from OP

The synthesis of esters of carboxyethyl(methyl)phosphinic acids (Figure 37) from the condensation of OP with methanol, n-octanol or benzyl alcohol was related in a recent patent assigned to Clariant[112]. These phosphinic acids were obtained after reaction times of more than 48 h, up to 56% yields. The products were then treated with different metal sources to yield the desired phosphinate salts.

The incorporation of about 12 wt% of the aluminum salt of methyl ester of carboxyethyl (methyl)phosphinic acid plus 6 wt% melamine cyanurate in glass fiber reinforced PBT gives a V-0 classification (1.6 mm) based on the UL94 criteria. On the other hand, a grade of PA 6.6 containing 20 wt% of the zinc salt of the same phosphinic acid achieves V-0 rating.

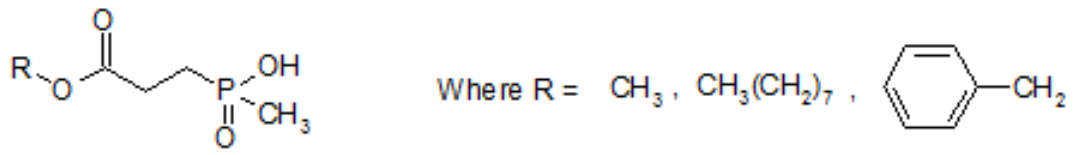

Figure 37 : Esters of carboxyethyl(methyl)phosphinic acid disclosed in the Clariant patent

The oxaphospholane oxide Exolit PE110 has been successfully used as a flame retardant monomer for PET fabrics (Trevira CS). Furthermore, its use as raw material for the synthesis of different varieties of carboxyethy(methyl)phosphinate derivatives (phosphinic acids and phosphinate salts) was the subject of several patents. FR performances of a number of structures from this class of phosphinates remain unknown and would be worth investigating in PBT.

2.4 Nanocomposites and nano-additives

There was from the past decades an abundant literature relating to the use of nano-fillers in plastics. At relatively low amount and with appropriate dispersion, these additives were reported to "boost" the thermal, mechanical or flame retardancy properties of materials. With regard to the limited fire proofing efficiency of some of these nano-additives (i.e. silica, metal oxides, layered clay silicates, graphene-based nano-particles, polyhedral oligomeric silsesquioxane), many attempts were made to combined them with conventional flame retardants. Layered clay silicates, graphene-based particles and polyhedral oligomeric silsesquioxanes are three classes of nano-additives, among the most investigated in the field of flame retardancy and will thus be hereafter described.

2.4.1 Nanocomposites

Layered clay silicates (especially montmorillonite) have surely been among the most widely investigated nano-particles in research for high performance materials. For a number of these composites, the nano-fillers may at relatively low contents provide better thermal and mechanical properties (mostly tensile strength and elastic modulus) when compared to neat polymers or macrocomposites and they are furthermore relatively inexpensive.

Depending on the strength of the interfacial interaction between the polymer and the nanoclay, the nanocomposite may achieve two distinctive morphologies: either intercalated or exfoliated (Figure 38)[113]. When the layered silicate presents poor compatibility with the polymer matrix, the former tends to aggregate into micro-size domains, with poor intercalation of the macromolecular chains into the clay galleries, and the material is no longer considered as nanocomposite but a microcomposite is obtained. A modification of nanoclays with organic cations (alkyl ammonium, alkyl phosphonium, alkyl imidazolium) can be performed in order to increase the compatibility and dispersion of the single clay platelets into the polymer matrix[54].

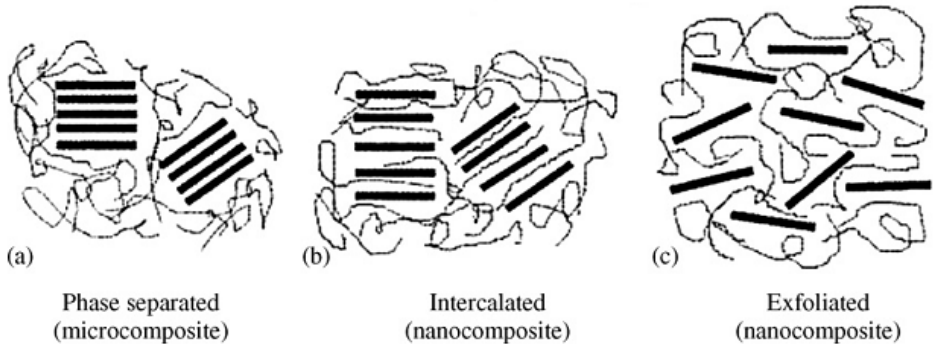

Figure 38 : Illustration of microcomposite, intercalated and exfoliated nanocomposite morphologies

The improvement of the fire behavior of polymers by layered silicates was mainly evidenced through forced flaming combustion scenarios, for instance in the cone calorimeter test. Driven by their lower surface free energy compared to the polymer[114,115] and the progressive gasification of this latter during the combustion process, the platelets migrate at the surface of the material and contribute to the constitution of an insulating carbonaceous-silicate barrier. In most cases, this phenomenon leads to a decrease of the Heat Release Rate (HRR) while the Total Heat Release (THR) of the material remains unchanged[116]. To some extent, the capacity of clays to migrate and to take part to an homogeneous reinforcement of the superficial char layer is influenced by the density, size and dispersion of clays, the morphology of the nanocomposite (intercalated, exfoliated of not) and the viscosity of the molten polymer[117]. It should be emphasized that organoclay modifiers, when having inferior thermal stabilities (i.e. ammonium), may earlier decompose during thermal degradation processes inducing the formation of acidic sites on the clay platelets. Those acidic sites may catalyze the formation of the char, but adversely accelerate the decomposition of the polymer, hence reducing its thermal stability.

In few studies[116,118], organomodified montmorillonites (OMMT), at loadings up to 2-3 wt%, were found to increase the thermal stability of PBT as observed through TGA measurements. Hwang et al[118] have for instance reported a slight increase of the onset temperature of degradation of the polyester in presence of MMT modified with stearylbenzyl dimethyl ammonium chloride. The temperature of the maximum mass loss rate and the residue yield were likewise increased for the nanocomposite, as well as the tensile strength. XRD and TEM analyses showed that the considered organoclay exhibited a mainly intercalated structure and was characterized by a rather good dispersion within the polymer matrix. Above 3 wt%, OMMT starts to agglomerate which results in the decrease of the tensile strength and stagnancy (not to say a decrease) of the thermal stability of PBT. Xiao et al[119] reported comparable results for a non-modified montmorillonite (Na^+MMT), incorporated at 3 wt% in PBT with increasing amount (0.5 to 3 wt%) of cetyl pyridinium chloride (CPC) as cationic compatibilizer. In cone calorimetry experiment, an optimized PBT/clay nanocomposite

formulation containing 1 wt% CPC showed a 24% decrease of the peak HRR as compared to the neat polymer, though the time to ignition of the latter was found to be slightly higher.

On the basis of TGA analyses, Yang et al[82] reported that 5 wt% montmorillonite modified with methyl tallow bis(2-hydroxyethyl) ammonium could slightly destabilize PBT, whatever glass fiber reinforced or not. The nanoclay has nevertheless beneficial effects on the tensile strength and modulus of the polyester and furthermore reduces its HRR and THR (Total Heat Release) in microscale combustion calorimetry experiments (PCFC). The OMMT besides showed no influence in ignition tests such as LOI and UL94. In this study, the nanoclay exhibits a main exfoliated structure, even in presence of a flame retardant additive such as aluminum hypophosphite. Different results were reported by Samyn et al[120] as the same OMMT (Cloisite 30B), incorporated with Exolit OP1240 in PBT, presented a low dispersion while the polymer chains were found to be poorly intercalated into the nanoclay gallery.

Graphene-based nano-particles (Figure 39) - especially graphene, expandable graphite, single-walled nanotubes (SWNTs) and multi-walled nanotubes (MWNTs) - are another class of nano-fillers reported to impart better fire properties to polymers[121-125].

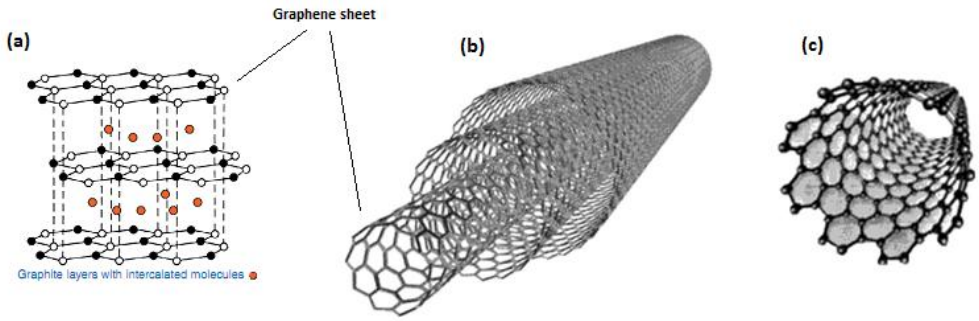

Figure 39 : Structural pattern of expandable graphite (a), MWNTs (b) and SWNTs (c)

Their flame retardancy mode of action is somewhat comparable to that of layered clay silicates. Upon decomposition, the carbon fillers accumulate at the surface of the molten polymer and form a char layer that acts as an insulator. To date, none of these fillers have been subjected to fundamental researches in flame retardancy of PBT, probably because they might have a negative impact on the electrical conductivity of the material.

POSS (polyhedral oligomeric silsesquioxanes) are inorganic cage-like hybrid molecules of silicon and oxygen whose silicon corner elements are covalently bonded to organic groups ($RSiO_{1.5}$). These organic groups, which can be of different nature (i.e. methyl, phenyl, silane, amine, isocyanate, etc), provide better compatibility of the silica-like nanocage with the polymeric matrix. POSS itself may display a variety of structural forms (Figure 40), including closed cages or opened cages with silanol end groups.

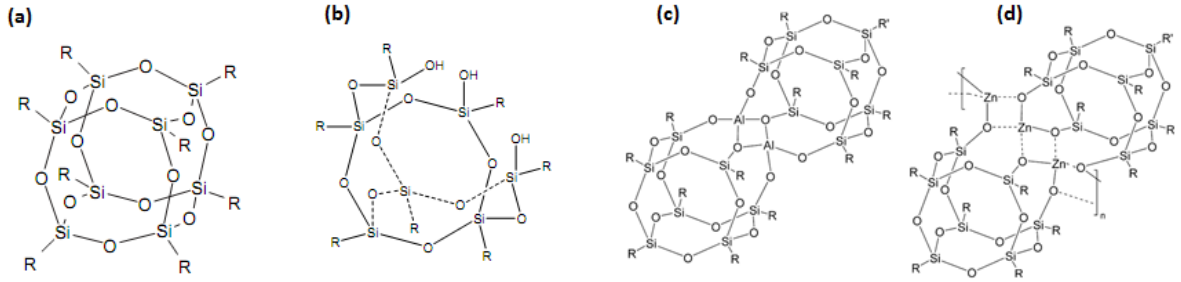

Figure 40: **Structure of some POSS; closed cage POSS (a), trisilanol POSS (b), dimeric Al-POSS (c), dimeric Zn-POSS (d)**

When subjected to thermal decomposition, POSS migrate at the surface of polymers and form an insulating ceramized layer that protects the underlying material from degradation. The ability of POSS to enhance the flame retardancy behavior of a defined material appears to be greatly dependent on the nature of the nano-particle under consideration. Fina et al[126] for instance reported that 10 wt% of the dimeric Al-isobutyl POSS in polypropylene (PP) leaded to a 43% decrease in the HRR as well as a substantial decrease of the CO/CO_2 release rate. The same amount of the dimeric Zn-isobutyl POSS brings about no improvement of the fire performances of the thermoplastic. Fire performances of PP even worsened when it was compounded with the single isobutyl POSS nano-cage.

2.4.2 Nanocomposites with conventional flame retardants

The approach consisting in combining traditional fire proofing has not yet been widely exploited in the flame retardancy of PBT. A few academic researches however proved that such combinations could be very promising.

Yang et al[82] have for instance showed that the substitution of aluminum hypophosphite (on a referential loading of 20 wt% in PBT/GF) by 5 wt% methyl tallow bis(2-hydroxyethyl) ammonium modified MMT did not change the LOI value and UL94 classification of the material. Interestingly, the incorporation of OMMT brings about further reduction of the HRR and THR in PCFC as well as superior tensile strength and elastic modulus compared to PBT/GF/20 wt% AHP. The clearer benefice brought by the AHP/OMMT combination is economical since OMMT is much more cost-effective than AHP. The authors recognized that OMMT contributed to the formation of a superficial carbonaceous-silicate layer, but it was also assumed that well dispersed nano-silicate platelets in the bulk polymer created “closed rooms” in which AHP and its decomposition products can adequately react with the decomposition products of PBT. Those mechanisms allow explaining the good performances of the AHP/OMMT combination, with regard to the significant condensed-phase mode of action of AHP.

Gallo et al[127,128] have reported that the combination of aluminum diethylphosphinate (Exolit OP1240) with nanometric particles of metal oxides such as Fe_2O_3 and TiO_2 could remarkably

improve the fire properties of unreinforced PBT. 10 wt% OP1240 in PBT achieve V-1 rating (3.2 mm) while substituting the phosphinate salt by 2 wt% of the metal oxides allows reaching the V-0 ranking. A V-0 classification has even been obtained with 5 wt% OP1240 and 2 wt% Fe_2O_3. Both TiO_2 and Fe_2O_3 were proved to increase the char residue in the burning polymer. While TiO_2 seems to favor polyarylate structures and polyaromatisation of PBT through coordinating with terephthalate residues, Fe_2O_3 was assumed to induce the homolytic cleavage of PBT chains, hence favoring crosslinking of the latter. According to the authors, high synergistic performances of metal oxides would be ascribed to their nanometric size and good dispersion in the PBT matrix.

On the other hand, Vannier et al[129] showed that substitution of only 1 wt% Exolit OP950 (on a referential loading of 10 wt%) by octamethyl POSS leaded to a significant decrease of the peak HRR of PET (- 24%) as well as an increase of its LOI value of 5 Vol%.

These various examples clearly illustrate the fact that the combination of low amount of nano-particles with traditional flame retardants may be an attractive way for improving fire properties of polymers.

2.5 Conclusion

The main additives used to flame retard PBT were reviewed in this second part. It has been found that three kinds of compounds generally accounted for the improvement of the polymer fire properties. Gas phase active agents such as halogenated compounds or alkylphosphinate salts appear to be reliable and effective substances with regard to the low propensity of PBT for charring. Good fire properties were also obtained when substituting part of these aforementioned substances by agents acting through fuel dilution such as melamine cyanurate. Char promoting flame retardants such as hyphophosphite salts and red phosphorus provides high fire properties as well and were somewhat found to be synergistic with high charring polymers, for instance polycarbonate or phenol formaldehyde resins. The combination of gas phase and condensed phase active substances is another attractive approach for enhancing the flammability behavior of PBT.

Halogenated compounds and red phosphorus are among all known families of flame retardants the most efficient. They nonetheless raised concerns regarding their potential toxicity or instability and therefore would get less and less consideration in academic and industrial researches. Phosphinates salts are environmentally friendly compounds which, besides being very effective flame retardants, may advantageously enhance the electrical properties of PBT. However, their high price and negative effects on the impact strength of the polymer might restrain their range of application.

An approach consisting in flame retarding PBT with nano-paticles has finally been discussed. Used alone, nano-particles may show some limitations but they should be worth being, at small loadings, combined with conventional flame retardants.

3. Conclusion

PBT is a polyester of the class of engineering thermoplastics that is used in a wide range of applications. As a material of choice for electrical and electronic equipments, it has to comply with severe requirements in term of flame retardancy.

A large proportion of PBT material is nowadays flame retarded with halogenated compounds. These compounds exhibit outstanding performances which allow them to be used at relatively low loadings. However, much effort has been made to withdraw them from the market because of their potential toxicity and hazardous impact on environment. A new class of environmentally friendly flame retardants, alkylphosphinates salts, is gaining more and more consideration as they could represent a reliable alternative to halogenated compounds. It is trusted that alkylphosphinate salts could impart excellent fire properties to PBT when combined with appropriate synergistic agents.

The main goal of this project is to find flame retardant systems that could compete with the well established FR solutions (i.e. brominated flame retardants, aluminum diethyl phosphinate) currently available on the market. This state of the art gives us clues to define the approaches which could be employed for that purpose. One of the retained approaches is to combine aluminum diethylphosphinate based systems with nano-particles. A second approach consists in synthesizing novel phosphinate salts to be used alone or eventually to combine to synergistic agents. These two approaches will be discussed in chapters 3 and 4 respectively. Chapter 2 will first describe the materials used in this project as well as the experimental techniques employed for the fire performance assessment of screened formulations and the comprehensive studies. The experimental procedures used for the synthesis of the novel phosphinate salts are also described in this chapter.

CHAPTER 2 – MATERIALS COMPOUNDING AND EXPERIMENTAL TECHNIQUES

This chapter is dedicated to the description of the materials, techniques and experimental protocols used in this work.

First the materials, namely PBT/GF, that has been used in this project as well as the compounding processes used to prepared the novel flame retarded PBT formulations will be described. The methods allowing the evaluation of the flame retardant behavior of materials will then be presented. The comprehension of the flame retardant modes of action is the key to conceive well-designed materials. This chapter hence details the analysis techniques that have been implemented to investigate the mechanisms of action of the developed FR systems.

While the first strategy of this project consists in developing flame retarded formulations based on synergistic mixtures of commercially available flame retarding agents (aluminum phosphinate salts) and nano-particles, the second approach consists in the development of novel flame retardants (also phosphinates salts) to improve the fire behavior of PBT. Synthesis procedures of these various substances are thus described in the second part of this chapter.

1. Materials, compounding and experimental techniques

1.1 Materials

The PBT grade used in this work is Ultradur B4520 (BASF). It exhibits a medium viscosity and rapid freezing injection molding properties. Its properties are reported in Table 4.

Table 4 : Properties of PBT Ultradur B4520[130]

Property	Nominal value	Unit
Specific gravity	1.3	-
Tensile strength (@ 23°C)	60	MPa
Elongation at beak (@ 23°C)	3.7	%
Flexural modulus (@ 23°C)	2300	MPa
Notched Izod Impact (@ 23°C)	43	J/M
Melting point	223	°C
Heat deflection temperature (@ 1.8 MPa)	60	°C

The various formulations discussed in this study were systematically prepared through melt blending process (see part 1.2) by mixing pellets of Ultradur B4520 and pellets of a 40 wt% glass fibers containing Ultradur B4520 (masterbatch) with the additives (flame retardants and co-additives). The quantities of pellets and additives introduced in the extruder were determined in order to obtain the desired percentage of each of the components (PBT, glass fibers, additives) in the final formulation. The Ultradur B4520 masterbatch was supplied by

BASF. Its properties are listed in Table 5. Glass fibers contained in the masterbatch are commercialized by PPG industries, under the trademark PPG 3786.

Table 5 : Properties of the masterbatch of glass fiber (40 wt%) reinforced Ultradur B4520 (data provided by BASF)

Property	Nominal value	Unit
Melting point	223	°C
Glass fiber content	39.6	wt%
Average glass fiber length	248	µm

1.2 Material compounding

The formulations were prepared using a DSM Xplore Micro15 twin screw micro-extruder (Figure 41) having a volume of 25 cm^3. PBT pellets (Ultradur B4520 and Ultradur B4520/GF masterbatch) and additives were melt mixed in nitrogen flow at 250°C for 3 minutes with a screw speed of 80 rpm. Raw materials were dried at least for one night at 60°C before use.

Bar specimens of 0.8 mm thick used to carry out the UL94 tests have been prepared with a DSM Xplore small scale injection molding machine (Figure 41). The melted formulations were directly collected from the micro-extruder by means of an injection unit and maintained in it at 270°C for 3 minutes before injection. The injection molding was performed in a conical shaped mould heated at 160°C with a pressure of 16 bars.

Samples needed to perform the LOI and Mass Loss Calorimeter (MLC) tests as well as UL94 bar specimens of 1.6 mm thick were obtained using a Darragon press (Figure 41) at 260°C with a pressure of 2 MPa.

µ-extruder DSM *Injection machine DSM* *Mechanical press Darragon*

Figure 41 : Picture of the various polymer processing techniques used during this study

1.3 Fire Testing Methods

This part of the chapter then describes the fire testing methods used to evaluate the flame retardant properties of the formulations. Fire behavior can be described through three

major parameters: the ignitability, the contribution to flame spread and the heat release. Depending on the material application fields, some specific tests can be implemented to simulate specific fire scenarios, but more generally, three tests are used to simulate the three parameters above-mentioned. These tests are the UL94, the Limiting Oxygen Index (LOI) and the Mass Loss Calorimeter (MLC) test.

1.3.1 UL94 vertical burning test

This small-scale test determines tendency of a material either to extinguish or to spread the flame once the specimen has been ignited[131]. Specimens are clamped vertically and exposed to a defined flame ignition source from the bottom for 10 seconds. The flame is applied twice if the sample self-extinguished after the first flaming. Cotton is also placed below the sample (Figure 42) to evaluate the presence or not of flaming drops.

Three classifications are assigned to materials based on their behavior regarding burning, flame propagation and dripping: V-2, V-1 and V-0, V-0 being the best ranking. If the material does not meet the criteria, it is non-classified at the UL94 test (NC). The criteria required for the ratings are presented in Table 6. The UL94 tests were realized on a Fire Testing Technology Limited equipment on strips 127x12,7x0.8 mm^3 and 127x12,7x1.6 mm^3 in accordance with the recommendations of the standard (ASTM D3801, IEC 707 or ISO 1210). The barrels are ignited by a blue flame (without cone) of 20 mm. The burner which generates the flame is fuelled by methane gas having a flow rate of 105 ml/min with a back pressure less than 10 mm of water. For each formulation, five bar specimens are tested after they underwent a preconditioning at 23±2°C for a minimum of 48 hours. Note that for some specific materials (i.e. those used for electrical/electronic applications), an additional set of five specimens has to be preconditioned in an air-circulating oven for 168 hours at 70±1°C prior to the test. The thickness of the strips can be 0.8, 1.6 or 3.2 mm. The thinner the barrel, the more severe is the test.

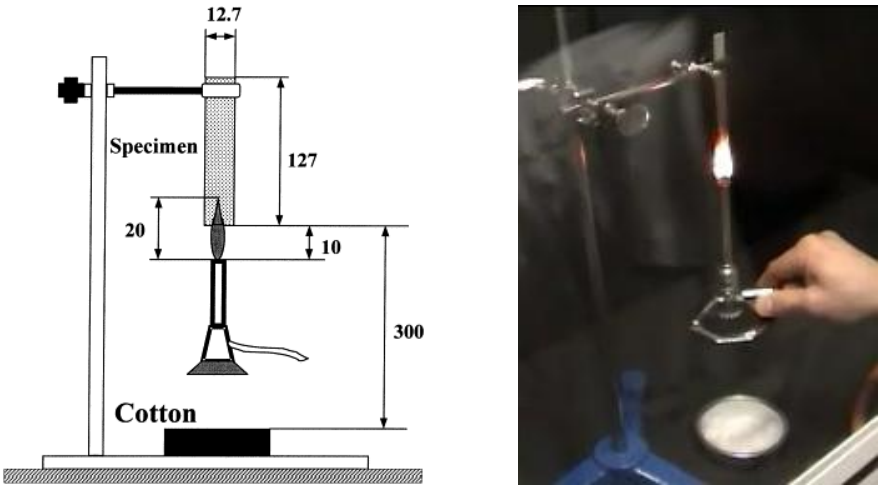

Figure 42 : Description of the vertical burning test UL94

Table 6 : Criteria for UL94 classifications

Criteria	V-0	V-1	V-2
Afterflame time for each individual flaming	≤10s	≤30s	≤30s
Afterflame+afterglow time for each individual specimen, after second flaming	≤30s	≤60s	≤60s
Total afterflame time for any condition set (5	≤50s	≤250s	≤250s
Cotton indicator ignited by flaming drops	No	No	Yes
Afterflame or afterglow of any specimen up to the holding clamp	No	No	No

1.3.2 Limiting Oxygen Index (LOI)

The Limiting Oxygen Index (LOI) is a standardized test (ISO 4589) which allows determining the minimum concentration of oxygen (in Vol%) in a nitrogen/oxygen mixture that is required for the combustion of a material in vertical position ignited by the top[132]. For a given oxygen concentration, the combustion time and the distance travelled by the flame are measured. The concentration in oxygen has to be increased if the combustion time is lower than 3 minutes and if the flame does not spread beyond 50 mm along the sample.

The testing specimen is fixed from the bottom in a nitrogen/oxygen gas circulating chamber where it is ignited by a butane/propane flame for a maximum period of time of 10s (Figure 43). Measurements were carried out with a Fire Testing Technology apparatus on strips of 100x10x3 mm^3. The margin of error of the obtained results is estimated at ± 1 Vol%.

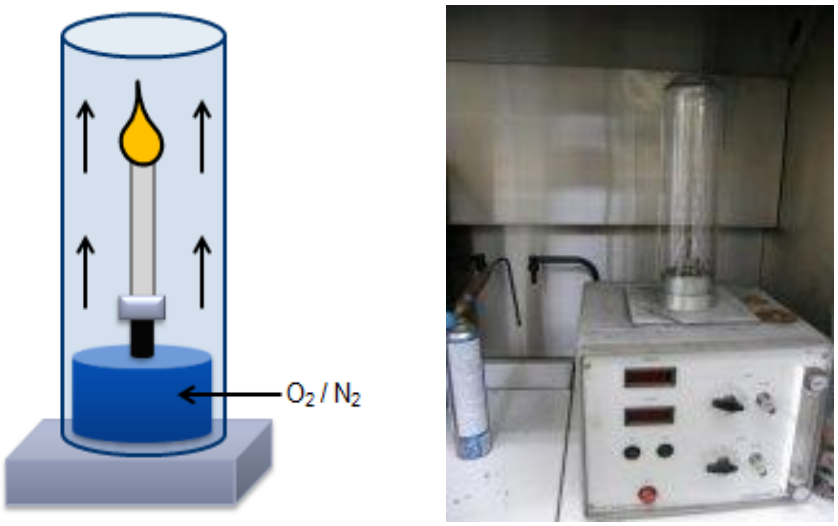

Figure 43 : Schematic representation of the LOI test

1.3.3 Mass Loss Calorimeter (MLC)

The mass loss calorimeter allows the simulation of the conditions of fire in a small bench scale according to ASTM E2102[133]. A schematic representation of the mass loss calorimeter is given in Figure 44. The core of the instrument is a radiant electrical heater in the shape of a truncated cone, irradiating a flat horizontal sample (100x100x3 mm^3) placed beneath it, at a preset heating flux (35 kW/m^2 to simulate a mild fire or 50 kW/m^2 for a developed fire). Ignition is provided by an intermittent spark igniter located 13 mm above the sample.

The mass loss calorimeter measures the temperature of the evolved gases using a thermopile located at the top of the chimney. The calibration of the heat release rate (HRR) is performed with methane. A methane flow of 0 to 6.7 ml/min is burnt above the sample holder to obtain a calibration curve of the heat release as a function of temperature.

Figure 44 : Schematic representation of a mass loss calorimeter

The measured parameters are the Heat Release Rate (HRR), the peak Heat Release Rate (pHRR), the Total Heat Release (THR) and the Time To Ignition (TTI). These parameters allow the evaluation of the contribution to fire of the material. Another parameter, namely the "Residue Yield" (RY), is determined by subtracting masses of the sample before and after the test. It allows evaluating the propensity of the material to form a carbonaceous char.

The MLC measurements were performed on a Fire Testing Technology mass loss calorimeter device at 50 kW/m^2 according to the ASTM E906 on specimens of 100x100x3 mm^3. All measurements were repeated at least two times to ensure good reproducibly of results. The margin of error is estimated at 10% for the different parameters.

1.4 Characterization of the materials degradation

Following the determination of improved flame retarded PBT/GF formulations, an analysis of the flame retardant modes of action was performed. The flame retardant mechanisms of

two aluminum phosphinates salts – one commercially available (Exolit OP1240), the other synthesized in the lab – are in particular compared.

As reported in the state of the art (chapter 1), flame retardant mechanisms may occurs both in the condensed and in the gas phases. Several FR mechanisms can operate which may result (or not) in the modification of the degradation pathway of the polymer (or else of the flame retardant). It thus results in the release of specific gaseous degradation products. To elucidate these mechanisms, it is hereafter proposed to investigate the thermal decomposition of the formulations as well as that of their various constituents (polymer, flame retardant systems) separately.

First the thermal decomposition of materials is characterized by thermogravimetric analysis. Through this technique, the characteristic temperatures of the degradation of materials are determined. Materials were thus heat treated at those temperatures and residues were collected. These residues were then analyzed using adapted analysis techniques in order to be able to propose the mechanisms occurring in condensed phase. As a complement, evolved gas analysis techniques were used to determine the nature of gaseous degradation products released by the materials.

In the following section, the methods implemented to understand the modes of action of flame retardant systems are presented.

1.4.1 ThermoGravimetric Analysis (TGA)

The ThermoGravimetric Analysis (TGA) is a technique in which the weight loss of a sample is monitored versus temperature while the sample is heated at a defined temperature ramp. The measurements can be carried out in oxidative (air) or inert atmosphere (nitrogen).

TGA measurements were carried out on a TA Instruments TGA Q5000IR with alumina crucibles. Balance and purge flow rates were set at 15 and 100 ml/min respectively. For all experiments, nitrogen was chosen as purge gas. The samples of about 20 mg were submitted to an isotherm at 50°C for 10 minutes then followed by a heating ramp of 10°C/min up to 800°C. Every TG analyses are repeated at least twice to ensure the reproducibility of the measurements.

It is noteworthy that the aluminum diethylphosphinate salt (Exolit OP1240) could not in its pure form be analyzed through TGA due to the conformation of the device (horizontal balance). Therefore the substance was investigated using a TA instruments SDT Q600. The purge flow rate (nitrogen) was set to 100 ml/min. The sample of about 15 mg was submitted to an isotherm at 50°C for 10 minutes then followed by a heating ramp of 10°C/min up to 800°C. Other materials such as neat PBT/GF and Exolit OP1240 containing PBT/GF were additionally analyzed by SDT Q600 to allow comparing data with those of pure Exolit OP1240.

- Comparison between experimental and calculated TGA curves:

In order to determine potential interactions between a polymer and flame retardant additives during the thermal degradation, a comparison between the experimental and a calculated TGA curves is performed. The calculated curve is obtained by linear combination of the TGA curves of each single component (polymer, additives) weighted by their respective mass fractions in the formulation. The interaction between components can also be illustrated by the difference weight loss curve ΔM (Eq.1):

$$\Delta M = M_{exp} - M_{calc}, \text{ with } M_{calc} = \sum x_i M_i \qquad \text{Eq.1}$$

with M_i the mass of the constituent i at given temperature and x_i the fraction of i in the formulation.

The ΔM curve allows to point out a potential increase or decrease in the thermal stability of the polymeric matrix related to the presence of one or several additives. When the experimental curve is higher than the calculated one (or when the ΔM curve is positive), the weight loss is higher than expected, showing that the reactivity of the polymer with the additives leads to a thermal stabilization of the material. On the opposite, if the experimental curve is lower than the calculated one (or when the ΔM curve is negative), a thermal destabilization occurs.

1.4.2 Condensed phase analysis

1.4.2.1 Thermal treatments

Thermal treatments consist in heating a sample in a furnace at a defined temperature (Heat Treatment Temperature; HTT) under a controlled nitrogen gas flow (Figure 45). The treatment temperatures were determined according to TGA curves as they correspond to the characteristic degradation steps of the systems.

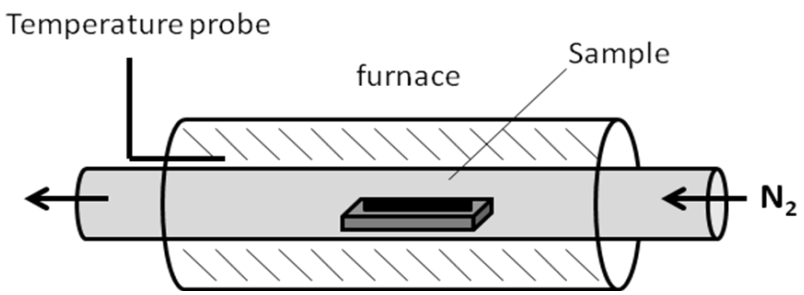

Figure 45 : Description of the tubular furnace used for thermal treatments

Samples were heat treated at a heating rate of 10°C/min (similar to the one used for the TGA measurements) from ambient to the HTT followed by an isotherm of two hours. The samples were then cooled to ambient temperature before being collected.

The residues obtained after thermal treatments were stored in a desiccators to avoid hydrolysis of the residues and then analyzed by solid state Nuclear Magnetic Resonance (NMR).

1.4.2.2 Solid State Nuclear Magnetic Resonance (NMR)

The nuclear magnetic resonance (NMR) in the solid state is a particularly effective tool to analyze the changes of chemical environment in a material.

In the solid state, i.e. a semi-crystalline or glassy polymer, the Chemical Shift Anisotropy (CSA, anisotropy of the magnetic moment) has a severe effect on the spectra in broadening the absorption peaks; this effect becomes worse when the mobility of the chains or molecules decreases[134]. Through a tensoral analysis of the magnetic moments in a molecule it is possible to demonstrate that there exists a "Magic Angle" with respect to the applied magnetic field at which rapid spinning of the solid sample leads to minimization of absorption line broadening due to CSA. This method is called "magic angle spinning" or MAS.

The low abundance of some atoms compared to the protons leads to poor absorption of the radiofrequency pulse in a FT-NMR experiment. This limitation can be overcome by exciting the protons in a sample, followed by a sequence of two series of long-time pulses which make the protons and the other nuclei resonate at the same frequency. This latter is called the "Hartman-Hahn" condition, and the process is called "cross-polarization" (CP). The time of polarization is called the "contact time" or "spin-lock time"[135].

Cross-polarization leads to a large enhancement of the excitation of the nuclei. The large number of protons in the sample however interferes with the decay of the isolated nuclei due to weak interactions of the spins. This dampening of the signal can be removed by strong radiofrequency signal which essentially holds the protons in a highly resonating state so they are not capable to absorb resonance from the nuclei. This is called "^{1}H decoupling" or "^{1}H dipolar decoupling" (DD)[136].

^{27}Al NMR Measurements were carried out on a Bruker Avance II 400 with a probe head of 3.2 mm using magic angle spinning (20 kHz). The repetition time was fixed at 2s for all samples, a minimum of 512 scans was necessary to obtain a satisfactory signal to noise ratio. Al in aqueous solution was used as a reference.

^{31}P NMR measurements were performed on the same spectrometer as above at a spinning rate of 13 kHz. Bruker probe heads equipped with 4 mm MAS assembly were used. Experiments have been carried out with ^{1}H dipolar decoupling because of the high relaxation time of the phosphorus nuclei (10 to 500 s). A repetition time of 120s was applied for all samples. H_3PO_4 in aqueous solution (85%) was used as reference.

^{13}C NMR measurements were performed on the same spectrometer with MAS (10 kHz), high-power ^{1}H decoupling and ^{1}H-^{13}C cross polarization (CP). A cross-polarization contact time of 2ms as well as a recycle delay of 5s were applied for all samples. The reference used to determine the chemical shifts is glycine.

Two-dimensional ^{27}Al-^{31}P D-HMQC: the spatial proximity between the phosphorus and aluminum sites was investigated with a 2D MAS-NMR D-HMQC (Dipolar Heteronuclear Multiple Quantum Coherence) sequence[137]. This NMR experiment uses the standard HMQC pulse sequence to produce heteronuclear coherences but an additional pulse scheme allows for the creation of through-space coherences in place of the standard through bonds signals obtained with the basic HMQC sequence. As a consequence, the 2D spectrum displays correlation signals between spatially close atoms. The ^{27}Al D-HMQC spectrum has been obtained with at 18.8 T (v_L(^{27}Al) = 208.4 MHz and v_L(^{31}P) = 323.8 MHz) on a Bruker spectrometer equipped with a 3.2 mm triple channels probe operating at a spinning frequency of 20 kHz. The through space correlations were created by a scheme pulse based on the SFAM (Simultaneous Frequency and Amplitude Modulation) technique[138] applied for 1 ms. The 2D spectrum was recorded with the following acquisition parameters: number of scans = 1536, recycle delay = 1s.

Two-dimensional ^{27}Al-^{27}Al MQMAS: in the solid state NMR of half integer quadrupolar nuclei (i.e. ^{27}Al: spin = 5/2), the 2nd order quadrupolar interaction (SQI) represents the dominant anisotropic broadening of the central transition (CT, +1/2 ↔ -1/2) and the symmetric multiple-quantum transitions (MQ, i.e. +3/2 ↔ -3/2 or +5/2 ↔ -5/2 for ^{27}Al). This 2nd order quadrupolar broadening may cause a severe decrease in the signal resolution if the nucleus (i.e. such as ^{27}Al) exhibits a large quadrupolar moment[139]. The SQI can only partially be averaged by MAS or eventually be reduced by performing NMR spectroscopy experiments at higher fields to yield an estimate of the range in isotropic resonances. A refinement of the chemical shift distributions can otherwise be performed by advanced techniques such as the two dimensional MQMAS[139,140]. This latter experiment allows for a separation of anisotropic interactions from isotropic interactions through correlating the symmetric MQ transitions phase coherences with the single quantum coherence of the CT. As a result, the 2D projection of the NMR spectrum of the half integer quadrupolar nucleus yields a slope of highly resolved isotropic signals free from both first and second order quadrupolar broadening. MQMAS spectra were collected at 18.8 T on a Bruker spectrometer equipped with a 3.2 mm triple channels probe operating at a spinning frequency of 20 kHz. The pulse sequence was composed of two hard pulses of durations of 4.4 µs and 1.4 µs and a selective pulse with a duration of 7 µs. The recycle delay was 1s and the number of scans 264.

1.4.3 Gas phase analysis

1.4.3.1 ThermoGravimetric Analysis (TGA) coupled with FTIR

Infrared spectroscopy exploits the fact that bonds have specific frequencies at which they rotate or vibrate corresponding to discrete energy levels. So, infrared absorptions at characteristic frequencies are related to chemical groups. Thus, TGA-FTIR could be used to analyze the evolved gases continuously during the degradation of a material[39,127,141].

In this technique, the FTIR spectrometer is connected to the TGA device via a heated transfer line. As gases evolve during the TGA experiment, they pass into the flow cell of the FTIR spectrometer where the infrared spectra are collected. The FTIR flow cell is compatible with all types of evolved gases and materials. Additionally, the large flow cell diameter provides high throughput and prevents spectral interference caused by deposits on the walls.

The experiments have been performed on the TA instruments TGA Q5000IR previously described coupled with a Nicolet is10 FTIR spectrometer from ThermoFischer. Parameters used to carry out the experiments are those described previously in part 1.4.1. The heat transfer line temperature is set at 225°C to avoid condensation of the evolved gases. The IR spectra were recorded in the 400-4000 cm^{-1} spectral range through the OMNIC software. The obtained spectra correspond to the accumulation of 8 scans with a resolution of 4 cm^{-1}.

1.4.3.2 Pyrolysis - Gas Chromatography/Mass Spectrometry analysis (Pyrolysis-GCMS)

Pyrolysis-GCMS was used in complement to the TGA-FTIR analyses. This technique provides an extremely sensitive tool to determine the nature of gases evolved during the thermal decomposition of a material[33-35,40,142].

The Pyrolysis-GCMS measuring system was provided by Shimadzu. An illustration of this system is found in Figure 46. A micro-furnace pyrolyzer (Frontier Lab PY-2020iD), a gas chromatograph equipped with a fused silica capillary column and a quadrupole mass spectrometer with an Electron-Impact (EI) ionization source (Shimadzu GCMS QP2010 SE) are directly connected in series.

Analyses are performed through a thermal desorption mode which consists in heating a sample at a defined temperature ramp in the pyrolyzer furnace while evolved gases condensate and accumulate at the top of the GC column. Right after reaching the desired temperature in the pyrolyzer furnace, condensed products are desorbed and separated in the GC column to finally be ionized (detection) in the mass spectrometer.

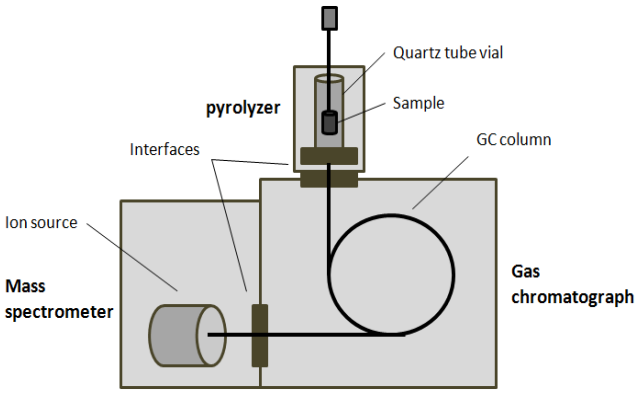

Figure 46 : Schematic representation of the Pyrolysis-GCMS measuring system

About 1.8 mg of the samples is added in a stainless steel sample cup. The latter is first placed at the upper position of the pyrolyzer, and then introduced into the centre of the pyrolyzer (inside a quartz tube vial) under an helium gas flow. In the pyrolyzer furnace, the temperature was initially set at 60°C and then raised to a defined temperature with a heating rate of 10°C/min. The temperature of the interface between the pyrolyzer and the GC injection port and the injection port were respectively set at 320°C and 250°C. A part of the carrier gas flow is reduced by a splitter so as to prevent clogging of the GC column as well as to prevent saturation of the signal during the detection of gases. Split parameters were empirically determined depending on the heat treatment temperature in the pyrolyzer. A 30 m-long capillary column was used and the linear velocity of helium as a carrier gas was 40 cm/s. The GC column temperature was maintained at 50°C during the whole heating treatment of samples in the pyrolyzer and then programmed up to 300°C at the rate of 20°C/min, followed by an isotherm of at least 1 hour at 300°C. Electron-Impact spectra were recorded at 70eV with a mass scan rate of 2 scan/s. Pyrograms and mass spectra were treated using a GCMS post-run analysis program (Shimadzu). The NIST mass spectral database was used for the identification of products.

2. Experimental procedures for the synthesis of novel phosphinate salts

This part relates to the synthesis of novel phosphinate salts whose chemical structures are modelled on the aluminum phosphinate salts from Clariant. It falls within the second approach of the project consisting in investigating the FR performances of novel phosphinates salts in PBT. This second approach aims at figuring out whether variation of the chemical structure of phosphinate salts allows improving the flame retardant properties of glass-reinforced PBT. It is then a further aim to have a better understanding of the mode of action of phosphinates as flame retardants in PBT.

Manifold phosphinate salts have been prepared in this project from the reactive substance Exolit PE110 (2-methyl-2,5-dioxo-1,2-oxaphospholane). Figure 47 depicts the global reaction scheme of syntheses with the corresponding denomination of products.

The following section encloses experimental procedures for the synthesis of the different products. First, the raw material and the techniques used to analyze the synthesized products are presented.

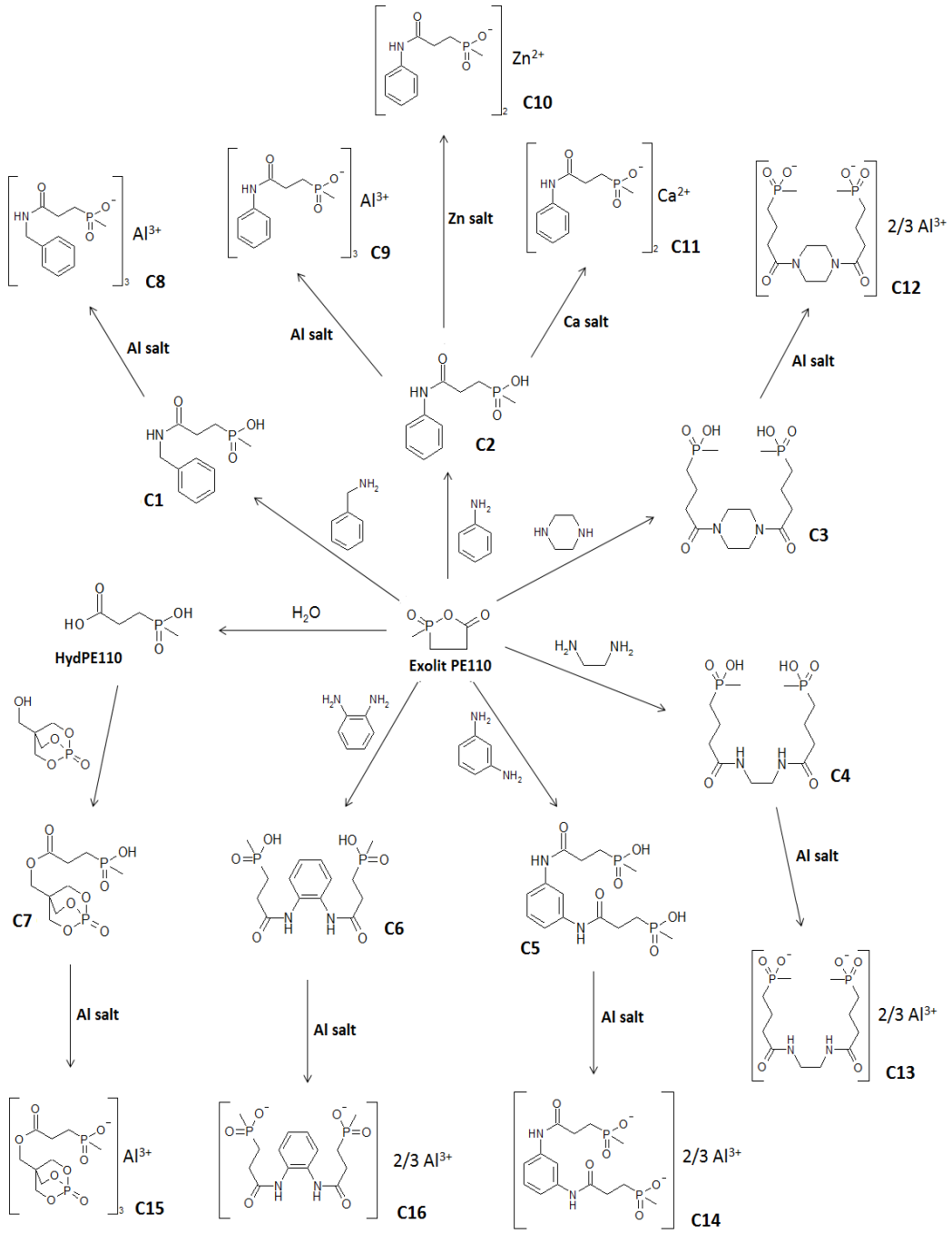

Figure 47: Synthesis scheme of the novel phosphinate salts

2.1 Materials and Techniques

Exolit PE110 was supplied by Clariant. 2,4,6-trioxa-1-phosphabicyclo[2,2,2]octane-4-methanol (PEPA) was provided by BASF. All other reagents and solvents were obtained from

commercial suppliers (Aldrich for instance) and used without further purification. ^{1}H, ^{13}C and ^{31}P liquid NMR spectra were recorded on a Varian INOVA 400, Varian VNMRS 500 or a Bruker DPX 360A spectrometer. Chemical shifts (δ) for ^{1}H and ^{13}C are given in parts per million (ppm) relative to $(CH_3)_4Si$ (TMS) as internal standard or relative to solvent signals. Chemical shifts (δ) for ^{31}P are given in parts per million (ppm) without referring to a specific standard. All spectra are reported in Appendix 1. ^{13}C, ^{31}P and ^{27}Al solid state NMR spectra were recorded on Bruker spectrometers operating at 300 MHz or 400 MHz resonance frequencies. The samples were introduced into zirconia rotors for analyses. The probehead diameter, rotational speed and pulse sequences used for each NMR experiment are reported in Appendix 1 along with spectra (with peak attributions).

Elemental analyses for carbon, hydrogen and nitrogen were performed with an Elementar micro cube CHN analyzer. The sample is weighed in a tin capsule and burned with O_2 under helium atmosphere. Different catalysts are used to convert the elements into specific compounds (C to CO_2, H to H_2O and N to N_2) which are then detected by a thermal conductivity detector (TCD). The initial weight of the sample is 1 - 10 mg, weighted in exactly on 0,001 mg. The quantification limit is 0,5 g/100 g and the measuring accuracy is ± 0,1 g/100 g.

Elemental analyses for oxygen were performed with an Eurovector EA analyzer. The sample is weighed in a silver capsule and pyrolyzed under helium atmosphere. The formed pyrolysis - gases are converted to specific compounds by catalysts, the oxygen is detected as CO by using a TCD. The initial weight of the sample is 0,1 – 5 mg, weighed in exactly on 0,001 mg. The quantification limit is 0,5 g/100 g and the measuring accuracy is ± 0,1 g/100 g.

Elemental analyses for aluminum, calcium and phosphorus were performed with a Vista Pro spectrometer system. The experiments are conducted as following: 0,1 g of the sample is added to a solution of Cs_2SO_4 as well as to a mixture of concentrated nitric acid and concentrated sulfuric acid. After solubilizing the sample with the oxidizing acids, the mixture is vaporized and the residue is dissolved in hypochloric acid. The relative percentages of Al, Ca and P of this solution are determined by means of atomic emission spectroscopy with inductive coupled plasma (ICP-AES). The standard deviation of the method is <2% rel.

- Two dimensional ^{31}P-^{31}P CP-RFDR experiment: A two-dimensional solid state NMR ^{31}P-^{31}P cross-polarization (CP) - radiofrequency driven recoupling (RFDR) experiment has been carried out to investigate the homonuclear correlations between the different phosphorus phases of **C9**. RFDR uses a radio-frequency pulse sequence that allows “recoupling” the dipolar couplings suppressed by MAS. It is therefore possible to determine the spatial proximity of phosphorus sites to within a substance[143]. The 2D ^{31}P-^{31}P CP-RFDR spectrum was collected at 9.4 T on a Bruker spectrometer equipped with a 4 mm triple channels probe operating at a spinning frequency of 10 kHz. The following acquisition parameters were used: number of scans = 64, recycle delay = 2s, CP contact time = 3 ms.

- TGA analysis of the synthesized products: the TGA measurements of the synthesized phosphinate salts were conducted in nitrogen flow on a TA Instruments SDT Q600 with alumina crucibles. The purge flow rate was set to 100 ml/min. The samples of about 15 mg were submitted to an isotherm at 50°C for 10 minutes then followed by a heating ramp of 10°C/min up to 600°C. Every TG analyses are repeated at least twice to ensure the reproducibility of the measurements.

2.2 Experimental procedures for the synthesis of the (di)phosphinic acids

● Synthesis of benzyl amide of carboxyethyl(methyl)phosphinic acid (C1)

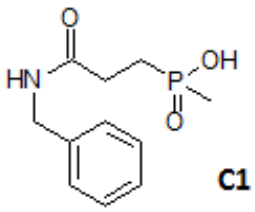

C1

Benzyl amine (89.5 g, 0.84 mol) was added dropwise to a solution of Exolit PE110/acetonitrile (112 g, 0.84 mol in 600 ml) stirred at about 60°C. The reaction mixture was then allowed to stir under acetonitrile reflux (80°C) for 4 hours. The phosphinic acid product started to precipitate out of the solution a few minutes following the addition of the amine. At last the mixture was cooled down to room temperature and the product was suction filtered and washed with acetonitrile. The resulting white solid was further dried overnight in a vacuum oven at 80°C to afford 194.9 g of **C1** (96.7% yield)**.**

^{1}H NMR (400 MHz, DMSO-d$_6$, stand. TMS): δ 8.48 (1H, t, H8, $^{3}J_{8\text{-}4}$ = 6.0 Hz), 7.31 (2H, ≈ t, H6, $^{3}J_{6\text{-}7/5}$ = 7.6 Hz), 7.25 (2H, d, H5, $^{3}J_{5\text{-}6}$ = 7.6 Hz), 7.23 (1H, t, H7, $^{3}J_{7\text{-}6}$ = 7.6 Hz), 4.27 (2H, d, H4, $^{3}J_{4\text{-}8}$ = 6.0 Hz), 2.36 (2H, m, H1), 1.82 (2H, m, H2), 1.28 (d, 3H, H3, $^{2}J_{3\text{-}P}$ = 14.0 Hz). **^{13}C NMR dec-^{1}H (126 MHz, DMSO, stand. DMSO):** δ 172.2 (d, C10), 140.4 (s, C11), 129.2 (s, C6), 128.2 (s, C5), 127.7 (s, C7), 43.2 (s, C4), 29.1 (s, C1), 27.3 (d, C2), 16.0 (d, C3).**^{31}P (^{1}H coupling) NMR (146 MHz, DMSO-d$_6$):** δ 46.6 (m).

● Synthesis of phenyl amide of carboxyethyl(methyl)phosphinic acid (C2)

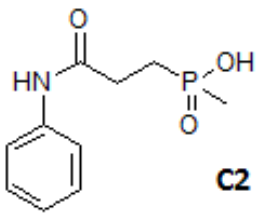

C2

To a solution of Exolit PE110 (147.5 g, 1.10 mol) in DMF (800 ml) stirred at about 80°C was added dropwise aniline (102.5 g, 1.10 mol). Following the addition of the amine, the reaction mixture was stirred for 4 hours at 100°C. The mixture was then cooled down to room

temperature and DMF was removed under reduced pressure to yield an orange/brun solid. The product was recrystallized in acetonitrile, collected by filtration and washed with methyl tert-butyl ether. The resulting white solid was further dried overnight in a vacuum oven at 80°C to afford 216.7 g of **C2** (86.7% yield).

^{1}H NMR (360 MHz, DMSO-d$_6$, stand. TMS): δ 10.02 (1H, s, H7), 7.58 (2H, ≈ dd, H4, $^{3}J_{4-5}$ = 8.3 Hz, $^{3}J_{4-6}$ = 1.1 Hz), 7.29 (2H, ≈ dd, H5, $^{3}J_{5-4}$ = 8.3 Hz, $^{3}J_{5-6}$ = 7.6 Hz), 7.03 (1H, tt, H6, $^{3}J_{6-5}$ = 7.6 Hz, $^{3}J_{6-4}$ = 1.1 Hz), 2.53 (2H, m, H1), 1.87 (2H, m, H2), 1.32 (3H, d, H3, $^{2}J_{3-P}$ = 14.1 Hz). **^{13}C NMR dec-^{1}H (126 MHz, DMSO-d$_6$, stand. DMSO):** δ 171.1 (d, C9), 140.2 (s, C10), 129.6 (s, C5), 124.0 (s, C6), 120.1 (s, C4), 30.2 (s, C1), 27.0 (d, C2), 16.2 (d, C3). **^{31}P (^{1}H coupling) NMR (146 MHz, DMSO-d$_6$):** δ 46.8 (m).

● **Synthesis of piperazine diamide of carboxyethyl(methyl)phosphinic acid (C3)**

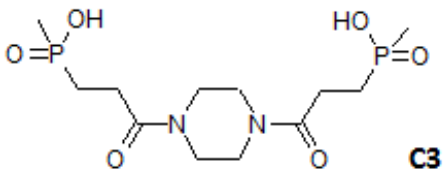

C3

To a solution of piperazine (48.8 g, 0.56 mol) in DMF (800 ml) stirred at about 60°C was slowly added Exolit PE110 (152 g, 1.13 mol), whereupon the diphosphinic acid product started to precipitate out of the solution. Because of the strong exothermicity of the reaction, the phospholane addition was metered so that the internal temperature did not rise above 130°C. After the end of the addition the reaction mixture was stirred for another 4 hours at 110°C. The mixture was at last cooled down to room temperature and the product was collected by filtration and washed with methanol. The resulting yellowish solid was further dried overnight in a vacuum oven at 80°C to afford 192.5 g of **C3** (95.9% yield).

^{1}H NMR (360 MHz, D$_2$O, stand. TMS): δ 3.65 (8H, m, H4), 2.73 (4H, m, H1), 2.08 (4H, m, H2), 1.53 (6H, d, H3, $^{2}J_{3-P}$ = 13.7 Hz). **^{13}C NMR dec-^{1}H (91 MHz, D$_2$O, stand. TMS):** δ 175.6 (dd, C5), 47.8/44.6 (dd, C4), 28.4 (m, C1), 27.9 (d, C2), 16.7 (dd, C3). **^{31}P (^{1}H coupling) NMR (146 MHz, D$_2$O):** δ 55.5 (m).

● **Synthesis of ethylene diamide of carboxyethyl(methyl)phosphinic acid (C4)**

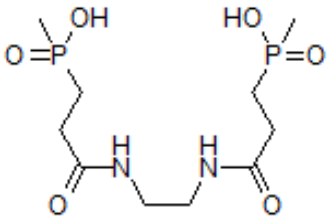

C4

To a solution of Exolit PE110 (163.4 g, 1.22 mol) in DMF (800 ml) stirred at about 60°C was added dropwise ethylene diamine (36.6 g, 0.61 mol), whereupon the diphosphinic acid

product precipitated out of the solution. Because of the strong exothermicity of the reaction, the phospholane addition was metered so that the internal temperature did not rise above 130°C. After the end of the addition the reaction mixture was stirred for another 3 hours at 110°C. The mixture was at last cooled down to room temperature and the product was suction filtered and washed with methanol. The resulting yellowish solid was further dried overnight in a vacuum oven at 80°C to afford 182.5 g of **C4** (91.3% yield).

^{1}H NMR (360 MHz, DMSO, stand. TMS): δ 3.13 (4H, s, H4), 2.30 (4H, m, H1), 1.83 (4H, m, H2) 1.30 (6H, d, H3). **^{13}C NMR dec-^{1}H (91 MHz, DMSO, stand. DMSO):** δ 39.1 (s, C4), 29.0 (s, C1), 27.0 (d, C2), 15.2 (d, C3). **^{31}P (^{1}H coupling) NMR (146 MHz, DMSO):** δ 46.4.

● **Synthesis of m-phenylene diamide of carboxyethyl(methyl)phosphinic acid (C5)**

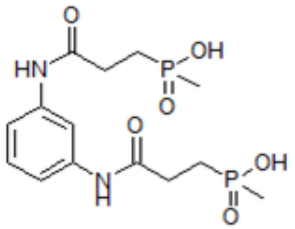

C5

To a solution of m-phenylene diamine (57.5 g, 0.53 mol) in DMF (800 ml) stirred at about 80°C was slowly added Exolit PE110 (142.5 g, 1.06 mol). Following the phospholane addition, the reaction mixture was stirred for a period of time of 4 hours at 110°C. The diphosphinic acid product started to precipitate out of the solution within 20 minutes after the end of the addition. The mixture was at last cooled down to room temperature and the product was suction filtered and washed with methanol. The resulting white solid was further dried overnight in a vacuum oven at 80°C to afford 178.9 g of **C5** (89.4% yield).

^{1}H NMR (400 MHz, DMSO-d$_6$, stand. TMS): δ 10.04 (2H, s, H7), 7.91 (1H, s, H4), 7.25 (2H, ≈ d, H5, $^{3}J_{5\text{-}6}$ = 7.6 Hz), 7.18 (1H, ≈ t, H6, $^{3}J_{6\text{-}5}$ = 7.6 Hz), 2.52 (4H, m, H1), 1.88 (4H, m, H2), 1.33 (6H, d, H3, $^{2}J_{3\text{-}P}$ = 14.0 Hz). **^{13}C NMR dec-^{1}H (91 MHz, DMSO-d$_6$, stand. DMSO):** δ 171.1 (d, C9), 140.4 (s, C10), 129.7 (s, C6), 114.9 (s, C5), 111.0 (s, C4), 30.2 (s, C1), 27.1 (d, C2), 16.2 (d, C3). **^{31}P (^{1}H coupling) NMR (146 MHz, DMSO-d$_6$):** δ 46.8 (m).

● **Synthesis of o-phenylene diamide of carboxyethyl(methyl)phosphinic acid (C6)**

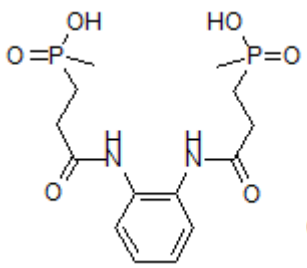

C6

To a solution of o-phenylene diamine (4.84 g, 0.045 mol) in DMF (60 ml) stirred at about 80°C was slowly added Exolit PE110 (12 g, 0.09 mol). The reaction mixture was then allowed to stir for a period of time of 4 hours at 110°C. The mixture was at last cooled down to room temperature and DMF was removed under reduced pressure to yield an orange viscous liquid. The product was recrystallized twice in methanol, after which it was collected by filtration and washed with methyl tert-butyl ether. The resulting white solid was further dried overnight in a vacuum oven at 80°C to afford 4.3 g of **C6** (25.5% yield).

^{1}H NMR (400 MHz, DMSO-d$_6$, stand. TMS): δ 9.64 (2H, s, H6), 7.54 (2H, ≈ t, H4 $J_{4\text{-}4/5}$ = 4.8 Hz), 7.11 (2H, ≈ t, H5, $^{3}J_{5\text{-}5/6}$ = 4.8 Hz), 2.58 (4H, m, H1), 1.95 (4H, m, H2), 1.37 (6H, d, H3, $^{3}J_{3\text{-}P}$ = 14 Hz). **^{13}C NMR dec-^{1}H (91 MHz, DMSO-d$_6$, stand. DMSO):** δ 171.6 (d, C8), 131.7 (s, C9), 125.7 (s, C4), 125.5 (s, C5), 30.0 (s, C1), 27.4 (d, C2), 16.0 (d, C3). **^{31}P (^{1}H coupling) NMR (146 MHz, DMSO-d$_6$):** δ 47.6 (m).

● **Synthesis of 2-carboxyethyl(methyl)phosphinic acid (hydrolyzed Exolit PE110, HydPE110)**

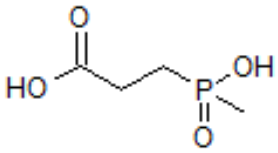

HydPE110

Exolit PE110 (50 g, 0.37 mol) was dissolved in distillated water (300 ml) at room temperature. The solution was allowed to stir for a period of time of 2 hours at 70°C. The mixture was then cooled down to room temperature and water was removed under reduced pressure to yield **C7** as a colorless viscous liquid. Afterward, the liquid product quickly crystallized into a yellowish solid, giving off large amount of heat. The resulting solid was further dried overnight in a vacuum oven at 60°C to afford 56.8 g of **HydPE110** (100% yield).

^{1}H NMR (360 MHz, DMSO, stand. TMS): δ 7.78 (s, H4, H5), 2.40 (2H, m, H1), 1.81 (2H, m, H2), 1.30 (3H, d, H3, $^{2}J_{3\text{-}P}$ = 14.1 Hz).

● **Synthesis of PEPA ester of carboxyethyl(methyl)phosphinic acid (C7)**

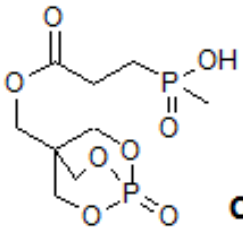

C7

A suspension of **HydPE110** (105.6 g, 0.69 mol) and Pentaerythritol Phosphate (PEPA) (125 g 0.69 mol) in toluene (1700 ml) was stirred at reflux for 20h. Traces of water were removed by azeotropic distillation using a Dean-Stark trap. In the course of the reaction, while monitoring removal of water, a brownish viscous phase was observed at the bottom of the

flask which slowly hardened and became a crystal solid. The reaction mixture was at last cooled down to room temperature and the crystal solid was collected by filtration and washed with methyl ethyl ketone. The crude solid, thinly crushed, was then washed two times with refluxing methyl ethyl ketone (1500 ml) for 1h30. The product was finally suction filtered, washed with methyl ethyl ketone and further dried overnight in a vacuum oven at 40°C to afford 187.2 g of **C7** (85.8% yield).

^{1}H NMR (360 MHz, DMSO, stand. TMS): δ 4.67 (6H, d, H5, $^{2}J_{5\text{-}P}$ = 6.98), 3.98 (2H, s, H4), 2.54 (2H, m, H1), 1.86 (2H, m, H2), 1.32 (2H, d, H3, $^{2}J_{3\text{-}P}$ = 13.9 Hz). **^{31}P NMR (146 MHz, DMSO):** δ 46.7 (1P, m, $P_{phosphinate}$), - 7.4 (1P, m, $P_{phosphate}$).

2.3 Experimental procedures for the synthesis of the (di)phosphinate salts

● **Synthesis of benzyl amide of carboxyethyl(methyl)phosphinate aluminum (C8)**

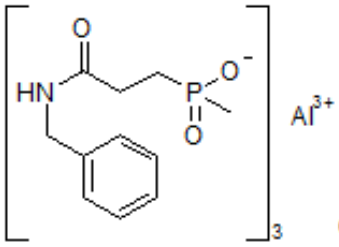

C8

To a solution of **C1** (160 g, 0.66 mol) in a water/ethanol mixture (800 ml/800 ml) stirred at room temperature was added aluminum triisopropylate (45.2 g, 0.22 mol). The reaction mixture was allowed to stir for a period of time of 9h at 80°C. The phosphinate salt progressively precipitated during the reaction, as a result of which the shear thickening behavior of the solution significantly increased. The mixture was then cooled down to room temperature and the product was suction filtered and washed abundantly with distillated water. The resulting white solid was dried two days in a vacuum oven at 80°C to afford 142,8 g of **C8** (86.3% yield).

Elemental Analysis. Calculated for $C_{33}H_{45}N_3O_9P_3Al$: C, 53.0; H, 6.1; N, 5.6; O, 19.3; P, 12.4; Al, 3.6 wt%. Found C, 52.1; H, 6.0; N, 5.5; O, 19.5; P*, 11; Al*, 4 wt%.

^{13}C solid state NMR - CP/MAS dec-^{1}H (Bo = 300 MHz, Probe-head = 4 mm, MAS = 5 kHz, CP ^{1}H-^{13}C contact time = 3ms, Recycle delay = 2s, scan = 10240): δ 174 (H1), 140-136 (H6), 134-120 (H7, H8, H9), 48-40 (H5), 33-24 (H2, H3), 19-12 (H4). **^{31}P solid state NMR - CP/MAS dec-^{1}H (Bo = 300 MHz, Probe-head = 4 mm, MAS = 10 kHz, CP ^{1}H-^{13}C contact time = 3ms, Recycle delay = 2s, scan = 1024):** δ 40.1, 36.3, 32.7. **^{27}Al solid state NMR - MAS (Bo = 300 MHz, Probe-head = 4 mm, MAS = 10 kHz, Recycle delay = 0.25s, scan = 122880):** δ -12.0.

* *imprecise data due to a lack of product for the analyses*

● **Synthesis of phenyl amide of carboxyethyl(methyl)phosphinate aluminum (C9)**

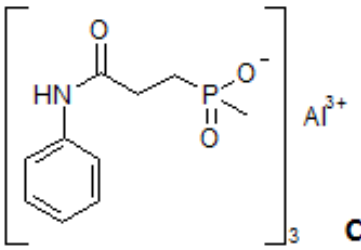

C9

This reaction was performed in an analogous manner to that for **C8,** using **C2** (160 g, 0.70 mol) and aluminum triisopropylate (47.9 g, 0.23 mol). The resulting white solid was dried for two days in a vacuum oven at 80°C to afford 149.3 g of **C9** (90.2% yield).

Elemental Analysis. Calculated for $C_{30}H_{39}N_3O_9P_3Al$: C, 51.1; H, 5.6; N, 6.0; O, 20.4; P, 13.2; Al, 3.8 wt%. Found C, 50.9; H, 5.5; N, 5.9; O, 21.1; P*, 11; Al*, 4 wt%.

^{13}C solid state NMR - CP/MAS dec-^{1}H (Bo = 300 MHz, Probe-head = 4 mm, MAS = 5 kHz, CP ^{1}H-^{13}C contact time = 3ms, Recycle delay = 2s, scan = 10240): δ 172 (H1), 140-135 (H5), 134-118 (H7, H8, H6), 36-24 (H2, H3), 19-12 (H4). **^{31}P solid state NMR - CP/MAS dec-^{1}H (Bo = 300 MHz, Probe-head = 4 mm, MAS = 10 kHz, CP ^{1}H-^{13}C contact time = 3ms, Recycle delay = 2s, scan = 1024):** δ 39.6, 38.2, 36.2. **^{27}Al solid state NMR - MAS (Bo = 300 MHz, Probe-head = 4 mm, MAS = 10 kHz, Recycle delay = 0.25s, scan = 122880):** δ -11,5.

* *imprecise data due to a lack of product for the analyses*

● **Synthesis of phenyl amide of carboxyethyl(methyl)phosphinate zinc (C10)**

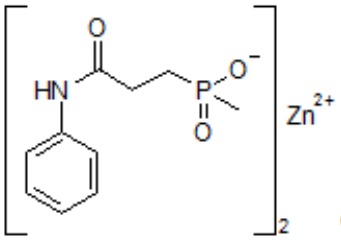

C10

A solution of NaOH (1.76 g, 0.044 mol) in water (25 ml) was added dropwise, with stirring, to **C2** (10 g, 0.044 mol). The reaction flask was introduced in a cold water bath and the addition of the aqueous sodium hydroxide was metered so as to forestall an increase of temperature in the mixture. After complete dissolution of the phosphinate, a solution of zinc acetate dihydrate (4.83 g, 0.022 mol) in water (25 ml) was added dropwise to the bulk synthesis whereupon the final product began to precipitate out. The reaction mixture was allowed to stir for 5h at room temperature. The mixture was then cooled down to room temperature and the product was suction filtered and washed with distillated water. The resulting white solid was dried two days in a vacuum oven at 80°C to afford 5.29 g of **C10** (46.4% yield).

Elemental Analysis. Calculated for $C_{20}H_{26}N_2O_6P_2Zn$: C, 46.4; H, 5.1; N, 5.4; O, 18.5; P, 12.0; Zn, 12.6 wt%. Found C, 46.4; H, 5.1; N, 5.4; O, 18.8; P, 11.7; Zn, 12.7 wt%.

^{13}C solid state NMR - CP/MAS dec-^{1}H (Bo = 400 MHz, Probe-head = 4 mm, MAS = 10 kHz, CP ^{1}H-^{13}C contact time = 2ms, Recycle delay = 5s, scan = 1024): δ 174-167 (H1), 140-135 (H5), 128 (H7), 125-119 (H8, H6), 33 (H2), 30-24 (H3), 19-12 (H4). **^{31}P solid state NMR - MAS dec-^{1}H (Bo = 400 MHz, Probe-head = 4 mm, MAS = 13 kHz, Recycle delay = 120s, scan = 8):** δ 53.2, 51.8, 46.2.

● **Synthesis of phenyl amide of carboxyethyl(methyl)phosphinate calcium (C11)**

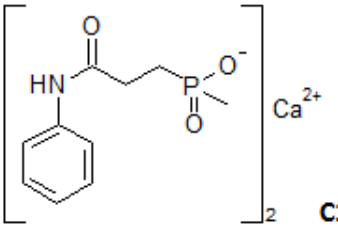

C11

This reaction was performed in an analogous manner to that for **C10,** using NaOH (1.76 g, 0.044 mol), **C2** (10 g, 0.044 mol) and calcium acetate hydrate (3.87 g, 0.022 mol). The resulting white solid was dried for two days in a vacuum oven at 80°C to afford 8,74 g of **C11** (80.8% yield).

Elemental Analysis. Calculated for $C_{20}H_{26}N_2O_6P_2Ca$: C, 48.8; H, 5.3; N, 5.7; O, 19.5; P, 12.6; Ca, 8.1 wt%. Found C, 45.4; H, 5.7; N, 5.2; O, 24.9; P, 8.3; Ca, 7.4 wt%.

^{13}C solid state NMR - CP/MAS dec-^{1}H (Bo = 400 MHz, Probe-head = 4 mm, MAS = 10 kHz, CP ^{1}H-^{13}C contact time = 2ms, Recycle delay = 5s, scan = 1024): δ 171 (H1), 138 (H5), 131 (H7), 122 (H8, H6), 32-22 (H2, H3), 15 (H4). **^{31}P solid state NMR - MAS dec-^{1}H (Bo = 400 MHz, Probe-head = 4 mm, MAS = 13 kHz, Recycle delay = 120s, scan = 8):** δ 42.0.

● **Synthesis of piperazine diamide of methyl-β-(carboxamid)ethylphosphinate aluminum (C12)**

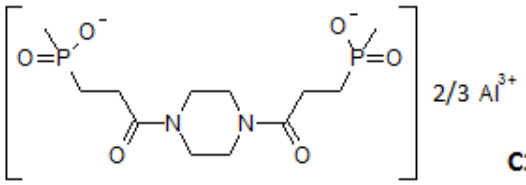

C12

To a solution of **C3** (150 g, 0.43 mol) in a water/ethanol mixture (750 ml/450 ml) stirred at room temperature was added aluminum triisopropylate (57.6 g, 0.28 mol). The reaction mixture was allowed to stir for 18h at 80°C. The phosphinate salt progressively precipitated

out from the solution over the course of the reaction. The mixture was then cooled down to room temperature and the product was suction filtered and washed abundantly with distillated water. The resulting white/yellowish solid was dried for two days in a vacuum oven at 80°C to afford 131.6 g of **C12** (84.0% yield).

Elemental Analysis. Calculated for $C_{36}H_{66}N_6O_{18}P_6Al_2$: C, 38.9; H, 6.0; N, 7.6; O, 25.9; P, 16.7; Al, 4.9 wt%. Found C, 34.3; H, 6.2; N, 6.3; O, 33; P, 14.7; Al, 5.3 wt%.

^{13}C solid state NMR - CP/MAS dec-^{1}H (Bo = 300 MHz, Probe-head = 4 mm, MAS = 5 kHz, CP ^{1}H-^{13}C contact time = 3ms, Recycle delay = 2s, scan = 10240): δ 171 (H1), 52-35 (H5), 35-20 (H2, H3), 20-9 (H4). **^{31}P solid state NMR - CP/MAS dec-^{1}H (Bo = 300 MHz, Probe-head = 4 mm, MAS = 10 kHz, CP ^{1}H-^{13}C contact time = 3ms, Recycle delay = 2s, scan = 1024):** δ 38.8. **^{27}Al solid state NMR - MAS (Bo = 300 MHz, Probe-head = 4 mm, MAS = 10 kHz, Recycle delay = 0.25s, scan = 122880):** δ -11,5.

● **Synthesis of ethylene diamide of carboxyethyl(methyl)phosphinate aluminum (C13)**

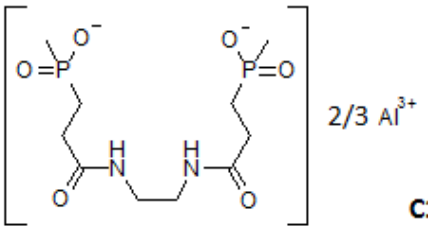

C13

To a solution of **C4** (140 g, 0.43 mol) in a water/ethanol mixture (700 ml/700 ml) stirred at room temperature was added aluminum triisopropylate (58.0 g, 0.28 mol). The reaction mixture was allowed to stir for a period of time of 9h at 80°C. The phosphinate salt progressively precipitated out from the solution over the course of the reaction. The mixture was then cooled down to room temperature and the product was suction filtered and washed abundantly with distillated water. The resulting white/yellowish solid was dried for two days in a vacuum oven at 80°C to afford 119.6 g of **C13** (81.1% yield).

Elemental Analysis. Calculated for $C_{30}H_{60}N_6O_{18}P_6Al_2$: C, 34.9; H, 5.9; N, 8.1; O, 27.9; P, 18.0; Al, 5.2 wt%. Found C, 32.5; H, 5.8; N, 7.6; O, 29; P, 17.0; Al, 5.6 wt%.

^{13}C solid state NMR - CP/MAS dec-^{1}H (Bo = 300 MHz, Probe-head = 4 mm, MAS = 5 kHz, CP ^{1}H-^{13}C contact time = 3ms, Recycle delay = 2s, scan = 10240): δ 171 (H1), 45-35 (H5), 35-22 (H2, H3), 20-10 (H4). **^{31}P solid state NMR - CP/MAS dec-^{1}H (Bo = 300 MHz, Probe-head = 4 mm, MAS = 10 kHz, CP ^{1}H-^{13}C contact time = 3ms, Recycle delay = 2s, scan = 1024):** δ 38.1, 35.6. **^{27}Al solid state NMR - MAS (Bo = 300 MHz, Probe-head = 4 mm, MAS = 10 kHz, Recycle delay = 0.25s, scan = 122880):** δ -11,5.

● **Synthesis of m-phenylene diamide of carboxyethyl(methyl)phosphinate aluminum (C14) – 1st route (14-1)**

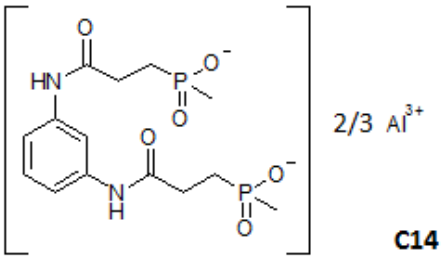

C14

To a solution of **C5** (10 g, 0.027 mol) in a water/ethanol mixture (100 ml/50 ml) stirred at room temperature was added aluminum triisopropylate (3.62 g, 0.018 mol). The reaction mixture was allowed to stir for a period of time of 23h at 80°C. The phosphinate salt progressively precipitated out from the solution over the course of the reaction. The mixture was then cooled down to room temperature and the product was suction filtered and washed abundantly with distillated water. The resulting white/yellowish solid was dried for two days in a vacuum oven at 80°C to afford 5.5 g of **C14** (52.8% yield).

^{13}C solid state NMR - CP/MAS dec-^{1}H (Bo = 300 MHz, Probe-head = 4 mm, MAS = 5 kHz, CP ^{1}H-^{13}C contact time = 3ms, Recycle delay = 2s, scan = 10240): δ 178-165 (H1), 143-133 (H5), 133-124 (H8), 124-102 (H7, H6), 37-21 (H2, H3), 21-10 (H4). **^{31}P solid state NMR - CP/MAS dec-^{1}H (Bo = 300 MHz, Probe-head = 4 mm, MAS = 10 kHz, CP ^{1}H-^{13}C contact time = 3ms, Recycle delay = 2s, scan = 1024):** δ 36.0. **^{27}Al solid state NMR - MAS (Bo = 300 MHz, Probe-head = 4 mm, MAS = 10 kHz, Recycle delay = 0.25s, scan = 122880):** δ 5, -11.0.

● **Synthesis of m-phenylene diamide of carboxyethyl(methyl)phosphinate aluminum (C14) – 2nd route (14-2)**

A solution of NaOH (30.9 g, 0.77 mol) in water (250 ml) was added dropwise, with stirring, to **C5** (145.6 g, 0.39 mol). The reaction flask was introduced in a cold water bath and the addition of the aqueous sodium hydroxide was metered so as to forestall an increase of temperature in the mixture. After complete dissolution of the phosphinate, a solution of aluminum sulfate hexadecahydrate ($Al_2O_{12}S_3.16H_2O$, 81.3 g, 0.129 mol) in water (350 ml) was added dropwise to the bulk synthesis, whereupon the final product began to precipitate out. The reaction mixture was allowed to stir for 2h at room temperature. The mixture was then cooled down to room temperature and the product was suction filtered and washed with distillated water. The resulting white solid was dried for two days in a vacuum oven at 80°C to afford 143.3 g of **C14** (96.2% yield).

Elemental Analysis. Calculated for $C_{42}H_{60}N_6O_{18}P_6Al_2$: C, 42.9; H, 5.1; N, 7.1; O, 24.5; P, 15.8; Al, 4.6 wt%. Found C, 39.9; H, 5.3; N, 6.4; O, 29; P, 13.3; Al, 4.6 wt%.

^{13}C solid state NMR - CP/MAS dec-^{1}H (Bo = 300 MHz, Probe-head = 4 mm, MAS = 5 kHz, CP ^{1}H-^{13}C contact time = 3ms, Recycle delay = 2s, scan = 10240): δ 178-165 (H1), 143-133 (H5), 133-124 (H8), 124-102 (H7, H6), 44-37 (?), (H2, H3), 21-10 (H4). **^{31}P solid state NMR - CP/MAS dec-^{1}H (Bo = 300 MHz, Probe-head = 4 mm, MAS = 10 kHz, CP ^{1}H-^{13}C contact time = 3ms, Recycle delay = 2s, scan = 1024):** δ 37.2. **^{27}Al solid state NMR - MAS (Bo = 300 MHz, Probe-head = 4 mm, MAS = 10 kHz, Recycle delay = 0.25s, scan = 122880):** δ -12.0.

● **Synthesis of PEPA ester of carboxyethyl(methyl)phosphinate aluminum (C15)**

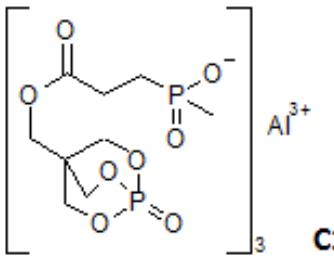

C15

A solution of NaOH (22.9 g, 0.57 mol) in water (300 ml) was added dropwise, with stirring, to **C7** (180 g, 0.57 mol). The reaction flask was introduced in a cold water bath and the addition of the aqueous sodium hydroxide was metered so as to forestall the increase of temperature of the mixture. After complete dissolution of the phosphinate, a solution of aluminum sulfate hexadecahydrate ($Al_2O_{12}S_3.16H_2O$, 59.9 g, 0.095 mol) in water (260 ml) was added dropwise to the bulk synthesis, whereupon the final product began to precipitate out. The reaction mixture was allowed to stir for 2h at room temperature. The mixture was then cooled down to room temperature and the product was suction filtered and washed with distillated water. The resulting white solid was dried for two days in a vacuum oven at 80°C to afford 20 g of **C15** (10.9% yield).

Elemental Analysis. Calculated for $C_{27}H_{45}O_{24}P_6Al$: C, 33.6; H, 4.7; O, 39.7; P, 19.2; Al, 2.8 wt%. Found C, 32.7; H, 5.0; O, 40.2; P, 14.3; Al, 3.2 wt%.

^{13}C solid state NMR - CP/MAS dec-^{1}H (Bo = 400 MHz, Probe-head = 4 mm, MAS = 10 kHz, CP ^{1}H-^{13}C contact time = 2ms, Recycle delay = 5s, scan = 1024): δ 178-165 (H1), 76 (H7), 57-64 (H5), 40-37 (H6), 31-21 (H2, H3), 20-10 (H4). **^{31}P solid state NMR - MAS dec-^{1}H (Bo = 400 MHz, Probe-head = 4 mm, MAS = 13 kHz, Recycle delay = 120s, scan = 8):** δ 36.3, -7.3. **^{27}Al solid state NMR - MAS (Bo = 400 MHz, Probe-head = 3.2 mm, MAS = 20 kHz, Recycle delay = 2s, scan = 512):** δ -11.5.

3. Conclusion

This chapter defined the materials, techniques and protocols used during the project to achieve the major challenge of this work: development of an innovative formulation to flame retard glass-reinforced PBT.

The basic polymer material and compounding processes used to prepare the flame retarded formulations for the screening phase of chapter 3 and chapter 4 were described. The testing methods used to determine the flame retardant properties (LOI, UL94, mass loss calorimeter) of the materials have also been presented. In this project, are investigated the flame retardant performances of two sorts of phosphinate salts in PBT. One is obtained from a commercial supplier (chapter 3), the other is conceived in the lab (chapter 4). Experimental procedures used for the synthesis of the novel phosphinate salts are gathered in the present chapter. Finally, the strategies implemented in chapter 5 to elucidate the flame retardant mode of actions of the phosphinate salts (TGA-FTIR, pyrolysis-GCMS, NMR) have been detailed. The next step, chapter 3, now consists in developing an innovative flame retardant PBT/GF formulation by using commercial phosphinate salts in combination with nano-particles.

CHAPTER 3 – DEVELOPMENT OF A NOVEL FLAME RETARDED PBT/GF FORMULATION BASED ON COMMERCIAL PHOSPHINATE SYSTEMS

The collaboration with BASF aims at finding potential flame retardants providing an optimized new fire retarded glass fiber reinforced PBT (PBT/GF) formulation. Following this line, two approaches have been chosen. The first one consists in the use of commercial flame retardants combined with synergistic agents. The second one consists in synthesizing novel flame retardant additives. The state of the art (chapter 1) allowed determining that one of the most valuable classes of non-halogenated flame retardants is phosphinate salts. Accordingly, our strategy focused on improving the fire behavior of the polyester by means of phosphinate based systems.

This present chapter deals with the research of synergistic agents for use with the aluminum phosphinate systems commercialized by Clariant, namely Exolit OP1240 and Exolit O1P200. These systems have proven FR efficiency in PBT. It is believed that the fire performances of PBT could be further improved by combining Exolit systems with other additives. Nano-particules appeared to be promising candidates with regard to the description of the related art.

The first part of this chapter is dedicated to the screening of the flame retardant combinations in glass fiber (25 wt%) reinforced PBT. For the hereafter tested formulations, as they are intended to be used for electronic/electrical applications, good results in the glow wire and UL94 tests must be achieved. In the present study, however, the screening was implemented only using the UL94 test with a view to reaching the required V-0 classification.

The second part will focus on an innovative flame retardant combination which showed the most promising performances in UL94: Exolit OP1240 + RDP bentonite (bentonite clay modified with Resorcinol Bis-Diphenylphosphate). The relative proportion of both additives in reinforced PBT was varied so as to optimize the efficiency of the combination. A comparative study is moreover performed to find out whether the modification of the bentonite clay by the RDP surfactant is relevant in terms of fire performance.

In the last part, the optimized formulation is tested through other fire test scenarios, namely the Limiting Oxygen Index (LOI) and the Mass Loss Calorimeter (MLC) tests, in order to fully evaluate the performances of the novel flame retardant combination.

1. Flame retardant screening

1.1 Flame retardant additives selected

The development of an innovative flame retarded PBT/GF formulation implies to judiciously select the flame retardant additives with regard to the extensive researches that have already been conducted. The prior art reviewed in chapter 1 helped to do this selection. Exolit OP1240 (aluminum diethylphosphinate) and Exolit OP1200 (Aluminum diethylphosphinate + melamine cyanurate) were chosen because of their excellent fire

performances in PBT. Both flame retardants were claimed to give V-0 rating (0.8 mm) to glass fiber (30 wt%) reinforced PBT at loading of 20 wt%[39,141]. Since such a loading tends to reduce the elongation at break and impact strength of the PBT material, it is possible to adjust the glass fibers content at 25 wt% so the mechanical properties of the polyester remain appropriate for the targeted applications.

Three classes of nano-particles were combined with the phosphinate-based Exolit: organo-modified clays, Polyhedral Oligomeric SilSesquioxane (POSS) and graphene based fillers. In the prior art (chapter 1), it was mentioned that such particles could have beneficial synergistic effects combined at low loadings with conventional flame retardants[54,129,144-150]. However, there is still no evidence that these nano-particles act as synergists with aluminum diethylphosphinate systems in PBT.

The tested particles are listed in Table 7. Further description of the flame retardant additives is depicted in Appendix 2.

Table 7 : Selected nano-additives: type, commercial name, supplier and loading in the formulation (PBT/GF/Exolit/nano-particle: 55%/25%/20-x%/x%)

Nano-filler type	Nano-filler type	Nano-filler name and supplier	Loading (wt%)
Organo-modifed layered clay	Methyl tallow bis(2-hydroxyethyl) ammonium modified Montmorillonite	*Cloisite 30B*, **Southern clay products**	2
	Potassium acetate modified Kaolinite	*VP cocoon 2125*, **Benefit** (experimental product supplied by Benefit)	
	Resorcinol bis(diphenyl phosphate) modified Bentonite	*RDP bentonite*, **Glen Burnie Technologies** (experimental product supplied by BASF)	
Polyhedral oligomeric silsesquioxane (POSS)	Octamethyl POSS (OM-POSS)	*OM-POSS*, **Hybrid Plastics**	2
	Aminoethyl Aminopropyl isobutyl POSS (AEAPI-POSS)	*AEAPI-POSS*, **Hybrid Plastics**	
	Trisilanol phenyl POSS (TSP-POSS)	*TSP-POSS*, **Hybrid Plastics**	
Graphite	Expandable Graphite (EG)	*ES 350 F5*, **Graphit Kropfmülh AG**	3
		Nord-Min 503, **Nordmann, Rassmann GmbH**	
Graphene	Graphene	*GraphEx* , **Ciba** (experimental product supplied by BASF)	3

Organoclays were proved to be efficient in polymers at loadings up to 5 wt%[54,116,118,119,146,147,150]. For the screening, they were tested at 2 wt%. Two experimental layered clays have been investigated besides the well-known organo-modified montmorillonite Cloisite 30B: potassium acetate kaolinite (VP cocoon 2125) and Resorcinol bis(Diphenyl Phosphate) bentonite (RDP bentonite). Kaolinite is a two sheet type clay mineral, from the category of phyllosillicates, with the chemical composition $Al_2Si_2O_5(OH)_4$. The two adjacent platelets of kaolinite are strongly held together by the hydrogen bonds formed between the interlamellar aluminol groups of the $Al_2(OH)_4$ octahedron and the oxygen of the SiO_4 tetrahedron[151,152]. The very short spacing between kaolinite platelets, stemming from these multiple hydrogen bonds, restricts the intercalation of large molecules. Modification of the clay by small molecules such as potassium acetate allows to greatly expand the interlayer distance between platelets (through breaking hydrogen bonds) and thereby to favor the intercalation of polymeric chains[152-154]. The potassium acetate modified kaolinite VP cocoon 2125 can be used for flame retardancy applications in polymers, as specified by its supplier (Benefit). On the other hand, bentonite is an impure clay mineral with a structure mostly consisting of montmorillonite (80%). RDP modified bentonite was recently developed by Glen Burnie Technologies to improve polymer exfoliate clay blends[155]. The proven flame retardant properties of RDP in PBT make it a valuable surfactant that might eventually enhance the flammability behavior of the polyester.

Three POSS were investigated: OctaMethyl POSS (OM-POSS), TriSilanol POSS (TSP-POSS) and Amino-Ethyl Amino-Propyl Isobutyl POSS (AEAPI-POSS). Small amounts of OMPOSS (1-2 wt%) were lately proved to be synergistic with phosphinate salts, for instance providing improved fire retardancy and smoke suppressant properties to PET in combination with zinc diethylphosphinate (Exolit OP950)[129]. OMPOSS was accordingly used at loading of 2 wt% in the present study. TSP-POSS and AEAPI-POSS were also tested in order to investigate the influence of POSS structures on the flammability behavior of PBT.

Were also used three types of graphene based particles, namely the two expandable graphites ES 350 F5 and NordMin 503 as well as an experimental graphene from Ciba (GraphEx). Expandable graphites are stacked sheets of graphene in which are inserted sulphuric acid, nitric acid or organic acids. Upon heating, acids decompose into gases that separate graphene sheets from each others and expand the graphite flakes[156-158]. The expandable graphite ES 350 F5 starts to expand at about 200°C. It was selected as it would easily delaminate in the PBT matrix during the processing (at 250°C), while the graphene sheets would break up under the effect of shear leading to an exfoliated morphology[159]. NordMin 503, showing an onset of thermal expansion at 300°C, and GraphEx, consisting in milled graphite nanoplatelets[160], were used for the sake of comparison. In the literature, graphene based particles are usually added to polymers at loadings up to about 10 wt%[159,161]. In the present study, the amount was fixed at 3 wt%.

1.2 Fire test results

The screening was performed using the UL94 fire test. The results obtained for the various flame retardant formulations are gathered in the tables presented below (Table 8 and Table 9). According to the UL94 standard[162], the bar specimens shall be tested after two specific aging conditions: first, in an unaltered state after 2 days at 25°C (2d-25°C), and then after an aging at 70°C for a full 7 days (7d-70°C). In order to optimize the screening, only samples that achieved V-0 rating at the 2d-25°C aging were further tested at the 7d-70°C aging.

The whole flame retardant compositions were kept at the amount of 20 wt% in the reinforced polymer containing 25 wt% GF. The novel compositions were accordingly prepared by substituting part of the phosphinate systems (OP1240 or OP1200) by the nano-particles.

1.2.1 Exolit OP1240 based combinations

Combinations of Exolit OP1240 with nano-particles are first investigated. The UL94 results obtained for the corresponding formulations are summarized in Table 8.

Table 8 : UL94 results obtained for the OP1240/nano-additives containing PBT/GF formulations

Co-additive	Composition (wt%)				UL-94, 0.8 mm bar			
	PBT	GF	OP1240	Co-additive	Conditioning	t1/t2[a] (s)	Dripping[b]	Rating
-	55	25	20	-	2d.25°C	3.6/7.4	N/D-N	V-1
-	55	25	20	-	7d.70°C	5.0/6.1	N/D-N	V-1
Cloisite 30B	55	25	18	2	2d.25°C	5.2/9.8	N	V-1
RDP Bentonite	55	25	18	2	2d.25°C	1.5/3.1	N	V-0
RDP Bentonite	55	25	18	2	7d.70°C	2.8/4.1	N/D-N	V-0
VP cocoon 2125	55	25	18	2	2d.25°C	2.2/3.1	N	V-0
VP cocoon 2125	55	25	18	2	7d.70°C	1.9/5.4	N/D-Y	V-2
EG-ES350F5	55	25	17	3	2d.25°C	9.0/3.6	N	V-1
EG-NordMin503	55	25	17	3	2d.25°C	2.2/5.1	N/D-N	V-0
EG-NordMin503	55	25	17	3	7d.70°C	2.8/2.3	N/D-Y	V-2
GraphEx	55	25	17	3	2d.25°C	6.4/6.4	N	V-1
OM-POSS	55	25	18	2	2d.25°C	2.0/3.6	N	V-0
OM-POSS	55	25	18	2	7d.70°C	2.7/3.8	N/D-N	V-0
AEAIP-POSS	55	25	18	2	2d.25°C	2.6/5.5	N	V-0
AEAIP-POSS	55	25	18	2	7d.70°C	3.8/2.6	N/D-Y	V-2
TSP-POSS	55	25	18	2	2d.25°C	3.6/5.0	N/D-N	V-0\V-1

[a] *t1 and t2, average combustion times after the first and the second application of the flame*

[b] *dripping after the first and second application of the flame. N = no dripping, D-N = dripping without ignition of cotton, D-Y = dripping with ignition of cotton*

The reference material containing 20 wt% OP1240 achieves a V-1 rating after the 2d-25°C and 7d-70°C aging. The sample is characterized by relatively high combustion times,

particularly after the removal of flame in the second application where non flammable drops are produced. These results are not in agreement with those reported by Braun et al[141], since it is claimed that comparable amount of OP1240 in PBT/GF gives a V-0 classification. The lower fire performances achieved in the present study are possibly explained by the fact that the materials hereby tested contain 25 wt% glass fibers while the ones investigated by the above-mentioned authors are filled with 30 wt% fibers. It is thus believed that the moderate increase of the proportion of combustible PBT (i.e. 5 wt%) at the expense of glass fibers would be detrimental to the flammability behavior of the material.

The substitution of 2 wt% OP1240 by Cloisite 30B prevents dripping of specimens but adversely increases their combustion times. The UL94 classification of the material (V-1) is therefore not changed. Different results are obtained when substituting OP1240 by other organoclays. Indeed, 2 wt% RDP bentonite or VP cocoon 2125 allows decreasing the average combustion times while preventing dripping of the polymer after the 2d-25°C aging. A V-0 ranking is reached for both corresponding materials. Interestingly, the flammability behavior of samples changes after the 7d-70°C aging. RDP bentonite still provides a V-0 rating, in spite of a slight increase of the combustion times and occurrence of nonflammable dripping for the material after the second ignition. On the contrary, the VP cocoon 2125 containing sample produces flammable drops and it is consequently classified V-2. It is noteworthy that VP cocoon 2125 dramatically impairs the mechanical properties of PBT/GF since the corresponding specimens were easily breakables (apparent fragility of specimens when breaking them by hand). One may notice that the torque (reciprocal to viscosity) monitored during the extrusion process severely dropped upon introducing the organo-modified kaolinite into the melted polymer. This could eventually results from the chemical interaction between the hydroxyl end surfaces of kaolinite and PBT chains (i.e. hydrolysis, grafting…)[163]. As a consequence, the PBT chains would be shortened which could explain the reduction of the material viscosity (so the increase of dripping) upon flame heating.

The UL94 performances of PBT/GF also depends on the nature of the graphite based fillers under investigation. 3 wt% ES 350 F5 prevents dripping but increases average combustion times, particularly after removal of flame in the first application. The material consequently achieves a V-1 classification after the 2d-25°C aging. At the same aging, V-0 rating is achieved with 3 wt% NordMin 503. The corresponding sample exhibits moderate average combustion times and it partially drops but without ignition of the cotton. The cotton however ignites after the 7d-70°C conditioning, therefore V-2 is obtained, due to the faster and more pronounced dripping of specimens after the second application of the flame. Throughout the test, worm-like microstructures, typical of expanded graphite flakes[164], are observed at the surface of samples containing NordMin 503 and ES 350 F5. NordMin 503 seems to expend more than ES 350 F5 during the fire test, judging by the greater extent of blowing of NordMin 503 specimens compared to the ES 350 F5 containing ones (Figure 48). Furthermore, some apparent holes can be distinguished in the char layer of the NordMin

503 containing material. The conjunction of blowing and holes formation generates some defects at the surface of the burning specimens[165], which could increase the heat flux in the bulk matter, hence favor the material dripping. In contrast, the ES 350 F5 containing bars exhibit a relatively flat surface aspect after the fire test. Since the thermal expansion temperature of ES 350 F5 is close to the processing temperature of PBT, one may reasonably assume that the graphite partly expended during the processing. As a result, the blowing effect that would have been induced by the graphite expansion through exposure of UL94 bar specimens to the flame would be partly lost.

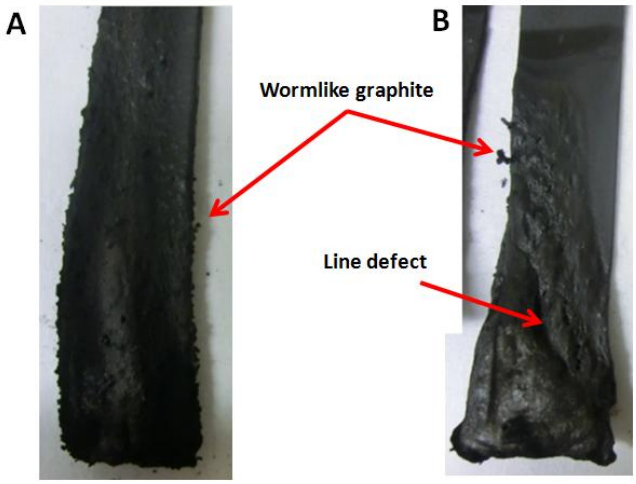

Figure 48 : Pictures of bar specimens after the UL94 test (2d.25°C); (A) OP1240/ES 350 F5 and (B) OP1240/NordMin 503 containing specimens

3 wt% GraphEx leads in some ways to the same performances than with 3 wt% ES 350 F5, providing a V-1 rating after a 2d-25°C aging. The experimental graphene from Ciba indeed prevents dripping of the material but increases its average combustion times.

The substitution of OP1240 by POSS particles somewhat tends to decrease the average combustion times. The samples containing 2 wt% OM-POSS or 2 wt% AEAIP-POSS do not drip after the 2d-25°C conditioning and therefore achieve a V-0 classification. 2 wt% TSP POSS provides a marginal V-0/V-1 rating because one specimen over the five tested exhibits a combustion time above 10s. After the 7d-70°C aging, the OM-POSS containing sample shows drops, but nonflammable ones, which allows maintaining the V-0 classification. On the opposite, inflamed cottons are obtained for the AEAIP-POSS containing sample which finally turns to V-2 rating.

This screening reveals that substitution of relatively small amount of Exolit OP1240 (2-3 wt%) by nano-particles does either not change the UL94 classification of PBT/GF/OP1240 (V-1) or improve it (V-0) after the 2d-25°C ageing. For those formulations which fulfill the V-0 rating at this aging condition, the fire properties worsened at the 7d-70°C ageing - excepted for the RDP bentonite and the OMPOSS containing samples - mostly due to an increase of

specimens dripping and subsequent tendency of drops to inflame the cotton. A full V-0 classification is finally obtained when substituting 2 wt% Exolit OP1240 by RDP bentonite or OMPOSS, while the reference material only reaches V-1 rating.

1.2.2 Exolit OP1200 based combination

The UL94 results obtained for the Exolit OP1200/nano-additives containing samples are summarized in Table 9.

Table 9 : UL94 results obtained for the OP1200/nano-additives containing PBT/GF formulations

Co-additive	Composition (wt%)				UL-94, 0.8 mm bar			
	PBT	GF	OP1200	Co-additive	Conditioning	t1/t2[a] (s)	Dripping[b]	Rating
-	55	25	20	-	2d.25°C	1.6/2.4	N	V-0
-	55	25	20	-	7d.70°C	1.9/1.8	N/D-Y	V-2
Cloisite 30B	55	25	18	2	2d.25°C	1.4/3.2	N	V-0
Cloisite 30B	55	25	18	2	7d.70°C	1.9/6.5	N/D-Y	V-2
RDP Bentonite	55	25	18	2	2d.25°C	2.5/4.4	N	V-0
RDP Bentonite	55	25	18	2	7d.70°C	2.4/1.2	N/D-Y	V-2
VP cocoon 2125	55	25	18	2	2d.25°C	4.4/6.2	N/D-N	V-1
EG-NordMin503	55	25	17	3	2d.25°C	4.5/3.0	N/D-Y	V-2
GraphEx	55	25	17	3	2d.25°C	2.7/4.3	N/D-Y	V-2
OM-POSS	55	25	18	2	2d.25°C	3.5/2.9	N	V-0
OM-POSS	55	25	18	2	7d.70°C	3.0/3.3	N	V-0
AEAIP-POSS	55	25	18	2	2d.25°C	1.9/3.3	N	V-0
AEAIP-POSS	55	25	18	2	7d.70°C	3.0/1.1	N/D-Y	V-2
TSP-POSS	55	25	18	2	2d.25°C	1.4/3.6	N	V-0
TSP-POSS	55	25	18	2	7d.70°C	1.7/1.9	N/D-Y	V-2

[a] *t1 and t2, average combustion times after the first and the second application of the flame*

[b] *dripping after the first and second application of the flame. N = no dripping, D-N = dripping without ignition of cotton, D-Y = dripping with ignition of cotton*

The reference material containing 20 wt% Exolit OP1200 achieves a V-0 classification after the 2d-25°C aging. It exhibits short combustion times after the removal of flame in the first and second applications and shows no dripping. UL94 performances however drastically decrease after the 7d-70°C aging as the tested specimens easily drip and ignite the cotton. A V-2 rating is accordingly achieved.

The substitution of 2 wt% OP1200 by Cloisite 30B and RDP bentonite does not alter the fire properties of the material - even if low increase in combustion times is observed - as the corresponding samples likewise achieve V-0 and V-2 rating respectively after the 2d-25°C and 7d-70°C aging. VP cocoon 2125 is the only organoclay that impairs the UL94 performances of PBT/GF, providing V-1 rating after the 2d-25°C aging. The modified kaolinite noticeably favors the increase of combustion times and promotes dripping of specimens, although drops are nonflammable. Again, the mechanical properties of the

OP1200/modified kaolinite containing material were strongly damaged (apparent fragility of the material upon breaking the bar specimens by hand) due to the shortening of PBT chains induced by the modified kaolinite during the melt extrusion process.

3 wt% of the graphene based fillers Nord-Min 503 and GraphEx have adverse effects on the flammability behavior of the polymer after the 2d-25°C aging. Substitution of OP1200 by these fillers causes flammable dripping during the second ignition. V-2 rating is consequently reached for those materials. The Nord-Min 503 containing sample also displayed the characteristic vermicular microstructures resulting from the expansion of graphite. On the other hand, the combination of GraphEx with OP1200 imparts to the bar specimens a much higher extent of intumescence than with O1P240 (Figure 49). A possible explanation for this could be that the melamine contained in OP1200 inflates the material by partially sublimating and releasing fuel dilution products[39,80]. This blowing effect would be further amplified by the accumulation of graphene particles at the surface of the material.

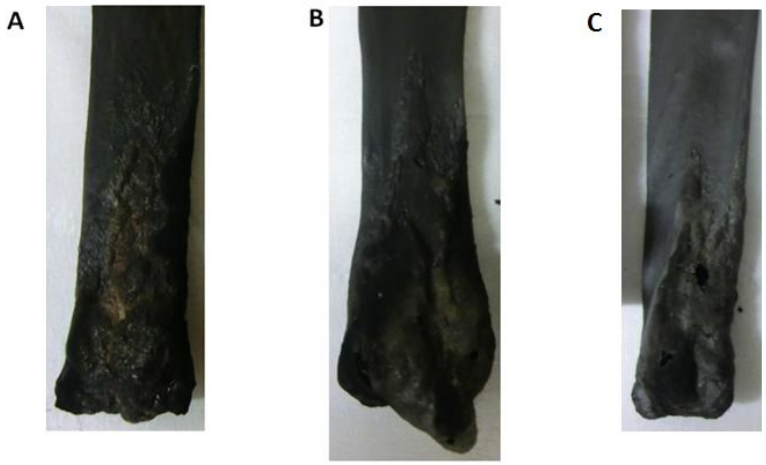

Figure 49 : Pictures of bar specimens after the UL94 test (2d.25°C); (A) OP1200, (B) OP1200/GraphEx (C) OP1240/GraphEx containing specimens

The three POSS particles have almost no influence on the fire properties of PBT/GF after the 2d-25°C aging. After the 7d-70°C aging, the presence of OM-POSS allows improving the UL94 performances of the polymer as it prevents dripping without significantly increasing combustion times of specimens. The OP1200/OM-POSS containing sample thus achieves a full V-0 classification. On the contrary, AEAIP-POSS and TSP-POSS do not help to suppress flammable dripping and the corresponding materials finally reach V-2 rating.

In conclusion, the substitution of Exolit OP1200 by nano-additives does generally not impart to PBT/GF better UL94 classification. The latter is preserved with most of the nano-additives except for the VP Cocoon 2125 and the graphene based fillers (Nord-Min 503 and GraphEx) which damage the fire properties of the material. Exolit OP1200 + OM-POSS was the only one combination capable of providing a V-0 classification after both aging conditions, showing even better performances than the reference sample (V-2 rating).

1.2.3 Conclusion

This screening demonstrates that small amount of nano-additives may have various effects depending on the phosphinate type system (OP1240 or OP1200). The nature of particles (i.e. structure, modifier type, etc) likewise appeared to be an influential criterion to enhance the performances of a single flame retardant system.

It is noteworthy that the reduction of the flammability performances of materials after a 7d-70°C aging was recurrently observed throughout the screening programme. According to some analyses performed at the UMET-ISP laboratory, including Differential Scanning Calorimetry (DSC) and Dynamic Mechanical Analysis (DMA), this phenomenon seems to be related to a rearrangement of the amorphous phases of PBT - which partially crystallize into imperfect crystallites - as the latter undergoes an ageing treatment above its glass transition temperature (50-60°C). To date, no clear correlation between the fire performances of samples and their physical transformation resulting from the 7d-70°C aging was found.

The graphene based fillers globally showed the lowest performances in terms of UL94 classification. These fillers should therefore be abandoned for the rest of the project. Moreover their high electrical conductivity could impair the tracking properties of PBT/GF.

The best performances were obtained by substituting 2 wt% OP1240 or OP1200 by OM-POSS. A V-0 classification was invariably obtained with both combined systems while pure OP1240 and OP1200 respectively provide a V-1 and V-2 classification after the 7d-70°C aging. A major drawback of OM-POSS is its high cost which might entail serious limitation for its commercial application as synergistic agent.

RDP bentonite also showed promising performances since it was found to improve the ranking of PBT/GF when combined with OP1240. No alteration of the UL94 properties of the material was noticed when substituting 2 wt% OP1200 by the organo-modified clay. An interesting feature of RDP bentonite is its cost which is much lower than that of the Exolit. The nano-additive was consequently selected for further optimization and tested in preference to OM-POSS.

2. Optimization and comparative study: Exolit OP1240/RDP bentonite flame retardant combination

The previous screening has revealed that the combination of Exolit OP1240 with RDP bentonite improved UL94 performances for PBT/GF. This part aims at finding the optimum ratio of both additives for which the highest performances would be obtained. The combination of Exolit OP1240 with basic bentonite and/or pure RDP is at last tested so as to determine whether the modification the bentonite clay by RDP provides reliable benefits for the fire properties of the material.

The optimization of the OP1240/RDP bentonite containing formulation was performed using the UL94 method. The formulations were only tested after the 7d-70°C aging, considering that not lower performances would be achieved after the 2d-25°C aging.

2.2 Optimization of the Exolit OP1240/RDP bentonite combination

A V-0 classification could be obtained at both aging conditions with the combination Exolit OP1240/RDP bentonite and Exolit OP1200/OM-POSS. On account of the high cost of OM-POSS, the combination Exolit OP1200/OM-POSS was not further considered for optimization. Focus has therefore been directed on the mixture of OP1240 and RDP bentonite. The UL94 results obtained for the various Exolit OP1240/RDP bentonite containing formulations are summarized in Table 10. Both additives were added up to 20 wt%. The only parameter that varies is the part by weight of Exolit OP1240 relative to that of RDP bentonite in the polymer.

Table 10 : UL94 results obtained for the OP1240/RDP bentonite containing PBT/GF formulations

Co-additive	Composition (wt%)				UL-94, 0.8 mm bar			
	PBT	GF	OP1240	Co-additive	Conditioning	t1/t2[a] (s)	Dripping[b]	Rating
-	55	25	20	-	7d.70°C	5.0/6.1	N/D-N	V-1
RDP Bentonite	55	25	19.5	0.5	7d.70°C	2.4/3.7	N/D-N	V-0
RDP Bentonite	55	25	19	1	7d.70°C	2.7/3.3	N/D-N	V-0
RDP Bentonite	55	25	18	2	7d.70°C	2.8/4.1	N/D-N	V-0
RDP Bentonite	55	25	17	3	7d.70°C	3.3/3.1	N/D-N	V-0
RDP Bentonite	55	25	16	4	7d.70°C	3.9/5.0	N/D-N	V-1
RDP Bentonite	55	25	15	5	7d.70°C	2.5/4.4	N/D-Y	V-2

[a] *t1 and t2, average combustion times after the first and the second application of the flame*

[b] *dripping after the first and second application of the flame. N = no dripping, D-N = dripping without ignition of cotton, D-Y = dripping with ignition of cotton*

It is observed that amount RDP bentonite up to 3 wt% keep giving a V-0 classification to PBT/GF/OP1240 formulation. The presence of the organoclay in a range between 0.5 to 3 wt% markedly helps to reduce the flaming combustion times of bar specimens but does not stop the dripping after the second ignition. Surprisingly, the combustion times of specimens remain relatively comparable whatever the amount of RDP bentonite considered. More surprising is the fact that only 0.5 wt% of RDP bentonite is sufficient to improve the fire properties of the polymer.

With 4 wt% RDP bentonite, the combustion times of specimens tend to increase. The corresponding material finally achieves a V-1 rating as two of the tested specimens burn above 10s. When 5 wt% OP1240 is substituted by the organoclay, the drops produced after the removal of flame in the second ignition are burning, and the material consequently reaches a V-2 rating.

These results allow concluding that, up to 3 wt%, the substitution of OP1240 by RDP bentonite ensures good UL94 performances to reinforced PBT (V-0 rating). The combination of 18 wt% Exolit OP1240 with 2 wt% RDP bentonite was finally established as optimal ratio as it offers a sufficient level of OP1240 substitution and would also authorize some larger deviations of additive contents - regarding the uncertainties in batch processing - without damaging the UL94 performances.

2.3 Comparative study: influence of RDP and non-modified bentonite on the fire properties of PBT/GF

After having defined the optimum ratio of Exolit OP1240 and RDP bentonite, it is important to find out whether the surface modification of the layered clay bentonite by RDP influences the flame retardancy of PBT. Table 11 gathers the UL94 results that have been obtained when combining OP1240 with non-modified bentonite and/or pure RDP.

Table 11 : UL94 results obtained when combining OP1240 with basic bentonite and/or pure RDP

Co-additive	Composition (wt%)				UL-94, 0.8 mm bar			
	PBT	GF	OP1240	Co-additive	Conditioning	t1/t2[a] (s)	Dripping	Rating
-	55	25	20	-	7d.70°C	5.0/6.1	N/D-N	V-1
RDP bentonite	55	25	18	2	7d.70°C	2.8/4.1	N/D-N	V-0
Bentonite	55	25	18	1.7	7d.70°C	12.0/12.5	N	V-1
RDP				0.3				
Bentonite	55	25	18	2	7d.70°C	9.7/15.5	N	V-1
RDP	55	25	19	1	7d.70°C	1.6/3.2	N/D-N	V-0
RDP	55	25	18	2	7d.70°C	2.1/2.6	N/D-N	V-0
RDP	55	25	17	3	7d.70°C	2.1/3.9	N/D-N	V-0
RDP	55	25	16	4	7d.70°C	5.9/4.5	N/D-Y	V-2
RDP	55	25	15	5	7d.70°C	3.2/8.5	N/D-Y	V-2

[a] *t1 and t2, average combustion times after the first and the second application of the flame*

[b] *dripping after the first and second application of the flame. N = no dripping, D-N = dripping without ignition of cotton, D-Y = dripping with ignition of cotton*

It is first to be noticed that the combination of 18 wt% OP1240 with 1.7 wt% basic bentonite and 0.3 wt% pure RDP - analogous amounts of bentonite and RDP contained in 2 wt% RDP bentonite - gives a V-1 classification to PBT/GF as a consequence of a substantial increase of the combustion times of specimens after both ignitions. Surprisingly, the material shows no dripping even though it was conditioned 7 days at 70°C prior to the test. The 2 wt% non organomodified bentonite containing sample achieves very similar performances, which demonstrates that the non-modified clay is the substance to be responsible for the strong increase of the combustion times and the anti-dripping effect. On the other hand, the substitution of OP1240 by 1 to 3 wt% pure RDP gives V-0 rating as it particularly confers short burning times to bar specimens. The burning times however increase with increasing

amount of RDP from 4 wt% to 5 wt%. At those contents, the material shows flammable drops and it is therefore classified V-2.

This study demonstrates that the modification of bentonite by RDP has a notable influence on the fire properties of PBT/GF. It indeed prevents an increase of the combustion times of specimens, which would normally be obtained in presence of the non-modified clay. Basic bentonite also exhibits anti-dripping properties that vanish when the clay is surface treated with the arylphosphtate oligomer. One may consider that dripping, when not flammable, is an advantage as it may drain off calories from the burning material and thus reduce combustion times. However, for all of the investigated samples, dripping does not occur after the first ignition. So the high combustion times of basic bentonite containing samples after the first ignition prove that the non-modified clay itself provides high intrinsic flammability to the material. On the other hand, RDP alone shows comparable properties to that of RDP bentonite, but the former may bloom out from the polymer which raises some concerns for the long term use of PBT/GF items. Pure RDP should therefore be avoided.

2.4 Conclusion

This part of the study showed that substitution of OP1240 by 0.5 to 3 wt% RDP bentonite improved the UL94 performances of PBT/GF. The combination of 18 wt% OP1240 and 2 wt% RDP bentonite has finally been defined as the optimal ratio to be incorporated in the reinforced polymer. The comparative study pointed out that the modification of bentonite by RDP was crucial to comply with the fire test requirements (V-0 rating). On the other hand, it was found that a “catalytic” amount of RDP bentonite (0.5 wt%) could be sufficient to enhance the flammability behavior of the polymer.

The upcoming part intends to fill out the characterization of the optimized formulation more completely through using other fire test scenarios (LOI, Mass Loss Calorimeter).

3. Investigation of the fire properties of the Exolit OP1240/RDP bentonite containing formulation (optimized) through the Limiting Oxygen Index (LOI) and Mass Loss Calorimeter (MLC) tests

Fire properties of the OP1240 (20 wt%) and OP1240/RDP bentonite (18 wt%/2 wt%) containing materials are evaluated thought the Limiting Oxygen Index (LOI) and the Mass Loss Calorimeter (MLC) tests. Since these two bench-scale tests involve different flame constraints (flame ignition of the material by the top for LOI and radiative heating for MLC) in comparison to UL94, they are important tools to fully characterize the performances of the OP1240/RDP bentonite system. LOI values and MLC data of both formulations are summarized in Table 12. Neat PBT/GF (75 wt%/25 wt%) was also tested for the sake of comparison. The heat release rate (HRR) and total heat release (THR) curves obtained in MLC are further depicted in Figure 50.

The incorporation of 20 wt% OP1240 in PBT/GF results in an increase of the LOI value from 19 to 42 Vol% (Table 12). This is in total agreement with data reported in the literature[141]. When substituting 2 wt% OP1240 by RDP bentonite, the LOI decreases from 42 to 41, which does not appear significant with respect to the margin of error of the measurement.

Table 12 : LOI and Mass Loss Calorimeter data of neat PBT/GF and flame retarded PBT/GF formulations (margin of error for pHRR, TTI and THR: 10%)

Composition	LOI (Vol%)	Mass loss (50 kw/m^2)			
		pHRR (kW/m^2)	TTI (s)	THR (MJ/m^2)	RY (%)
PBT + 25wt% GF	19 ± 1	332 ± 33	70 ± 7	41 ± 4	32.7 ± 0.3
+ 20wt% OP1240	42 ± 1	147 ± 15	60 ± 6	31 ± 3	39.4 ± 0.5
+ 18wt% OP1240 + 2wt% RDP bentonite	41 ± 1	107 ± 11	57 ± 6	26 ± 3	41.6 ± 0.3

pHRR : peak Heat Release Rate; TTI: time to ignition; THR: Total Heat Release; RY: Residue Yield

In mass loss calorimeter, neat PBT/GF exhibits a time to ignition of 70s. The HRR curve of the non-flame retarded polymer presents an initial sharp maximum of 332 kW/m^2 at 119s, followed by a sudden decrease to 50 kW/m^2 after 230s due to the formation of a surface barrier by the accumulation of glass fibers[41]. The HRR then gradually decreases between 230s and 550s.

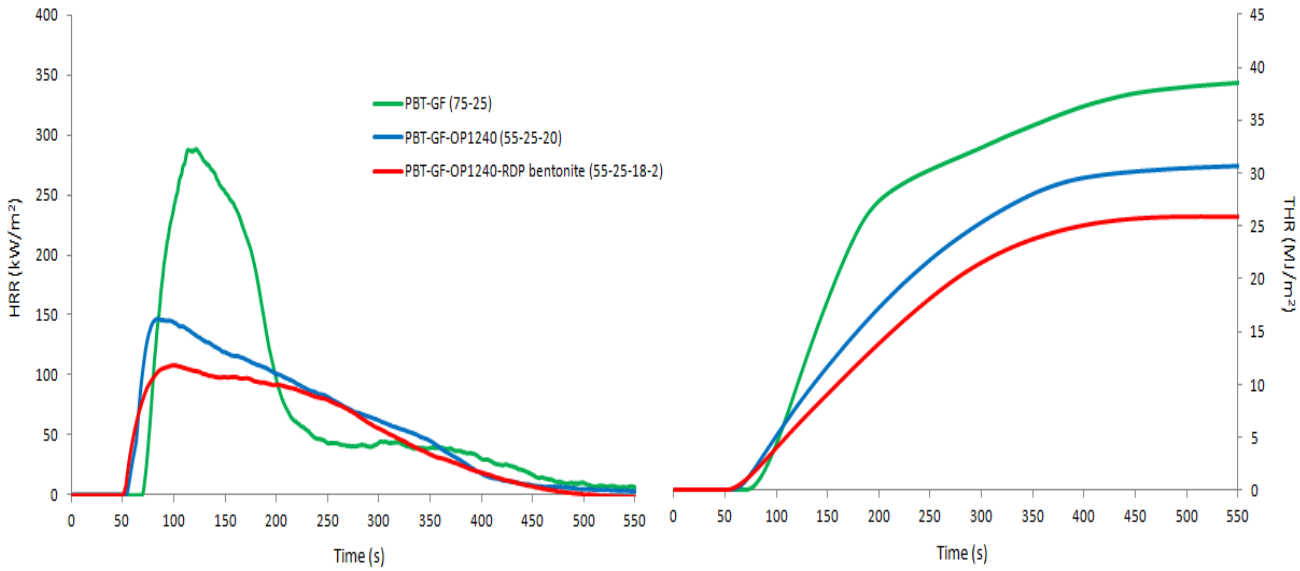

Figure 50 : HRR and THR curves of neat PBT/GF (green), PBT/GF/20wt%OP1240 (blue) and PBT/GF/18wt%OP1240/2wt%RDP bentonite (red)

Incorporation of 20 wt% OP1240 to the reinforced PBT leads to a slight decrease of the time to ignition (from 70s to 60s), while the peak HRR is strongly reduced by 56%. The peak HRR of the flame retarded sample (147 kW/m^2) is rapidly attained after 88s and HRR then

progressively decreases to 500s. The THR is reduced by 24% (decrease from 41 to 31 MJ/m^2). Such reduction of the pHRR and THR values are consistent with data of the literature[141,166]. The presence of RDP bentonite further improves the HRR profile of the material. Whereas the substitution of OP1240 by RDP bentonite does not significantly alter the time to ignition, it brings about a reduction of the peak HRR from 147 to 107 kW/m^2 (-27%) as well as a reduction of the THR from 31 to 26 MJ/m^2 (-16%).

At flame-out, the residue of PBT/GF consists in a loose network of glass fibers without almost any char remaining. That of both flame retarded materials is constituted of swollen char composites of strong consistency (Figure 51).

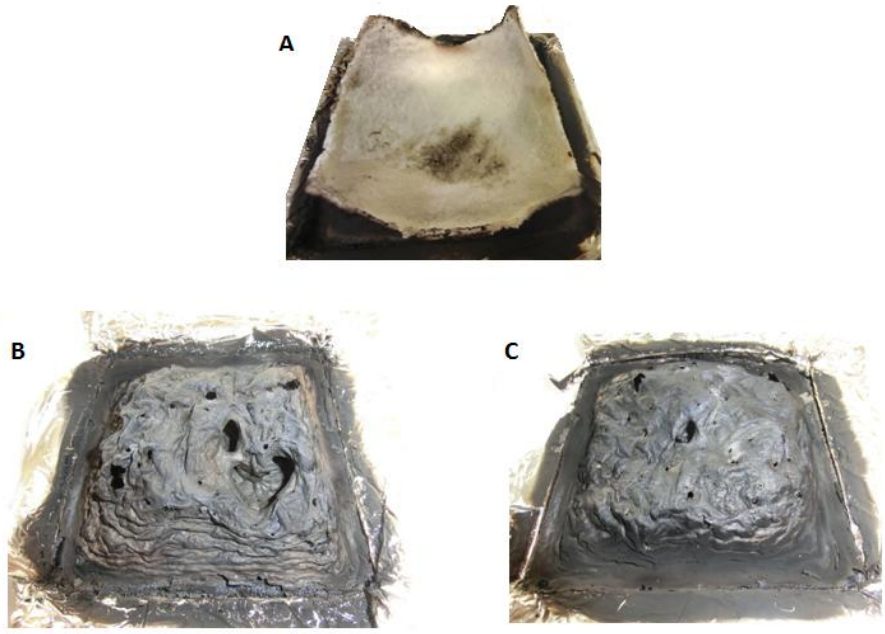

Figure 51 : Pictures of residue samples collected after the Mass Loss Calorimeter test; PBT/GF (A), PBT/GF/20wt%OP1240 (B), PBT/GF/18wt%OP1240/2wt%RDP bentonite (C)

According to Table 12, the presence of the flame retardant systems in the polymer allows increasing the char yield from 7 to 9 wt%. Comparable increases were observed by Braun et al[141]. They were attributed to the char promoting properties of the flame retardant systems. The blowing of the flame retarded samples provides further evidence that a cohesive char is formed acting as a surface barrier and taking part in the reduction of the HRR and flame spread. The residue of the 20 wt% OP1240 containing material has an irregular aspect and it presents some big size holes. That of the RDP bentonite containing sample seems smoother and it presents fewer and smaller holes. Furthermore, Table 12 shows that the substitution of OP1240 by RDP bentonite results in a 2.2 wt% increase of the residue weight fraction compare to the 20 wt% OP1240 containing PBT/GF sample which should mainly accounts for the portion of inert clay (≈ 1.7 wt%). It is well established that nanoclays alone enhance the fire performances of polymers in cone calorimetry (notably the pHRR) as they migrate at the surface of materials and form (or else reinforce) a protective shield reducing the diffusion of

combustible products in the gas phase[114-116]. One can assume that RDP bentonite would act in a similar way provided that the substitution of OP1240 by RDP bentonite improves the MLC parameters of PBT/GF (especially the pHRR) and that the surface aspect of the residue of the OP1240/RDP bentonite containing sample seems more homogeneous and cohesive than that of the OP1240 containing one. With the presence of flame retardants and glass fibers, however, phenomena could be more complex. Yet Samyn[167], while investigating the combination of aluminum diethylphosphinate Exolit OP1230 and the organoclay cloisite 30B in PA 6, showed that no interaction occurred between the two additives during the thermal degradation. Therefore, the assumption that RDP bentonite would migrate and form a protective barrier remains pausible.

4. Conclusion

In this chapter, a first approach has been explored to develop a novel flame retarded GF (25 wt%) - PBT formulation. Two commercial phosphinate type systems - Exolit O1P240 and Exolit OP1200 - were investigated in combination with various nano-particles, namely organo-modified clays, POSS and graphene based particles.

The screening campaign, implemented through using the UL94 testing method, showed that the performances achieved by the tested formulations were contingent on the type of phosphinate systems and nano-particles. Among nano-particles, the Octamethyl-POSS (OM-POSS) and Resorcinol Bis(Diphenyl Phosphate) modified bentonite (RDP bentonite) were both found to improve the UL94 ranking of the reinforced PBT at loading of 2 wt% in substitution of OP1240, while the enhancement of the UL94 performances of the OP1200 containing PBT/GF sample could be obtained only with OM-POSS. Finally, RDP bentonite was chosen for further investigation in preference to OM-POSS since this latter is particularly expensive.

The following study focused on the OP1240/RDP bentonite flame retardant combination as promising alternative to the sole use of Exolit O1P240. An optimization campaign showed that the substitution of 0.5 to 3 wt% OP1240 (initially at loading of 20 wt%) by RDP bentonite allowed to upgrade the UL94 performances of the reinforced polymer to a V-0 classification after 7d-70°C aging being in compliance with the requirements. A comparative study demonstrated that the modification of the bentonite clay by RDP was indispensable to promote such enhancement. It was finally determined that the optimum amounts of OP1240 and RDP bentonite to be incorporated in the polymer would be respectively of 18 wt% and 2 wt%.

Compared to 20 wt% OP1240, the combination of 18 wt% OP1240 and 2 wt% RDP bentonite neither is beneficial nor is detrimental to the polymer through the LOI test. Better performances were however obtained in Mass Loss Calorimeter as the substitution of the

Exolit by the organo-modified bentonite resulted in the reduction of the pHRR and THR of the polymer from 27% and 16% respectively.

Through this first approach, the industrial challenge was finally achieved: developing a novel PBT/GF formulation (55 wt% PBT/25 wt% GF/18 wt% OP1240/2 wt% RDP bentonite) with improved flame retardant properties. A next step could consist of investigating the flame retardant mode of action of the Exolit OP1240/RDP bentonite combination in reinforced PBT to elucidate the type of interactions occurring between both additives or between the additives and the polymer during the burning process.

The next chapter (chapter 4) deals with the synthesis of a variety of phosphinate based salts for flame retardancy applications in PBT/GF. This study falls within the framework for the second approach of this project consisting in developing a novel flame retarded PBT/GF formulation using self-synthesized phosphinate type systems.

CHAPTER 4 – DEVELOPMENT OF A NOVEL FLAME RETARDED PBT/GF FORMULATION BASED ON SELF-SYNTHESIZED PHOSPHINATE SALTS

The previous chapter (chapter 3) dealt with the improvement of the flame retardant properties of PBT through combining commercial phosphinate salts with nano-particles. The fire behavior of PBT could successfully be enhanced by substituting a small quantity of aluminum diethylphosphinate (Exolit OP1240) by the organoclay RDP bentonite. The objectives of our first strategy have thus been achieved.

Phosphinate salts remain a valuable choice for the flame retardancy of PBT. It is logical to inquire what are the most appropriated phosphinates (in terms of chemical structure) to afford to the polymer outstanding flame retardant properties. The prior art (chapter 1) provided some clues about the FR performances of a multitude of phosphinate based products. However, there still are untapped routes in the research of efficient flame retardants of this type for PBT. Our second approach therefore intends to explore one of these routes. In this respect, the present chapter sets out to describe the synthesis of novel phosphinate salts and to study their fire performance in glass reinforced PBT.

A convenient way to synthesize novel phosphinate salts modeled on the chemical structure of the Clariant's products (diethyl phosphinate salts) was by using the oxaphophoslane oxide Exolit PE110. Through reacting this latter with nucleophilic reagents it is possible to design manifold phosphinic acids that can be afterward transformed into salts. Interestingly, it appeared that some phosphinate salts from this category were not fully explored for flame retardancy applications in PBT. This raises obvious questions: would these phosphinates salts bring better FR performances than the Clariant's phosphinates currently available on the market? If not, can we improve the FR performances of these novel phosphinate salts by combining them with other substances or synergists? We will attempt to answer these questions in the present chapter.

The first part of this chapter describes the preparation of the phosphinate salts. The syntheses are performed in a two step process. In the first step, nucleophilic reagents, namely 2,4,6-trioxa-1-phosphabicyclo[2,2,2]octane-4-methanol (PEPA) and various amines (aniline, benzyl amine, phenylene diamine, piperazine and ethylene diamine), are reacted with Exolit PE110 to give a series of products derived from ethyl methyl phosphinic acid. In the second step, the phosphinic acid derivatives are converted into phosphinate salts. The purities and thermal stabilities of the novel phosphinate salts will be discussed.

The second part of this chapter aims at investigating the flame retardancy performances of the novel phosphinates salts in reinforced PBT. Fire tests were performed throught using the UL94 method and the Limiting Oxygen Index (LOI). The phosphinates salts that showed the highest fireproofing performances are at last optimized (research of optimum ratios in the polymer) and tested in combination with traditional flame retardants or synergists (including OM-POSS and RDP bentonite) in order to design high-performing flame retardant systems.

1. Synthesis and characterization of novel phosphinate salts

This part is dedicated to the synthesis of the novel phosphinate salts that will be used to flame retard PBT/GF. The synthesis methods as well as the purity of the products are discussed. The first step (1) and second step (2) of syntheses - respectively synthesis of phosphinic acids (1) and conversion of phosphinic acids into salts (2) - are described in two distinctive sections. Through elemental and solid state NMR analyses, a particular effort is made to fully characterize the phosphinate salts. At last, the thermal stability of the salts is investigated. It is important to explain the motivations that led us to choose the raw materials. That is the purpose of the following section.

1.1 Survey: selection of the raw materials

The synthesis of novel phosphinate salts, as part of the strategy of this PhD project, is not an easy task since numerous structures have already been investigated and are yet extensively related in patents[77-79,168-171].

A convenient way to develop novel phosphinate salts was nonetheless found which consisted in using the 2-methyl-2,5-dioxo-1,2-oxaphospholane (Exolit PE110). Several patents have already referred to this substance as raw material for the synthesis of phosphinic acids and their corresponding salts[109-112]. The synthesis of the phosphinic acids especially involves a single "condensation" of the phospholane oxide with nucleophilic alcohol or amine reagents (Figure 52).

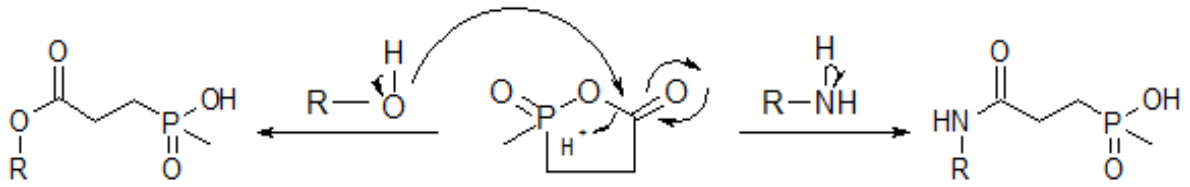

Figure 52 : "Condensation" of Exolit PE110 with nucleophilic alcohol or amine reagents

Whereas the salts of phosphinic acids derived from the reaction of Exolit PE110 with conventional alcohols were lately patented by Clariant[112] and proved to be effective in PBT, we found so far no evidence relating to the synthesis and fire performances of similar phosphinate salts derived from reaction of Exolit PE110 with non-halogenated amine reagents. From these observations, it has been undertaken the synthesis of a series of phosphinates salts by first reacting Exolit PE110 with different varieties of (di)amines as well as one non-conventional alcohol (PEPA), secondly by converting the resulting phosphinic acids into phosphinate salts (Figure 53).

The nucleophilic reagents to be reacted with Exolit PE110 were chosen mainly for three reasons. The first one is that some of these reagents, namely piperazine, ethylene diamine

and m-phenylene diamine, have already been employed for the preparation of nitrogen containing diphosphinic acids.

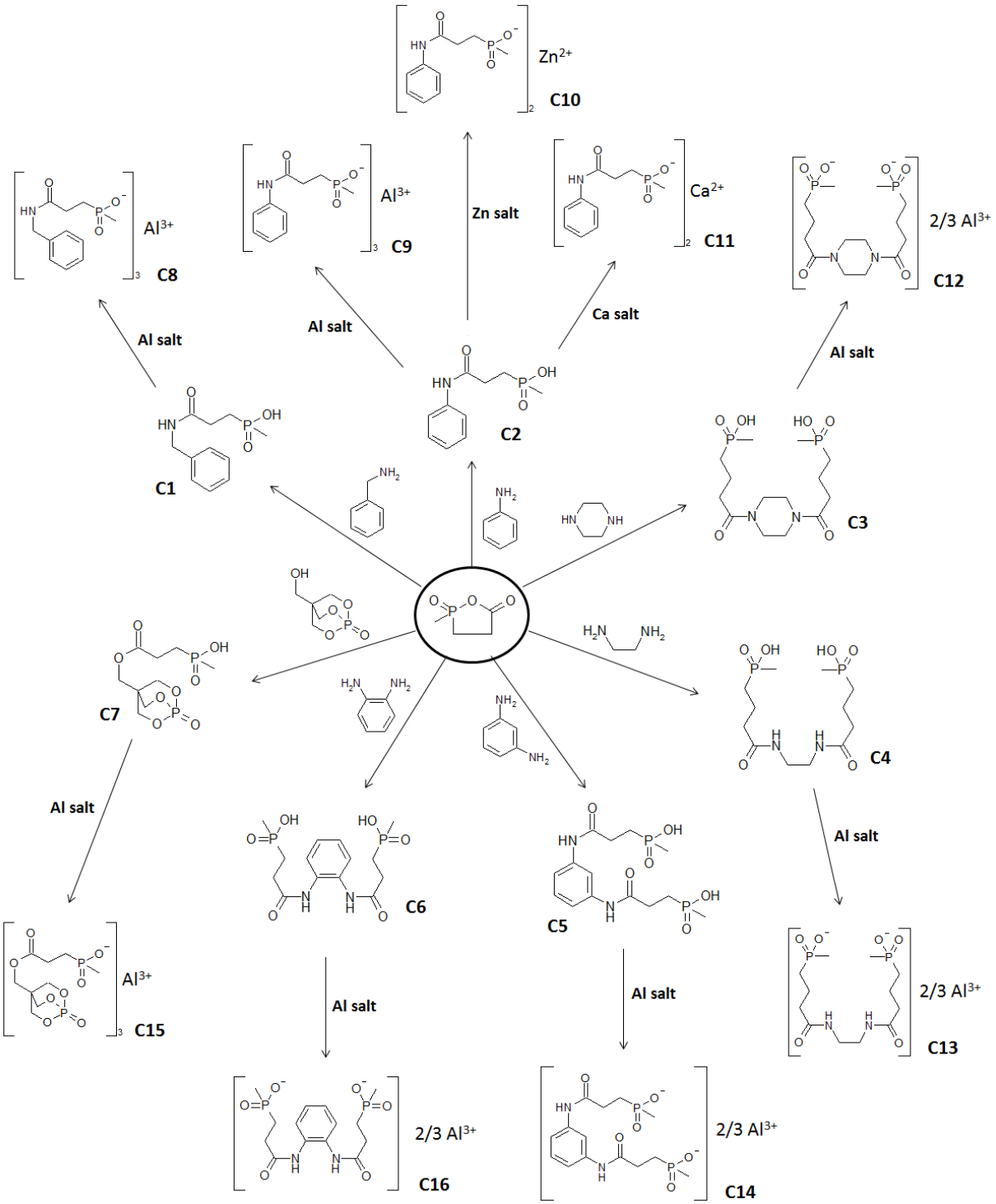

Figure 53 : Synthesis scheme of various phosphinate salts

These diphosphinic acids, whose syntheses are reported by Blöcker in a patent assigned to Hoechst[111], were claimed to provide V-0 rating (1.6 mm) to PBT/GF at loading between 11 and 15 wt%. On account of their symmetrical structure, these diphosphinic acids exhibit

relatively high thermal stabilities which allow them to be processed with PBT without significant degradation. Nevertheless, the acidic functional group of these flame retardants should have a negative effect on the integrity of the polyester chain structure. In our opinion, this shortcoming can be overcome by neutralization of the acid radical with metal cations. On the other hand, the salts would exhibit higher thermal stabilities as compared to the acids[110].

Nucleophilic reagents such as o-phenylene diamine, aniline or benzyl amine got secondly selected for the sake of comparison. Indeed, to what extent would the thermal stability and effectiveness of the phosphinate salts be affected when using a phenylene diamine derivative with an amine group in ortho-position or when using mono-functional arylamines? Again, what would be the influence of reducing the phosphorus rate of the flame retardants on their respective effectiveness in the polymer (e.g. P% = phenylene diamine based salts > aniline based salts > benzyl amine based salts)?

PEPA was selected as it is a well-known charring agent that has been particularly used in intumescent systems[172-175]. It is believed that the covalent grafting of PEPA on the phosphinate residue could somewhat promote the PBT charring during the burning process, so favor a condensed phase mechanism. This may perhaps operate as a supplement to the gas phase mode of action of the alkylphosphinate moiety which should normally prevail in the polyester[39,80].

The preferred metal cation for the neutralization of the P-OH acid functionality was the aluminum as it was clearly demonstrated that aluminum salts are more effective than other metal salts in PBT[80]. It will be shown later in this chapter that the aluminum salt of the aniline based phosphinate (**C9**, Figure 53) provides the best performances among the synthesized products. As a consequence, the zinc and calcium salts of the same phosphinate (**C10** and **C11** respectively) were also prepared to draw a comparison with their analogous aluminum salt.

1.2 Synthesis and characterization of phosphinic acids

Here are described the syntheses of the phosphinic acids from the oxaphospholane oxide Exolit PE110. Since the PEPA based phosphinic acid (**C15**) was prepared through a different synthesis route in comparison to that of the amine based products, it will be the subject of a specific section in this part.

1.2.1 Syntheses involving amine reagents

The syntheses of the amine based phosphinic acids were principally performed following the Blöcker's procedures[111]. In most case, DMF was used as solvent and the mixtures were heated for 3-4 hours at 100-110°C Table 13.

Table 13 : Synthesis of amine based phosphinic acids

Amine reagent (product)	Equivalent to Exolit PE110	Solvent	Temperature (°C)	Time (h)	Purification method	Product Yield (%)
Benzyl amine **(C1)**	1	ACN	80	4	Filtration, washing with acetonitrile	96.7
Aniline **(C2)**	1	DMF	100	4	Recrystallization in acetonitrile	86.7
Piperazine **(C3)**	0.5	DMF	110	4	Filtration, washing with methanol	95.9
Ethylene diamine **(C4)**	0.5	DMF	110	3	Filtration, washing with methanol	91.3
m-phenylene diamine **(C5)**	0.5	DMF	110	4	Filtration, washing with methanol	89.4
o-phenylene diamine **(C6)**	0.5	DMF	110	4	Recrystallization in methanol (x2)	25.5

On account of its relatively high toxicity, DMF is usually not the preferred solvent for industrial syntheses, however it appeared to be very convenient for the syntheses of the diphosphinic acids **C3**, **C4** and **C5** because these latter readily precipitate from the solution after their formation. On the other hand, the addition of Exolit PE110 to the solution of amines in DMF (or counterwise) had to be carefully monitored as a safety measure due to the strong exothermic feature of reactions. This was particularly true for the syntheses involving piperazine and ethylene diamine since the resulting phosphinic acids (**C3** and **C4** respectively) precipitated almost instantly during the addition step. Contrary to the other diphosphinic acids, the o-phenylene diamine based diphosphinic acid **C6** did not precipitated out from the DMF solution. The ^{1}H NMR analysis of the crude product from this synthesis (Figure 54) shows that Exolit PE110 reacts incompletely with o-phenylene diamine as **C6** is obtained together with fraction of mono-functionalized phosphinate intermediate and unreacted phospholane. The reaction was less favorable due to the too close proximity of the amino groups of o-phenylene diamine that would have cause an effect of steric congestion. Finally, **C6** was obtained in low yield (25.5%) because it was only partially recovered after two recrystallizations in methanol.

The synthesis of the benzyl amine based phosphinic acid **C1** was carried out using another solvent, namely acetonitrile. For this particular reaction, acetonitrile was suitable because **C1** precipitates from the solution after partial conversion of the reactants. The diphosphinic acids **C3**, **C4**, **C5** and **C6** would surely not have been obtained in acetonitrile if one considers

that the mono-functionalized diamine intermediates would have precipitated before functionalization of the second free amine group.

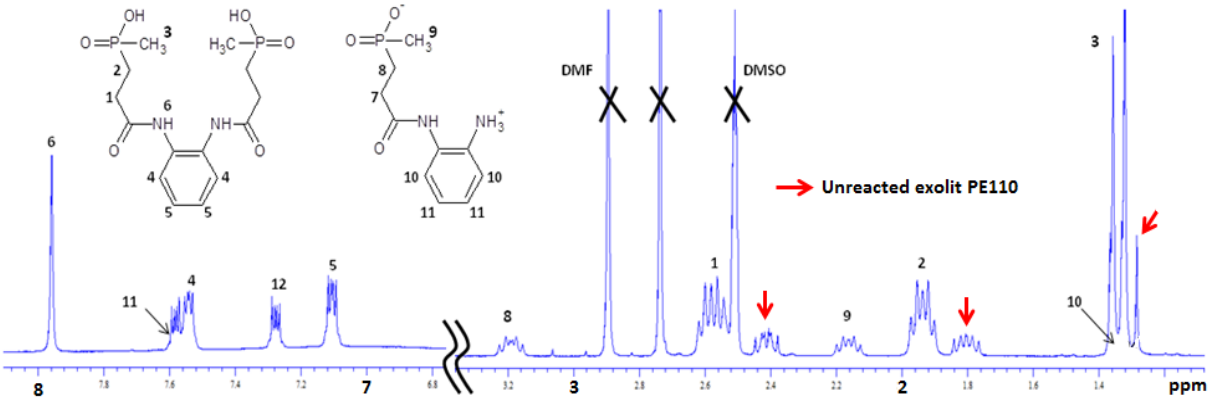

Figure 54 : ^{1}H NMR spectrum of the crude product from the C6 synthesis (in DMSO-d$_6$)

The phosphinic acid **C2**, prepared from the mono-functional aniline, was synthesized in DMF. Indeed, aniline exhibits lower reactivity compared to benzyl amine due to the fact that the lone pair of electrons on the aniline nitrogen atom is delocalized on the aromatic ring. DMF was therefore preferred in this case because it allowed one to apply a more elevated temperature, hence to provide further energy to the reaction and to ensure a better reactivity of aniline toward Exolit PE110. The purification of **C2** afterward required to evaporate DMF, then to recrystallize the final product in acetonitrile.

The whole phosphinic acids were globally afforded in good yields and purities. ^{1}H, ^{13}C and ^{31}P spectra of the products are reported in Appendix 1. Regarding compounds **C1** and **C4**, the ^{31}P (^{1}H coupling) NMR analysis undeniably proves that this is the phosphinic acid derivative which is obtained and not the phosphinamide derivative as one might suspect (Figure 55). As illustrated in Figure 56, the ^{31}P NMR spectrum of **C1** exhibits a sextuplet centered at 46.6 ppm whose pattern stems from the spin-spin coupling (^{2}J) between the phosphorus and the alpha-protons (-C**H**$_2^{\alpha}$-**P**(OOH)-C**H**$_3^{\alpha}$). Each of the peaks of the sextuplet shows splitting and broadening due to a further coupling between phosphorus and the beta-protons (-C**H**$_2^{\beta}$-CH$_2$-**P**(OOH)-CH$_3$).

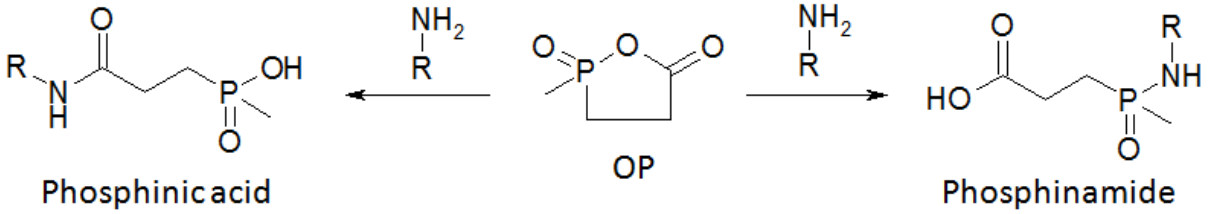

Figure 55 : Potential reactivity of oxaphospholane oxide with nucleophilic reagents

If the amine reagent had preferentially reacted on the phosphonyl function of Exolit PE110, the phosphorus peak of **C1** would have been otherwise much more complex. Indeed, an

additional splitting would have come out from the coupling of phosphorus with the N-H and CH_2 protons of the amine residue (-**P**(O)-N**H**-C**H$_2$**-C_6H_5)[176,177]. The signals of these protons would have been themselves splitted in ^{1}H NMR. Regarding compounds **C2**, **C5** and **C6**, the evidence of the reaction of amine groups on the carbonyl function of Exolit PE110 is brought out by ^{1}H NMR and ^{13}C NMR analyses[178,179] for the N-H protons and the aromatic carbons of these products show up as singlets and not doublets.

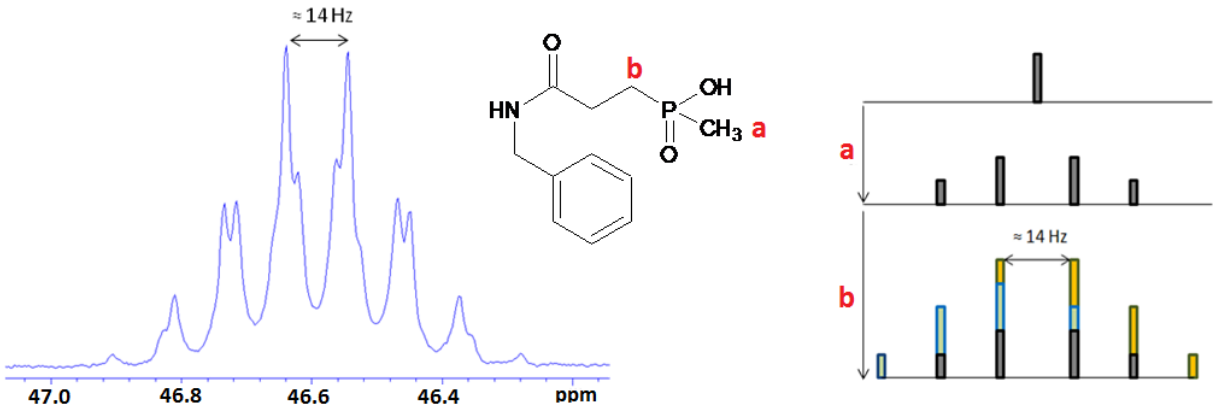

Figure 56 : ^{31}P NMR spectrum of C1 (in DMSO-d$_6$) with schematic representation of the coupling between phosphorus and alpha protons.

It is noteworthy that the ^{31}P (^{1}H coupling) NMR signal of the piperazine based diphosphinic acid **C3** exhibits a higher multiplicity than that of the other products (Figure 57). With ^{1}H decoupling, **C3** presents two symmetrical ^{31}P signals distant from about 0.1 ppm, whereas the other products show only one peak.

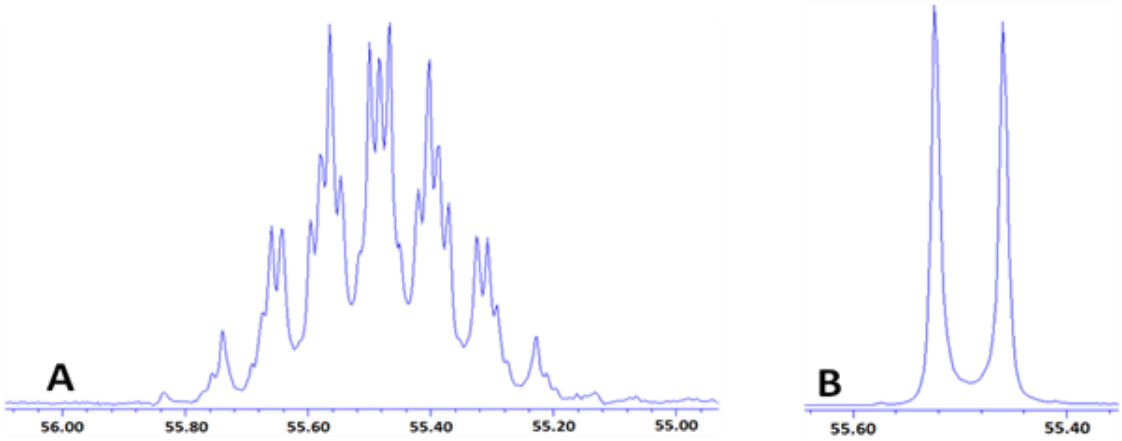

Figure 57 : ^{31}P NMR spectrum of C3 (in D_2O): (A) ^{1}H coupling; (B) ^{1}H decoupling

The two ^{31}P peaks of **C3** were ascribed to each of the phosphorus of the product. It means that these phosphorus have different chemical environments. This unexpected multiplicity can still be observed on the ^{13}C (^{1}H decoupling) NMR spectrum of **C3** (Appendix 1) by the duplication of the peaks assigned to the carbon amide and the CH_2 carbons of the piperazine residue. In ^{1}H NMR, CH_2 protons of the piperazine residue show up as a multiplet (≈

quadruplet) which contrasts with the singlet normally found for piperazine based compounds with a symmetrical structure[180-182]. It is thus assumed that **C3** adopts a preferential conformation in solution which generates an asymmetric environment around its structure. This favored conformation is very likely to be explained by the restrained mobility of the piperazine cycle, the restricted rotation of the amide bonds and/or the steric congestion effects engaging the bulky alkylphosphinate moieties.

1.2.2 Synthesis involving PEPA

Few publications[107,108] have reported that the reaction of alcohols on Exolit PE110 leads to the formation of the phosphinic ester derivatives owing to the preferential attack of hydroxyl groups on the phosphonyl function of the phospholane. A Clariant patent[112] discloses that phosphinic acid derivatives could be obtained by simply mixing an equimolar ratio of the phospholane and alcohols in solution but it implies long reaction times and the products are sometimes obtained in low yields. As an illustration, stirring benzyl alcohol with Exolit PE110 (solvent not specified) for a period of time of 70h at 60°C would afford the corresponding phosphinic acid in 49% yield. In order to explore further the reactivity of Exolit PE110, the synthesis with benzyl alcohol was reproduced in chloroform (bp ≈ 60°C) with lower reaction time (4h). Moreover, for the sake of comparison, the reaction was also performed in DMF at 100°C (Figure 58). For both reactions, the ^{1}H NMR spectra of the crude products show an almost complete conversion of the reactants with exclusive formation of the phosphinic ester derivative (Figure 59, reaction performed in $CHCl_3$). Such formation is particularly evidenced by the coupling of the CH_2 protons of the benzyl alcohol residue (doublet at 5.05 ppm) with phosphorus and the subsequent high multiplicity of the ^{31}P NMR signal of products. Then, the synthesis of the PEPA based phosphinic acid **C7** from PEPA and Exolit PE110 was attempted in DMF following the above-mentioned procedure but, again, the phosphinic ester derivative was obtained instead of the desired phosphinic acid (Figure 58).

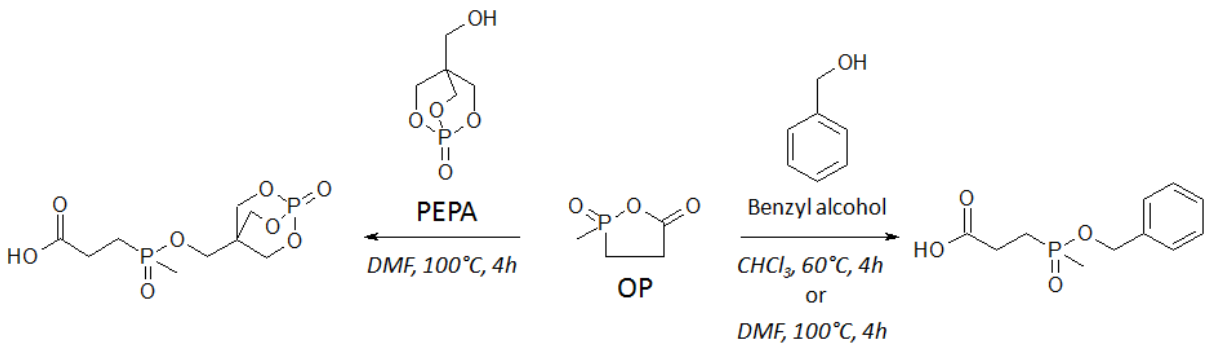

Figure 58 : Reactivity of oxaphospholane oxide with PEPA and benzyl alcohol

These experiments demonstrate that the short-term reaction between Exolit PE110 and an alcohol does not provide the phosphinic acid. The latter would only be obtained after long reaction times, according to the Clariant patent. It indicates that formation of the phosphinic

ester derivative is kinetically favored. Having regard to that fact that the reaction is reversible, the phosphinic acid derivative, as thermodynamic product, would accumulate in the bulk synthesis over time.

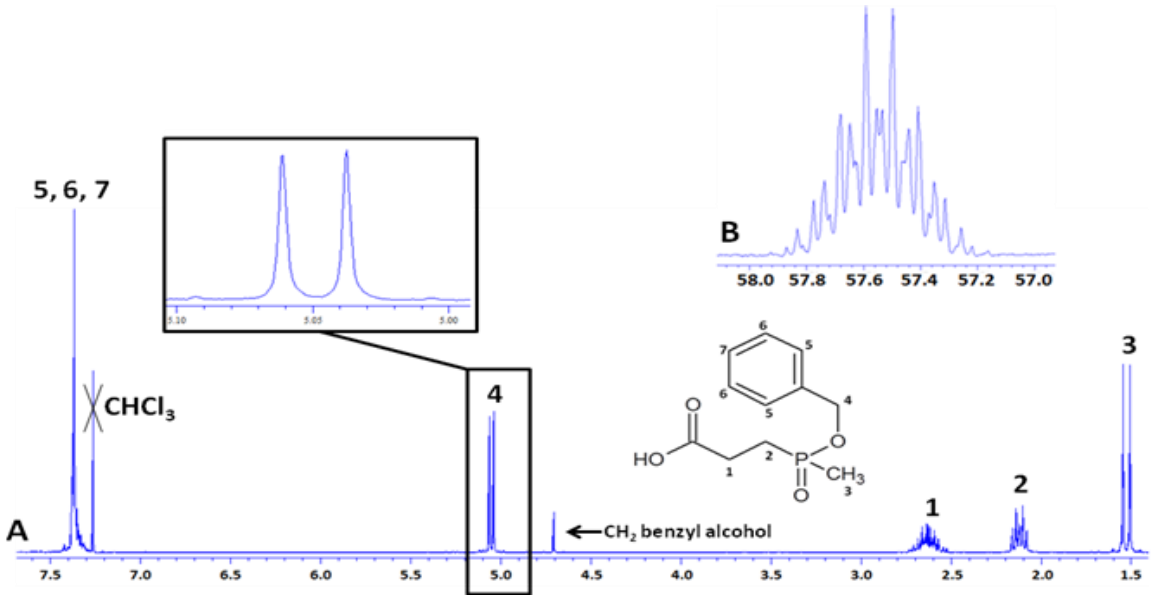

Figure 59 : Crude product from the reaction between exolit PE110 and benzyl alcohol operated in $CHCl_3$: (A) ^{1}H NMR; (B) ^{31}P NMR - ^{1}H coupling (in $CDCl_3$)

In order to obtain **C7** with appreciable yield, another route was investigated involving the condensation between PEPA and the hydrolyzed form of Exolit PE110 (2-carboxyethyl(methyl)phosphinic acid) via a Fischer type esterification. The reaction should be performed by using a Dean Stark trap to remove the water resulting from the esterification, and thus to favor the quantitative production of the esterified product. The success of this reaction is based on the assumption that if the PEPA based phosphinic acid derivative is the thermodynamic product, it would be more largely obtained than the phosphinic ester derivative owing to the reversible feature of Fischer esterifications[183].

Prior to the esterification, it was necessary to hydrolyze Exolit PE110. This reaction is simply performed by stirring a solution of the phospholane in demineralized water at 70°C. The hydrolyzed phospholane is obtained in 100% yield.

The esterification of hydrolyzed phospholane with benzyl alcohol was carried out as a first trial. The reaction was performed in refluxing toluene, for 20h, using a large excess of benzyl alcohol and a catalytic amount of p-toluenesulfonic acid. The ^{1}H NMR spectrum of the resulting crude product (Figure 60) reveals that the desired phosphinic acid (**C7'**) is effectively obtained along with two byproducts, namely dibenzyl ether and the benzyl phospho-ester derivative of **C7'**. These two byproducts, which respectively stem from the further esterification of the phospho-acid function of **C7'** and the dimerization of benzyl alcohol (Figure 61), are obtained in relatively significant percentages. Their formation was

believed to be due to a too large excess of alcohol associated to a too strong acidity of the bulk reaction.

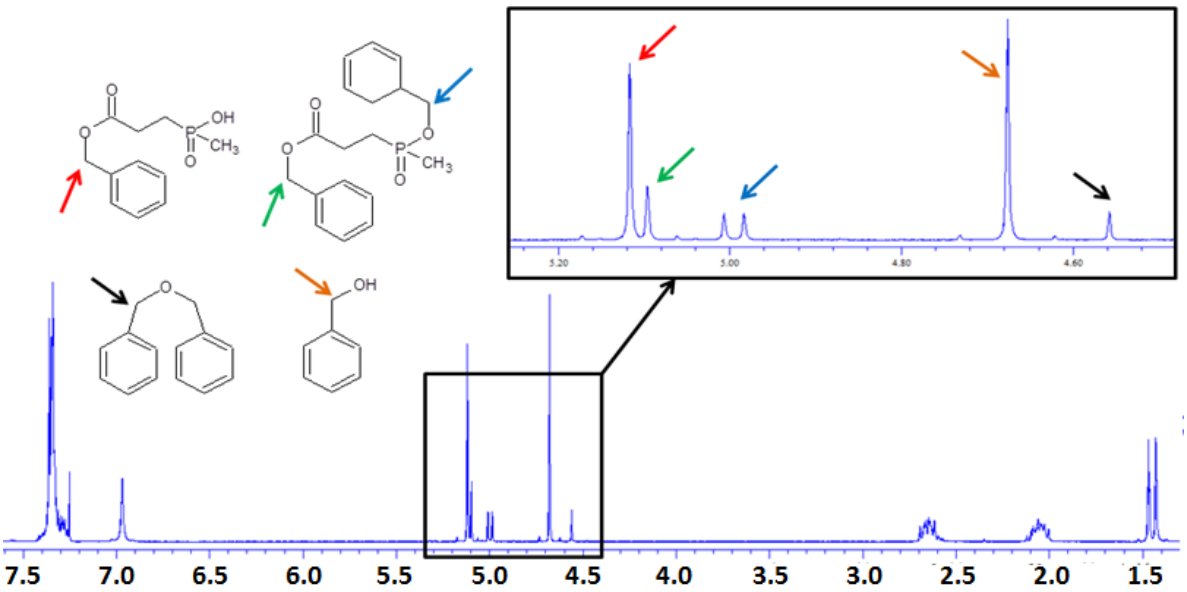

Figure 60 : ^{1}H NMR spectrum of the crude product from the esterification of hydrolyzed phospholane with benzyl alcohol (in $CDCl_3$)

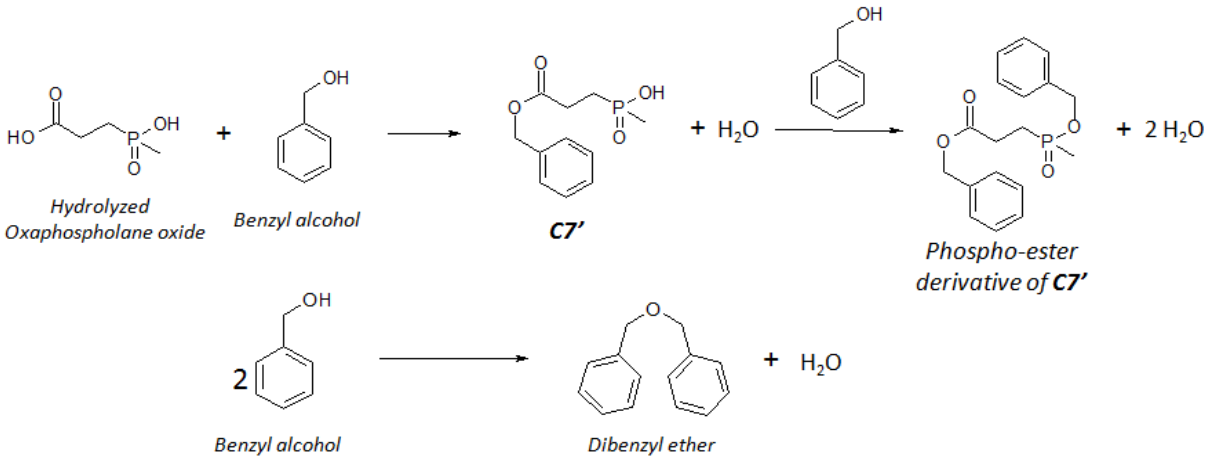

Figure 61 : Esterification reaction between hydrolyzed phospholane and benzyl alcohol

In the light of these observations, the PEPA based phosphinic acid **C7** was prepared through the same conditions than that for **C7'** but using an equimolar ratio of PEPA and hydrolyzed phospholane and without p-toluenesulfonic acid. According to ^{1}H NMR measurements, the resulting crude product mainly contains **C7** with moderate amounts of reactants and unidentified by-products. It may be concluded that the sole presence of the two reactants is sufficient to trigger the esterification, surely because this latter is self-catalyzed by the carboxylic and phosphinic acid functions of the hydrolyzed phospholane.

The recrystallization of **C7** was attempted using numerous solvents. Protic solvents such as methanol, ethanol and iso-propanol should be proscribed because the carbo-ester and phospho-ester functions of **C7** are subjected to trans-esterifications at high temperatures. Ketones, ethers, esters were also tried with no success. Finally, **C7** was washed using methyl ether ketone. The solvent is convenient to remove part of the impurities but it should be used in large quantity so the product can be obtained with acceptable purity. At last, the desired product is obtained in 85.8% yield and it contains residual amount of impurities (Figure 62).

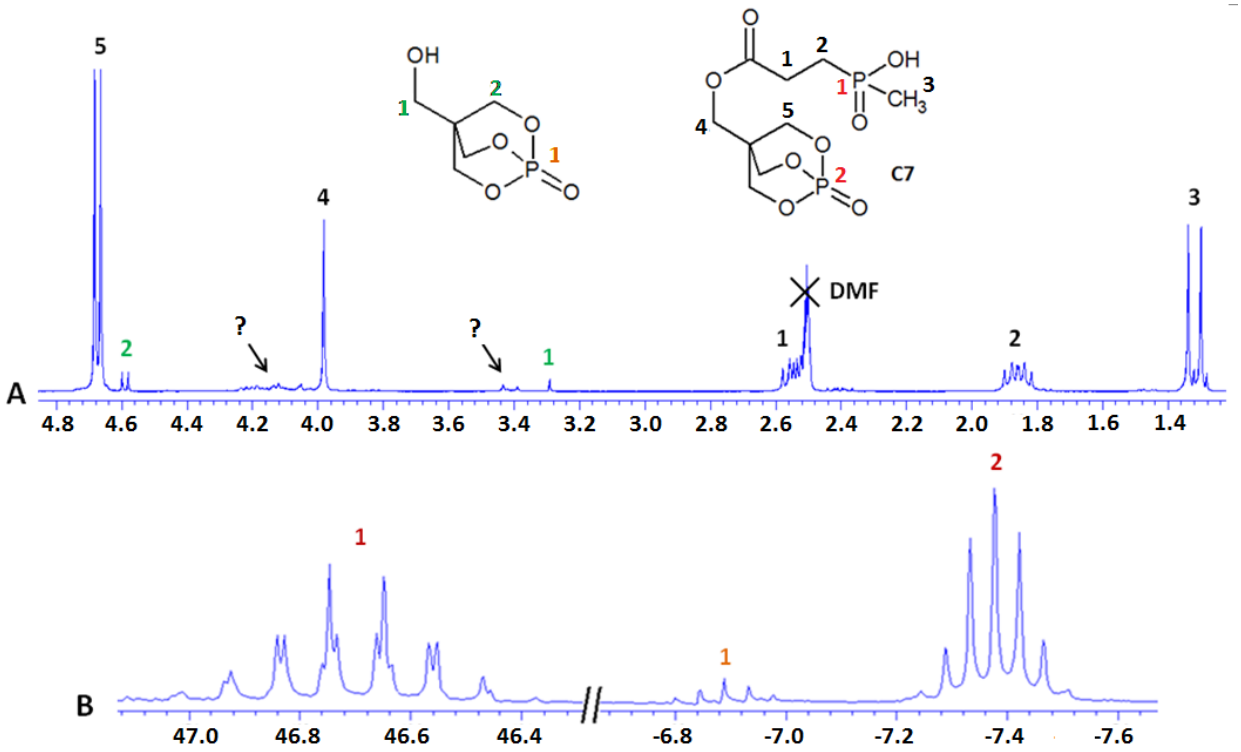

Figure 62 : C7 after washing with methyl ether ketone: (A) ^{1}H NMR; (B) ^{31}P NMR (in DMSO-d$_6$)

1.2.3 Conclusion

The seven phosphinic acid derivatives hereby synthesized were obtained with good purities, either through direct "condensation" of the nucleophilic reagents (amines) with Exolit PE110 or by an alternative pathway consisting first in hydrolyzing Exolit PE110, secondly in esterifying the hydrolyzed phospholane oxide with the nucleophilic reactant (PEPA). The products were also obtained in good yields excepted the o-phenylene diamine based diphosphinic acid (**C6**). As a consequence, **C6** was not further investigated in this project because it would have necessitated substantial amount of Exolit PE110 to be produced in sufficient quantity.

The following section focuses on describing the conversion of the phosphinic acids into aluminum salts. Additionally, it is described the synthesis of the calcium and zinc salts from

the aniline based phosphinic acid **C2**. The structure and purity of salts are evaluated through elemental analysis and solid state NMR.

1.3 Conversion of phosphinic acids into salts

This part deals with the conversion of phosphinic acids into phosphinate salts. First are described the preparation of aluminum salts. As we will show later, the aniline based phosphinate aluminum (**C9**) exhibits the best FR properties. In order to investigate the influence of the metal cation of phosphinates on the fire behavior of PBT, the calcium and zinc analogues of **C9** were also prepared. This will be the subject of a specific section in this part.

1.3.1 Preparation and characterization of aluminum salts

The synthesis of the aluminum salts was performed following laboratory procedures as well as procedures from the patent literature[184]. Operating conditions for each of the syntheses carried out are gathered in Table 14.

Table 14 : Conversion of the phosphinic acids into aluminum salts

Phosphinic acid (product)	Metal source	medium	Temperature (°C)	Time (h)	Yield (%)
C1 (C8)	$[(CH_3)_2CHO]_3Al$	H_2O/EtOH	80	9	86.3
C2 (C9)	$[(CH_3)_2CHO]_3Al$	H_2O/EtOH	80	9	90.2
C3 (C12)	$[(CH_3)_2CHO]_3Al$	H_2O/EtOH	80	18	84.0
C4 (C13)	$[(CH_3)_2CHO]_3Al$	H_2O/EtOH	80	9	81.1
C5 (C14-1)	$[(CH_3)_2CHO]_3Al$	H_2O/EtOH	80	23	52.8
C5 (C14-2)	1) NaOH 2) $Al_2O_{12}S_3.16H_2O$	H_2O	rt	2	96.2
C7 (C15)	1) NaOH 2) $Al_2O_{12}S_3.16H_2O$	H_2O	rt	2	10.9

Most of the aluminum phosphinate salts, including **C8**, **C9**, **C12**, **C13** and **C14-1**, were prepared using aluminum triisopropylate as aluminum precursor. The phosphinic acids were mixed with the aluminum source in amount equivalent to the valence of aluminum. The reactions were performed in a water/ethanol medium at 80°C. The phosphinate salts undergo a progressive precipitation during the reaction and they are finally recovered by filtration. It should be mentioned that aluminum triisopropylate is very insoluble in water.

Therefore mixing ethanol and water allowed increasing the speed conversion of reactants by facilitating the solubilization of the isopropanol released by the aluminum precursor.

Three of the aluminum phosphinates, namely **C8**, **C9** and **C13**, were obtained in relatively good yields and with a minimum period of time of 9h. A longer time was required to obtain **C12** as the latter underwent slower precipitation during the reaction. Despite a stirring of about one day (23h), **C14-1** could not be obtained in more than 53% yield. To improve the yield of **C14**, another route was explored consisting first in converting **C5** into sodium salt using NaOH. The resulting sodium phosphinate salt was then converted into aluminum salt by using aluminum sulfate. Through this synthesis pathway, which is performed in water at room temperature, **C14** (**C14-2**) could finally be obtained in 96% yield. This second procedure was also implemented for the synthesis of **C15** since **C7** proved to be unstable under the operating conditions of the first procedure. **C15**, however, was obtained in yield as low as 11%.

Figure 63 depicts the result of elemental analyses for the synthesized aluminum phosphinates (except **C14-1**). Through a graphic representation, measured mass fractions (exp.MF) for each element of the products are compared to theoretical values (theo.MF). The method used to determine theo.MF is depicted in Appendix 3. Data of the analyses are further gathered in Table 15.

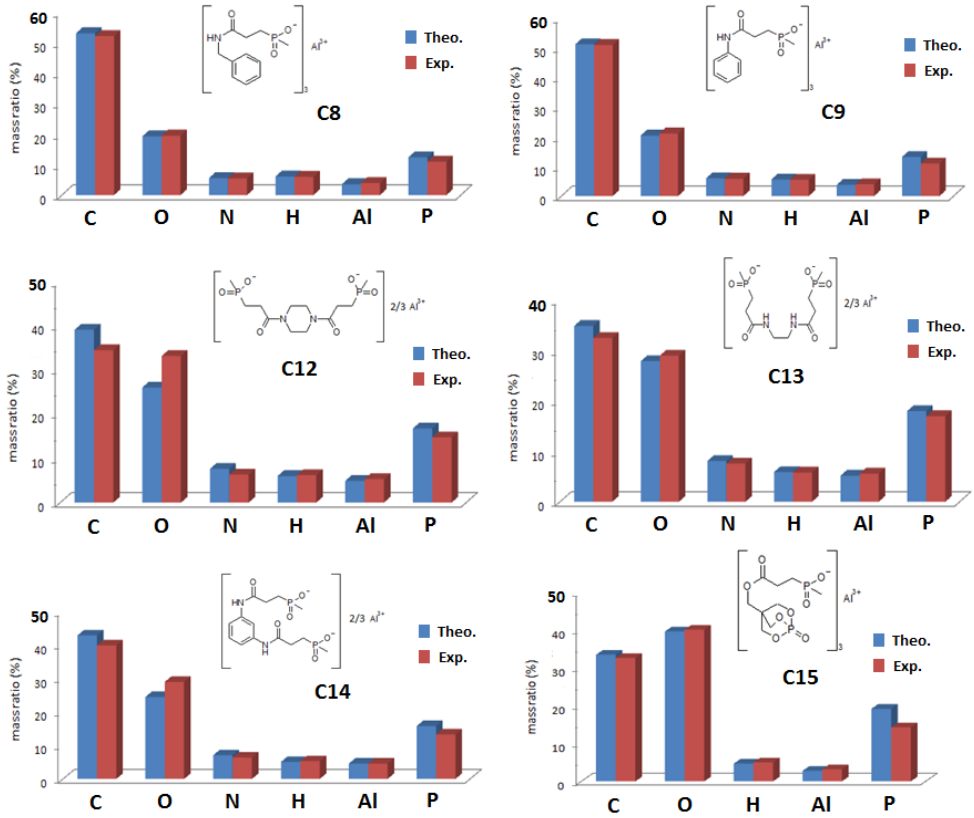

Figure 63 : Elemental analysis of the synthesized phosphinate salts; theoretical (blue) vs experimental (red) mass fractions of elements

Table 15 : Elemental analysis of the synthesized phosphinate salts; theoretical vs experimental mass fractions of elements

		Element (wt%)						
		C	O	N	H	Al	P	Total
C8	Theo.	53.0	19.3	5.6	6.1	3.6	12.4	100
	Exp.	52.1	19.5	5.5	6.0	4*	11*	98.1
C9	Theo.	51.1	20.4	6.0	5.6	3.8	13.2	100
	Exp.	50.9	21.1	5.9	5.5	4*	11*	98.4
C12	Theo.	38.9	25.9	7.6	6.0	4.9	16.7	100
	Exp.	34.3	33*	6.3	6.2	5.3	14.7	99.8
C13	Theo.	34.9	27.9	8.1	5.9	5.2	18.0	100
	Exp.	32.5	29*	7.6	5.8	5.6	17.0	97.5
C14-2	Theo.	42.9	24.5	7.1	5.1	4.6	15.8	100
	Exp.	39.9	29*	6.4	5.3	4.6	13.3	98.5
C15	Theo.	33.6	39.7	-	4.7	2.8	19.2	100
	Exp.	32.7	40.2	-	5.0	3.2	14.3	95.4

* *imprecise data due to a lack of product for the analyses*

It is first to be noted that the exp.MF for **C8** and **C9** are very close to the theoretical values. Only the exp.MF of phosphorus appears slightly lower but the value is probably underestimated due to the uncertainty and imprecision of the measurement for this element Table 15.

The exp.MF for **C12**, **C13**, and **C14-2** are also relatively well correlated to theo.MF, though perceptible differences can be noted for some of the analyzed elements. For these three products, indeed, the exp.MF of oxygen and aluminum appear higher than the theo.MF while the opposite is observed with carbon, nitrogen and phosphorus. Such a deviation would suggest the presence of water[185-188], hydroxo groups (HO^-) or oxygen dianionic (O^{2-}, i.e. Al-O-Al) in the salt structures[189-191]. A recalculation of the elemental composition of **C12**, **C13** and **C14-2** was performed on basis of an empirical formula containing two Al atoms, so theoretically three diphosphinate molecules. The method used for the calculations is presented in Appendix 3. The results are depicted in Table 16. For compounds **C12** and **C13**, it is observed that the composition in carbon, phosphorus and nitrogen globally decreases in the same order of magnitude (in percent) compared to the compositions of the theoretical formulas. This indicates that the proportion of phosphinate is lower than expected. For **C14-2**, the percent reduction of phosphorus is markedly lower than that of carbon and nitrogen. It is very likely that the proportion of phosphorus is underestimated in this case which again proves the difficulty of quantifying phosphorus with accuracy through elemental analyses. Thus, considering that the reduction of the fraction of diphosphinates is equal to the percent reduction of carbon (arbitrary choice among other elements), empirical formulas (obeying to

the neutrality rule) were proposed for the three products as followings (the methodology used to determine these empirical formulas is also given in Appendix 3):

- for **C12**: $Al_2(\mathbf{C3}^{2-})_{2.4}(O^{2-})_{n/2}(OH^-)_{1.2-n/2}(H_2O)_{4.1+n/2}[O]_{1.2}$; where $1.2 < n < 0$

- for **C13**: $Al_2(\mathbf{C4}^{2-})_{2.6}(O^{2-})_{n/2}(OH^-)_{0.8-n/2}(H_2O)_{1.0+n/2}[H]_{0.4}$; where $0.8 < n < 0$

- for **C14-2**: $Al_2(\mathbf{C5}^{2-})_{2.8}(O^{2-})_{n/2}(OH^-)_{0.4-n/2}(H_2O)_{2.8+n/2}[O]_{1.4}$; where $0.4 < n < 0$

Table 16 : Elemental composition of C12, C13 and C14-2, established from results of elemental analyses

		Elemental composition					
		C	O	N	H	Al*	P
C12	$C_{Theo.}$	36	18	6	66	2	6
	$C_{Exp.}$	29.1	21.0	4.6	62.6	2.0	4.8
	$C_{Exp.}/C_{Theo.}$%	80.8	116.7	76.7	94.8	100	80.0
C13	$C_{Theo.}$	30	18	6	60	2	6
	$C_{Exp.}$	26.1	17.5	5.2	55.4	2	5.3
	$C_{Exp.}/C_{Theo.}$%	87	97.2	86.6	92.3	100	88.3
C14	$C_{Theo.}$	42	18	6	60	2	6
	$C_{Exp.}$	39.0	21.3	5.4	61.7	2	5.0
	$C_{Exp.}/C_{Theo.}$%	92.9	118.3	90.0	102.8	100	83.3

** Calculations established on the basis of an empirical formula containing 2 aluminums*

These formulas, though perhaps not strictly representative of the actual structure of salts, allow at least giving an account of their content in aqua (H_2O)/hydroxo (OH^-)/oxo (O^{2-}) species. The excess of hydrogen or oxygen (denoted [H] and [O] in the formulas) may arise from the approximation in the calculation and the imprecision in the measurements. One may not exclude, however, that more water as well as more hydroxo and oxo groups could be contained in the products. Basically, the diphosphinate content in salts remains relatively high, particularly for **C14-2**. The lowest diphosphinate content would be achieved for **C12**. Furthermore, **C12** shows the highest amount in aqua/hydroxo/oxo species, with a particularly high concentration of water, while the water content is the lowest in **C13**.

As for compound **C15**, there are very good correlations between exp.MF and theo.MF except for the phosphorus which shows a significant reduction of 4.9 wt% (-25.5%) compared to its theoretical value. One can tentatively assume that part of the P=O group from PEPA would be lost by hydrolysis during the salt formation leaving some free hydroxyl groups of pentaerythritol linked to the phosphinate moiety. According to Table 16, the total mass of elements measured for **C15** is only of 95.4 wt%. It could suggest the presence in the salt of undetected elements such as sodium or sulfur (from sulfate) that could substitute for the

fraction of P=O lost by hydrolysis. On the other hand, it should not be excluded that the detection of phosphorus would have been imprecise.

Solid state NMR was used to characterize the phosphinate salts. In Figure 64 and Figure 65, are respectively compared the ^{13}C and ^{31}P solid state NMR spectra of salts with those of the corresponding phosphinic acids. Figure 66 depicts the ^{27}Al solid state NMR spectra of salts. Note that the spectra of salts (including chemical shift assignments) can also be found in Appendix 1.

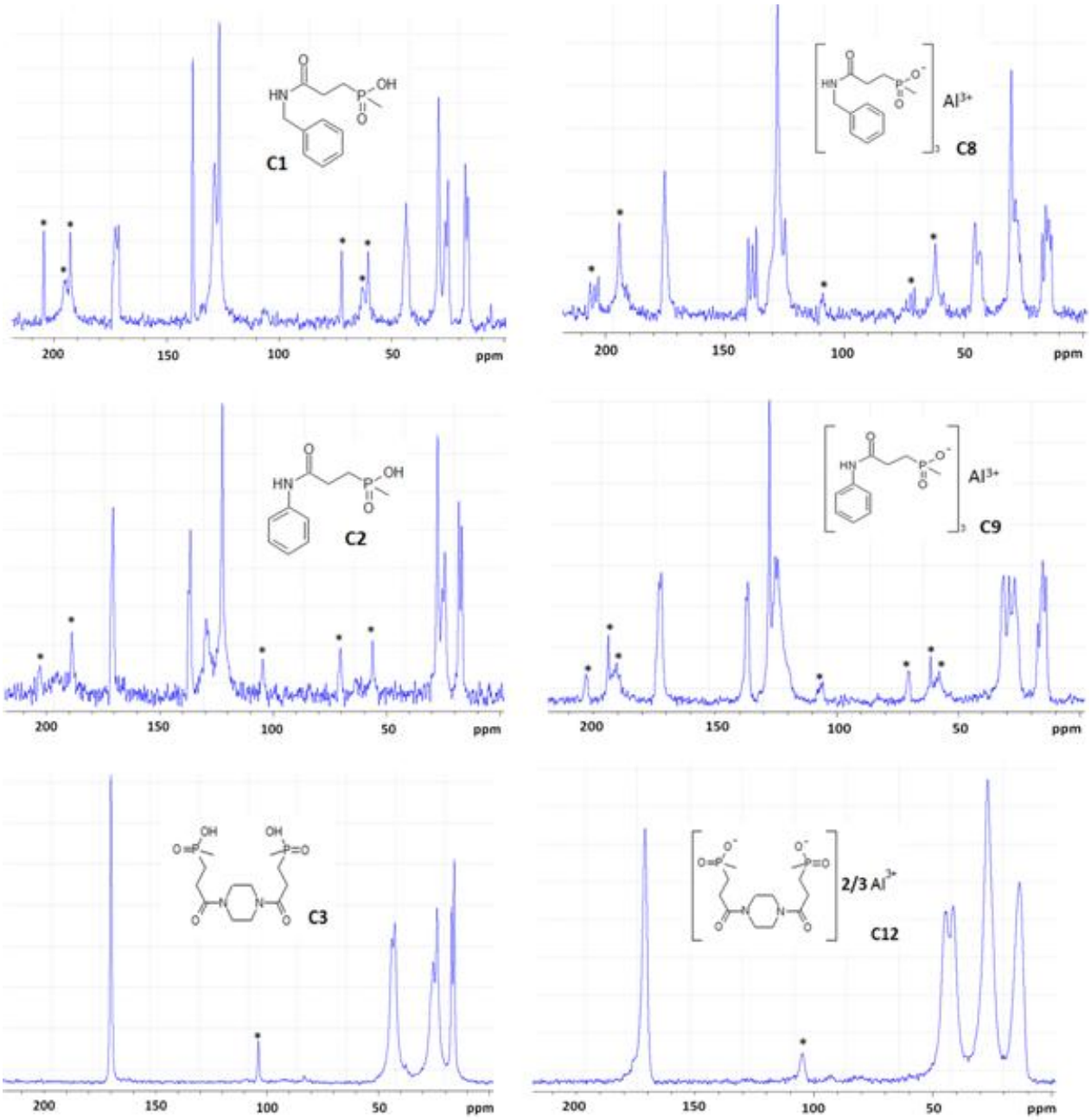

(continued below)

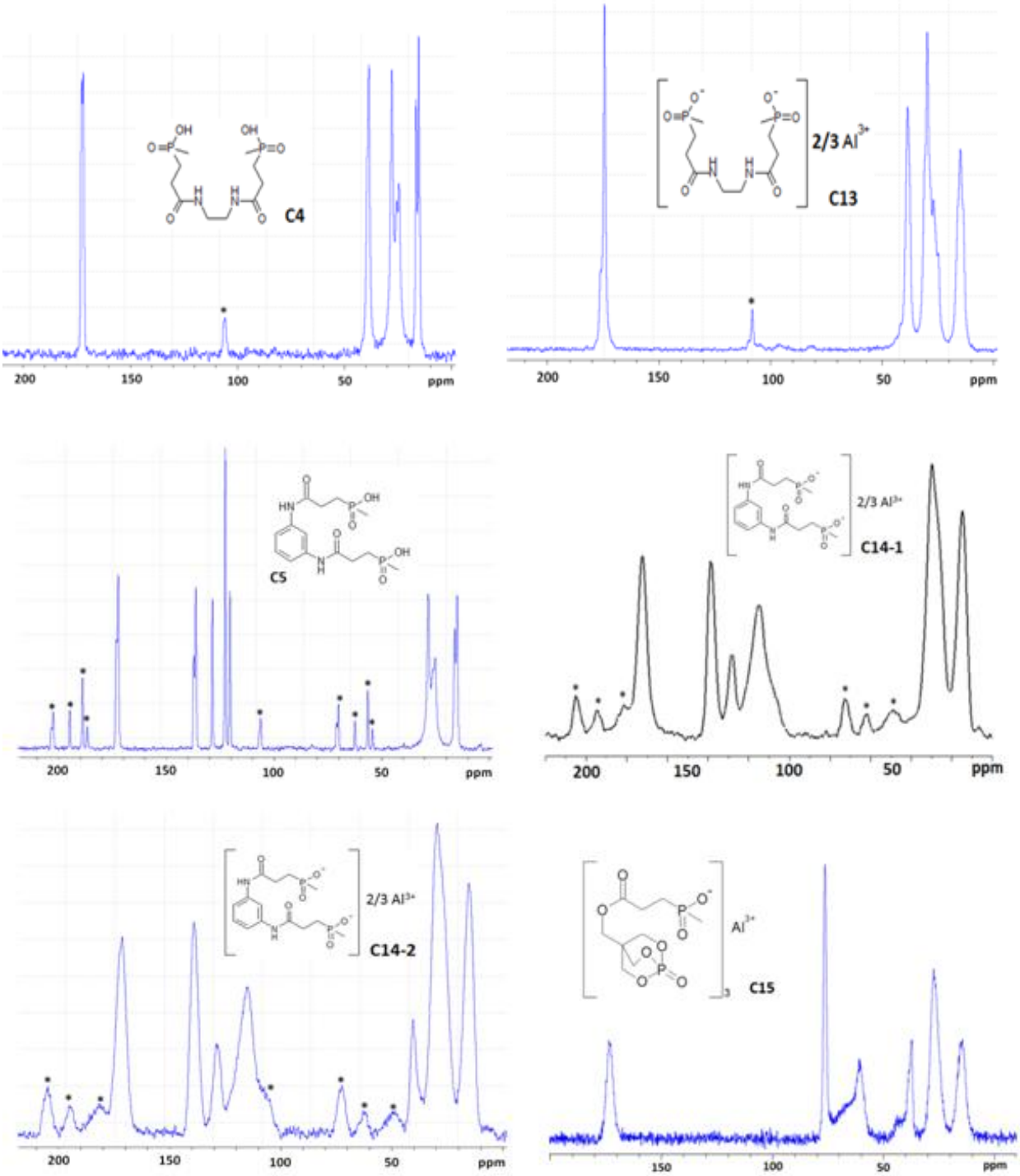

Figure 64 : ^{13}C (CP/MAS) solid state NMR spectra of the phosphinate salts and corresponding phosphinic acids. * denotes spinning sidebands.

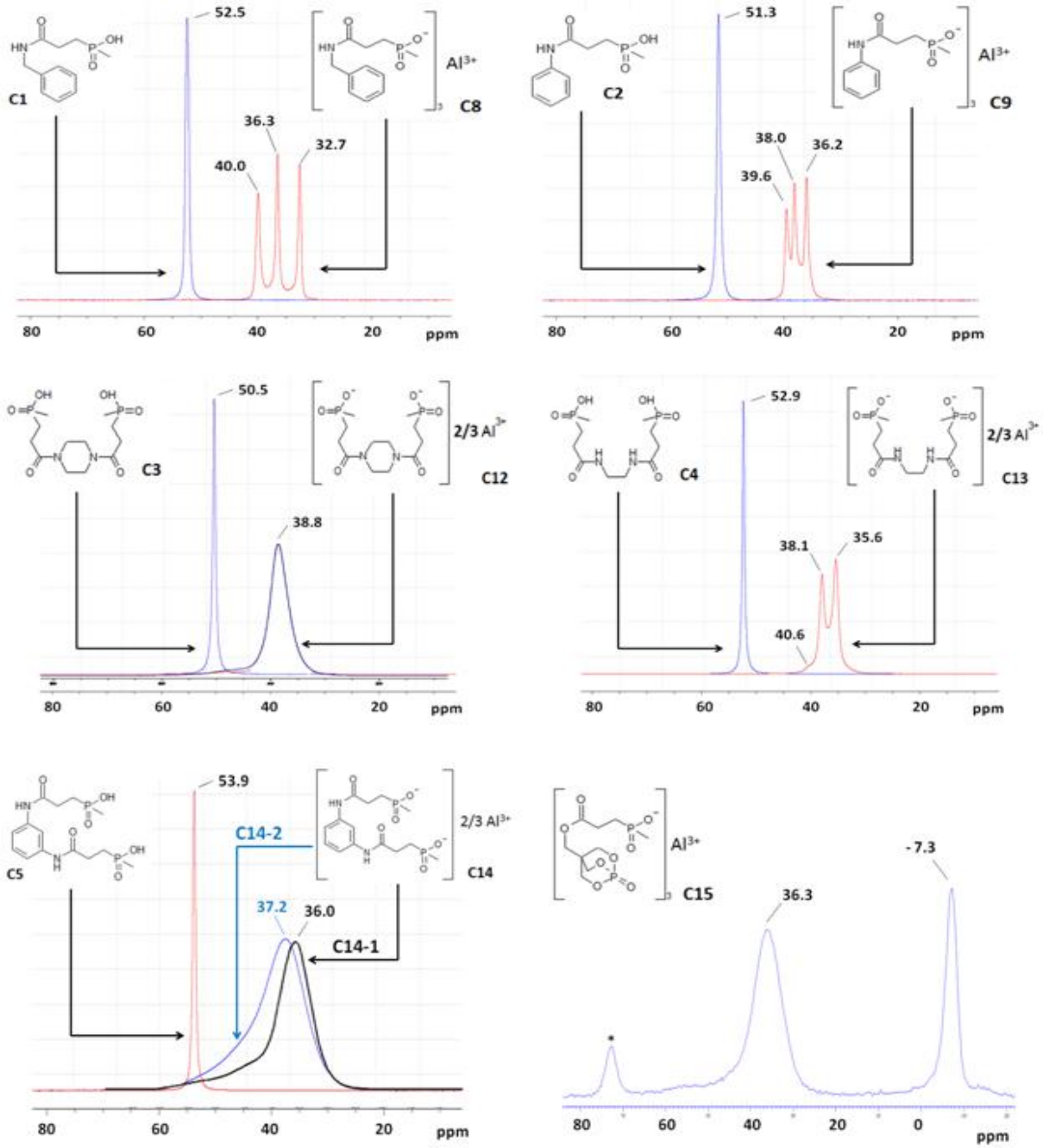

Figure 65 : ^{31}P solid state NMR spectra of the phosphinate salts and corresponding phosphinic acids. * denotes spinning sidebands. A CP/MAS pulse sequence was used for all compounds except C15 whose analysis was done through direct observation of ^{31}P.

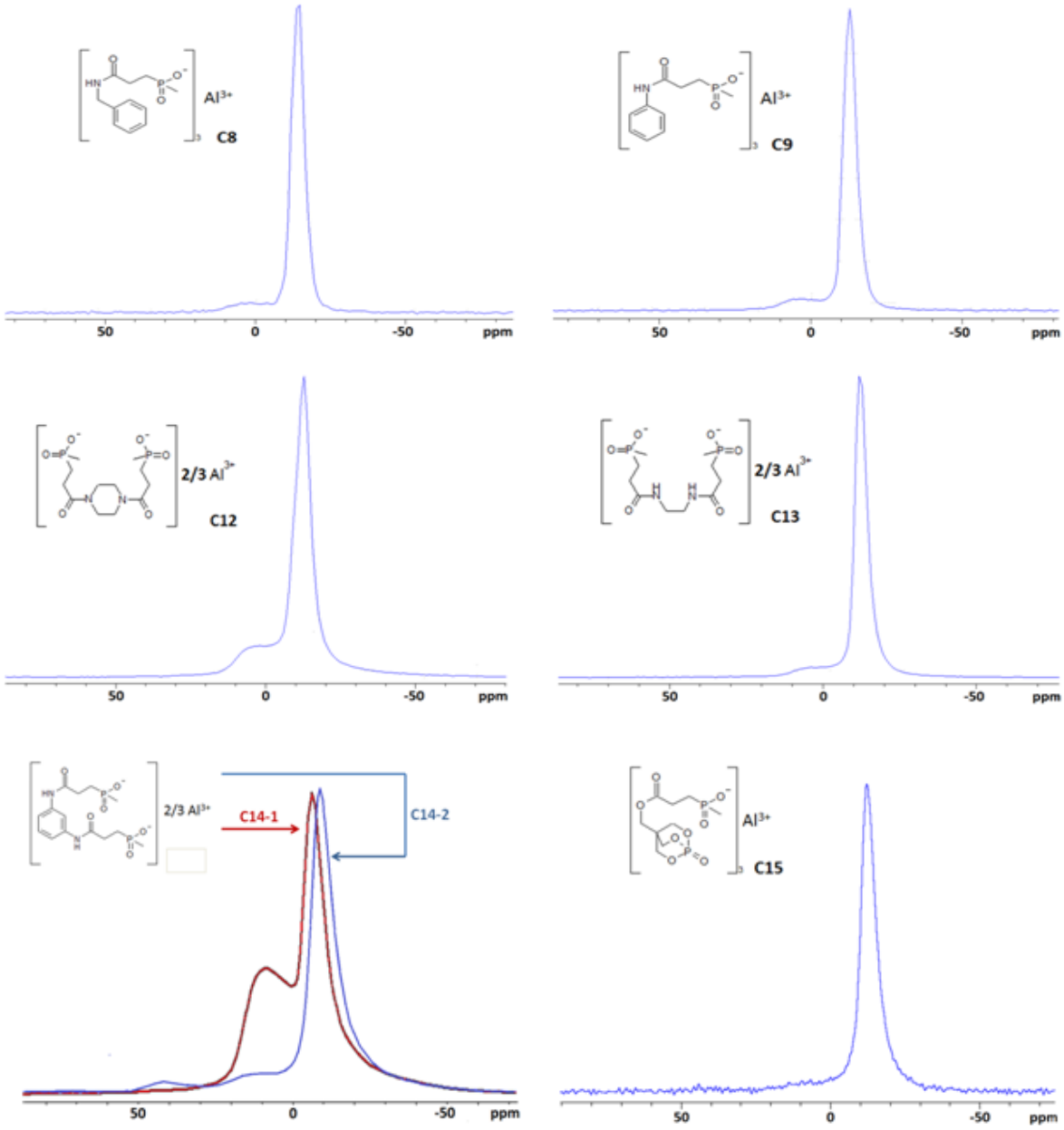

Figure 66 : ^{27}Al solid state NMR spectra of the phosphinate salts

It should first be noted the relatively close similarity between the ^{13}C signals of **C8**, **C9**, **C12** and **C13** and that of their corresponding phosphinic acids (Figure 64), though chemical shifts and/or multiplicities of signals may present some slight variations. Since carbon nuclei are not influenced by homonuclear (dipolar) or quadrupolar couplings, these variations shall be explained by a modification of chemical environments in salts, resulting from changes in the conformational arrangement of phosphinate moieties and the coordination of these latter with aluminum. The ^{13}C resonances of **C8**, **C9** and **C13** are relatively sharp (especially those of **C8** and **C9**); their line width is comparable to that of the ^{13}C signals of phosphinic acids which indicates that these salts exhibit rather well-defined crystal structures. On the contrary, the ^{13}C NMR patterns of compounds **C14-1**, **C14-2** exhibit very broad signals. It

indicates that these salts have an amorphous structure. If compared to the ^{13}C spectrum of **C5**, the peaks observed for **C14-1** and **C14-2** are consistent with what would be expected. However, an additional peak can be seen at 40 ppm on the spectrum of **C14-2** that is not observed for **C14-1**. The reason for this remains unknown. The ^{13}C spectrum of compounds **C15** shows unexpected broad bands in the left side hand of the resonances at 61 ppm (**C**H_2COO) and 38 ppm (-**C**CH_2O-P). Based on assumptions from elemental analyses, these broad bands could be assigned to the carbons of some PEPA residues that were partially or completely hydrolyzed[173].

In ^{31}P NMR analysis, all of the synthesized salts present the typical ^{31}P resonance of aluminum phosphinates (centered around 36-38 ppm)[192]. The ^{31}P spectra of **C8, C9** and **C13** display several phosphorus signals, namely three for **C8** and **C9**, and two for **C13**. Another small signal can also be observed for **C13** at 40.6 ppm, probably assigned to some phosphorus sites isolated from the general structure of the salt (i.e. separated phases at the periphery or at the junction of crystals). The presence of multiple phosphorus resonances indicates that the salts have either multiple polymorphic forms or else a unique crystal structure with different phosphorus sites. The possibility of a quadrupolar coupling between phosphorus and aluminum (typically of 15-30 Hz for aluminophosphate complexes[193]) is to be ruled out on account of too high frequency between the phosphorus peaks (in the range of 447-193 Hz). A dipolar ^{31}P-^{31}P correlation experiment, depicted in Figure 67, was performed with compound **C9**.

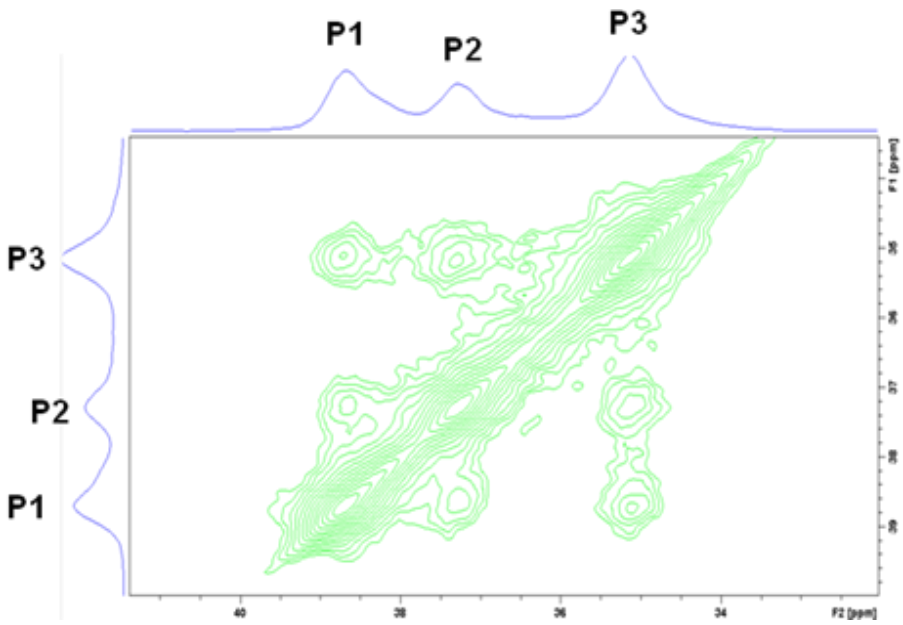

Figure 67 : Two dimensional (2D) solid state NMR analysis of C9 : ^{31}P-^{31}P cross-polarization (CP) - radiofrequency driven recoupling (RFDR) experiment

It clearly demonstrates that the different phosphorus nuclei of **C9** have a short spatial proximity as they show evidence of dipole-dipole interactions with each other[194]. Therefore

it is possible to conclude that the three phosphorus sites of **C9** are located in the same crystallite. One may assume that **C8** and **C13** likewise exhibit only one crystalline form wherein the phosphinate moieties would have diverse chemical environments. It is noteworthy that these multiple chemical environments can also be visualized from the ^{13}C signals of **C8**. For instance, the quaternary carbon of the aryl group of **C8** shows up as a threefold signal (corresponding to three environments) centered on 139 ppm.

The ^{31}P signal of the phosphinate groups of compounds **C12**, **C14-1**, **C14-2** and **C15** shows only one broad band. The width of bands (especially that of **C14-2**) confirms the assumption of a more disordered structure for these salts. One may particularly remark that the ^{31}P band of both **C14-1** and **C14-2** spreads out over a relatively wide range of frequencies up to the ^{31}P resonance of the phosphinic acids. Thus, the presence of residual phosphinic acids in the salt structures can be considered. The downfield side of the ^{31}P signal of **C14-1** shows distinctive overlapping resonances (at least two, at 45 ppm and 54 ppm), which would be consistent with the existence of several phosphinate species (i.e. aluminate-hydrate-phosphinate clusters). Weak shoulders can also be distinguished downfield from the dominant resonance of **C12** (at 48 ppm) and **C15** (at 55 ppm). Contrary to the other salts, the ^{31}P NMR analysis of compound **C15** was performed by direct observation (and not through cross-polarization). Our intent was to carry out an accurate integration of the phosphorus signals of the phosphinate group (at 36 ppm) and of PEPA (at -7.3 ppm) so as to properly compare the relative proportion of both phosphorus in the salt (theoretically in a ratio 1:1). The analysis of **C15** was performed using a high MAS (20 kHz) to prevent overlapping of the sidebands with the isotropic signals of phosphorus. Thus, it has been determined that the integration ratio of signals of the phosphinate group and PEPA ($Int_{PEPA}/Int_{phosphinate}$) was of about 0.72 which means that the quantity of phosphinate groups in the salt is 39% higher than the quantity of PEPA. This result brings about a supplementary proof that fraction of the phosphorus from PEPA got lost by hydrolysis during the salt synthesis.

The ^{27}Al NMR analyses of salts confirm most of the observations made through ^{13}C and ^{31}P NMR. The salts exhibit a main signal centered around -12 ppm (hereinafter reffered to as S1), corresponding to the typical chemical shift of octahedral Al atoms coordinated to eight framework oxygen atoms with phosphorus in the second coordination sphere[192,195]. The relative symmetry of the line shape of S1 in spectra of **C8**, **C9** and **C13** proves that Al is located in an isotropic environment which is again consistent with a crystal arrangement. The line shape of S1 in spectra of **C12** and **C15** is comparable to that of **C8**, **C9** and **C13**, though a little bit broader and asymmetric. It signifies that the surrounding of Al atoms in **C12** and **C15** is relatively isotropic, hence the salts have a certain degree of structural order. On the opposite, the same signal in spectra of **C14-1** and **C14-2** exhibits a broad asymmetric line shape characteristic of the combination of significant distributions of isotropic chemical shift and second-order quadrupolar broadening. It undeniably indicates that these salts are mainly amorphous.

In all spectra, another band (reffered to as S2) with an apparent isotropic chemical shift at 5 ppm (Al in octahedral geometry) can be seen as a broad shoulder downfield from S1. In the literature[195-199], this band is assigned to aluminate-hydrate complexes (containing possibly also hydroxo groups). The surface area of S2 is relatively small and almost equivalent for **C8**, **C9**, **C13** and **C14-2** which appears surprising with regard to elemental analyses. Indeed, the latter showed that **C13** and **C14-2** contained more aqua/hydroxo/oxo species than **C8** and **C9**. An explanation could be that the water contained in **C13** and **C14-2** is not directly coordinated to aluminum (moisture) and/or that the content in aqua/hydroxo/oxo species in these salts would have been overestimated. It is not excluded besides that signals originating from mixed aluminate-phosphinate-hydrate species would be superimposed upon the signal S1[188,195,200]. One should finally take into consideration the fact that the drying period of salts was not rigorously the same in between analyses. It is noteworthy that an additional broadened band of low intensity is observed at 39 ppm in the spectrum of **C14-2**. This band, attributed to a fivefold-coordinated aluminum (pentahedral geometry)[201,202], is likely to arise from the amorphous feature of the salt. The surface area of S2 is significantly higher in the spectrum of **C12**, even more in the spectrum of **C14-1**, which is consistent with the results of the elemental analysis. In these cases, S2 clearly overlaps with S1 and it suggests an apparent quadrupolar broadening towards high frequencies. This testifies from the amorphous feature of aluminate-hydrate species. S2 is hardly distinguishable in the spectrum of **C15** which is not contradictory with elemental analyses.

1.3.2 Preparation and characterization of zinc and calcium salts of the aniline based phosphinic acid

The synthesis of the zinc and calcium salts of **C2** was performed based on procedures described in the literature[203]. Table 17 depicts the materials and operating conditions used for both syntheses.

Table 17 : Conversion of the phosphinic acid C2 into zinc and calcium salts

Phosphinic acid	Metal source	medium	Temperature (°C)	Time (h)	Yield (%)
C2	1) NaOH 2) $[CH_3CO_2]_2$ Zn.2H_2O	H_2O	rt	5	(**C10**) 46.4
C2	1) NaOH 2) $[CH_3CO_2]_2$ Ca. H_2O	H_2O	rt	5	(**C11**) 80.8

C10 and **C11** were prepared in an analogous manner to that for **C14-2**, using the respective zinc and calcium acetate salts as metal sources. The salts were respectively obtained in 46.4% and 80.8% yields.

The results of elemental analyses for the salts are depicted in Figure 68 and Table 18.

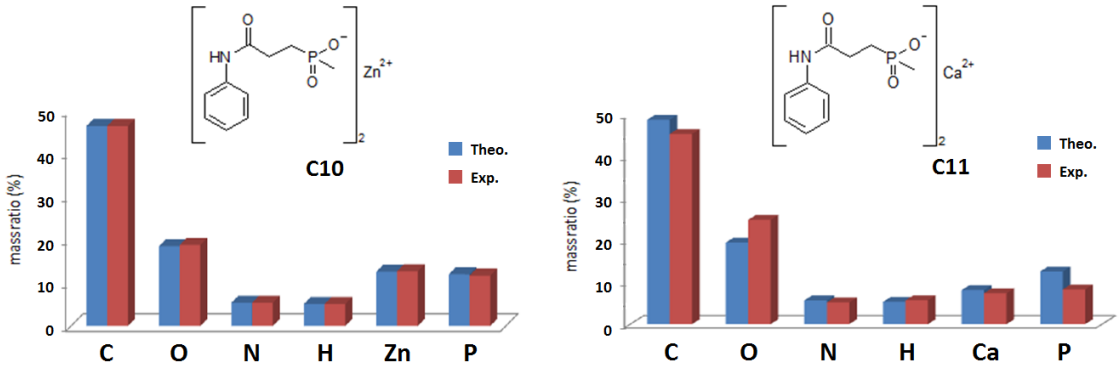

Figure 68 : Elemental analysis of the synthesized zinc and calcium salts of C2; theoretical (blue) vs experimental (red) mass fractions of elements

Table 18 : Elemental analysis of the synthesized zinc and calcium salts of C2; theoretical vs experimental mass fractions of elements

		Element (wt%)						
		C	O	N	H	Me*	P	Total
C10	Theo.	46.4	18.5	5.4	5.1	12.6	12.0	100
	Exp.	46.4	18.8	5.4	5.1	12.7	11.7	100.1
C11	Theo.	48.8	19.5	5.7	5.3	8.1	12.6	100
	Exp.	45.4	24.9	5.2	5.7	7.4	8.3	97.0

Very good correlations are obtained between the exp.MF and theo.MF of **C10**. For **C11**, the fraction of oxygen is higher than expected while fractions of carbon, nitrogen, phosphorus and calcium are on the contrary lower. As for the aluminum based salts, this deviation indicates that the calcium salt contains aqua/hydroxo/oxo species. Similarly to **C12**, **C13** and **C14-2**, the elemental composition of **C11** was determined (Table 19) considering one calcium for two phosphinate residues.

Table 19 : Elemental composition of C11 established from results of elemental analyses

		Elemental composition					
		C	O	N	H	Ca*	P
C11	$C_{Theo.}$	20	6	2	26	1	2
	$C_{Exp.}$	20.5	8.4	2.0	30.6	1	1.5
	$C_{Exp.}/C_{Theo.}$%	102.5	140.0	100.0	117.7	100	75.0

** Calculations established on the basis of an empirical formula containing 1 calcium*

According to Table 19, there is an almost perfect adequacy between the carbon, nitrogen and calcium contents of **C11**. The still large reduction of phosphorus is attributed to the imprecision in the measurements. Considering, therefore, that **C2** was converted into calcium salt in stoichiometric proportion, the followings formula is proposed for **C11**: Ca(**C2**$^{-}$)$_2$(H_2O)$_{2.3}$[O]$_{0.1}$. This formula demonstrates that the calcium salt contains at least two structural water molecules.

The ^{31}P and ^{13}C solid state NMR spectra of **C10** and **C11** are compared to that of **C2** in Figure 69 and Figure 70 respectively. Those spectra are further depicted in Appendix 1.

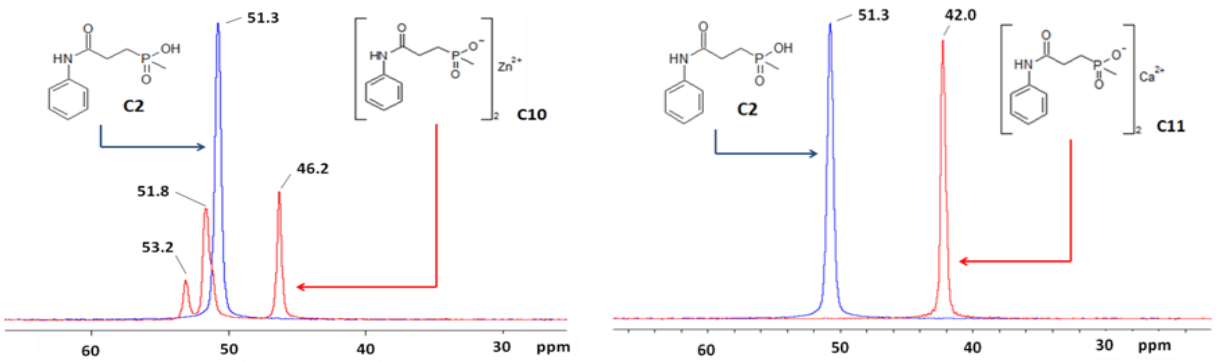

Figure 69 : ^{31}P solid state NMR spectra of C2, C10 and C11. * denotes spinning sidebands. (see Appendix 1 for further details of acquisition parameters)

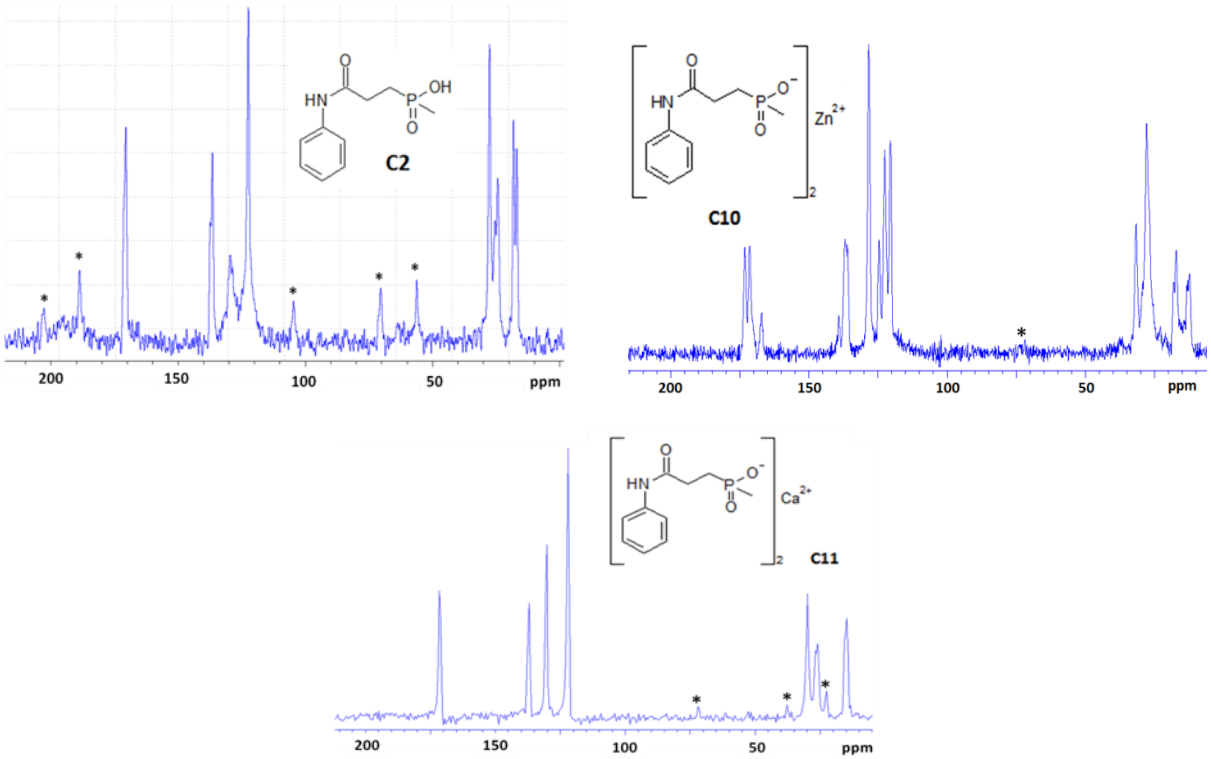

Figure 70 : ^{13}C (CP/MAS) solid state NMR spectra of C2, C10 and C11. * denotes spinning sidebands. (see Appendix 1 for further details of acquisition parameters)

Both **C10** and **C11** present well-defined crystal structures. The ^{31}P NMR spectrum of **C10** exhibits three sharp resonances at 46.2, 51.8 and 53.2 ppm ascribed to three different phosphorus sites. It is noteworthy that a similar ^{31}P NMR pattern was reported by Vannier et al[204] for the zinc salt of diethylphosphinic acid (OP950). The three-fold splitting of the phosphorus signal - originating from three variations in the molecular arrangements of the phosphinate residues in the salt - can also be inferred from the ^{13}C spectrum of **C10**, notably from the resonances of the carbon amid (-**C**ONH-) and that of the quaternary carbon of the aromatic group. The latter indeed show up as "triplets" respectively centered at 171 and 138 ppm.

For **C11**, only one sharp resonance is observed in ^{31}P NMR that shifted to 9 ppm upfield from the phosphorus resonance of **C2**. Yet the ^{13}C spectrum of **C11** appears quite similar to that of **C2**. By contrast with **C10**, the NMR signals of **C11** show no splitting which suggests that the phosphinate residues of **C11** have only one specific arrangement in the salt structure.

1.3.3 Conclusion

This part dealt with the conversion of several phosphinic acids into phosphinate salts. The yield and purity of salts appeared to greatly depend on the nature of the phosphinic acid, the metal precursor as well as the metal itself.

The monofunctional phosphinic acids **C1** and **C2** were successfully converted into aluminum salts from aluminum triisopropylate. The resulting salts (**C8** and **C9** respectively) are obtained in good yields and purities. From the same metal source, the aluminum salts derived from the difunctional phosphinic acids **C3** and **C4** (**C12** and **C13**) were obtained in slightly lower yields whereas the aluminum salt derived from **C5** (**C14-1**) was obtained in relatively low yield. Elemental and NMR analyses demonstrated that fraction of aqua/hydroxo/oxo species was contained in **C12**, **C13** and **C14-1**. While the concentration of such species remained low in **C12** and **C13**, it was found to be particularly important in **C14-1**. Another synthesis route consisting in using aluminum sulfate as metal source (with prior conversion of phosphinic acid into sodium salt), allowed affording **C14** (**C14-2**) in much better yield and with reduced concentration in aqua/hydroxo/oxo species. Aluminum sulfate was also used to prepare the salt derived from the PEPA based phosphinic acid **C7** (**C15**). In this case, the salt was obtained in very low yield. Moreover, **C15** presents relatively low amount of aqua/hydroxo/oxo species, while part of the P=O group from the PEPA residue is lost by hydrolysis during the salt synthesis.

The zinc and calcium salts of **C2** (**C10** and **C11**) were respectively prepared from zinc and calcium acetates. **C10** was obtained in limited yield but with excellent purity. **C11** was obtained in higher yield, however, it contains structural water molecules.

The synthesized phosphinate salts are characterized through TGA in the next section. The thermal decomposition behavior of salts is evaluated and it is compared to that of phosphinic acids and PBT/GF.

1.4 Thermal behavior of the phosphinate salts

Thermogravimetric analysis (TGA) was used as an easy and highly informative tool to determine the thermal stabilities of phosphinate salts. Through this technique, it is a first purpose to characterize further the synthesized products. One should expect for instance that the phosphinate salts exhibit higher thermal stabilities than their respective phosphinic acids or else exhibit sufficient stabilities to endure the PBT processing. In some cases, the TGA analysis may prove to be a valuable method to understand, at least partially, the mechanisms involved in the flame retardancy of polymers[96,97]. Since a variety of related phosphinates was hereby obtained, it could be possible to partly elucidate their mode of action by simply comparing their thermal stability with that of PBT. This is the second purpose of this part.

The thermogravimetry curves of the phosphinic acids, the phosphinate salts and PBT/GF in an inert atmosphere are depicted in Figure 71. The detailed TGA data are summarized in Table 20.

Among aluminum salts, **C8** and **C9** achieve the lowest thermal stabilities. The onset temperature for mass loss of **C8** (T_{onset} = 293°C) is slightly lower compared to that of **C9** (T_{onset} = 314°C) but both products globally exhibit similar behavior with respective weight losses of 70% and 68% up to 600°C. Interestingly, weight losses of the two salts occur in a temperature range close to that of PBT which could be a key asset for the flame retardancy of the polymer. As predicted, the mass loss of **C1** (T_{onset} = 200 °C) and **C2** (T_{onset} = 180°C) starts at much lower temperature than that of their corresponding salts. It furthermore occurs in one single stage with no residue left beyond 350°C which contrasts with the multiple weight loss stages (at least three) displayed on the TG curves of the salts. It proves that the conversion of acids into salts not only increases the stability of products but change their degradation pathways.

The mass loss of the PEPA based phosphinate salt **C15** starts at 339°C and it occurs in one main step that almost exactly matches with the decomposition stage of PBT/GF. The remaining residue of **C15** at 600°C (appearing as a highly swollen char on visual observation) represents 41% of the initial mass of the product. The weight loss of **C7** (T_{onset} = 300°C) - the corresponding phosphinic acid of **C15** - occurs at lower temperatures than **C15**, but **C7** still exhibits a relatively high thermal stability, notably compared to the other mono-functional phosphinic acids **C1** and **C2**. In contrast to **C1** and **C2**, **C7** shows incomplete weight loss and leaves a char residue (also highly swollen) of 28% at 600°C. This represents a difference of

only 13% compared to the residue yield of **C15**. Thus, it shows that **C7** exhibits inherent charring properties as it was suspected prior to the syntheses.

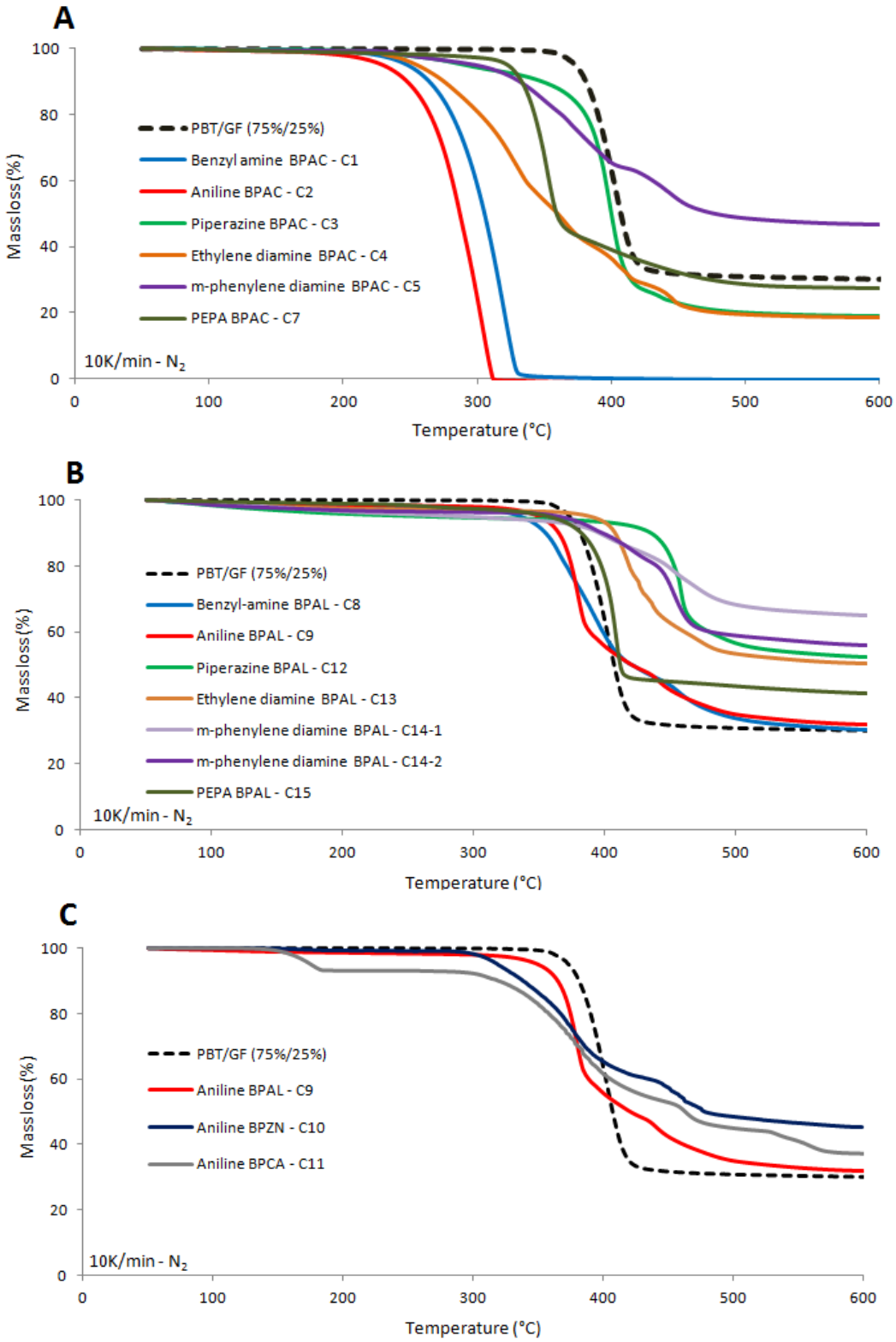

Figure 71 : TG curves of glass fiber (25 wt%) reinforced PBT, phosphinate salts and corresponding phosphinic acids; heating rate 10K.min^{-1}

Table 20 : TGA data of PBT/GF and the synthesized products

	T_{Onset} * (°C)	T_{MLR} ** (°C)	Residue yield at 600°C (wt%)
PBT/GF (75%/25%)	335	404	30.6
Benzyl amine BPAC - **C1**	200	320	0
Aniline BPAC - **C2**	180	305	0
Piperazine BPAC - **C3**	215	397	18.9
Ethylene diamine BPAC - **C4**	211	333	18.7
m-phenylene diamine BPAC - **C5**	226	377	46.7
PEPA BPAC - **C7**	300	351	27.6
Benzyl amine BPAL - C**8**	293	388	30.2
Aniline BPAL - **C9**	314	379	31.7
Aniline BPZN - **C10**	291	384	45.4
Aniline BPCA - **C11*** **	293	384	36.4
Piperazine BPAL - **C12**	403	458	52.5
Ethylene diamine BPAL- **C13**	360	419	50.4
m-phenylene diamine BPAC - **C14-1**	340	453	64.9
m-phenylene diamine BPAC - **C14-2**	336	459	55.9
PEPA BPAL- **C15**	332	407	41.3

** T_{onset} : Onset temperature degradation*
*** T_{MLR} : Temperature at maximum mass loss rate*
****T_{Onset} of the second mass loss step*

The aluminum salts **C12**, **C13** and **C14** exhibits high thermal stabilities due to the fact that the phosphinic acids from which they are synthesized are already highly stables. It is noteworthy that the TG curves of these salts show a low mass loss rate from the ambient temperature to the onset degradation temperature. This decrease is likely to result from the release of water. The latter is particularly significant for **C12** and **C14-1** as it represents a weight loss of about 8%. Globally, **C12**, **C13** and **C14** undergo major part of their weight loss after complete decomposition of PBT/GF. These salts furthermore present high residue yields at 600°C (around 53% for **C12**, **C13** and **C14-2**). **C12** presents the highest stability among the phosphinate salts with a T_{onset} of 68°C higher than that of neat PBT/GF. The largest difference between the stability of a salt and that of its corresponding phosphinic acid is observed for **C13** and **C4**. **C4** starts losing weight at 211°C and it undergoes a constant and gradual mass loss up to 500°C leading to a residue of about 19%. The conversion of **C4** into **C13** allows increasing the T_{onset} to 360°C (+ 149°C) and the residue yield to 50% (+ 31%). There is a lesser extent of variation between the stability of **C14-2** and that of **C5**. It arises from the fact that **C5**, besides having an elevated thermal stability (with a particularly low mass loss rate), exhibits the highest residue yield (48%) among the phosphinic acids. The conversion of **C5** into **C14-2** increases the T_{onset} from 226°C to 336°C (+ 110°C) while the residue yield is finally increased by only 9%. Note that the TG curves of **C14-1** and **C14-2** present some differences. Both compounds show comparable T_{onset}, however, the residue

yield of **C14-1** (65%) is higher than that of **C14-2** (56%). Since **C14-1** contains more aqua/hydroxo/oxo species than **C14-2**, this difference is explained by the fact that a higher fraction of volatile species, mostly organics, would evolve from **C14-2** during the thermal analysis.

The zinc salts of **C2** (**C10**) exhibits multiple mass loss stages that seem to be equivalent to that of the aluminum salt **C9**. Compared to **C9**, however, **C10** has lower T_{onset} (291°C), lower mass loss rate and superior residue yield at 600°C (45%). The TG curve of **C11** would appear quite equivalent to that of **C10** without occurrence of two additional mass loss stages, the first one between 140°C and 181°C, and the second one between 525°C and 575°C. FTIR analysis of the gases evolved from **C11** confirmed that the first mass loss occurring between 140°C and 181°C corresponded to the release of 7% water (Figure 72). It exactly represents the loss of two molecules of water from the structure of **C11** as established in the previous section.

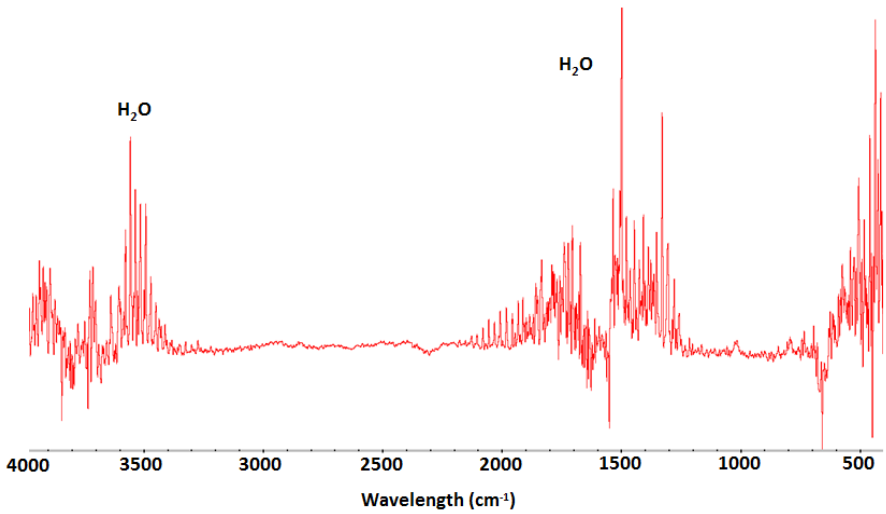

Figure 72 : FTIR spectrum of gases evolved from C11 at 165°C during the TGA analysis

1.5 Conclusion

This part has described the synthesis and then the conversion into metal salts (mostly aluminum) of a variety of phosphinic acids derived from the oxaphospholane oxide Exolit PE110. The synthesized products have been thoroughly characterized by NMR, elemental analyses and thermogravimetric analyses. Finally, eight phosphinate salts (**C8**, **C9**, **C10**, **C11**, **C12**, **C13**, **C14-2**, **C15**) could be obtained in sufficient purities and with good thermal stabilities.

The aluminum salt derived from the benzyl amine based phosphinic acid (**C8**) and the aluminum, zinc and calcium salts derived from the aniline based phosphinic acid (**C9**, **C10** and **C11** respectively) achieved the highest purities. Even if the salt **C11** contains structural water (as evidenced by elemental and TG analyses), it should be easily removed by a thermal

treatment. The aluminum salt derived from the PEPA based phosphinic acid (**C15**) seems to have been obtained in relatively good purity, though part of the P=O group from the PEPA residue (≈24%) would apparently be lost by hydrolysis during the salt synthesis. The aluminum salts derived from the piperazine, ethylene diamine and m-phenylene diamine based phosphinic acids (**C12**, **C13** and **C14-2** respectively) were also successfully synthesized, but they contain a certain concentration of aqua/hydroxo/oxo species. This may, however, not be so detrimental for flame retardant applications as these salts still contain high proportion of diphosphinates and particularly high phosphorus percentages.

The synthesized salts exhibit a large diversity of thermal stabilities. Through TG analyses, the salts derived from mono-functional phosphinic acids (**C8**, **C9**, **C10**, **C11** and **C15**) lose weight in a temperature range close to that of the decomposition of PBT/GF. Compared to their aluminum analogue **C9**, the zinc and calcium salts **C10** and **C11** exhibit lower onset temperatures of weight loss as well as lower mass loss rates and they show higher residue yields at high temperature. The salts derived from di-functional phosphinic acids (**C12**, **C13** and **C14-2**) start to lose weight after decomposition of PBT and they present particularly high residue yields.

The third part will consist in evaluating the fire performances of the various synthesized salts in glass fiber reinforced PBT. The most efficient salts will be combined with commercial flame retardants and synergistic agents in the prospect of improving further the flammability behavior of the polymer.

2. Flame retardant properties of the novel phosphinate salts

In this part, the flame retardant properties of the synthesized phosphinate salts in PBT/GF are evaluated. The salts are tested alone first, and then in combination with commercial flame retardants and synergistic agents.

The fire performances of materials are investigated through the UL94 (1.6 mm) testing method and the LOI test. First trials were performed with materials containing a loading (arbitrarily chosen) of 15 wt% of the flame retardants. The amount of flame retardants was adjusted when necessary. For the sake of comparison, the fire performances of Exolit OP1240 containing formulations, which were prepared in the same conditions as the novel formulations were also tested.

2.1 Fire testing of the aluminum phosphinates containing formulations

The flame retardant properties of the synthesized aluminum phosphinates in the reinforced PBT are first investigated. The UL94 and LOI results obtained for the corresponding formulations are summarized in Table 21.

.

Table 21 : UL94 and LOI results obtained for the aluminum phosphinates containing PBT/GF formulations

Aluminum salt (FR)	Composition (wt%)			LOI (Vol%)	UL-94, 1.6 mm bar			
	PBT	GF	FR		Conditioning	t1/t2[a] (s)	Dripping[b]	Rating
Exolit OP1240	60	25	15	43	2d.25°C	5.5/3.8	N	V-1
Exolit OP1240	59	25	16	44	2d.25°C	2.3/3.4	N	V-0
C8	60	25	15	40	2d.25°C	5.3/1.0	N/D-Y	V-2
C8	57	25	18	-	2d.25°C	1.5/1.7	D-Y/D-Y	V-2
C9	60	25	15	50	2d.25°C	3.5/3.4	N/D-Y	V-2
C9	59	25	16	-	2d.25°C	3.7/7.0	N/D-Y	V-2
C9	58	25	17	50	2d.25°C	2.4/3.9	N/D-N	V-0
C9	58	25	17	-	7d.70°C	6.6/2.8	N/D-Y	V-2
C9	58	25	18	-	2d.25°C	4.0/4.4	N	V-0
C12	60	25	15	25	2d.25°C	21.2[F]/-	D-Y/-	NC
C13	60	25	15	25	2d.25°C	29.3/17.2[F]	D-Y/D-Y	NC
C13	50	25	20	27	2d.25°C	23.4/16.4	D-Y/D-Y	V-2
C14-2	60	25	15	22	2d.25°C	25.0/15.3[F]	D-Y/D-Y	NC
C15	58	25	17	24	2d.25°C	34.3[F]/-	D-Y/-	NC
C15	55	25	20	25	2d.25°C	28.5[F]/-	D-N/-	NC

[a] *t1 and t2, average combustion times after the first and the second application of the flame*

[b] *dripping after the first and second application of the flame. N = no dripping, D-N = dripping without ignition of cotton, D-Y = dripping with ignition of cotton*

[F] *bars burn up to the holding clamp*

With no occurrence of dripping melt, the 15 wt% OP1240 containing formulation (taken as a reference) does achieve V-1 rating. Even though, in terms of average burning times, the material fulfills the conditions for a V-0 classification, the V-1 rating is justified by the fact that two specimens burn above 10s, especially after the first application of the flame. It is therefore necessary to increase the amount of OP1240 to 16 wt% so the material may reach V-0.

15 wt% **C8** or **C9** provides a V-2 classification to reinforced PBT due to the fact that burning drops are produced by UL94 specimens after removal of flame in the second application. As illustrated in Figure 73, the **C8** and **C9** containing materials flow markedly more under the flame than the OP1240 containing sample, however, they produce relatively limited amounts of burning drops while their respective average burning times are fairly comparable to that of the reference sample.

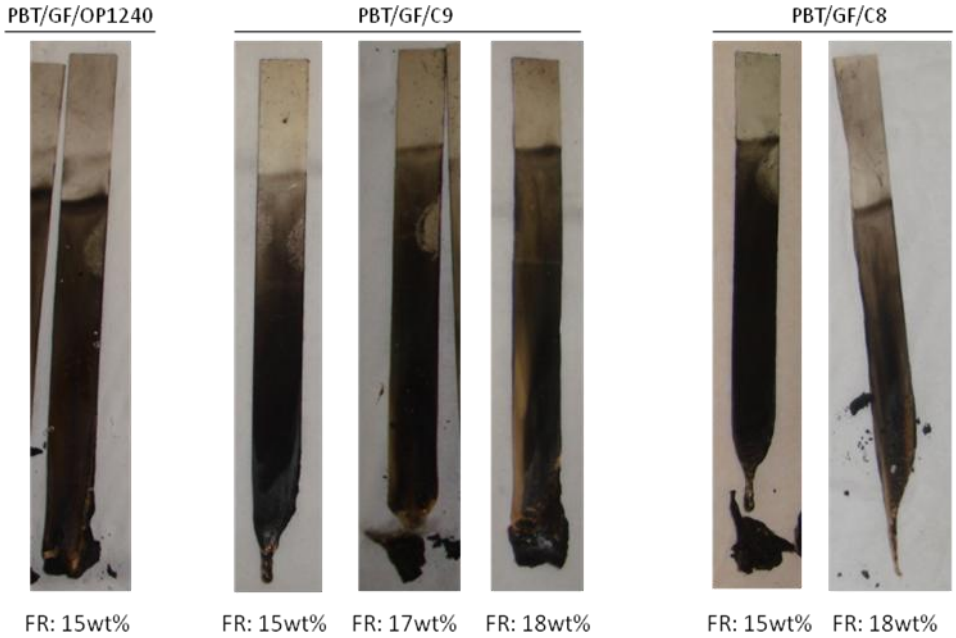

Figure 73 : Bar specimens after the UL94 test (2d.25°C)

Interestingly, the material containing 15 wt% **C9** achieves very high LOI value (50 Vol%) which is significantly higher than the LOI of the sample containing 15 wt% OP1240 (43 Vol%). This demonstrates that there are no absolute correlations between fire results in UL94 and LOI. The LOI value of the material containing 15 wt% **C8** is also high (40 Vol%) but inferior to that of the material containing 15 wt% **C9** which suggests that **C9** is more efficient than **C8**.

C9 provides a V-2 ranking at amounts up to 16 wt%. Increasing the amount of **C9** from 15 to 16 wt% does not improve the UL94 result of the material as higher average combustion times (especially after the second application of the flame) are achieved with the highest FR content. This is due to the fact that burning drops take a longer time to fall away from the bar specimens. At 17 wt% **C9**, a V-0 classification is finally reached after the specimens were conditioned 2 days at 25°C. Nonetheless, this classification turns to V-2 when the sample is conditioned 7 days at 70°C which is consistent with the results discussed in the third chapter. The LOI value of the polymer levels off at 50 Vol% with contents of **C9** of either 15 wt% or 17 wt%. On the other hand, increasing the amount of **C8** from 15 to 18 wt% does not change the UL94 rating of the material (V-2). A higher content of **C8** would rather tend to increase the dripping behavior of PBT as evidenced by the appearance of burning drops after the first application of the flame (Table 21 and Figure 73). This suggests that **C8** has opposite effects on the melt flow of PBT upon heating. This could possibly be caused by a faster degradation of the polymer during the burning process or a degradation of the polymer during the processing. This last assumption is favored since the samples were very breakables. Contrary to **C8**, the compound containing **C9** still provides V-0 rating at 18 wt% in the reinforced polymer, the sample presenting relatively low average combustion times and no dripping (Table 21 and Figure 73).

The products **C12**, **C13** and **C14-2**, appear much less efficient than **C8** and **C9** as formulations containing 15 wt% of these di-phosphinate salts are not classified in the UL94 test. Such formulations exhibit particularly high burning times, besides producing extensive amount of flammable drops, and they moreover all burn up to the holding clamp. The **C12** containing formulation achieves the lowest performances as the corresponding bar specimens burn completely after removal of flame in the first application. 15 wt% **C13** or **C14-2** brings about similar performances in the UL94 test. The di-phosphinate salts also achieve low performances through the LOI test. The highest LOI value, namely 25 Vol%, is obtained for the **C12** and **C13** containing (15 wt%) samples. This represents an increase of 6 points compared to the LOI value of the non-flame retarded polymer (19 Vol%). It thus evidences that **C12** and **C13** have some flame retardant action. A LOI value of only 22 Vol% is achieved for the **C14-2** containing formulation, making **C14-2** the least efficient of the di-phosphinate salts. Owing to the fact that **C13** presents the highest phosphorus percentage (17 wt% according to elemental analyses), it was further tested at 20 wt% in the polymer. Thus, an increase of the amount of **C13** from 15 to 20 wt% allows increasing the LOI value of only 2 points (27 Vol%), while the sample reaches V-2 rating in the UL94 with still high combustion times.

Formulations of reinforced PBT with 17 wt% or 20 wt% **C15** do not allow to achieve any of the UL94 rankings as, for both formulations, complete burning of specimens occurs after removal of flame in the second application. **C15** nevertheless shows some flame retarding properties since it provides a LOI of 24 and 25 Vol% at loading of respectively 17 and 20 wt%.

It can be concluded that a high phosphorus rate is not a prerequisite to improve the flammability behavior of PBT since the best fire performances are achieved with the aluminum phosphinates (namely **C8** and **C9**) having the lowest phosphorus percentages. On the other hand, there is a high disparity between FR efficacies of the mono-functional phosphinate salts (**C8** and **C9**) and that of the di-functional phosphates salts (**C12**, **C13**, **C14-2**). It appears to be somewhat related to inherent thermal stabilities of products. Indeed, poor flame retarding performances are achieved for **C12**, **C13** and **C14-2** whose TG curves (see part 1.4.) showed that they degrade at higher temperature than PBT. Moreover, their residue yields were the highest. On the opposite, good performances are obtained with **C8** and **C9** that degrade in a temperature range around that of PBT and whose residue yields were the lowest. It means that flame retardants (a least that from the category of products hereby investigated) are hardly efficient when they have too high thermal stabilities compared to PBT. Poor performances were obtained with a product such as **C15** whose TG curve almost perfectly superimposed upon the TG curve of PBT and whose residue yield was intermediate between that of mono-functional phosphinates (**C8**, **C9**) and di-functional phosphinates (**C12**, **C13**, **C14-2**). The low efficacy of **C15** can originate from its peculiar chemical nature involving a different mode of degradation or it might result from a too high thermal stability of the salt (particularly as regards to its residue yield in TGA). Yet it is not

straightforward to propose a relevant explanation for the low efficiency of **C15** without further investigation of degradation mechanisms.

Finally, the highest performances were achieved with **C9**, which at loading of 17 wt% gives a V-0 rating (2d.25°C) together with a LOI of 50 Vol% to reinforced PBT. **C8** only provides a V-2 rating at 15 wt% or 18 wt% and the material reaches an excellent LOI of 40 Vol% with 15 wt% **C8**. Thus, further attention should be paid to these salts.

2.2 Fire performances of the zinc and calcium salts of the aniline based phosphinic acid

The following section aims at investigating the influence of the metal of the salts on the flammability behavior of PBT/GF. Since **C9** has proven high flame retardant efficiency, its zinc and calcium analogues (**C10** and **C11** respectively) were also evaluated. Table 22 summarized the UL94 and LOI results obtained for the **C10** and **C11** containing formulations.

It should be remarked that **C11** was exposed to a thermal treatment at 200°C for 5 min prior to its processing with PBT. This treatment aimed to remove the structural water contained in the salt.

Table 22 : UL94 and LOI results obtained for the C9, C10 and C11 containing PBT/GF formulations

Aluminum salt (FR)	Composition (wt%)			LOI (Vol%)	UL-94, 1.6 mm bar			
	PBT	GF	FR		Conditioning	t1/t2[a] (s)	Dripping[b]	Rating
C9	58	25	17	50	2d.25°C	2.4/3.9	N/D-N	V-0
C10	58	25	17	22	2d.25°C	13.8/18.8	D-Y /D-Y	NC
C11	58	25	17	23	2d.25°C	18.0/27.0[F]	D-Y/D-Y	NC

[a] *t1 and t2, average combustion times after the first and the second application of the flame*

[b] *dripping after the first and second application of the flame. N = no dripping, D-N = dripping without ignition of cotton, D-Y = dripping with ignition of cotton*

[F] *bars burn up to the holding clamp*

It appears from Table 22 that **C10** and **C11** present low flame retardant efficiencies in the reinforced PBT. The incorporation of 17 wt% of the salts in the polymer does allow increasing its LOI of only 3-4 points, while none of the UL94 ranking could be reached for both formulations. The latter produce burning drops and they achieve high combustion times, particularly the **C11** containing sample whose bar specimens completely burn after removal of flame in the second application. The reason justifying that the **C10** containing material is not classified in the UL94 is that one of its bar specimens burn above 30s.

In conclusion, the nature of the cationic metal center has a drastic influence on the flame retarding properties of the aniline based phosphinate salt. Since the zinc and calcium salt **C10** and **C11** show an almost similar inability to flame retard PBT/GF, the fire performances of formulations should be to some extent related to the thermal stabilities of the salts.

Indeed, **C10** and **C11** exhibit similar TG curves (see part 1.4.) which are both characterized by lower T_{onset}, higher residue yields, hence lower mass rate amplitudes as compared to the TG curve of **C9**. Assuming that the synthesized phosphinates exhibit a prevailing gas phase mode of action (by analogy with the aluminum and zinc salts of the diethyphosphiniate[80]), **C10** and **C11** would therefore release a lower amount of active species in the gas phase, while such release would occur earlier and at lower rate (so with less efficiency) compared to **C9**. It is not to be excluded, however, that condensed phase activities take place in the burning PBT and that the metal cationic center plays an non negligible role in these mechanisms[80].

2.3 Fireproofing combinations: combination of the aluminum salts of the aniline and benzyl amine based phosphinates with commercial flame retardants and synergistic agents

As seen in the last two sections, **C8** and **C9** showed the most attractive properties to flame retard PBT. It is now of interest to figure out whether these salts can bring about improved fire performances to the polymer when they are combined with commercial flame retardants or synergistic agents.

2.3.1 Selection of the co-additives

The additives to be combined with **C8** and **C9** were selected taking into account the investigations reported in the third chapter and on the state of the art. These additives are summarized in Table 23.

RDP bentonite and OM-POSS were selected as they proved, below 3 wt%, to be good synergistic agents for use with Exolit OP1200 and Exolit OP1240 (see chapter 3). These nano-particles were accordingly combined with **C8** and **C9** at loading as low as 1-1.5 wt%.

PTFE is a well-known anti-dripping agent that is commonly used for flame retardancy applications[62,205,206]. It was chosen here because the main shortcoming of PBT formulations containing **C8** or **C9** is their tendency to drip, hence to inflame cottons during the UL94 test. Amounts of PTFE up to 0.5 wt% are usually required to prevent dripping of samples. So for the present test, PTFE was used at loading of 0.5 wt%.

Melamine polyphosphate was selected because it was successfully used in combination with phosphinate salts for applications in thermoplastics (i.e. Exolit OP1311)[207]. Aluminum hypophosphite was finally chosen because it has proven flame retardant properties in PBT[82,83] and because it is characterized by high phosphorus content.

Table 23 : Selected co-additives: type, commercial name, supplier and loading in the formulation

Co-additive type	Co-additive type	Co-additive name and supplier	Loading (wt%)
Organo-modifed layered clay	Resorcinol bis(diphenyl phosphate) modified Bentonite	*RDP bentonite*, **Glen Burnie Technologies** (experimental product supplied by BASF)	1
Polyhedral oligomeric silsesquioxane (POSS)	Octamethyl POSS (OM-POSS)	*OM-POSS*, **Hybrid Plastics**	1.5
Fluorinated polymer	Polytetrafluoroethylene (PTFE)	*PTFE powder SST-5,* **Shamrock**	0.5
Melamine salts	Melamine polyphosphate (MPP)	*Melapur 200*, **BASF (Ciba)**	5
Phosphinate salt	Aluminum hypophosphite	*Phoslite IP-A*, **Italmach**	8.5

2.3.2 Fire performances of the fireproofing combinations

In Table 24 and Table 25, are respectively depicted the fire test results (UL94 and LOI) obtained for the **C8** and **C9** containing formulations.

Table 24 : UL94 and LOI results obtained for the C8 + co-additive containing PBT/GF formulations

Co-additive	Composition (wt%)				LOI (Vol%)	UL-94, 1.6 mm bar			
	PBT	GF	C8	Co-additive		Conditioning	t1/t2[a] (s)	Dripping[b]	Rating
-	60	25	15	-	40	2d.25°C	5.3/1.0	N/D-Y	V-2
-	57	25	18	-	-	2d.25°C	1.5/1.7	D-Y/D-Y	V-2
OM-POSS	60	25	13.5	1.5	39	2d.25°C	15.2/1.8	D-Y/D-Y	V-2
RDP Bentonite	57	25	14	1	-	2d.25°C	9.9/1.0	D-Y/D-Y	V-2
RDP Bentonite	57	25	17	1	-	2d.25°C	1.6/1.4	D-Y/D-Y	V-2
PTFE	60	25	14.5	0.5	36	2d.25°C	8.1/1.2	N/D-Y	V-2
MPP	55	25	15	5	34	2d.25°C	14.1/0.5	D-Y/D-Y	V-2

[a] *t1 and t2, average combustion times after the first and the second application of the flame*

[b] *dripping after the first and second application of the flame. N = no dripping, D-N = dripping without ignition of cotton, D-Y = dripping with ignition of cotton*

By first examining Table 24, it should be noted that the substitution of **C8** by 1.5 wt% OM-POSS or 1 wt% RDP bentonite (on basis of a formulation containing 15 wt% **C8**) does not modify the UL94 ranking of the material (V-2). In fact, the presence of nano-particles (particularly OM-POSS) increases the combustions time of specimens after the first application of the flame which leads to the formation of flammable drops. Further to that, the LOI value of the material is slightly reduced from 40 to 39 Vol% with substitution of **C8** by

OM-POSS. On the other hand, the combination of 17 wt% **C8** and 1 wt% RDP bentonite brings about the same UL94 results as with 18 wt% **C8**. Apart from a moderate increase of the combustion time of specimens after removal of flame in the first application, the substitution of a slight amount of **C8** by PTFE has no real influence on the UL94 results. The LOI, however, significantly decreases from 40 to 36 Vol%. The combination of 5 wt% MPP and 15 wt% **C8** leads to an antagonist effect as the material achieves higher combustion time at UL94 and lower LOI compare to the sample containing only 15 wt% **C8**.

As observed in Table 25, the substitution of **C9** by 1.5 wt% OM-POSS (on basis of a formulation containing 15 wt% **C9**) seriously damages the flammability performances of reinforced PBT. There is indeed a clear antagonism between OM-POSS and **C9** which is evidenced by the important decrease of the LOI value from 50 to 38 Vol%. Furthermore, OM-POSS greatly promotes the combustion and dripping of bar specimens in UL94 to such an extent that the material is not classified anymore (see in Figure 74 a comparison between burned specimens containing or not OM-POSS).

Table 25 : UL94 and LOI results obtained for the C9 + co-additive containing PBT/GF formulations

Co-additive	Composition (wt%)				LOI (Vol%)	UL-94, 1.6 mm bar			
	PBT	GF	C9	Co-additive		Conditioning	t1/t2[a] (s)	Dripping[b]	Rating
-	60	25	15	-	50	2d.25°C	3.5/3.4	N/D-Y	V-2
-	59	25	16	-	-	2d.25°C	3.7/7.0	N/D-Y	V-2
-	58	25	17	-	50	2d.25°C	2.4/3.9	N/D-N	V-0
-	58	25	17	-	-	7d.70°C	6.6/2.8	N/D-Y	V-2
OM-POSS	60	25	13.5	1.5	38	2d.25°C	37.0/17.0	D-Y/D-Y	NC
RDP Bentonite	57	25	14	1	49	2d.25°C	12.2/5.1	D-Y/D-Y	V-2
RDP Bentonite	57	25	15	1	48	2d.25°C	8.8 /5.4	N/D-Y	V-2
RDP Bentonite	57	25	16	1	-	2d.25°C	2.4/4.9	N/D-N	V-0
RDP Bentonite	57	25	16	1	-	7d.70°C	5.7/4.5	N/D-N	V-1
PTFE	60	25	14.5	0.5	36	2d.25°C	12.8/5.8	N/D-Y	V-2
MPP	55	25	15	5	-	2d.25°C	17.4/0.8	N /D-Y	V-2
phoslite	60	25	8.5	8.5	25	2d.25°C	37.2[F]/-	D-Y/-	NC

[a] *t1 and t2, average combustion times after the first and the second application of the flame*

[b] *dripping after the first and second application of the flame. N = no dripping, D-N = dripping without ignition of cotton, D-Y = dripping with ignition of cotton*

[F] *bars burn up to the holding clamp*

The combination of **C9** with 1 wt% RDP bentonite shows interesting properties depending on the total concentration of additives (**C9** + RDP bentonite). When the overall additive content is of 15 wt%, the formulation achieves V-2 rating with higher average combustion times (and further production of burning drops after the first application of the flame) compared to the formulation containing 15 wt% **C9**. An increase of the additive content to 16 wt% (15 wt% **C9** + 1 wt% RDP bentonite) shows no benefit in UL94 compared to 16 wt% **C9**. With 16 wt% **C9** +

1 wt% RDP bentonite, a V-0 rating (2d.25°C) could finally be reached (see bar specimens in Figure 74), similarly to the sample containing 17 wt% **C9** alone. V-0 rating turns to a V-1 rating when the sample underwent an ageing treatment of 7 days at 70°C. Therefore, mixture of 16 wt% **C9** + 1 wt% RDP bentonite achieves better UL94 classification than **C9** alone at loading of 17 wt%. As it was previously observed for the OP1240 based formulations (chapter 3), the substitution of **C9** by RDP bentonite tends to slightly reduce the LOI value of the material.

Similarly to **C8**, the substitution of 0.5 wt% **C9** by PTFE does significantly decrease the LOI value (from 50 to 36 wt%). The UL94 rating is preserved, but an increase of the average burning times of the sample is still observed in presence of the fluorinated polymer. The use of 5 wt% MPP is not more beneficial with 15 wt% **C9** than with 15 wt% **C8** as seen through the UL94 test. The combustion time of bar specimens after the first application of the flame likewise increases when adding MPP up with **C9** in the polymer, while after removal of flame in the second application a plain part quickly brake off from specimens and inflames the cotton.

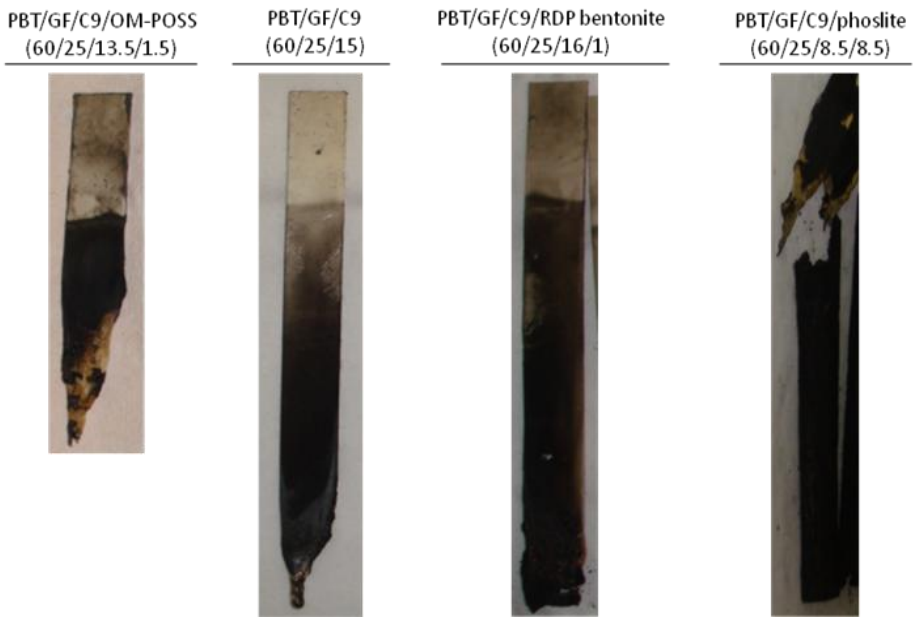

Figure 74 : Bar specimens after the UL94 test (2d.25°C)

The combination of **C9** with the aluminum hypophosphite (phoslite) provides very low performances to reinforced PBT, both in the LOI and UL94 tests. A LOI value of only 25 Vol% is achieved for the material. The latter is furthermore not classified in the UL94 test as complete burning of specimens occurs after removal of flame in the first application. As illustrated in Figure 74, the bar specimens swell up during the UL94 test, releasing an important amount of fumes, and they break as full part from the clamp.

In conclusion, few of the co-additives tested with **C8** and **C9** show beneficial properties. Whereas good performances were achieved when combining OM-POSS with Exolit OP1200 or Exolit OP1240, the nano-particle is found to be antagonistic with the synthesized phosphinates, particularly with **C9**. PTFE does not exhibit the expected anti-dripping properties and it even tends to worsen the flammability behavior of materials although it is used in very low amount. For both **C8** and **C9** (15 wt%) containing materials, the addition of 5 wt% MPP decreases the fire performances and the combination of **C9** with phoslite leads to poor flame retardant properties. So far, the most interesting performances are achieved when combining 16 wt% **C9** with 1 wt% RDP bentonite. This fireproofing combination provides a V-0 and a V-1 rating to the reinforced PBT respectively after the 2 days (25°C) and 7 days (70°C) ageing. It is therefore better than the sole use of 17 wt% **C9**.

2.4 Conclusion

In this section, the flame retarding properties of the synthesized phosphinate salts in the reinforced PBT were investigated. It appeared that the FR efficiency of salts was somewhat related to their thermal stability rather than their phosphorus content. The di-functional phosphinate salts (**C12**, **C13** and **C14-2**) exhibited poor efficiencies probably because of their too high thermal stabilities compared to the polymer. On the opposite, good performances were obtained with the mono-functional phosphinates **C8** and **C9** as these salts degrade in a temperature range close to that of PBT. **C9** was found to be particularly efficient as it provides a V-0 (1.6 mm) rating (2d.25°C) at loading of 17 wt% and a LOI of 50 Vol% to reinforced PBT. The PEPA based phosphinate (**C15**) shows poor efficiency but no clear conclusion could be drawn to explain this since the product degrades in the same temperature range than PBT, as observed for **C8** and **C9**. On the other hand, the zinc and calcium analogues of **C9** (**C10** and **C11**) were found to be much less efficient that **C9**. It proves that the metal cation plays a key role in flame retarding performances of phosphinates.

The combination of **C8** and **C9** with commercial flame retardants (MPP, phoslite) and synergistic agents (OM-POSS, RDP bentonite, PTFE) was also experienced. None of the fireproofing combinations provided satisfactory FR properties except the combination of 16 wt% **C9** with 1 wt% RDP bentonite. The latter gives a V-0 and V-1 rating after conditioning the bars respectively for 2 days (25°C) and 7 days (70°C) whereas V-0 and V-2 rating were achieved with 17 wt% **C9** alone in the reinforced PBT.

3. Conclusion

Novel phosphinate salts were synthesized from the commercial oxaphospholane oxide Exolit PE110. These salts, whose structure is derived from ethyl methyl phosphinate, exhibited FR efficiencies in reinforced PBT depending on the type of metal cation or the structural variation of the residue “grafted” on the phosphinate basis. Narrowing the focus on

aluminum salts, it appears that the best FR performances are achieved for the salts whose thermal stabilities are close to that of PBT. Salts having too high thermal stabilities compared to PBT achieved poor FR performances. These observations lead us to assume that the enhancement of the fire behavior of PBT should mainly proceed through a gas phase mode of action. Thus, phosphinate salts of too high thermal stabilities exhibit low FR performances as they would release insufficient amounts of active species (i.e. phosphorus) in the gas phase during the PBT degradation. On the other hand, the nature of the metal cation coordinated to phosphinate is an important parameter to take into consideration in the improvement of the flame retardant properties of PBT. With regards to the results obtained in the present study, aluminum phosphinate salts would appear much more efficient than calcium or zinc salts.

Among the synthesized salts, there is one that exhibited very promising FR properties: the aluminum salt of the aniline based phosphinate **C9**. The latter proved to be a bit less effective than Exolit OP1240 in considering the UL94 test but better considering the LOI. The various tests performed came to define an optimized PBT formulation that contains 16 wt% **C9** + 1 wt% RDP bentonite. Thus, RDP bentonite was found to be a good synergistic agent when used with the phosphinate salt **C9** which is in agreement with the result of chapter 3. **C9** might undoubtly surpasses the performances of OP1240 if it is combined with the suitable co-additives. This shall open up new prospects in the research of improved flame retardant PBT/GF formulations.

The understanding of the flame retardant modes of action is another important part of this project. Such an approach is crucial to design high performing flame retardant materials. The last chapter therefore intends to investigate and to compare the flame retardant modes of action of Exolit OP1240 and **C9** in reinforced PBT.

CHAPTER 5 – FLAME RETARDANCY MECHANISM OF PHOSPHINATE SALTS IN REINFORCED PBT: COMPARISON BETWEEN COMMERCIAL AND SELF-SYNTHESIZED FLAME RETARDANT MODES OF ACTION

The industrial challenge has been achieved: developing novel, efficient, flame retardant glass fiber reinforced PBT formulations using commercial and self-synthesized phosphinate salts. Chapter 3 has demonstrated that the combination of 18 wt% of the commercial phosphinate salt Exolit OP1240 with 2 wt% of the organoclay RDP bentonite brought improved flame retardancy performances as shown with the UL94 and the cone calorimeter tests while the LOI is maintained. In chapter 4, the synthesis of the aluminum salt of the aniline based phosphinate **C9** was described. This novel phosphinate provided excellent flame retardant properties to reinforced PBT, even better when it was combined with RDP bentonite.

The present chapter aims at investigating and comparing the flame retardant mechanisms of both phosphinates **C9** and Exolit OP1240 in reinforced PBT. We will particularly attempt to answer the following questions:

- Are the flame retardants decomposing thought an analogous route, whether outside or inside the polymer, and do they act according to the same FR mode of action (i.e. gas and/or condensed phase)?

- What is the influence of the flame retardants on the degradation pathway of the polymer? Is this degradation pathway similar to that for the pure PBT/GF? If not, to which extent would the flame retardants modify the nature, proportion and/or production sequence of the degradation products of PBT and what would be the mechanisms involved in such modification.

- Does the polymer itself influence the degradation pathway of the flame retardants and would it play a key role in the improvement of the flammability of the material?

Thus, the first part of this chapter investigates the thermal degradation pathway of the pure reinforced PBT. Various methods have been used, including TGA-FTIR and pyrolysis-GCMS for the analysis of the degradation products released in the gas phase as well as solid state NMR measurements to study the condensed phase of the material. This first part will be crucial to thoroughly compare the decomposition routes of the flame retarded and non-flame retarded polymer.

The second and last part of this chapter will be properly dedicated to the flame retardant properties of the two phosphinate salts (**C9** and Exolit OP1240) in the reinforced PBT. The thermal degradation pathway of the pure flame retardants as well as that of flame retarded PBT will be explored. Special emphasis will be put on the comparison between the FR modes of action of both phosphinate salts.

It should be remarked that the amount of each component in the material hereafter analyzed (flame retarded or not) have been intentionally chosen to be equivalent to the relative amount of the same components in the optimized (complete) formulations containing RDP bentonite. This methodology was indeed more convenient for future

prospects regarding the investigation of the synergistic effect between phosphinate salts and RDP bentonite. Thus, three formulations have been investigated in this part. The first formulation is PBT/GF. It contains a mass percentage of PBT and GF of respectively 69.9 wt% and 30.1 wt%. It corresponds to the relative mass percentage of both components in the optimized PBT (58 wt%)/GF (25 wt%)/**C9** (16 wt%)/RDP bentonite (1 wt%) formulation. The latter was also used as reference to determine the mass percentage of PBT, GF and **C9** in the PBT/GF/**C9** formulation studied below (second formulation). So for this second formulation, the mass percentages of PBT, GF and **C9** were of 58.9 wt%, 25.3 wt% and 16.2 wt% respectively. The third formulation investigated is PBT/GF/OP1240. In this case, the mass percentages of PBT, GF and OP1240 used were respectively 56.1 wt%, 25.5 wt% and 18.4 wt%. It corresponds to the relative amount of the three components in the optimized PBT (55 wt%)/GF (25 wt%)/OP1240 (18 wt%)/RDP bentonite (2 wt%) formulation. It is to be noted that the study of FR + RDP bentonite systems will not be addressed in the present work.

1. Thermal degradation behavior of glass fiber reinforced PBT

The flame retardant behavior of a material depends on the degradation reactions, the rearrangements and/or recombinations occurring in the condensed and gas phases. In order to determine the flame retardant mode of action of the phosphinate salts, it is necessary to investigate the reactions occurring during the thermal degradation of the pure reinforced PBT and that occurring in the polymer flame retarded with the salts.

This first part focuses on the study of the thermal degradation of pure glass fiber reinforced PBT. The latter has been widely reported in the literature[33-35,142,208] and it was fully discussed in the state of the art (chapter 1). As mentioned earlier, PBT is a low charring polymer and its degradation occurs in an apparent single stage with release of well characterized effluents and production of low amount of char residue. The nature and proportion of the PBT degradation products released in the gas phase can nonetheless differ depending on the PBT grade, the equipment and the experimental conditions used during analyses. Therefore, study of the thermal degradation of PBT using our own experimental methods is necessary so as to draw relevant conclusions and comparisons on the FR modes of action of phosphinate salts.

1.1 Thermal degradation

The thermal degradation of PBT/GF was studied by thermogravimetric analysis (TGA). The experiment was carried out under nitrogen atmosphere where pyrolytic degradation reactions are prevalent. The TGA curve (TG) as well as the derivative TG curve (DTG) of the PBT/GF material are pictured in Figure 75.

The degradation of reinforced PBT occurs in a single step from 330 to 450°C with a maximum degradation rate at 400°C, leading to a residue of 33.3 wt%. Inert glass fibers mostly accounts for the mass of the final residue, that is to say 30.1 wt%. The final char yield attributed to the polymer is thus of only 3.2 wt%. It is in accordance with data of the literature[34,39].

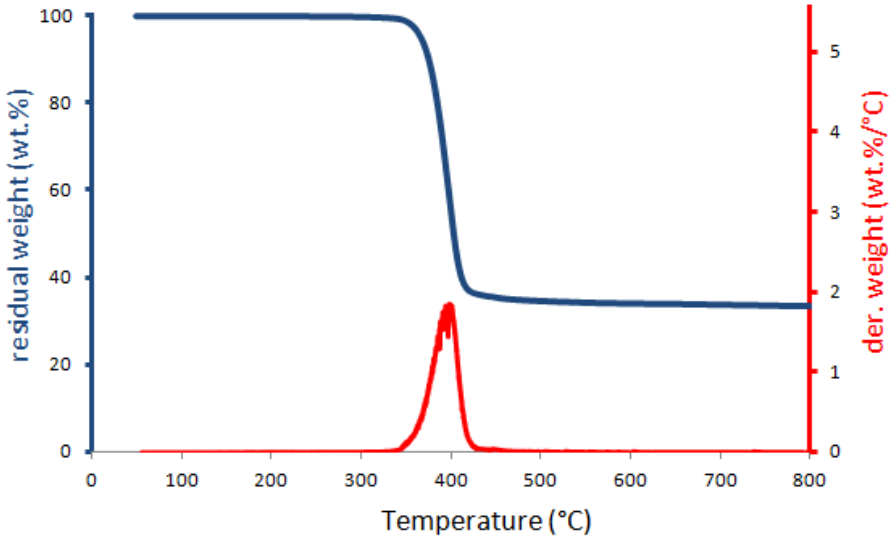

Figure 75 : TG and DTG curves of PBT/GF (10°C/min in nitrogen)

1.2 Evolved gases

The analysis of the gas phase was performed through TGA-FTIR and Pyrolysis-GCMS. The former technique allows detecting in real time gaseous products evolved from the sample during the thermal degradation. The second technique was used in complement to the first one. The analysis is performed using a thermal desorption mode which consists of heating the sample in a pyrolyzer module - at the same heating rate (10 K/min) as the one used in TGA-FTIR - while evolved gases condense and accumulate at the top of the GC column. The separation and analysis of gases in the GCMS unit is started right after reaching the desired temperature in the pyrolyzer. The methodology applied for pyrolysis-GCMS analyses was the same for almost all materials investigated in this chapter. For each product or formulation two samples were systematically analyzed: a first sample was heated to the temperature corresponding to the middle part of the mass loss slope in TGA while a second sample was heated to a temperature close to the end of TG weight loss. This methodology allowed monitoring the evolution of gases released throughout the degradation.

FTIR spectra versus temperature of gases evolved during the TG analysis of PBT/GF are presented in Figure 76. Attributions of the IR bands are gathered in Table 26. Band assignments were obtained from a few studies reported in the literature[39,80,127,128,209]. It is worth mentioning that a slight delay between the detection of evolved gases in FTIR and the

mass loss in TGA can be observed because some of the evolved gases can condense in the transfer line heated at 250°C. Figure 77 depicts the pyrograms recorded during the thermal desorption phase of degradation products in the GCMS, after heat treatment of the sample to 390°C and 470°C in the pyrolyzer. Mass spectra of detected products are depicted in Appendix 4.

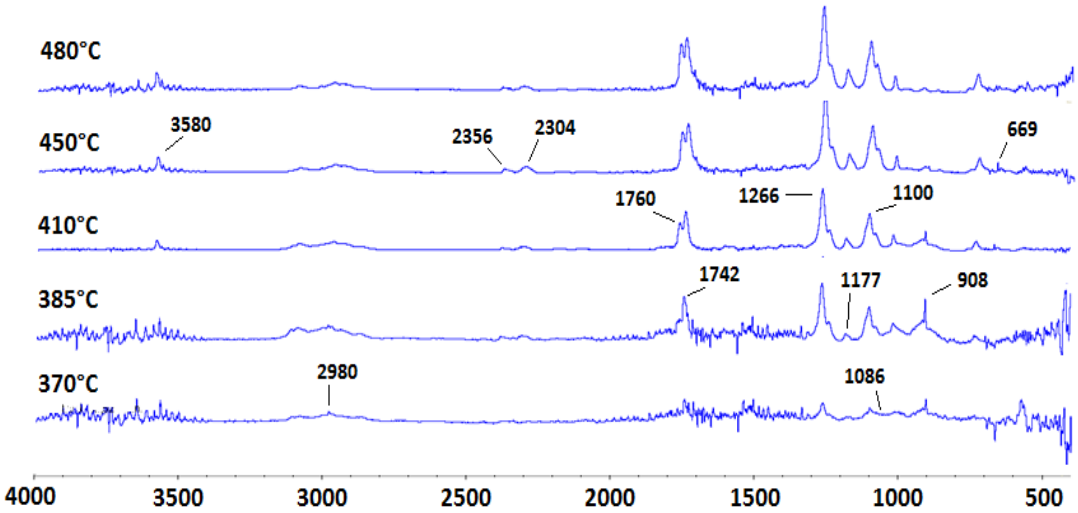

Figure 76 : FTIR spectra of the gases evolved during the thermal degradation of PBT/GF (in N_2 atmosphere) at characteristic temperatures

Table 26 : Attribution of the IR bands of the gases evolved during degradation of PBT/GF in nitrogen[39,80,127,128,209]

Decomposition products	FTIR/cm^{-1}
THF	**2980** (CH_2 stretch), **1086** (asym. ring vibration)
Butadiene	**908** (-C=C-H wag)
CO_2	**2356** (CO_2 asym. stretch), **2304** (CO_2 sym. stretch), **669** (CO_2 bend)
H_2O	**4000-3400** (O-H stretch)
Benzoic acid	**3580** (O-H stretch), **1760** (C=O sym. stretch)
Esters	**1742** (C=O stretch), **1266** (C-O-C asym. stretch), **1100** (C-O-C sym. stretch)

Water, THF, butadiene, carbon dioxide, benzoic acid and ester derivatives were identified through TGA-FTIR which is in accordance with the literature[39,127]. THF and water are the first degradation products to be released. These are followed by the release of butadiene, esters, CO_2 and benzoic acid. Throughout the pyrolysis-GCMS measurements, the most volatile products such as THF, butadiene, carbon dioxide and water could not be detected as they run directly through the GCMS transfer line without accumulating at the top of the GC column during the heating phase of the sample in the pyrolyzer.

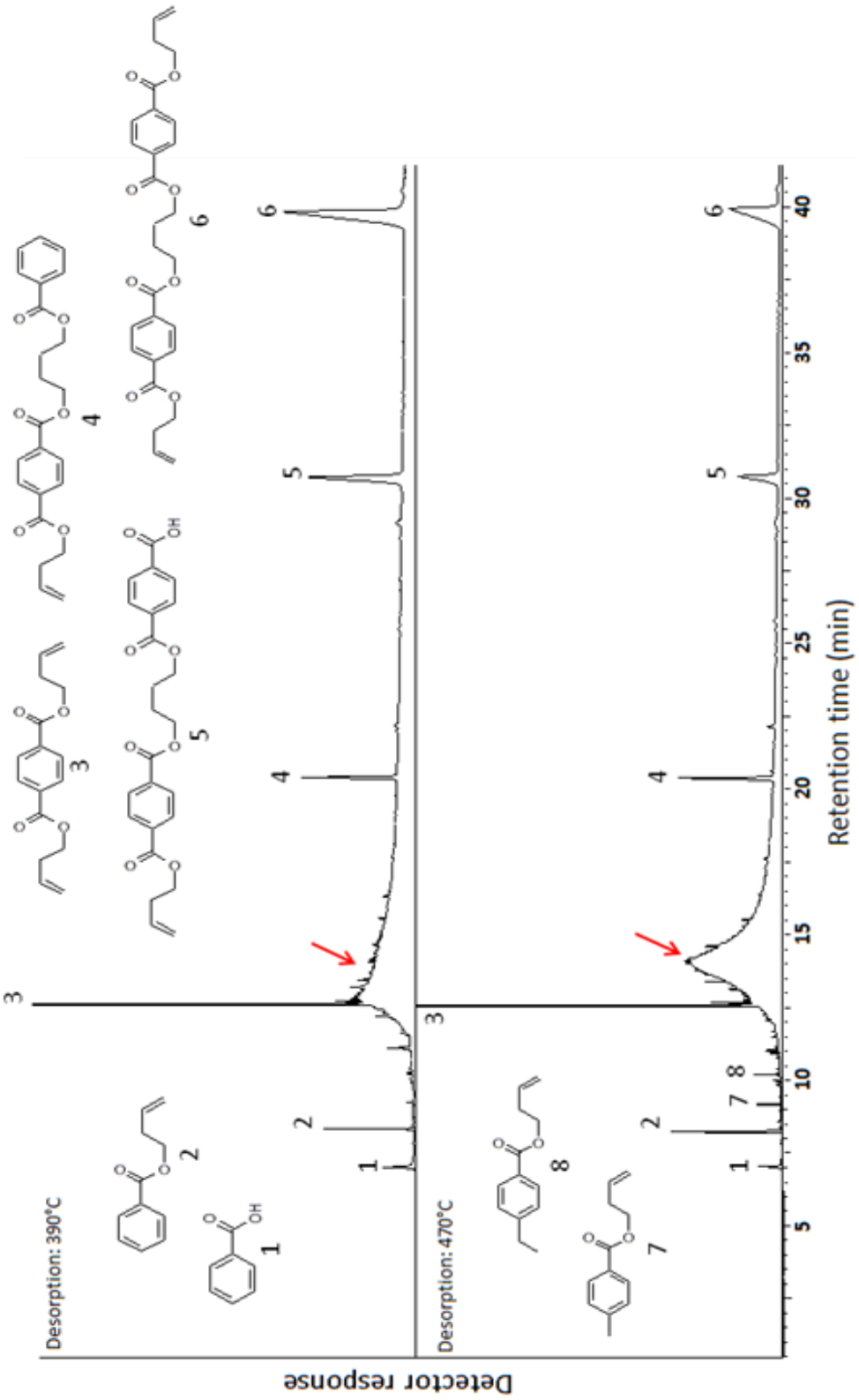

Figure 77 : Chromatogram of the gases evolved during the thermal treatment of PBT/GF to 390°C (above) and 470°C (below) in helium atmosphere; heating rate in the pyrolyzer: 10°C/min

The pyrograms depicted in Figure 77 allow providing details on the chemical structure of ester derivatives (peak 2, 3, 4, 5, 6) prevalently released during the degradation. Similar

esters were identified by Ohtani et al[35]. Unlike the results reported by the same authors, however, the proportion of evolved benzoic acid (reciprocal to the surface area of the peak) is relatively low while oligomeric esters of benzoic acid and of terephthalic acid (peak 4, 5 and 6) are released in significant proportions. This is due to the fact that the thermal treatment of samples has not been carried out in the same conditions. In the present study, the sample has been thermally treated through a constant heating rate (10K/min) from 60°C to fixed temperatures. In the Ohtani study, the sample was directly introduced in the pyrolyzer pre-heated at 590°C (pyrolysis). In the latter case, the material underwent more severe heating conditions involving faster degradation processes and production of a higher proportion of low boiling point degradation products.

On the other hand, the pyrograms exhibit a broad massif centered at 13.8 s (red arrow). It is attributed to species which could not be finely separated in the column. The mass spectra taken out from this massif (see Appendix 4) reveals the presence of a large quantity of terephthalic acid plus a number of degradation products that could not be identified. During the first half of the PBT/GF decomposition (desorption at 390°C), oligomeric esters corresponding to the peaks 5 and 6 are obtained in relatively high proportion. With increasing degradation temperature (desorption at 470°C), the proportion of terephthalic acid and esters of smaller molecular weight (peak 2, 3 and 4) increases while the release of esters of higher molecular weight (peak 5 and 6) tends to level off or even decrease. This is obviously due to a further degradation of the polymer. The pyrogram obtained after heat treatment of the sample to 470°C exhibits two supplementary peaks attributed to the butenyl ester of benzoic acid substituted by a methyl (peak 7) and an ethyl (peak 8) group on the aromatic ring. These compounds have never been reported in the literature. As they result from minor degradation processes (small area of peaks), they will not be considered in the decomposition model discussed below.

1.3 Analysis of the PBT/GF residue

In order to investigate the degradation residue of the PBT/GF material, the latter was submitted to a thermal treatment as following: it was heated in nitrogen flow, to temperature above that corresponding to the end of mass loss in TGA, in this case 600°C. It is noteworthy that the mass lost during the thermal treatment of the sample was compared to that of the TGA. Slight differences can be observed, attributed to heat and mass transfer phenomena occurring in the heat-treated strips (UL94 bar specimen) and not in the powder used for TGA. The treatment was validated as the mass loss of the heat treated sample was in the same range of the one observed in TGA at the same temperature. The same methodology was applied for the investigation of the residue of other samples discussed below in this chapter. For all samples, the mass losses will thus be presented as comparison elements but not commented on.

The residue obtained after thermal treatment of the PBT/GF material to 600°C is pictured in Figure 78. Before the treatment, the material consists of a strip of white polymer. After the treatment, the material is black and it contains lots of holes. Its rugged surface reveals the presence of a glass fiber network.

The degradation residue was analyzed using ^{13}C CP/MAS solid state NMR to determine its chemical structure. A stacking of the ^{13}C NMR spectra of the material before and after the thermal treatment is depicted in Figure 79. It should be remarked that the signal intensity on the spectrum of the residue (spectrum B) was increased to facilitate the peaks observation.

The ^{13}C spectrum of the degradation residue exhibits a broad signal centered at 130 ppm attributed to aromatic and alkylenic carbons in amorphous structural arrangements. Neither aliphatic carbons (spectrum A, peaks 8, 9, 10, 11) nor carbons from the carbonyl functions (spectrum A, peak 1) remain after the treatment to 600°C. Solid state NMR measurements – supported by TGA analyses - allow concluding that PBT produces a relatively low amount of carbonaceous char when decomposing.

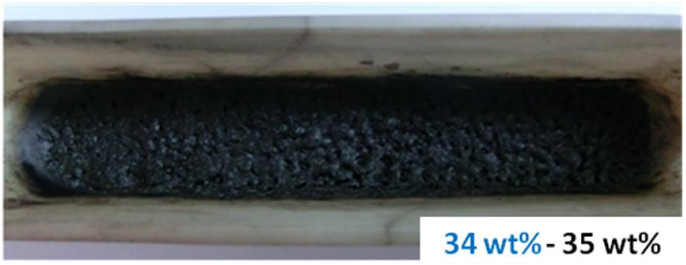

Figure 78 : Picture of the residue of PBT/GF obtained after thermal treatment to 600°C in nitrogen. In blue: expected mass loss (according to TGA), in black: experimental mass loss

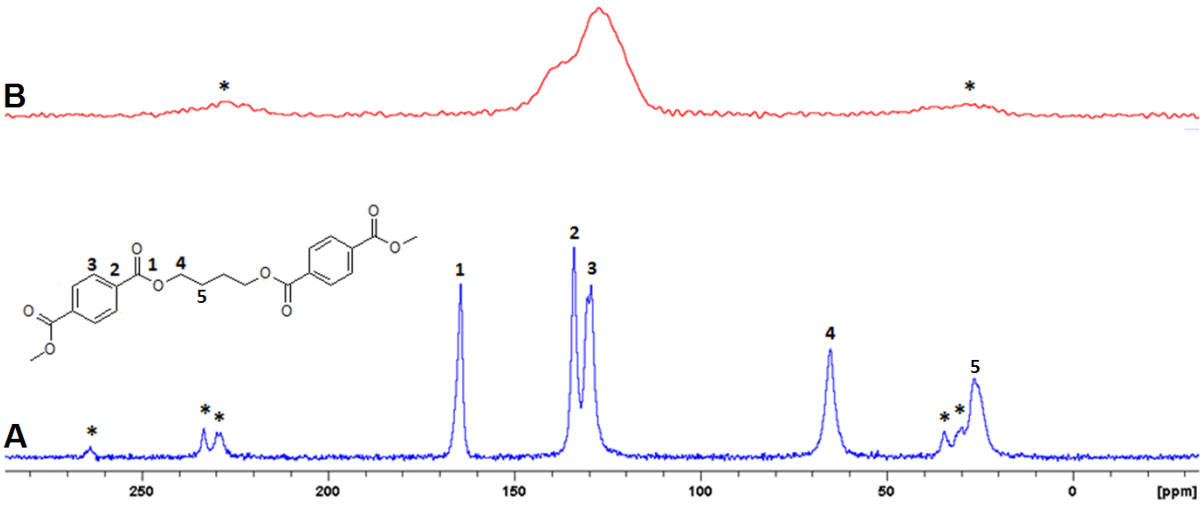

Figure 79 : ^{13}C CPMAS solid state NMR spectra of the PBT/GF material before (spectrum A) and after (spectrum B) thermal treatment at 600°C in nitrogen (*spinning side bands)

1.4 Degradation mechanism

Most of the information provided by the gas and condensed phase analyses are consistent with data of the literature[33-35,39,141]. The degradation pathway of PBT/GF is then pictured in Figure 80.

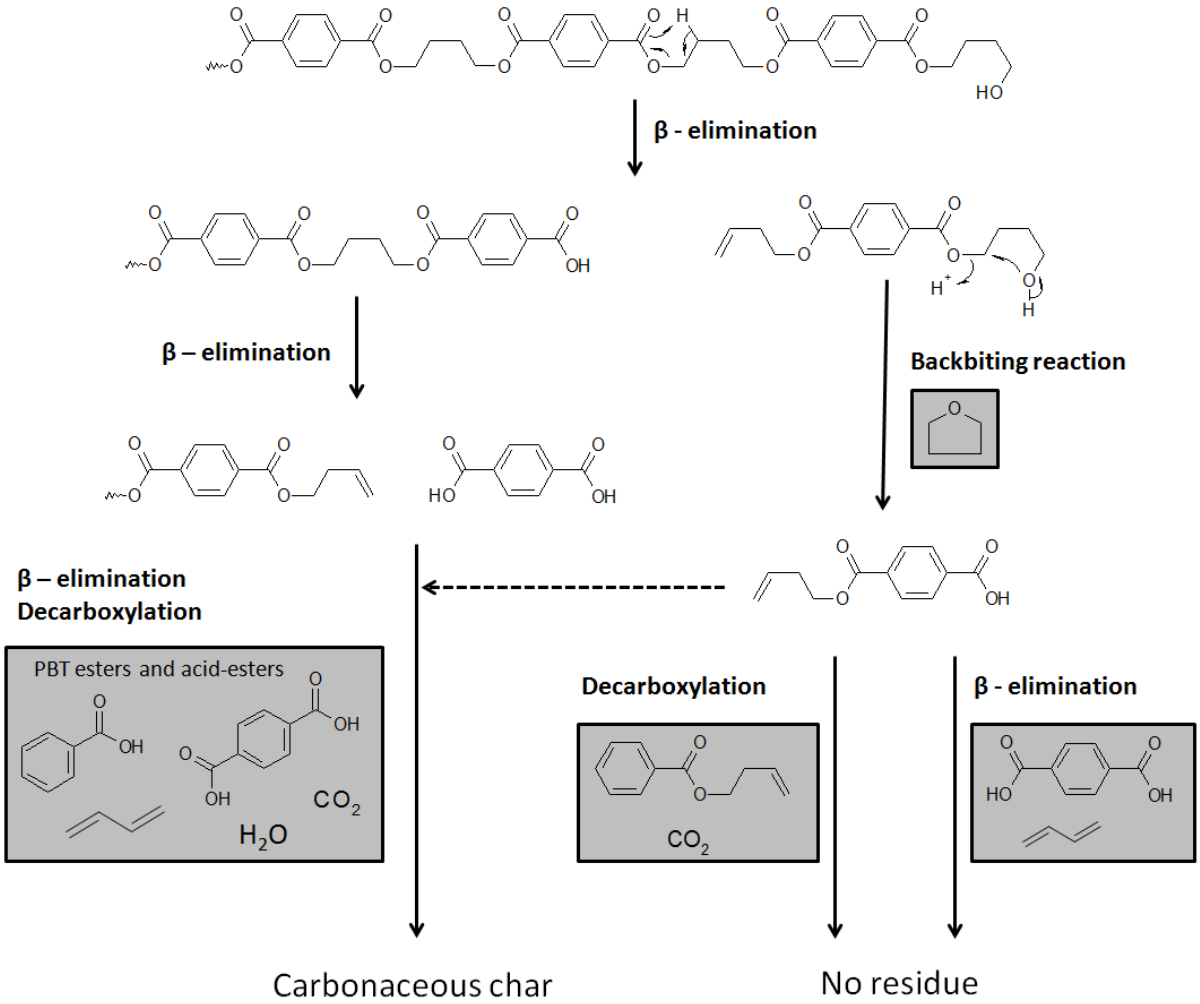

Figure 80 : PBT/GF degradation scheme (detected gaseous decomposition products in grey)

PBT mainly decomposes through a beta elimination process, leading to the formation of acid and vinyl end-chain groups[33-35]. Decarboxylation of acids and further beta elimination processes lead to the formation and subsequent liberation of CO_2, butadiene and aromatic acids, esters and acid-esters. This degradation route does not result in char production[39,141]. Pyrolysis-GCMS analyses demonstrated that under the thermal conditions used, the aromatic acids, esters and acid-esters prevalently released by PBT/GF in the gas phase were terephthalic acid, dibutenyl ester of terephthalic acid and oligomers with vinyl, acid and/or phenyl end groups. It should be noticed that terephthalic acid could not be observed in FTIR since the di-acid condenses in the transfer line connecting the TGA apparatus to the FTIR module[39]. On the other hand, a small quantity of THF is released at the beginning of the PBT degradation. THF can be obtained through several decomposition pathways, including a

backbiting cyclisation reaction[210,211] of butanediol end chain radicals (see degradation scheme) or a cyclisation of free butanediols generated by hydrolyses of PBT[33,141]. These degradation routes do not result in residue formation. A solid residue is however formed when THF is obtained through cyclisation of intra-chain butanediol and/or end-chain butenyl groups[33]. These processes are induced by proton transfer reactions. Finally, some minor degradation reactions lead to the formation a low proportion of carbonaceous char residue.

2. Thermal degradation behavior of glass fiber reinforced PBT flame retarded with aluminum phosphinate salts

To determine the influence of the phosphinate salts (**C9** and exolit OP1240) on the chemical degradation pathway of the PBT, it is necessary to compare the thermal degradation mechanism of the pure and of the flame retarded material. The same methodology as for the pure reinforced PBT was followed to determine the degradation pathway of the material flame retarded with both commercial and self-synthesized phosphinates.

The decomposition of PBT/GF/**C9** is first investigated in this part. Then, it will be discussed the decomposition of PBT/GF/OP1240 to highlight the differences and similarities between both phosphinate salts in terms of FR properties.

2.1 PBT/GF flame retarded with the aniline based phosphinate aluminum C9

Before investigating the degradation behavior of the PBT/GF/**C9** formulation, it is indispensable to understand how pure **C9** decomposes. This is the purpose of the first subsection.

2.1.1 Thermal decomposition behavior of C9

2.1.1.1 Thermal degradation

As shown in Figure 81, the thermal degradation of **C9** occurs in several steps between 310°C and 600°C, leading to a residue of 35.8 wt%. A first step occurs between 310°C and 385°C (1) and it is characterized by a sharp mass loss of about 32 wt%. The second degradation step occurs between 385°C and 450°C (2). It corresponds to a mass loss of about 20 wt%. The convoluted shape of the DTG curve indicates that complex degradation phenomena take place in this range of temperature. The third step occurs between 450°C and 482°C (3) and the fourth step between 482°C and 600°C (4). Mass losses of about 7 wt% and 4 wt% are respectively recorded for these two last degradation stages.

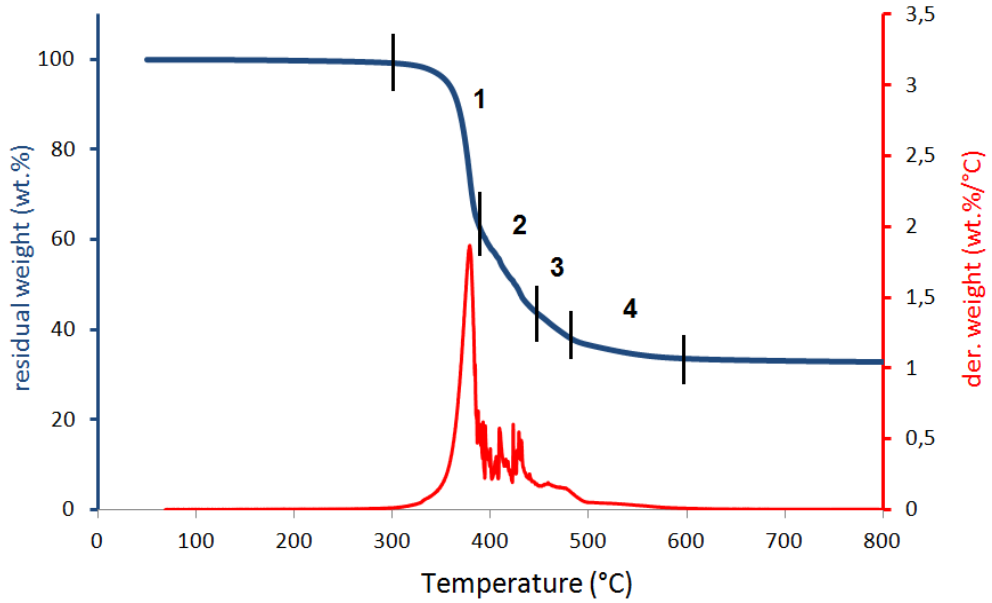

Figure 81 : TG and DTG curves of C9 (10°C/min in nitrogen)

2.1.1.2 Evolved gases

As for the PBT/GF material, the gas phase analysis for C9 was performed using TGA-FTIR and pyrolysis-GCMS. The FTIR spectra of C9 obtained at characteristic temperatures are pictured in Figure 82. Band assignments are given in Table 27. The pyrograms recorded after heat treatment of C9 to 390°C and 600°C are depicted in Figure 83. Mass spectra of detected products are found in Appendix 4.

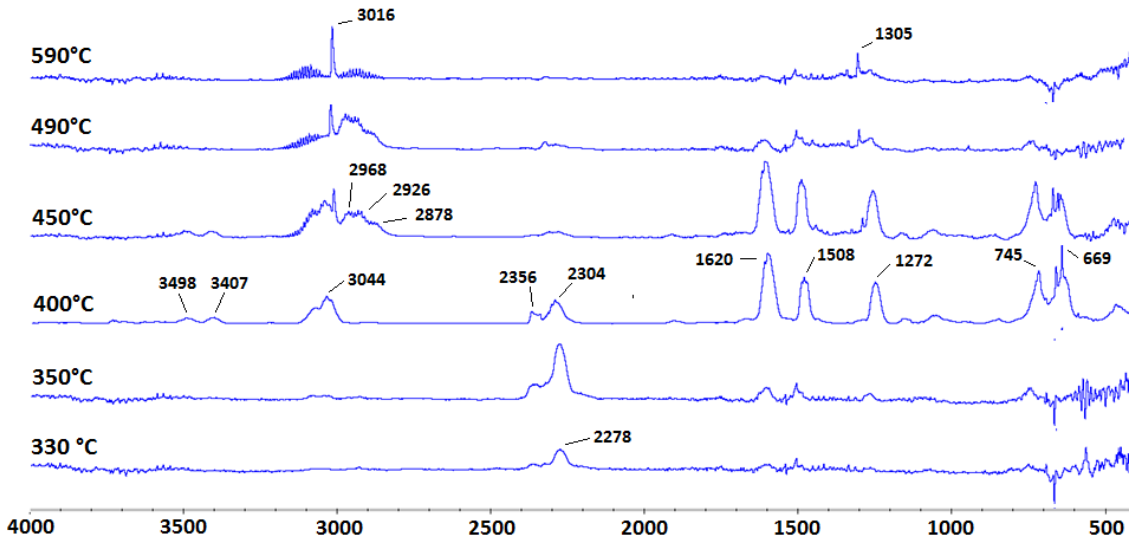

Figure 82 : FTIR spectra of the gases evolved during the thermal degradation of C9 (in N_2 atmosphere) at characteristic temperatures

Table 27 : Attribution of the IR bands of the gases evolved during degradation of C9 in nitrogen[209]

Decomposition products	FTIR/cm^{-1}
Isocyanate	**2278** (N=C=O asym. stretch)
Aniline	**3498** (NH_2 asym. stretch), **3407** (NH_2 sym. stretch), **3044** (=C-H stretch), **1620** (NH_2 bend), **1508** (C-C ring stretch), **1272** (C-N stretch), **745** (NH_2 wag)
CO_2	**2356** (CO_2 asym. stretch), **2304** (CO_2 sym. stretch), **669** (CO_2 bend)
Products containing CH_3/CH_2 groups	**2968** (CH_3 stretch), **2926** (CH_2 stretch), **2878** (CH_3 stretch)
CH_4	**3016** (C-H stretch), **1305** (CH_4 asym. bend)

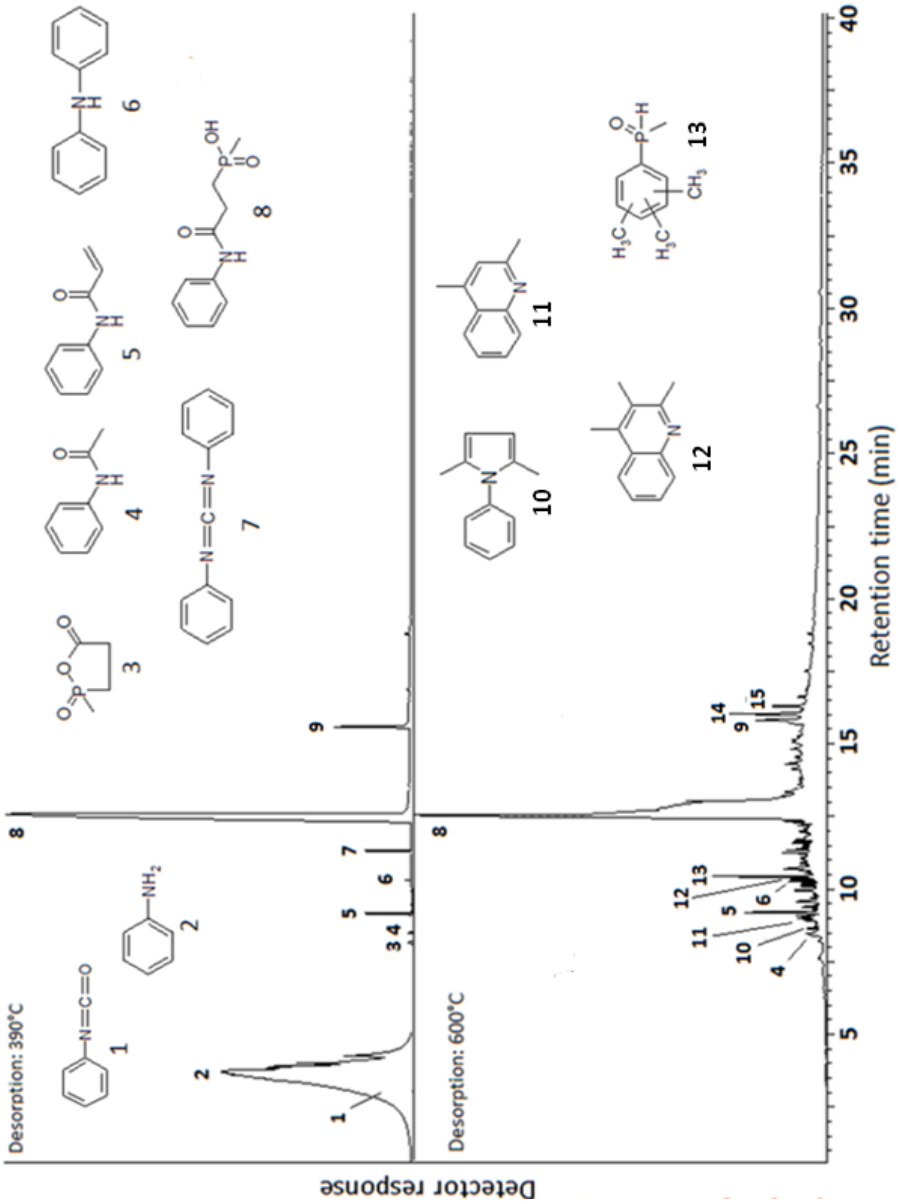

Figure 83 : Chromatogram of the gases evolved during the thermal treatment of C9 to 390°C (above) and 600°C (below) in helium atmosphere; Heating rate in the pyrolyzer: 10°C/min

According to FTIR analyses, three major products, namely isocyanate, carbon dioxide and aniline, are released during the first degradation step. The characteristic band of isocyanate (2278 cm^{-1}) is observed at the beginning of the decomposition. This band is likely to be attributed to phenyl isocyanate since it is clearly identified in the pyrogram of the product by a peak superimposed on the peak of aniline (peak 1 in Figure 83). The release of phenyl isocyanate is then followed by the evolution of carbon dioxide and aniline. The proportion of aniline in the gas phase appears particularly high as shown by the strong intensity of signals in FTIR and GCMS (peak 2). Examination of the pyrogram of **C9** after heat treatment to 390°C allows identifying a fourth product (peak 8) that is released in relatively high quantity during the first degradation step. The heaviest fragment ion observed on the mass spectrum of this product (Figure 84) exhibits a molecular weight of 209 m/z which coincides with a dehydrated form of the aniline based phosphinic acid **C2**.

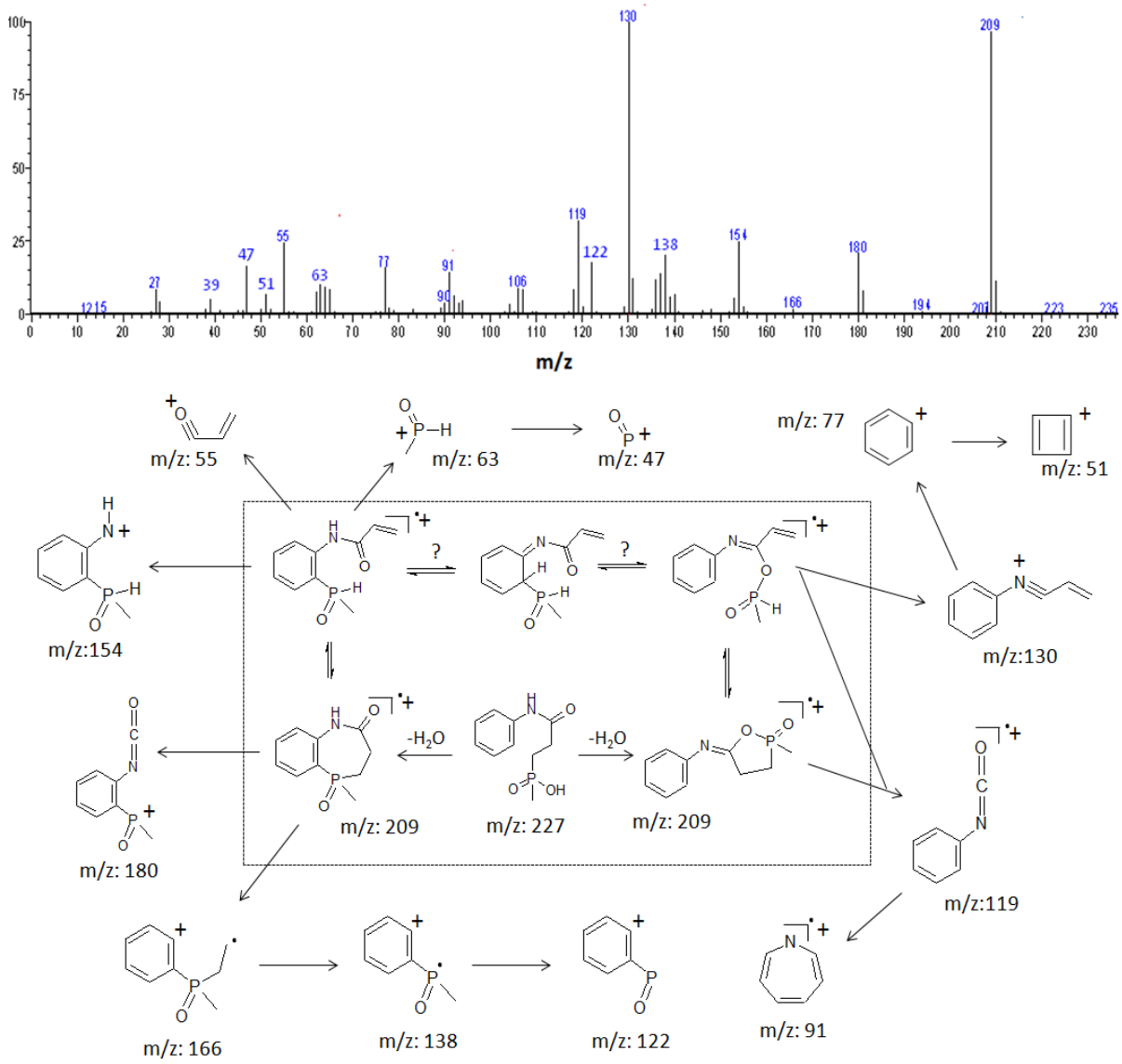

Figure 84 : Mass spectrum of the product 8 (Figure 83) evolved by heat treatment of C9; the proposed fragmentation pattern of the product is pictured below the spectrum

Generally, phosphorus based compounds such as phosphinic acids cannot be easily analyzed in GCMS due to their high polarity[212]. It could be that **C2** undergoes a transformation (dehydration) when traveling in the gas chromatography column[213]. The dehydrated product transits more readily in the GC column and it is hence detected by the mass spectrometer. Haake et al[214] also highlighted the fact that some phosphinic acids exhibited a tendency to form anhydrides on heating under vacuum. One can therefore reasonably assume that dehydration of **C2** would occur in the mass spectrometer. However, one cannot be certain whether dehydration of **C2** effectively occurs in the GC column or in the mass spectrometer or whether it is released in the gas phase as a dehydrated compound. In Figure 84, is proposed the fragmentation pattern of **C2**. It was established on the basis that **C2** underwent intra-molecular cyclization upon dehydration. Some characteristic fragment ions (i.e. 47, 51, 55, 63, 77, 91 and 119 m/z) have been deduced from the literature[107,214] and database resources (i.e. NIST). In order to explain the formation of all fragments, two cyclic molecules of 209 m/z had to be considered. These molecules are potentially inter-transformable or obtained through an independent cyclization mechanism. Most of the fragment ions could be recovered from the dehydrated **C2** obtained through aromatic cyclization. However, cyclization of **C2** by the oxygen amide had to be envisaged to give account of the presence of fragment ions with a molecular weight of 130 and 119 m/z.

On the other hand, heat treatment of **C9** to 390°C generates some minor products such as the OP (Exolit PE110), phenyl acetamide, acrylanilide, diphenylamine and benzenamine (N, N') methanetraylbis (respectively corresponding to peaks 3, 4, 5, 6, 7). An additional peak with a retention time towards 15.5 s (peak 9) can be observed. No substance could be found matching with the corresponding mass spectrum (see Appendix 4). The presence of fragment ions of 51, 77 and 130 m/z in the mass spectrum of product 9 may suggest that the latter contains aniline residues or derivatives. Besides, the substance is likely to contain a P=O group as evidenced by the presence of the fragment ion of 47 m/z.

The FTIR analysis shows that the release of carbon dioxide decreases rapidly while that of aniline is still pursued in the second degradation step. There are new products that are liberated during this stage, including low amount of methane as well as substances containing CH_3 and CH_2 groups. In the third degradation step, the release of aniline decreases, that of methane and CH_3/CH_2 containing products increases. The fourth degradation step corresponds to the sole liberation of methane. The formation of methane probably stems from the bond scission of P-CH_3 groups left in the residue[39,128,141]. In the pyrogram of **C9** thermally treated to 600°C, the peak characteristic of the dehydrated form of **C2** is intense. The product is apparently released after the first degradation step. Peaks of phenyl isocyanate and aniline could not be observed as both products travelled across the GCMS before the detection phase. On the other hand, numerous peaks are observed in the pyrogram. It proves that multiple degradation reactions occur in the decomposing salt which is consistent with the convoluted shape of the DTG curve of **C9** in the second and third

degradation step. Peak 5 (acrylanilide) as well as peaks 9, 13, 14 and 15, exhibit relatively noticeable intensities. Peak 13 is assigned to an aliphatic-aromatic phosphine oxide that was already described by Balabanovich while investigating the thermal degradation of OP (Exolit PE110)[107]. The mass spectrum of this phosphine oxide (Figure 85, spectrum A) exhibits two major signals (167 m/z and 182 m/z) that are also recovered in mass spectra of products 14 and 15 (Figure 85, spectrum C and D).

Products 14 and 15 possibly contain residues related to the phosphine oxide 13. However, their respective structure could not be resolved owing to the too high complexity of fragmentations occurring in the mass spectrometer. To a number of the other small peaks displayed by the pyrogram, the database resources often associate molecules whose structures are derived from methyl-substituted heterocyclic aromatic amines (i.e. quinolines, pyrroles, indoles, pyridine, carbazole…). However, with the exception of products 10, 11, and 12, the mass spectra of molecules do not show sufficient correlations with the proposed structures. Yet, the release of such molecules in the gas phase should be in agreement with the signals of aliphatic groups (particularly -CH_3 stretch) in FTIR. Pericyclic reactions as well as various types of other rearrangements would explain the formation of these heterocyclic molecules.

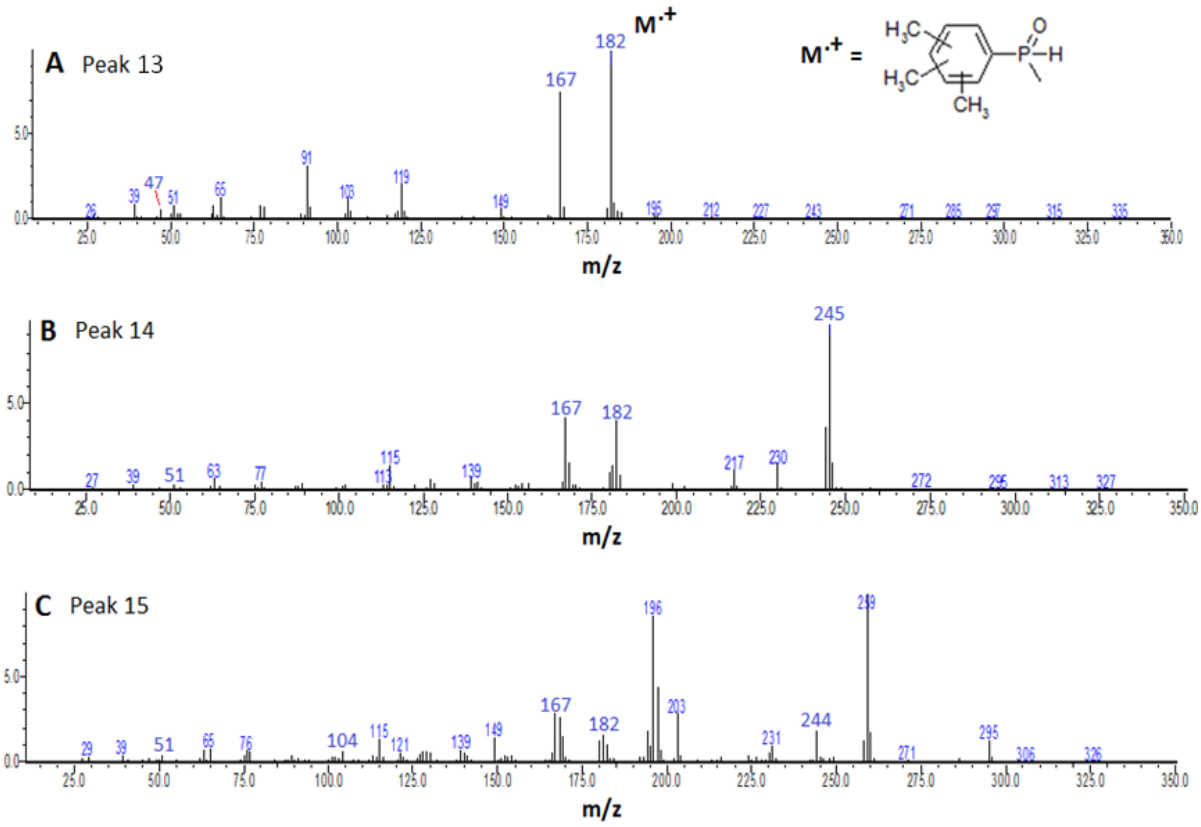

Figure 85 : Mass spectra of product 14 (spectrum A), product 15 (spectrum B) and product 16 (spectrum C) evolved by heat treatment of C9

In order to determine whether the phosphinic acid **C2** is liberated as such or in its dehydrated form during thermal decomposition of **C9**, an additional experiment was performed. It consisted in heating **C9** in a round bottom flask to 400°C under nitrogen. A glass tube was connected to the flask whose outlet part was dived in liquid nitrogen to condense volatile degradation products. Thus, evolved gases that condensed on the wall of the round bottom flask and in the nitrogen trap system were collected, dissolved in DMSO-d_6 and analyzed using liquid state NMR. The ^{1}H NMR spectra of the collected degradation products are depicted in Figure 86. According to NMR analyses, the product collected in the nitrogen trap system exclusively contains aniline. The product collected on the wall of the round bottom flask consists for the most part of a mixture of aniline and of the phosphinic acid **C2**. It can be concluded that upon thermal decomposition, **C9** effectively releases **C2** in the gas phase. Dehydration of the phosphinic acid therefore occurs in the GCMS apparatus.

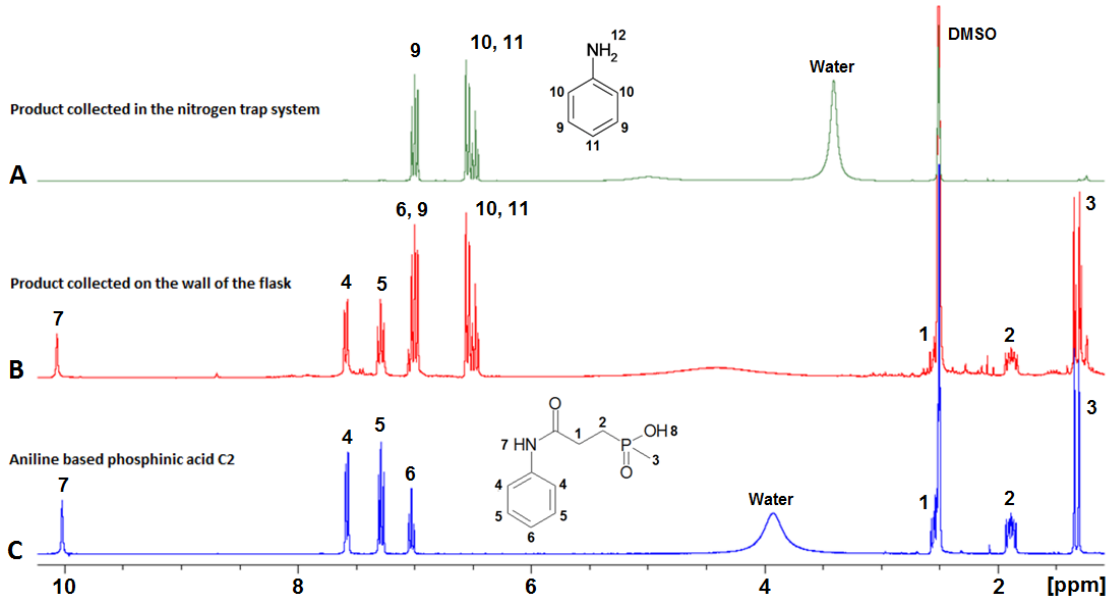

Figure 86 : ^{1}H NMR spectrum of the degradation products evolved during thermal treatment of C9 to 400°C in nitrogen atmosphere; (A) - pure C2, (B) - degradation products collected on the wall of the round bottom flask, (C) - degradation products collected in the nitrogen trap system

2.1.1.3 Analysis of the residue

The residue obtained after thermal treatment of **C9** to 600°C was analyzed through ^{13}C CP/MAS, ^{31}P MAS and ^{27}Al MAS solid state NMR. The spectra are gathered in Figure 87.

As viewed in chapter 4, the phosphinate salt **C9** exhibits three sharp ^{31}P resonances at 39.6, 38 and 36.2 ppm. When treating the sample to 600°C, the phosphinate signals disappear yielding two broad bands centered at 4 and -30 ppm. The band at 4 ppm is attributed to phosphonate species while the band at -30 ppm is characteristic of phosphates. The successive oxidation of phosphinates into phosphonates, then into phosphates, during thermal decomposition processes is widely reported in the literature[39,127,128,141,167,192].

The ^{27}Al NMR spectrum of **C9** after thermal treatment presents three broad overlapping resonances corresponding to aluminum oxide sites in tetrahedral (34 ppm), pentahedral (4 ppm) and octahedral (-17 ppm) geometries. They are attributed to the presence of aluminum phosphonates and aluminum phosphates[167,192]. A ^{31}P-^{27}Al correlation NMR experiment (HMQC) performed on the thermal degradation residue of the flame retarded PBT material (Appendix 5) has highlighted that phosphonates much greatly contributed in the signals at 4 and -17 ppm than phosphates while both phosphonate and phosphate species equally contribute in the resonance at 34 ppm. It signifies that the oxidation of phosphinate species into phosphonates and phosphates is accompanied by a modification of Al-O(P) sites from an octahedral (six-fold) toward a tetrahedral (four-fold) coordination geometry, passing through a transitory pentahedral (five-fold) geometry.

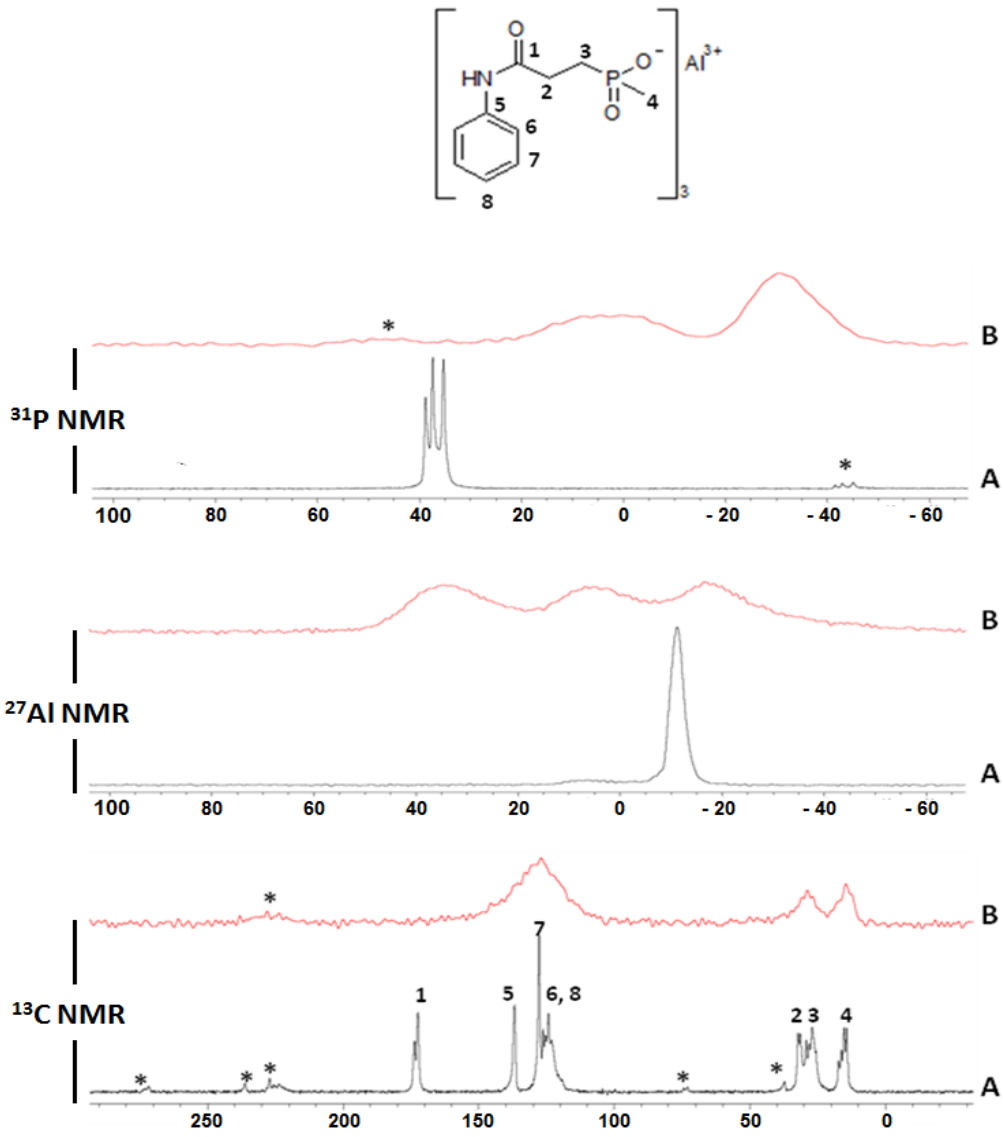

Figure 87 : ^{13}C CPMAS, ^{31}P MAS and ^{27}Al MAS solid state NMR spectra of C9 before and after the thermal treatment at 600°C in nitrogen; (A) - before treatment, (B) - after treatment (* spinning side bands)

The ^{13}C NMR spectrum of **C9** treated at 600°C exhibits a broad band at 128 ppm ascribed to amorphous aromatic and ethylenic species (char). Two bands are also observed at 30 and 15 ppm coinciding with the aliphatic groups of the untreated phosphinate salt. The signal at 15 ppm can be surely attributed to the P-CH_3 methyl group. It would be consistent with the liberation of methane in the late stage of the thermal decomposition of **C9** as well as the presence of phosphonates in the residue. The signal at 30 ppm should be attributed to residual ethylenic groups linked to the phosphorus (-HNC(O)-**<u>CH_2-CH_2</u>**-P(OO^-)-CH_3) but these may not be attached to the amide function (-**<u>HNC(O)</u>**-CH_2-CH_2-P(OO^-)-CH_3) since the latter is not observed in the ^{13}C NMR spectrum.

2.1.1.4 Degradation mechanism

The information collected from gas and condensed phase analyses allow establishing a global scheme for the thermal decomposition of **C9** (<u>Figure 88</u>).

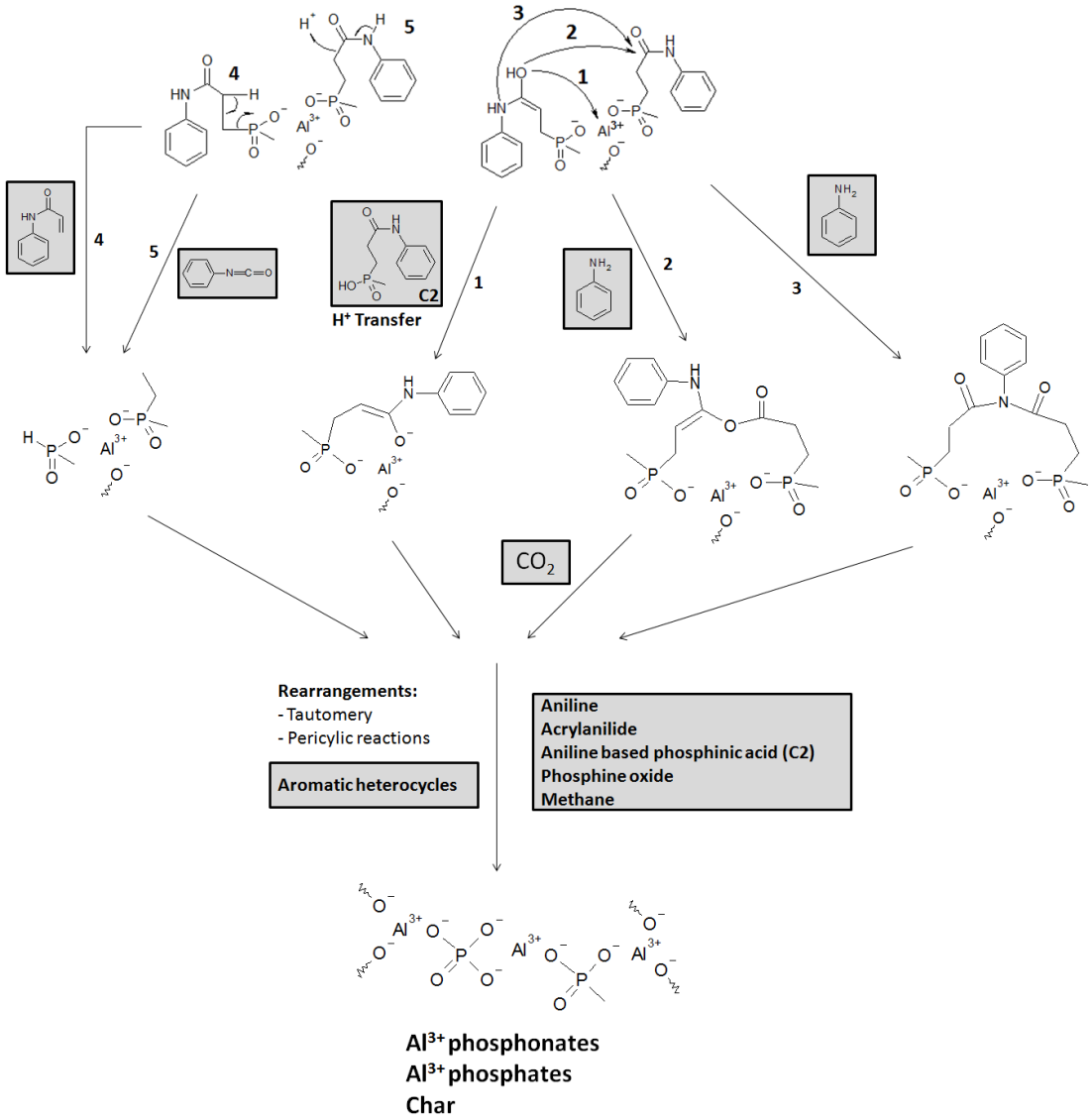

Figure 88 : C9 degradation scheme (detected gaseous decomposition products in grey)

Minor degradation products such as OP, phenyl acetamide, diphenylamine and benzenamine (N, N') methanetraylbis were not considered in the degradation model. Phenyl isocyanate is first released in the gas phase. It is obtained through bond scission between the carbon amide and the carbon in beta position from the phosphorus (5). This leads to the production of ethylmethyl phosphinate. Phenyl acrylanilide is obtained by elimination with subsequent formation of H-(methyl)phosphinate[214] (4). Aniline and CO_2 are released in the same time during the first degradation step. To account for this, and to particularly explain the formation of CO_2, the following mechanism (2) is proposed: the oxygen amide transforms into hydroxyl by tautomery. Hydroxyl attacks the carbon amide of an adjacent phosphinate which results in the elimination of aniline. This is directly followed by decarboxylation and liberation of CO_2. Another mechanism was envisaged for the elimination of aniline which involves an attack of carbon amides by the nitrogen amide of adjacent phosphinates (3). It leads to the formation of succinimide.

Along with these degradation pathways, volatilization of the aniline based phosphinic acid **C2** occurs. Polarization of the carbonyl bonds of amide functions by aluminum and subsequent hydrogen transfer (1) reactions is proposed to explain the primary formation of the phosphinic acid **C2**[215]. The second and third degradation steps imply a further liberation of aniline, acrylanilide and **C2** as well as volatilization of phosphine oxides (i.e. aliphatic-aromatic phosphine oxide) and heterocyclic aromatic (i.e. quinolines, pyrroles…). The latter products originate from complex rearrangements (i.e. pericyclic reactions) within the degrading material. In the condensed phase aluminum phosphonates are first produced. Aluminum phosphonates then degrade into transitory aluminum phosphonates with penta-coordinated aluminum.

The oxidation of phosphonates into phosphates leads to the release of methane (bond scission of P-CH_3 groups) during the third and fourth degradation steps. This oxidation operates with a transition of the Al-O(P) coordination from an octahedral or pentahedral geometry to a tetrahedral geometry. A char residue is produced all along the degradation process of **C9**.

2.1.2 Thermal decomposition of PBT/GF flame retarded with C9

In this part, it is investigated the thermal degradation of PBT/GF flame retarded with the aluminum salt of the aniline based phosphinic acid **C9**.

2.1.2.1 Thermal degradation

TG and DTG curves (experimental and calculated) of PBT/GF filled with **C9** are presented in Figure 89. It is noteworthy that the experimental and the calculated TG curves are very close to each other, except between 310°C (onset temperature of decomposition) and 380°C

where the degradation of the flame retarded material (experimental) appears to be slightly accelerated. It means that a slight destabilization occurs in this range of temperature.

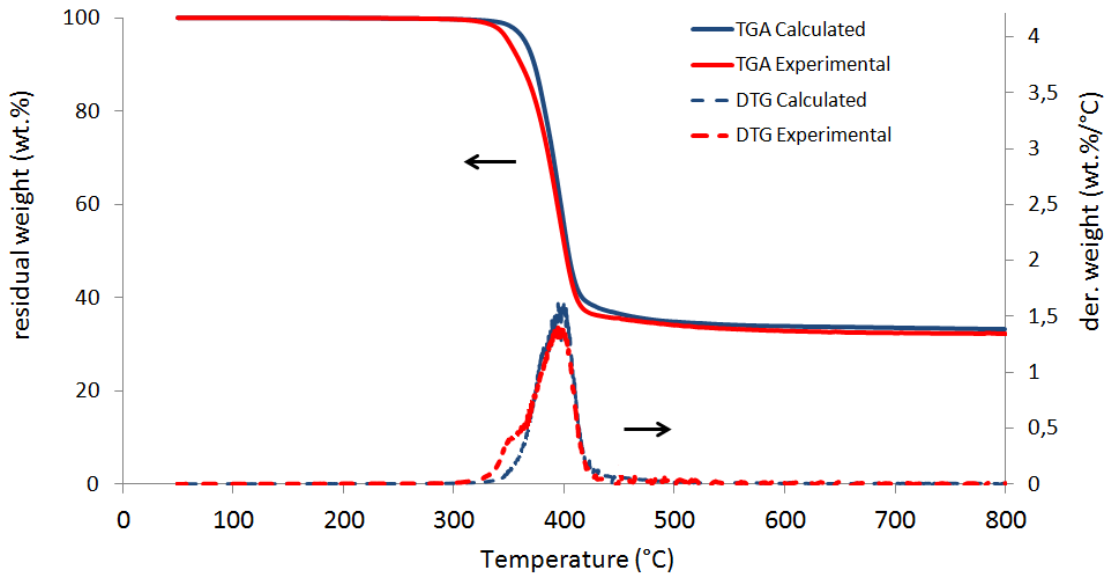

Figure 89 : TG and DTG curves of PBT/GF/C9 (10°C/min in nitrogen)

One can define two degradation steps. The first step from 310 to 380°C exhibits a mass loss of about 23.4%. The second step between 380 and 600°C is characterized by a mass loss of 43.4%. As evidenced by the almost perfect overlay of both calculated and experimental TG curves, there would be no significant chemical interaction between **C9** and PBT in this second step. A residue of 33.2 wt% remains at the end of the experiment as expected.

2.1.2.2 Evolved gases

As for pure PBT/GF and **C9**, the analysis of gases evolved by the PBT/GF/**C9** formulation was performed through FTIR and pyrolysis-GCMS. First, a stacking of FTIR spectra recorded at characteristic temperatures during the TG analysis of the material is presented in Figure 90. Band assignments are gathered in Table 28. It appears that the gaseous degradation products released by the flame retarded polymer are similar to those found for neat PBT/GF. This includes water, THF, CO_2, butadiene, benzoic acid and ester derivatives. Some additional products such as isocyanate (assumed to be phenyl isocyanate) and methane can be observed. These are gases arising from the degradation of **C9**. The phosphinate salt shall probably contribute in the release of part of the CO_2. Interestingly, the characteristic signals of aniline are not present on the spectra, whereas these signals were particularly intense on the FTIR spectra of the pure flame retardant. This suggests that aniline evolves differently in the PBT/GF matrix.

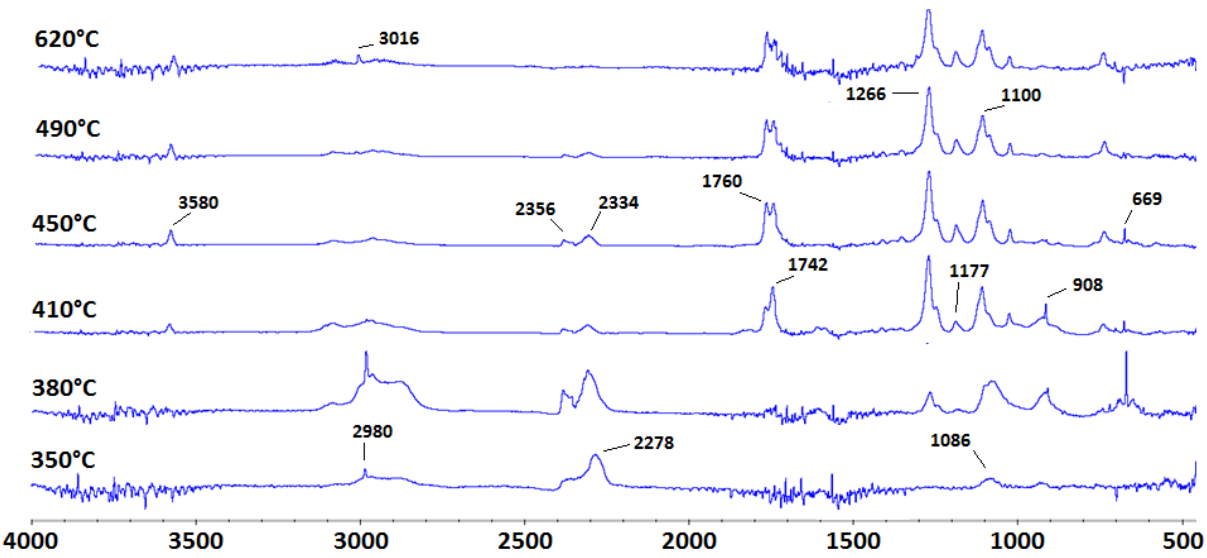

Figure 90 : FTIR spectra of the gases evolved during the thermal degradation of PBT/GF/C9 (in N_2 atmosphere) at characteristic temperatures

Table 28 : Attribution of the IR bands of the gases evolved during degradation of PBT/GF/C9 in nitrogen; the underlined band positions are used to determine the evolved gas release rate of products[39,80,127,128,209]

Decomposition products	FTIR / cm^{-1}
Isocyanate	**2278** (N=C=O asym. stretch)
THF	**2980** (CH_2 stretch), **1086** (asym. ring vibration)
CO_2	**2356** (CO_2 asym. stretch), **2304** (CO_2 sym. stretch), **669** (CO_2 bend)
Butadiene	**908** (-C=C-H wag)
H_2O	**4000-3400** (O-H stretch)
Benzoic acid	**3580** (O-H stretch), **1760** (C=O sym. stretch)
Esters	**1742** (C=O stretch), **1266** (C-O-C asym. stretch), **1100** (C-O-C sym. stretch)
CH_4	**3016** (C-H stretch), **1305** (CH_4 asym. bend)

Figure 91 illustrates the evolved gas release rate of the decomposing flame retarded polymer. The evolution curves of gaseous products were drawn on the basis of the intensity of characteristic FTIR signals (see underlined band positions in Table 28).

The release of isocyanate and THF (also water which was not reported in the graph) occurs at the beginning of the decomposition (from about 310°C). Then liberation of CO_2 and THF increases to reach a maximum towards 375 - 380°C. It is accompanied by a low evolution of ester derivatives. This stage corresponds to the first degradation step of the sample. In the second degradation step, it is observed a sharp increase in the release rate of esters and benzoic acid along with an increase in the release of butadiene and a second peak of CO_2

emission. This degradation step is in accordance with to the standard decomposition scheme of pure PBT/GF. A third degradation step can be observed at higher temperatures corresponding to the release of CH_4.

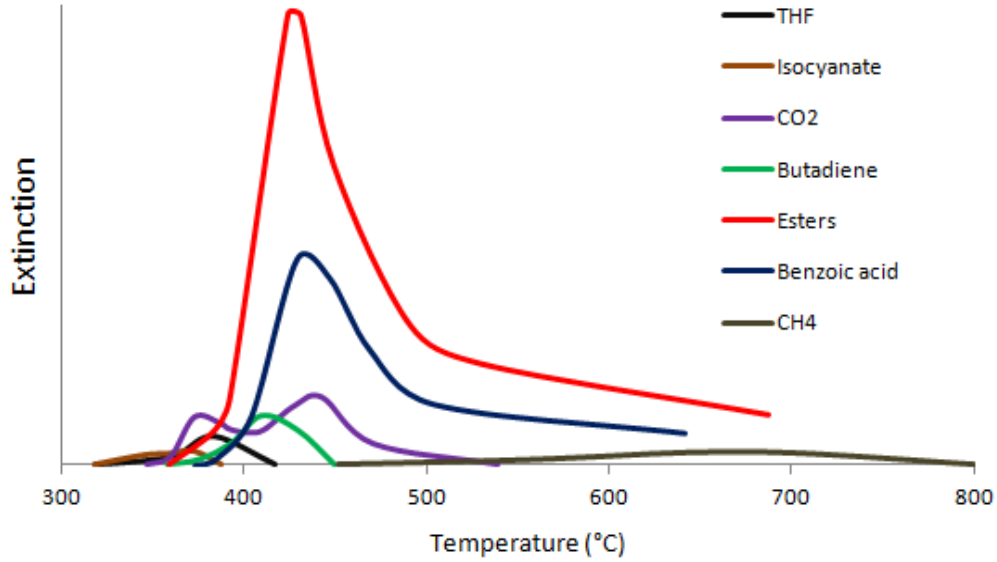

Figure 91 : Evolved gas release rate of the PBT/GF/C9

In Figure 92, the pyrograms recorded after the flame retarded sample underwent heat treatments to 390°C and 470°C (similar treatments than for PBT/GF) are presented. The mass spectra of products are found in Appendix 4. The main gaseous products evolved when PBT degrades are the same than those obtained on the pyrograms of pure PBT/GF: benzoic acid (peak 3), terephthalic acid (broad massif centered around 13.5 s), alkenyl esters of benzoic acid and of terephthalic acid (peaks 4, 7, 9, 14), oligomers of PBT with vinyl, acid and/or phenyl end groups (peaks 11, 12, 13).

Besides, the relative intensity of peaks for these products is comparable to that for the non-flame retarded polymer whatever the heat treatment considered (390°C or 470°C). This gives further proof that the flame retardant has relatively limited effects on the degradation pathway of the polyester as well as on the release rate of its degradation products. One may however remark the presence of new degradation products of PBT (in relatively low amounts) such as the mono-butenyl ester of terephthalic acid (peak 7) and the butadiol dibenzoate (peak 15). These products were also reported in the literature[33,35]. Products resulting from the decomposition of **C9** can also be clearly identified on the pyrograms, notably phenyl isocyanate (peak 1), aniline (peak 2), OP (peak 5) and the dehydrated form of the aniline based phosphinic acid **C2** (peak 8). On the contrary to the FTIR analysis, the GCMS analysis confirms that aniline is effectively released in the gas phase. As for the OP (peak 5), it seems to be produced in larger quantity when **C9** is incorporated in the polymer than when the flame retardant is "pyrolyzed" in pure form. However, the oxaphospholane oxide is only observed upon heat treatment of the flame retarded sample at 390°C while it is not

observed at 470°C. As it is a particularly reactive compound, it may possibly recombine with other substances over time. Another explanation is that the oxaphospholane is mostly released during the first part of the degradation and therefore its signal would be less intense on the pyrogram of the material treated to 470°C.

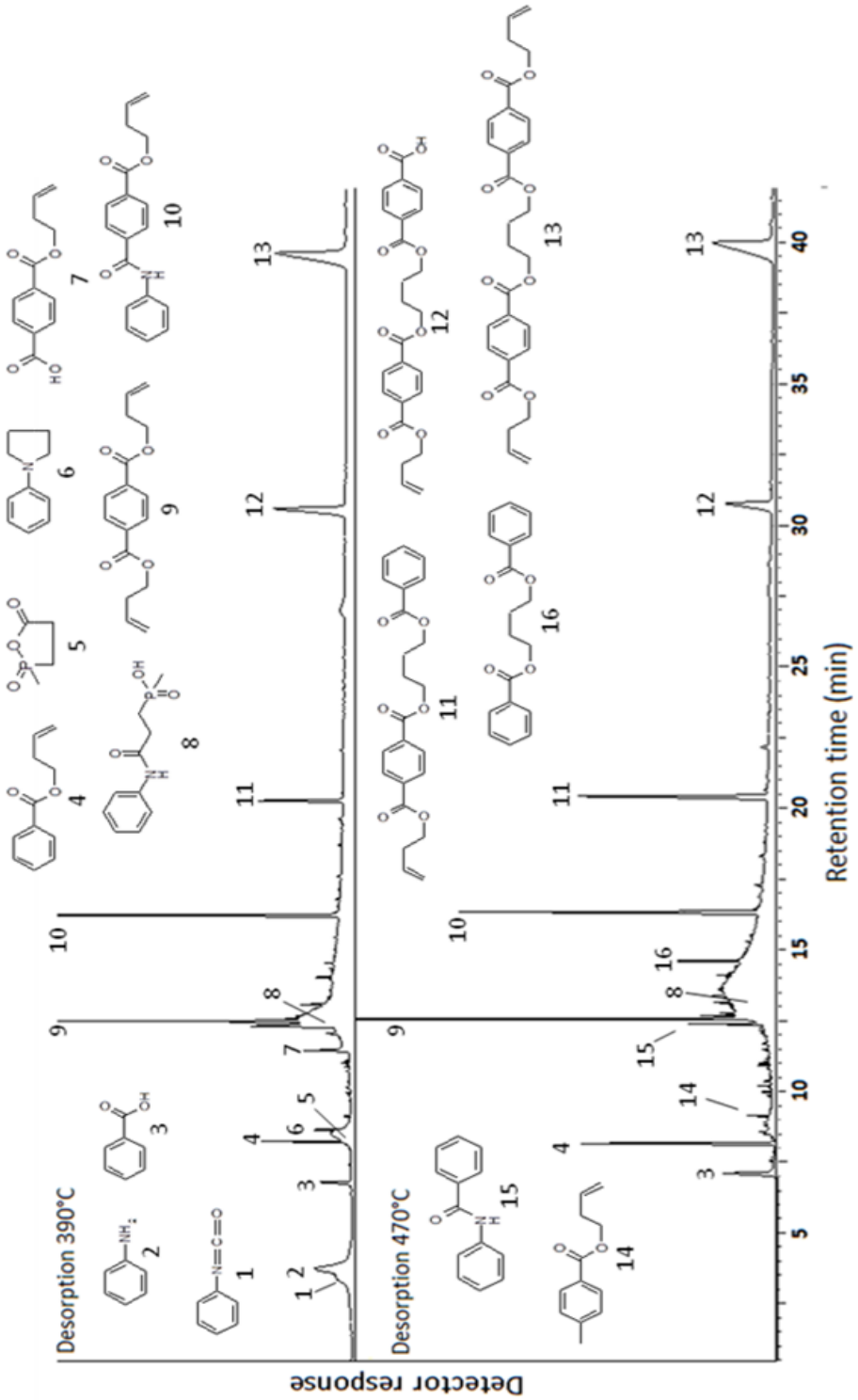

Figure 92 : Chromatogram of the gases evolved during the thermal treatment of PBT/GF/C9 to 390°C (above) and 470°C (below) in helium atmosphere; heating rate in the pyrolyzer: 10°C/min

The presence of an additional peak of high intensity, denoted as 10 in the pyrograms, is attributed to the mono-butenyl ester of terephthalic acid amidified by aniline. This product results from aminolyse of PBT chains by aniline. Note that an analogous product of lower molecular weight – the N-phenyl benzamide (peak 14) – is also detected after thermal treatment of the flame retarded polymer at 470°C. The aminolyse of PBT has already been related by Balabanovich while investigating the effect of melamine on the thermal decomposition of PBT[71]. In this study, the reaction occurred between PBT esters and ammoniac, the latter arising from the condensation of melamines. The author also noticed the formation of substituted melamines. These are generated from an addition reaction of melamine to the double bonds of butadiene or butenyl end-chain radicals of PBT. In the present study, a similar compound can be detected but with aniline instead of melamine (peak 6). As product 6 is released in relatively low amount, it will not be considered in the decomposition model.

Finally, GCMS analyses demonstrate that part of the aniline released by **C9** reacts with PBT during the thermal decomposition. This is consistent with the fact that aniline is not detected in FTIR.

2.1.2.3 Analysis of the residue

The PBT/GF/**C9** sample was heat treated at 600°C in nitrogen atmosphere. A picture of the solid residue obtained is depicted in Figure 93.

The residue of the flame retarded sample is not significantly different compared to that of the pure PBT/GF (see Figure 78) except that holes appear a little bit larger. This is due to the fact that the flame retarded formulation contains less glass fibers. Furthermore, previous analyses showed that the flame retardant did not promote the polymer charring but rather tended to release degradation products in the gas phase. The apparent inhomogeneity of the residue surface is therefore explained by an extensive bubbling of the polymer during the decomposition through the release of gaseous species.

Figure 93 : Picture of the residue of PBT/GF/C9 obtained after thermal treatment to 600°C in nitrogen. In blue: expected mass loss (according to TGA), in black: experimental mass loss

As previously, the solid residue was analyzed through ^{13}C CP/MAS, ^{31}P MAS and ^{27}Al MAS. Corresponding spectra are gathered in Figure 94.

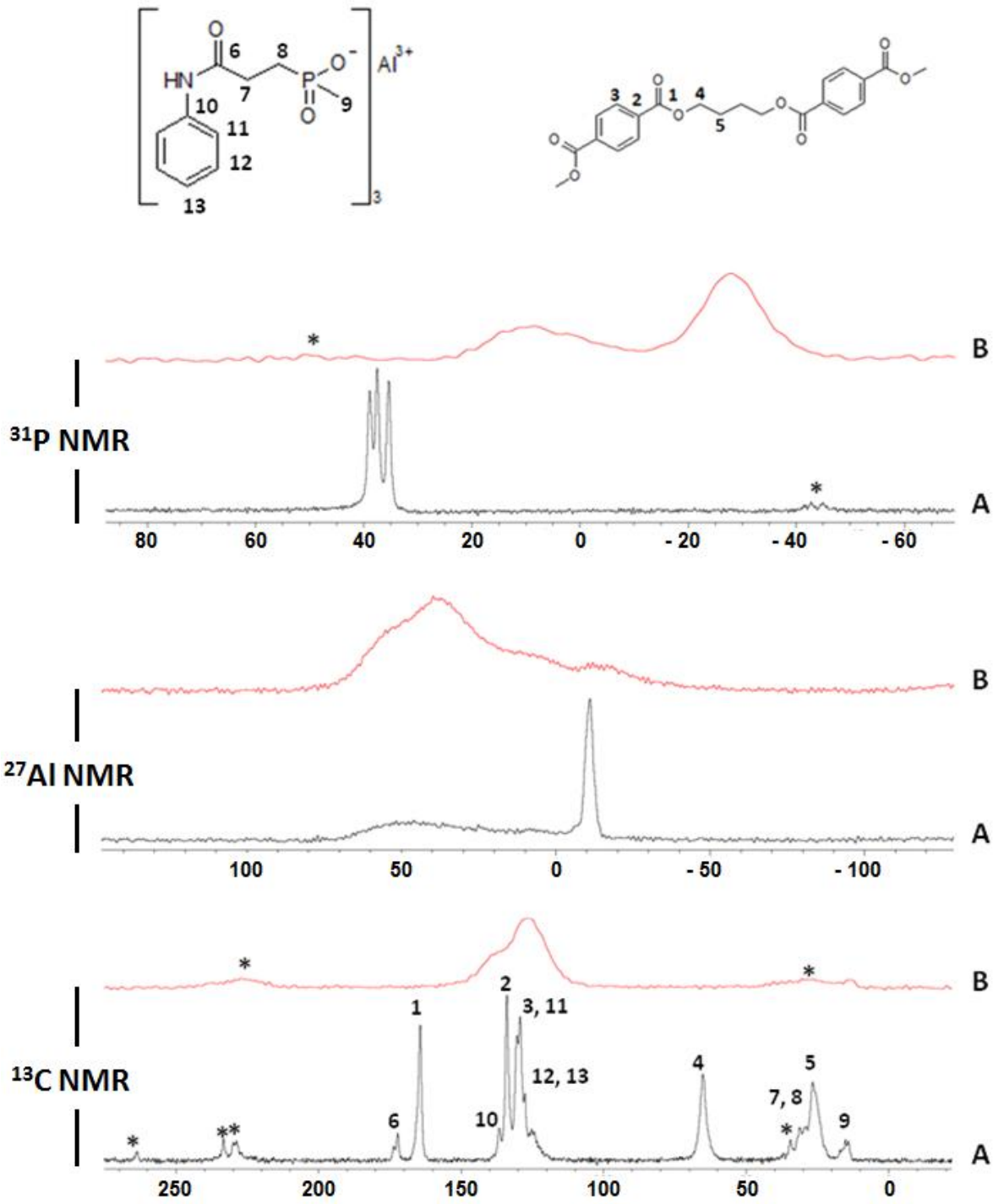

Figure 94 : ^{13}C CPMAS, ^{31}P MAS and ^{27}Al MAS solid state NMR spectra of PBT/GF/C9 before and after the thermal treatment to 600°C in nitrogen; (A) - before treatment, (B) - after treatment

The characteristic signals of phosphonates (6 ppm) and phosphates (-30 ppm) are observed on the ^{31}P NMR spectrum of the treated flame retarded sample. The broadness and relative surface area of these signals are somewhat comparable to those of the pure flame retardant treated at the same temperature. It gives further evidence that the evolution of **C9** is relatively independent from that of PBT.

On the ^{27}Al NMR spectrum of the non-treated material, it is observed the expected resonance of alumino-phosphinate species at -12 ppm. However, the spectrum exhibits another broad and asymmetric band (with apparent quadrupolar broadening) centered around 50 ppm. This signal is attributed to amorphous alumino oxide species contained in glass fibers[216]. This has been confirmed through performing a NMR experiment on the non-flame retarded PBT/GF (Appendix 5). After the thermal treatment, the Al signal of glass fibers remains unchanged while that of alumino-phosphinates disappeared, replaced by three apparent signals at 40 ppm, 8 ppm and -17 ppm. Similarly to pure **C9**, these bands are respectively attributed to the tetrahedral, pentahedral and octahedral Al-O(P) sites of alumino-phosphonate and alumino-phosphate species. As these resonances overlap with the Al resonance of glass fibers, supplementary bands (due to novel aluminum species) should not be detected in the spectrum. Thus, to differentiate isotropic resonances from the quadrupolar broadening of the glass fiber signal, a two dimensional ^{27}Al-^{27}Al MQMAS experiment was performed. This experiment was conducted using a very high field spectrometer (18.8 T) in order to increase the resolution of the spectrum and to further reduce the quadrupolar interaction of aluminum. The corresponding 2D spectrum is depicted in Figure 95. The isotropic signals correspond to the spots on the black axis. The black arrow emphasizes spreading of the signal of glass fiber out of this axis (on the right side hand). This spreading is attributed to the quadrupolar broadening. It is effectively observed that only three bands are present on the spectrum except that ascribed to glass fibers.

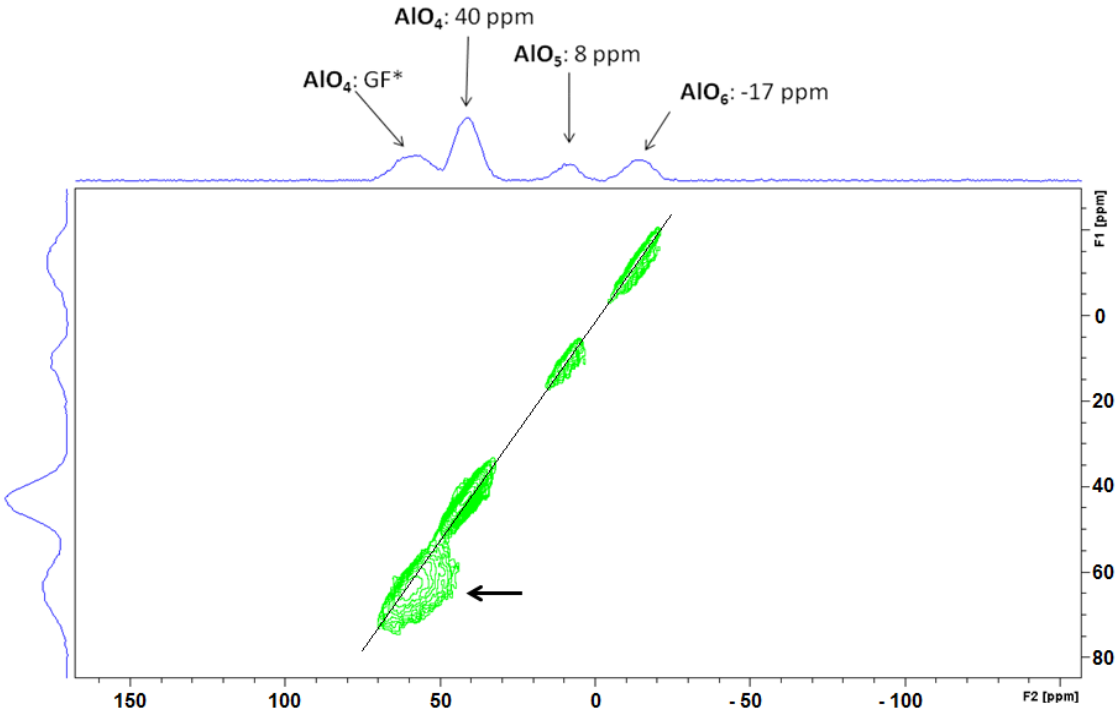

Figure 95: 2D ^{27}Al-^{27}Al MQMAS NMR spectra of the PBT/GF/C9 material after the thermal treatment to 600°C in nitrogen; 800 MHz NMR spectrometer; GF: Al signal of glass fibers

The ^{13}C NMR analysis of the PBT/GF/**C9** formulation complements the previous results. After treatment to 600°C, the sample mostly exhibits a broad band centered at 130 ppm corresponding to carbonaceous residues (aromatic and ethylenic carbons). The signal is similar to that observed for the PBT/GF sample treated at the same temperature. A char residue resulting from the decomposition of **C9** may slightly contribute in the intensity of this broad resonance. One can further remark the presence of the low intense signal at 15 ppm assigned to the CH_3 groups linked to phosphorus as previously observed when **C9** alone was heat treated at the same temperature.

2.1.2.4 Degradation mechanism

Gas and condensed phase analyses allow establishing a degradation mechanism for the PBT/GF/**C9** formulation. A schematization of this mechanism is depicted in Figure 96.

Degradation of PBT and of the flame retardant **C9** globally occurs in the same way as for the separated components. However, a slight destabilization of the material occurs at the beginning of the degradation which is marked by a maximum in the release rate of THF and CO_2 (TGA-FTIR, 1st degradation step).

During the first degradation step, water and phenyl isocyanate are released followed by THF, CO_2 and a limited proportion of ester derivatives. The release of aniline by **C9** should occur during this first step and would be concomitant with the material destabilization. Indeed, part of the aniline reacts with PBT through aminolyse of ester bonds. From this, it results the formation of PBT with butanediol and N-phenyl benzamide end chain groups. As aniline accelerates the PBT chain scission and provokes a faster production of butanediol end chain groups, the release rate of THF and CO_2 increases rapidly (first peak release rates) and the liberation of ester derivatives starts sooner[71,80]. With the exception of some additional aminolyse reactions, PBT degrades without significant interaction with the flame retardant, releasing butadiene, CO_2, ester derivatives, terephthalic acid and benzoic acid during the second decomposition step.

The pyrolysis-GCMS measurements showed that **C9**, when incorporated in PBT/GF, released the aniline based phosphinic acid **C2** as main phosphorus based gaseous product. Contrary to what was observed for the pure flame retardant, a non-negligible proportion of the oxaphospholane Exolit PE110 is also liberated, mostly during the first part of the degradation. This should be explained by the fact that the water generated by PBT partly hydrolyzes the amide functions of the aluminum phosphinate leading to the formation of 2-carboxyethyl(methyl)phosphinate. The latter is evolved either in the di-acid form or in the cyclized from (oxaphospholane oxide). The supplement of aniline evolved through this mechanism may interact with PBT and take part in the destabilization of the material. On the other hand, part of the CO_2 detected in FTIR should arise from the decomposition of **C9** as previously demonstrated for the pure flame retardant. The volatilization of acrylanilide,

phosphine oxides and aromatic heterocycles (see degradation pathway of pure **C9**) is also assumed but these degradation products are released in low quantity and thus could not be detected neither by FTIR or GCMS. The emission of CH_4, resulting from the bond scission of P-CH_3 groups, is observed at the end of the decomposition. Aluminum phosphonates and phosphates remain in the final residue as well as low amount of carbonaceous char.

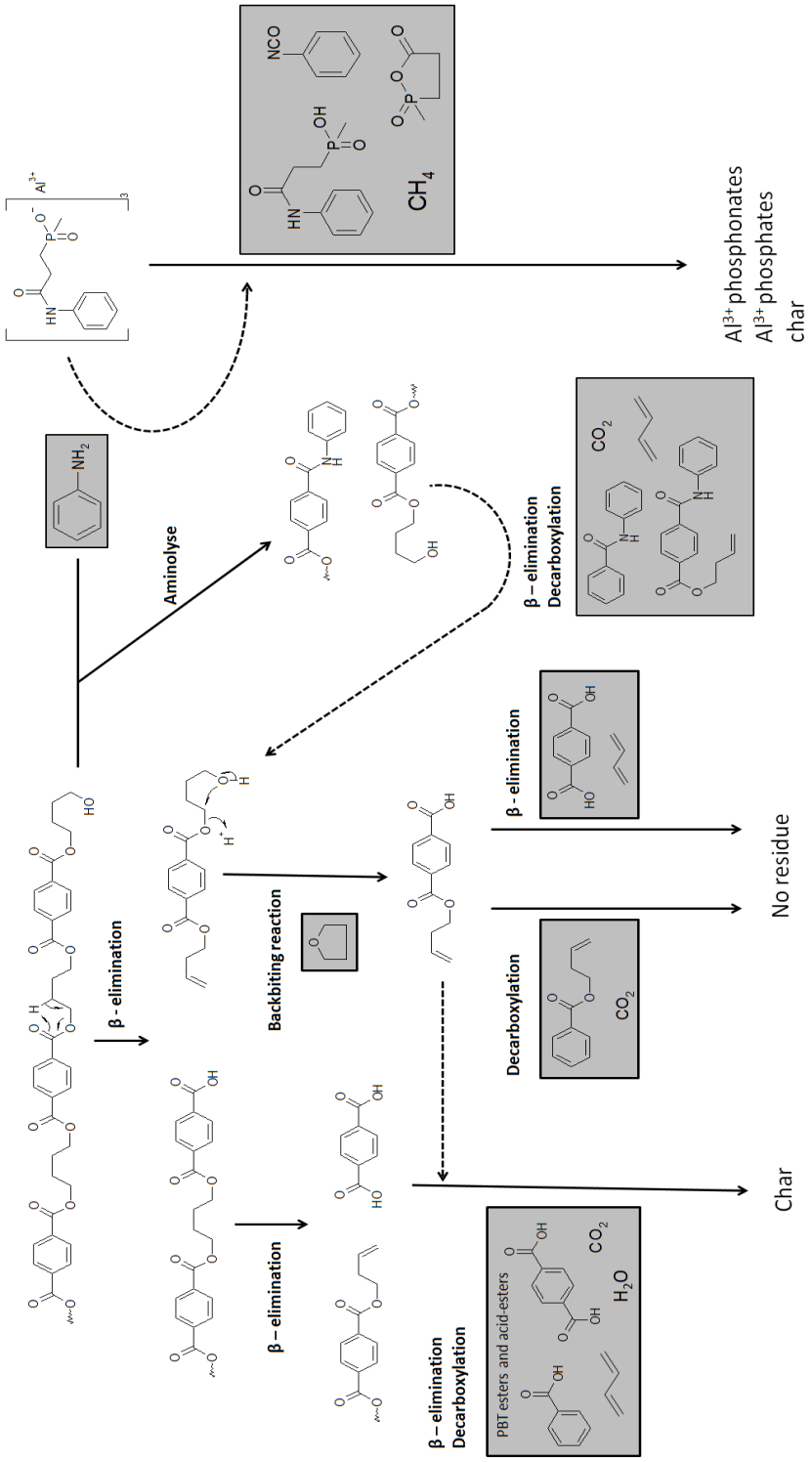

Figure 96 : PBT/GF/C9 degradation scheme (detected gaseous decomposition products in grey)

2.1.2.5 Conclusion

In this part, the thermal degradation mechanism of glass fiber reinforced PBT flame retarded with the aluminum salt **C9** was investigated. TGA-FTIR analyses combined to pyrolysis GCMS and solid state NMR experiments allowed demonstrating that the polymer and the flame retardant mostly decomposed independently from each other. A few interactions nonetheless occur. Particularly, the aniline released by **C9** splits the PBT chains through aminolysis of ester bonds.

A clear gas phase mode of action is established for **C9**. While PBT degrades almost completely and produces low amount of char, the aniline based phosphinic acid **C2** is prevalently released by **C9** during the thermal decomposition of the material. The phosphinic acid acts in the gas phase through quenching the combustion reactions fed by fuel degradation products of PBT. Experiments have proved that the flame retardant exhibited no condensed phase mode of action (no char promotion).

The next part is dedicated to the study of the flame retardant mode of action of Exolit OP1240 in the reinforced PBT. It aims at comparing the FR modes of action of the commercial flame retardants to that of the self-synthesized one.

2.2 PBT/GF flame retarded with the aluminum phosphinate salt Exolit OP1240

The degradation scheme of PBT/GF flame retarded with Exolit O1240 has been described by Braun et al[39,141]. However, in order to compare the FR mechanisms of OP1240 and **C9**, it is important to elucidate the thermal degradation the PBT/GF/OP1240 material using our own experimental methods. The thermal decomposition of pure Exolit OP1240 will thus be firstly discussed.

2.2.1 Thermal decomposition of Exolit OP1240

2.2.1.1 Thermal degradation

According to Braun et al[39], the thermal behavior of pure OP1240 in nitrogen atmosphere strongly depends on the experimental conditions used. This is due to the fact that the phosphinate salt can either decomposes or sublimates as complete molecule. Figure 97 presents the thermogravimetric analysis of the aluminum diethylphosphinate. It occurs in a single step from 390°C to 520°C with a maximum degradation rate at 475°C, leading to stable residue of 9.2 wt%. The onset temperature for weight loss of OP1240 is comparatively higher than that of **C9** (390°C vs 310°C), however, the former produces a much smaller percentage of residue at 800°C (9.2 wt% vs 35.8 wt%). The final residue of OP1240 appears like a carbonaceous expanded material (visual observation in the pan after the experiment).

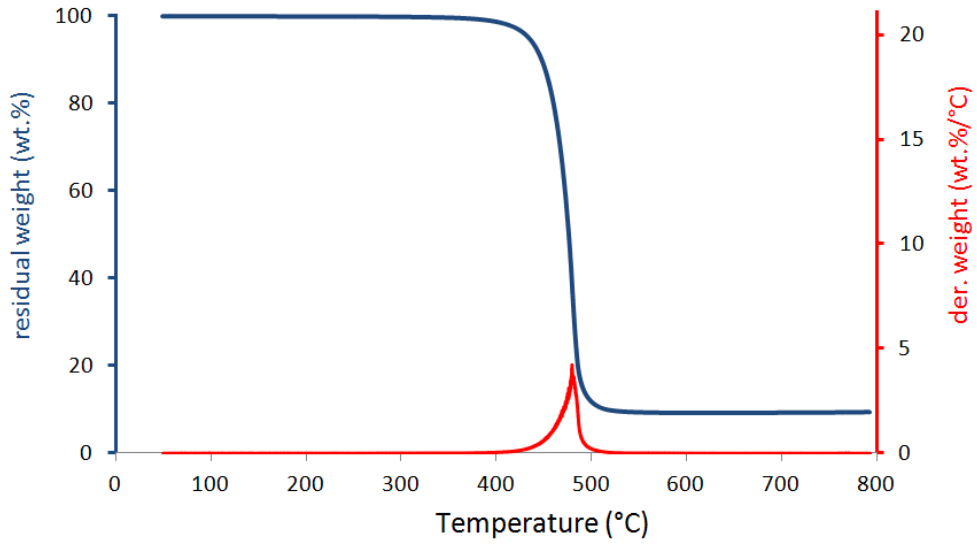

Figure 97 : TG and DTG curves of Exolit OP1240 (10°C/min in nitrogen)

2.2.1.2 Evolved gases

As shown by TGA, the carbonization of Exolit OP1240 to char suggests that the phosphinate releases degradation products in the gas phase. In order to characterize these degradation products, OP1240 was analyzed through pyrolysis-GCMS. Figure 98 depicts the pyrograms recorded after the phosphinate salt underwent heat treatments of 475°C (maximum mass loss rate) and 600°C (end of degradation). Mass spectra of the detected products are gathered in Appendix 4.

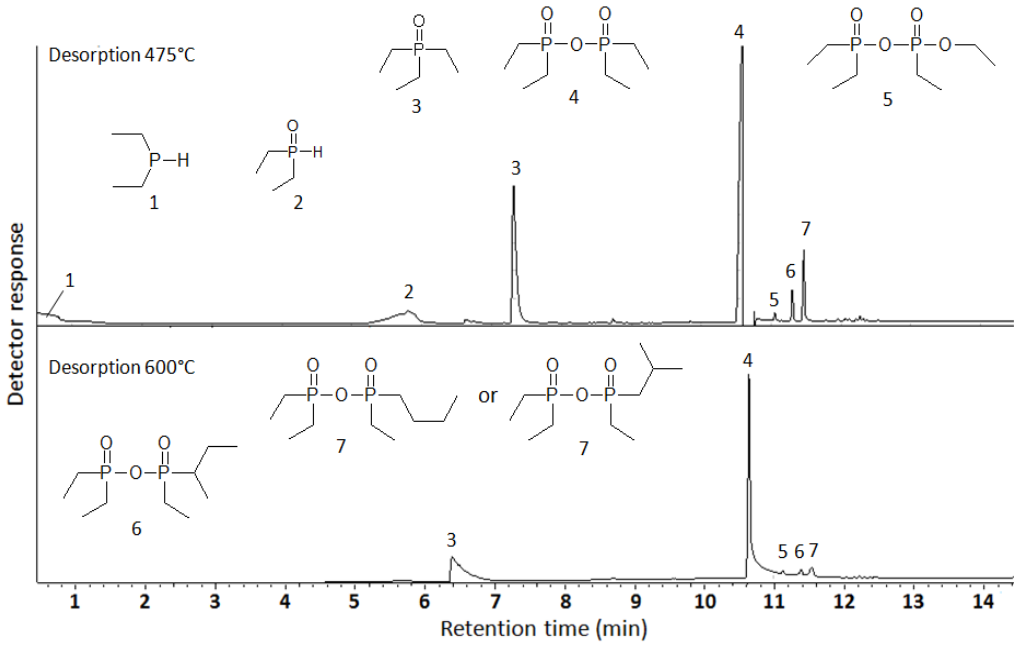

Figure 98 : Chromatogram of the gases evolved during the thermal treatment of Exolit OP1240 at 475°C (above) and 600°C (below) in helium atmosphere; heating rate in the pyrolyzer: 10°C/min

Two major degradation products are released by OP1240 during the whole decomposition process. There are the triethyl phosphine oxide (peak 3) and the dimeric anhydride of diethylphosphinic acid (peak 4). Three other anhydrides, denoted as 5, 6 and 7, are released mostly during the first part of the decomposition. In Figure 99, is presented the mass spectra of the different anhydrides. A fragmentation pattern is proposed below each spectrum.

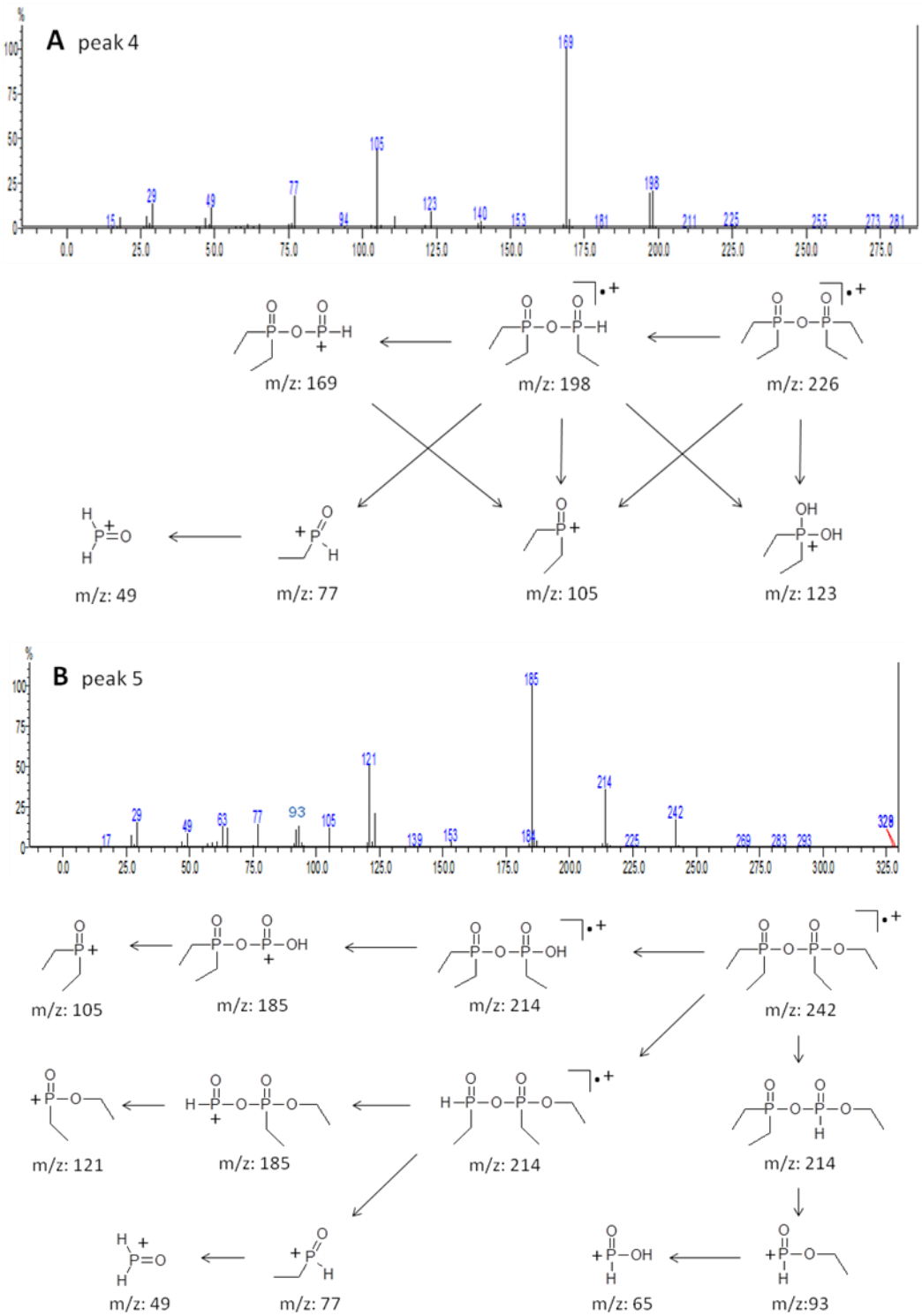

Continued below

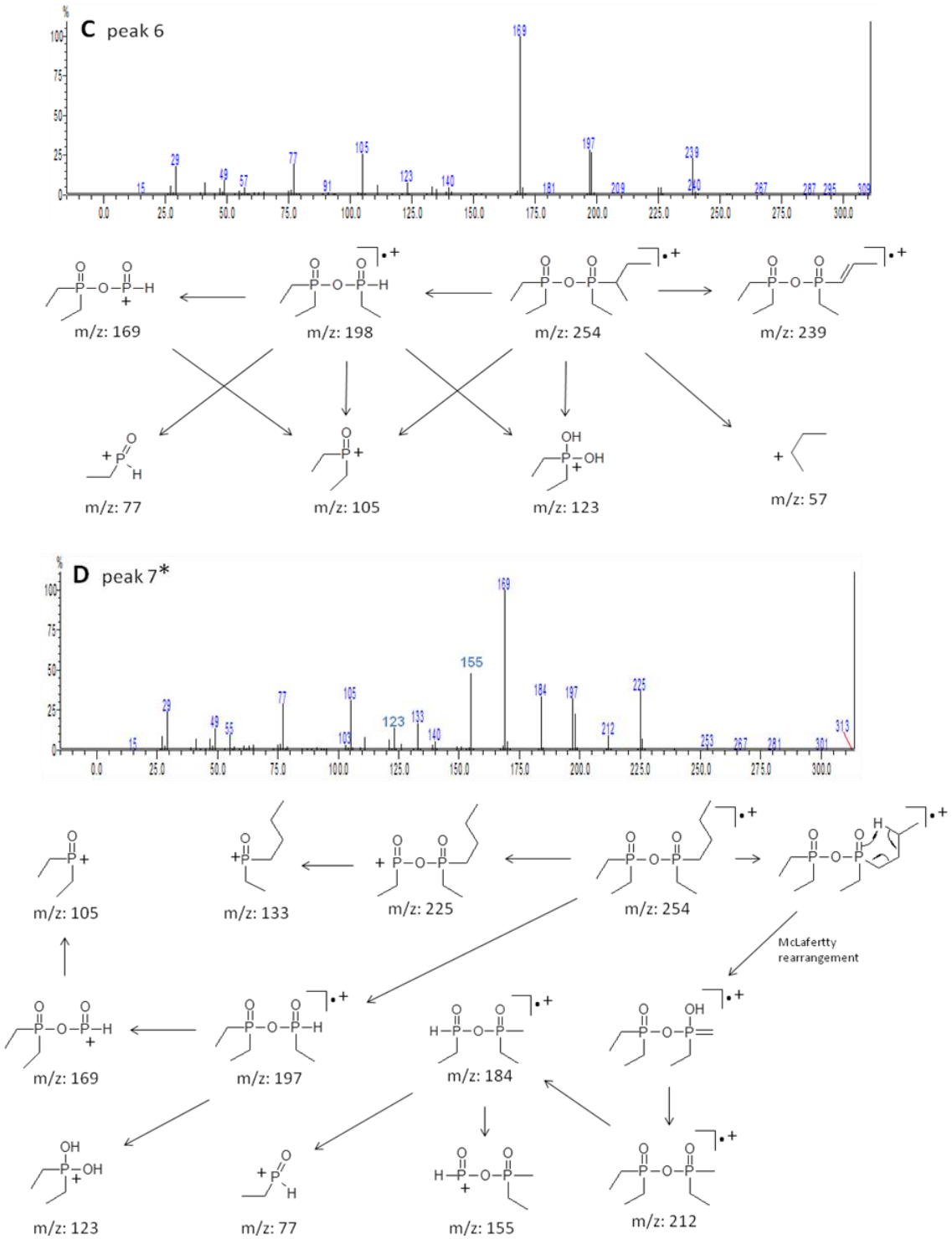

Figure 99 : Mass spectra of the products 4 (spectrum A), 5 (spectrum B), 6 (spectrum C) and 7 (spectrum D) evolved by heat treatment of Exolit OP1240; the proposed fragmentation patterns are pictured below the spectra; * product 7 may either contain the n-butyl or the isobutyl residue

Product 5 is the result of the condensation of one diethylphosphinic acid with the ethyl phosphonic acid ethyl ester. This compound is obtained in low quantity and should not be considered in the decomposition model. Peaks 6 and 7 are attributed to two different

isomers of the butyl ethyl phosphinic acid condensed with diethyl phosphinic acid. Product 7 is most likely composed of the n-butyl or the isobutyl residues. For this compound, the formation of fragment ions of 212, 184 and 155 m/z in mass spectrometry must involve a "McLafferty rearrangement" whereupon a P-CH_3 group is obtained[214]. This rearrangement is only achievable with the presence of n-butyl or isobutyl residues. Product 6 should therefore contain the residue sec-butyl. On the other hand, diethyl phosphine (peak 1) and H-diethyl phosphine oxide (peak 2) are detected during the first part of the decomposition. It is worth mentioning that several signals, among which ethene, overlap with the signal of diethyl phosphine (see Appendix 4). The release of ethene would be in agreement with data of the literature[39,141,192].

Interestingly, the diethylphosphinic acid is not observed on pyrograms whereas it was clearly identified as a degradation product of OP1240 in a few studies[39,192]. The phosphinic acid is very likely to be released in the gas phase but one can suspect that the product self-condenses in the mass spectrometer to form the corresponding dimeric anhydride (peak 4)[214]. The evolution of other anhydrides (products 5, 6 and 7) during the decomposition process of OP1240 is likewise uncertain. These anhydrides might also be formed by condensation reactions in the GCMS apparatus.

2.2.1.3 Analysis of the residue

Exolit OP1240 was heat treated at 600°C in nitrogen atmosphere. The obtained residue was analyzed through ^{13}C, ^{31}P and ^{27}Al solid state NMR. Corresponding spectra are gathered in Figure 100.

The ^{31}P and ^{27}Al NMR spectra of the residue of OP1240 are quite comparable to the spectra of the residue of **C9**. Aluminum diethylphosphinate accordingly decomposes into alumino-phosphonate (^{31}P: 6 ppm) and alumino-phosphate species (^{31}P: - 30 ppm)[167,192]. As for **C9**, the coordination of the OP1240 phosphorus species with aluminum varies from an octahedral geometry (^{27}Al: - 12 ppm) to a tetrahedral geometry (^{27}Al: 36 ppm), transiting through a pentahedral geometry (^{27}Al: 6 ppm). The ^{13}C NMR analysis also shows that upon treating OP1240 to 600°C, some char is formed while a still significant proportion of aliphatic groups (i.e. ethyl groups bonded to phosphorus, bands at 20 and 8 ppm) remain in the condensed phase. The resonance at about 12 ppm, which is observed on the ^{13}C spectrum of the heat treated sample but not on that the untreated one, might be attributed to aliphatics hydrocarbons different than those of the ethyl groups linked to phosphorus.

It is noteworthy that an important proportion of white powder has been found to accumulate on the wall of the quartz tube in which was performed the thermal treatment of OP1240. The ^{13}C, ^{31}P and ^{27}Al solid state NMR spectra of this powder are depicted in Figure 101. The resonances observed on spectra are characteristics of the aluminum phosphinate

salt. Thus, it confirms that OP1240 not only decomposes but also sublimates during the thermal treatment.

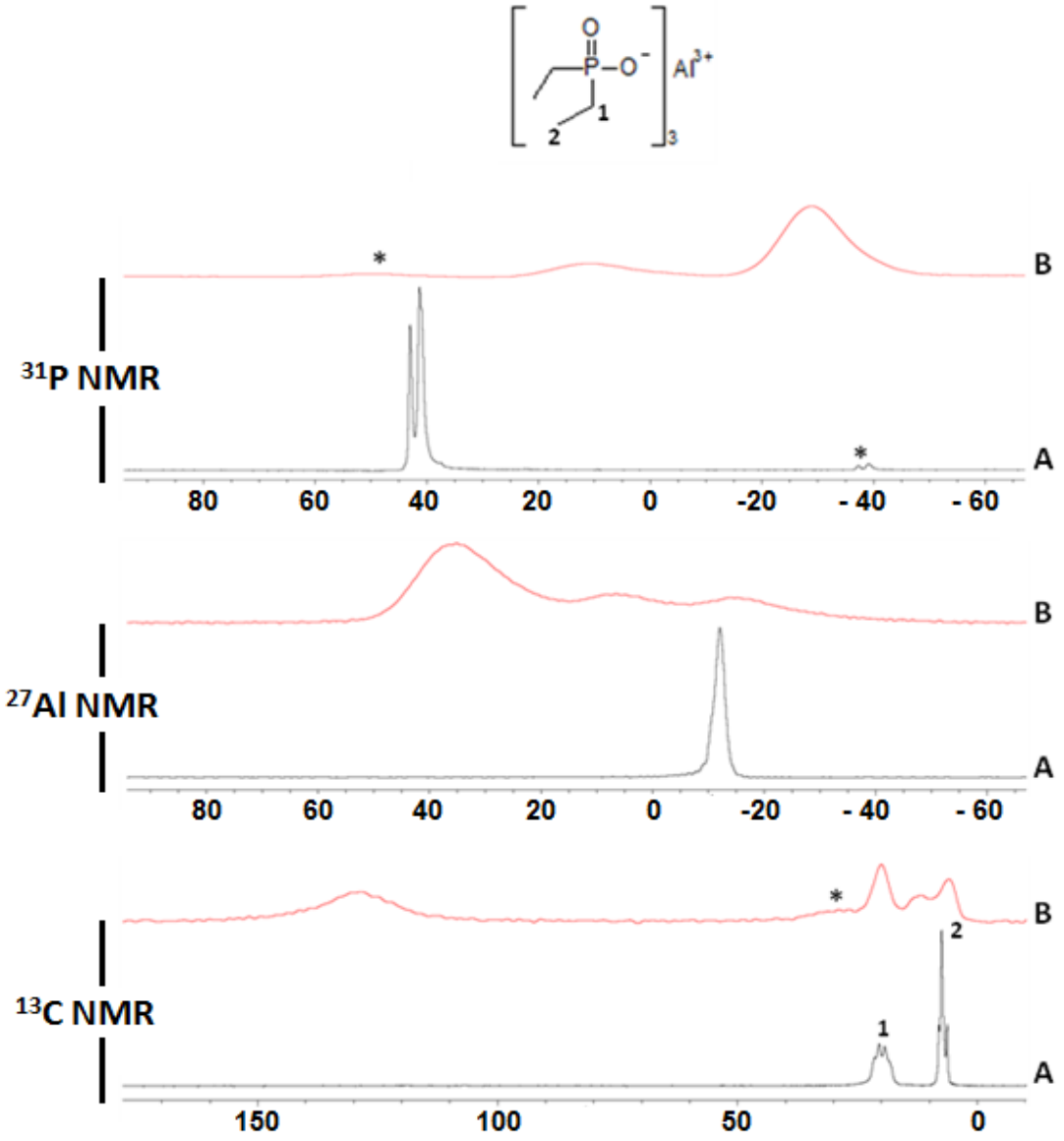

Figure 100 : ^{13}C CPMAS, ^{31}P MAS and ^{27}Al MAS solid state NMR spectra of Exolit OP1240 before and after the thermal treatment at 600°C in nitrogen; (A) - before treatment, (B) - after treatment

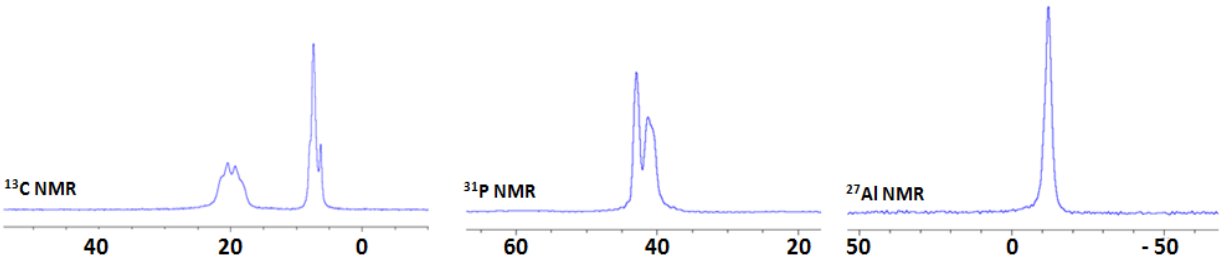

Figure 101 : ^{13}C CPMAS, ^{31}P MAS and ^{27}Al MAS solid state NMR spectra of the white powder collected on the wall of the quartz tube after thermal treatment of Exolit OP1240 in nitrogen

2.2.1.4 Degradation mechanism

The degradation scheme of Exolit OP1240 is pictured in Figure 102.

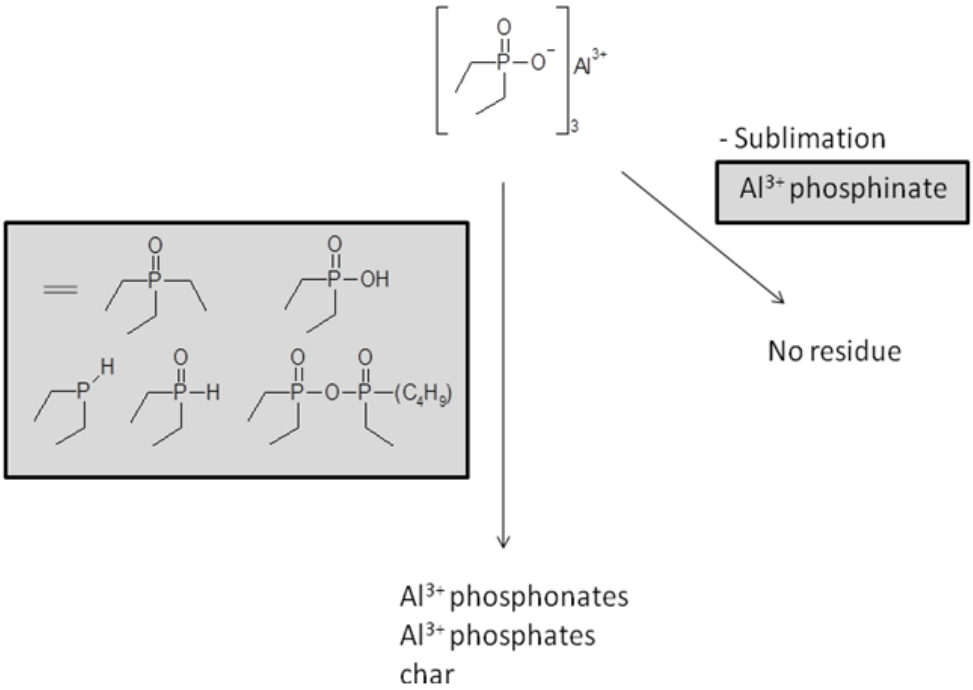

Figure 102 : Exolit OP1240 degradation scheme (detected gaseous decomposition products in grey)

It has been demonstrated through TGA that Exolit OP1240 exhibited a high thermal stability. The latter appeared higher than that of **C9**. Moreover, the commercial and self-synthesized phosphinates are characterized by different thermal behaviors. On the contrary to **C9**, part of the OP1240 sublimates during thermal treatments. In parallel with its sublimation, OP1240 undergoes degradation. It leads for the most part to the formation of alumino-phosphonates, alumino-phosphates and some char in condensed phase along with the release of ethene, diethyl phosphinic acid (detected as a dimeric anhydride), diethyl phosphine and phosphine oxides (H-diethyl and triehtyl phosphine oxides) in the gas phase. Two phosphinic acid anhydrides were additionally identified in GCMS. They result from the condensation of diethyl phosphinic acid with butyl ethyl phosphinic acids. It is not sure whether the condensation of such products occurs during the decomposition or during the transfer of gases in the GCMS apparatus.

The formation of alumino-phosphonate and alumino-phosphate residues during the decomposition of OP1240 follows the same scheme as for **C9**: diethyl phosphinates transform into transitory ethyl phosphonates, then into phosphates[192]. Part of the ethene is released when phosphonate oxidizes into phosphates[39]. Note that the formation in condensed phase of phosphorus based substances of higher oxidation state (i.e.

phosphonates, phosphates) is compensated by the reduction of phosphinate species into phosphine and phosphine oxide. Such behavior was already reported in the case of zinc phosphinate salt[204].

2.2.2 Thermal decomposition of PBT/GF flame retarded with Exolit OP1240

This part deals with the thermal degradation of PBT/GF flame retarded with Exolit OP1240. A special emphasis will be laid on establishing a comparison between the decomposition modes of PBT/GF/OP1240 and PBT/GF/**C9**.

2.2.2.1 Thermal degradation

TG and DTG curves (experimental and calculated) of PBT/GF flame retarded with OP1240 are presented in Figure 103.

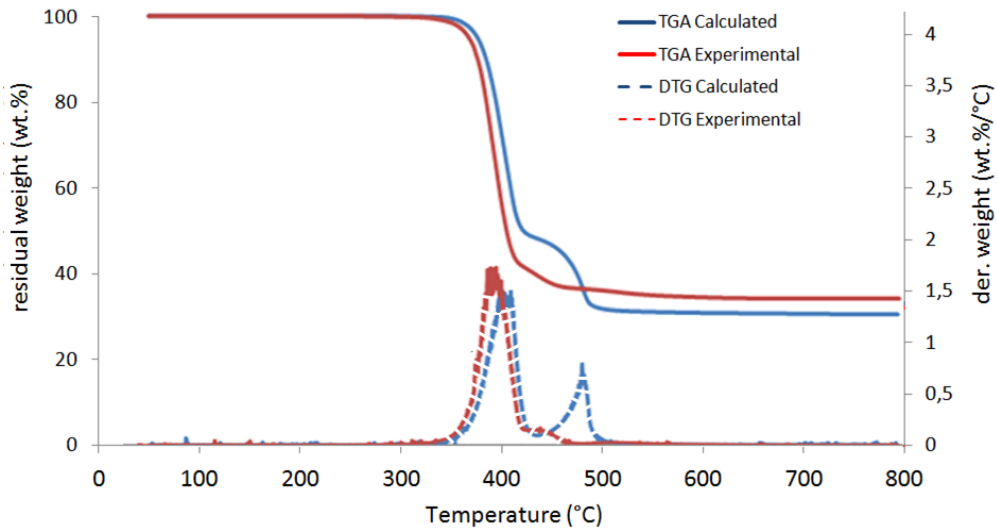

Figure 103 : TG and DTG curves of PBT/GF/OP1240 (10°C/min in nitrogen)

The calculated formulation exhibits two distinct weight loss steps, the first one between 325°C and 420°C (- 50.2 wt%) attributed to the decomposition of PBT, the second one between 420°C and 590°C (- 18.4 wt%) ascribed to the decomposition of both PBT and OP1240. Experimentally, incorporating OP1240 in PBT/GF leads to a modification of the thermal decomposition behavior of the material. This suggests chemical interactions between the flame retardant and the polymer: a slight destabilization of the material is observed during the first mass loss step. It is characterized by a decrease of the onset temperature of degradation and by a higher mass loss rate as well as by an increase in the size of the mass loss step (- 57 wt%). Two successive degradation steps are then observed for the experimental formulation. The first one between 415°C and 460°C corresponding to a weight loss of 5 wt% and a second minor one between 460°C and 590°C corresponding to a mass loss of 3.1 wt%. At 800°C, the experimental formulation shows a residual mass of 3.6

wt% higher than the one expected which allows assuming that OP1240 promotes charring of the polymer. These results are consistent with the literature[39,141].

2.2.2.2 Evolved gases

The FTIR analysis of gases released during the thermal degradation of the PBT/GF/OP1240 material is presented in Figure 104. Attribution of the FTIR signals is given in Table 29. As for the formulations previously investigated (PBT/GF and PBT/GF/**C9**), PBT/GF/OP1240 degrades through releasing water, THF, butadiene, CO_2, benzoic acid and ester derivatives.

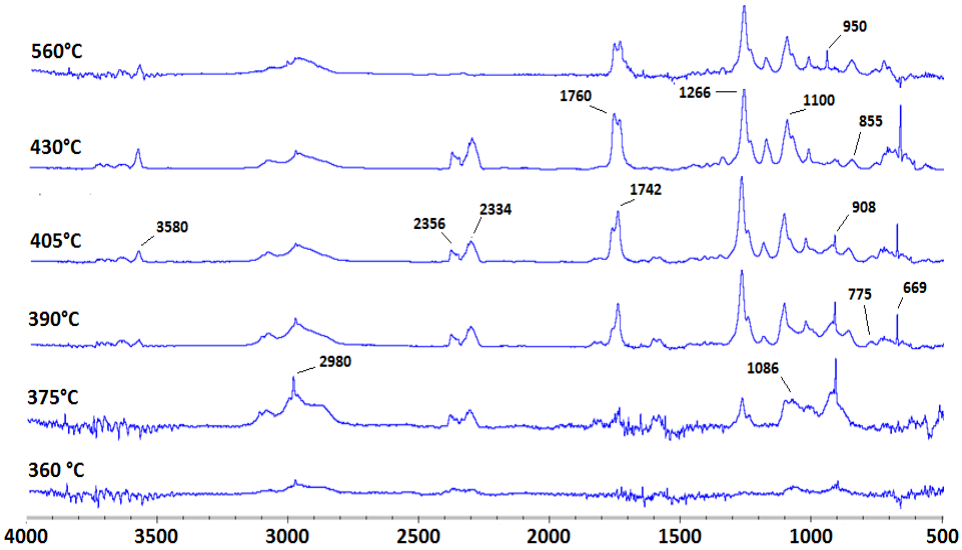

Figure 104 : FTIR spectra of the gases evolved during the thermal degradation of PBT/GF/OP1240 (in N_2 atmosphere) at characteristic temperature

Table 29 : Attribution of the IR bands of the gases evolved during degradation of PBT/GF/OP1240 in nitrogen; the underlined band positions are used to determine product release rates[39,80,127,128,209]

Decomposition products	FTIR / cm^{-1}
Phosphinic acid	**855**,**775** (P-O phosphinic acid)
THF	**2980** (CH_2 stretch), **1086** (asym. ring vibration)
CO_2	**2356** (CO_2 asym. stretch), **2304** (CO_2 sym. stretch), **669** (CO_2 bend)
Butadiene	**908** (-C=C-H wag)
H_2O	**4000-3400** (O-H stretch)
Benzoic acid	**3580** (O-H stretch), **1760** (C=O sym. stretch)
Esters	**1742** (C=O stretch), **1266** (C-O-C asym. stretch), **1100** (C-O-C sym. stretch)
Ethene	**950** (CH_2 wag)

Benzene, which has not been observed up to now, shows up as a novel degradation product of PBT that would be released at an advanced stage of the decomposition. It is indeed

characterized by a broad signal at about 667 cm^{-1} (see FTIR spectrum at 430°C) superimposed on the signal of CO_2 (669 cm^{-1})[39,141]. Diethylphosphinic acid and ethene are obtained from the Exolit OP1240 degradation.

The signal extinction of evolved gases versus temperature (except for water and benzene) is presented in Figure 105. The first step of the decomposition starts with the release of H_2O, THF, butadiene, esters, CO_2, benzoic acid and phosphinic acid. Then it is observed a second peak release of THF and phosphinic acid while the liberation of CO_2 and benzoic acid reaches a maximum. One can note that an important amount of CO_2 evolves during the degradation of PBT/GF/OP1240 as suggested by the large surface area of the evolution curve of the gas. It would indicate that the material undergoes extensive decarboxylation. The release of ethene starts with the second degradation step. This step is marked by a noticeable inflection in the evolution curves of CO_2 and esters. Benzene is also released during this step. The third degradation step defined in TGA corresponds to the release of ethene.

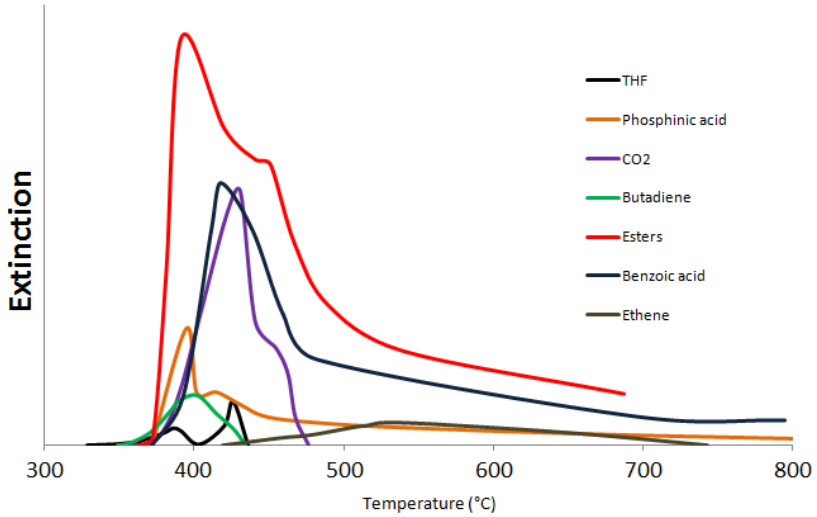

Figure 105 : Evolved gas release rate of the PBT/GF/OP1240

The Pyrolysis-GCMS analysis allows providing further indications on the degradation products released by the material. In Figure 106, is depicted the pyrogram recorded after the material underwent a thermal treatment at 390°C. The mass spectra of evolved products are depicted in Appendix 4. Gaseous products resulting from the PBT decomposition are basically the same than those found for the PBT/GF and PBT/GF/**C9** formulations. However, if considering the same heat treatment temperature (390°C), significant differences can be observed between the pyrogram of the PBT/GF/OP1240 formulation and that of the PBT/GF (Figure 77) and PBT/GF/**C9** (Figure 92) formulations. Indeed, the surface area of the peaks of low boiling point products (particularly those of benzoic acid and mono-butenyl ester of terephthalic acid) appears greater in the pyrogram of PBT/GF/OP1240 than in the pyrograms PBT/GF and PBT/GF/**C9**. Conversely, the surface area of the peaks of high boiling point oligomeric ester and acid-esters appears greater for PBT/GF and PBT/GF/**C9** than for

PBT/GF/**C9**. Hence, relative to high boiling point products, a higher amount of low boiling point products is released by the PBT/GF/OP1240 material. It indicates that PBT undergoes a greater extent of degradation in presence of OP1240 than in presence of **C9**.

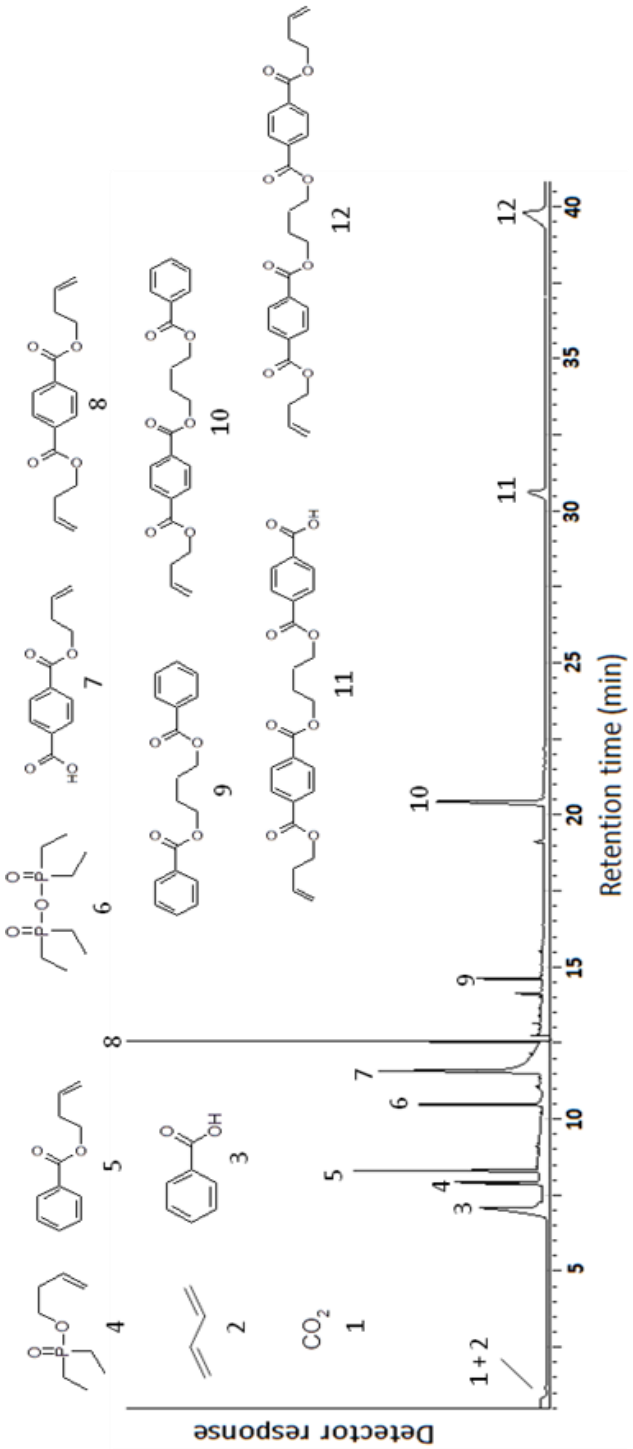

Figure 106 : Chromatogram of the gases evolved during the thermal treatment of PBT/GF/OP1240 to 390°C° in helium atmosphere; heating rate in the pyrolyzer: 10°C/min

Thus, it would corroborate the results of the FTIR analysis showing that a larger proportion of CO_2 would be released by PBT/GF/OP1240 compared to PBT/GF/**C9**. This is confirmed further by the fact that the signals of butadiene and CO_2 (peak 1 and 2) can be observed on the chromatogram. Another particularity of PBT/GF/OP1240 is that the broad signal of terephthalic acid is not properly detected. It is very likely that the di-acid preferentially decarboxylates into the benzoic acid during the degradation of the material[39].

Two more degradation products are observed on the pyrogram, namely the dimeric anhydride of diethyl phosphinic acid (peak 6) and the diethylphosphinic acid butenyl ester (peak 4). As previously proposed, product 6 is the result of the condensation of two molecules of diethyl phosphinic acids in the GCMS apparatus. This assumption is substantiated by the fact that diethyl phosphinic acid is detected through the FTIR analysis while not through pyrolysis-GCMS. Product 4 appears like a new substance that has never been mentioned in the literature. Its mass spectrum and corresponding fragmentation pattern are depicted in Figure 107.

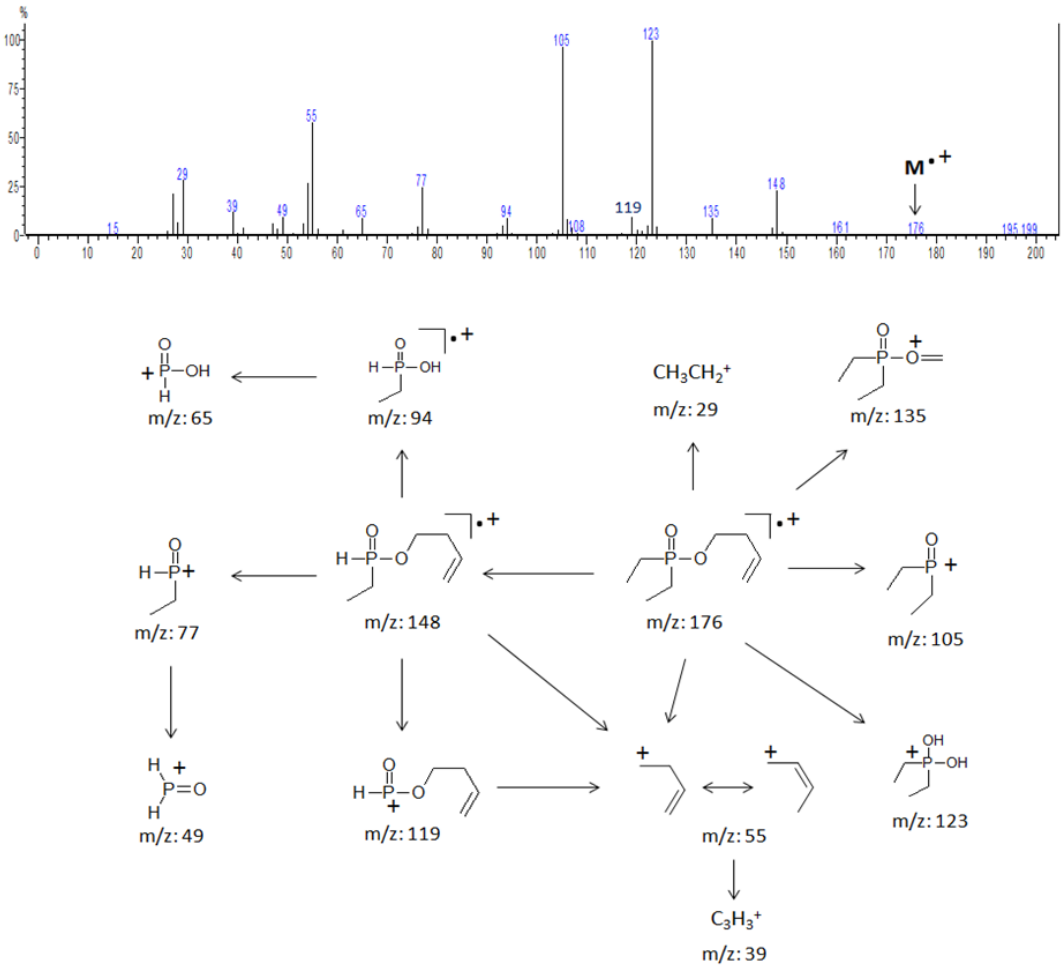

Figure 107 : Mass spectrum of the product 6 (Figure 106) evolved by heat treatment of PBT/GF/OP1240; the proposed fragmentation pattern of the product is pictured below the spectrum

At first sight, product 4 originates from an addition reaction of diethyl phosphinic acid to the double bonds of butadiene. Its formation may take place in condensed phase or in gas phase. Another possible route to explain the formation of product 4 will be discussed below with insight on the global decomposition scheme of PBT/GF/OP1240.

2.2.2.3 Analysis of the residue

The PBT/GF/OP1240 material was heat treated at 600°C in nitrogen atmosphere. A picture of the obtained residue is presented in Figure 108. The surface of the residue of PBT/GF/OP1240 appears more homogeneous comparatively to that of PBT/GF/**C9**. In particular, PBT/GF/OP1240 does not present the large-sized holes which have been observed for PBT/GF/**C9**. This can be explained by the fact that OP1240 promotes the polymer charring on the contrary to **C9**.

Figure 108 : Picture of the residue of PBT/GF/OP1240 obtained after thermal treatment at 600°C in nitrogen. In blue: expected mass loss (according to TGA), in black: experimental mass loss

The ^{13}C, ^{31}P and ^{27}Al NMR spectra of the material, before and after the thermal treatment, are gathered in Figure 109. The residue of PBT/GF/OP1240 exhibits the same ^{31}P and ^{27}Al resonances as those observed for the residue of PBT/GF/**C9** (alumino phosphonates and phosphates). However, for the residue of PBT/GF/OP1240, the surface area of the ^{31}P signal of phosphonate species appears particularly low comparatively to that of the ^{31}P signal of phosphates. The ratio between the surface areas (integrations) of ^{31}P phosphonate and ^{31}P phosphate signals ($IntPO_3/IntPO_4$) was calculated. This ratio is of 0.15 and 0.43 respectively for the residue of PBT/GF/OP1240 and the residue of PBT/GF/**C9**. These results prove that for a same heat treatment, the evolution of phosphinates toward phosphates is more extensive for OP1240 than for **C9**. It may suggest that PBT/GF/OP1240 releases a higher amount of phosphorus in the gas phase than PBT/GF/**C9**.

The ^{13}C NMR spectrum of the residue of PBT/GF/OP1240 only displays a broad band centered at 130 ppm attributed to carbonaceous char (aromatic and alkylenic carbons). The absence of the alkyl signals, notably that of ethyl bonded to phosphorus, is consistent with the low proportion of phosphonate species in the residue.

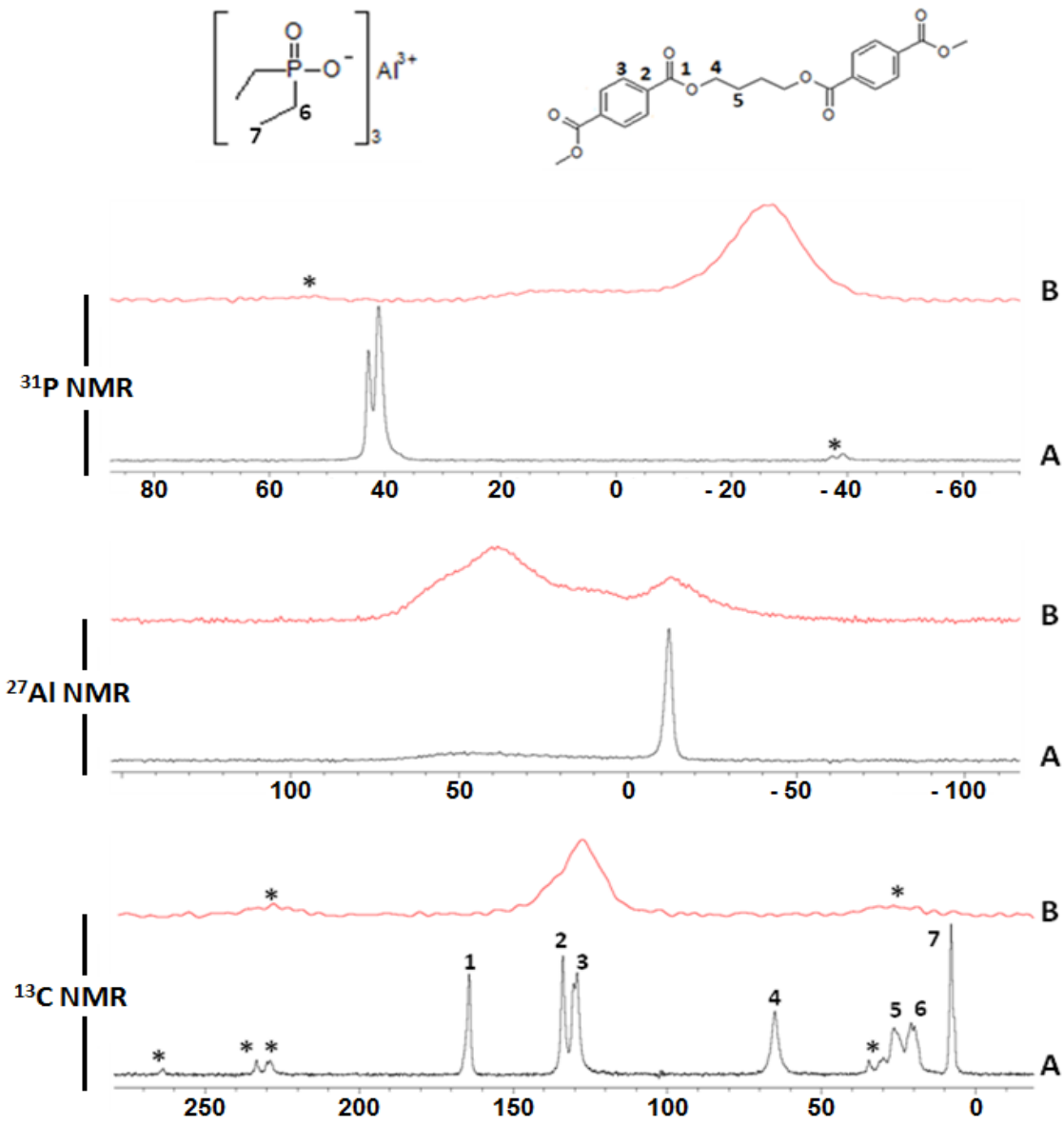

Figure 109 : ^{13}C CPMAS, ^{31}P MAS and ^{27}Al MAS solid state NMR spectra of PBT/GF/OP1240 before and after the thermal treatment to 600°C in nitrogen; (A) - before treatment, (B) - after treatment

2.2.2.4 Degradation mechanism

The proposed degradation scheme of PBT/GF/OP1240 is depicted in Figure 110. The information provided by the different analyses performed on PBT/GF/OP1240 (TGA-FTIR, pyrolysis GCMS, solid state NMR) are for the most part consistent with the results reported by Braun et al[39,141]. Along with the standard decomposition processes of PBT, interaction occur between PBT and Exolit OP1240. The release of diethyl phosphinic acid starts right from the beginning of the degradation of the material and proceeds by proton transfer reactions between the terephthalic acid end chain groups (formed by β-elimination of PBT) and the phosphinate residues linked to aluminum. Aluminum terephthalate-phosphinate salts are consequently produced in condensed phase[39]. Aluminum terephthalate-

phosphinate complexes ultimately degrade into aluminum phosphates while specific products such as benzene (together with CO_2) and ethene (by scission of P-C_2H_5 bonds) are released in the gas phase[39].

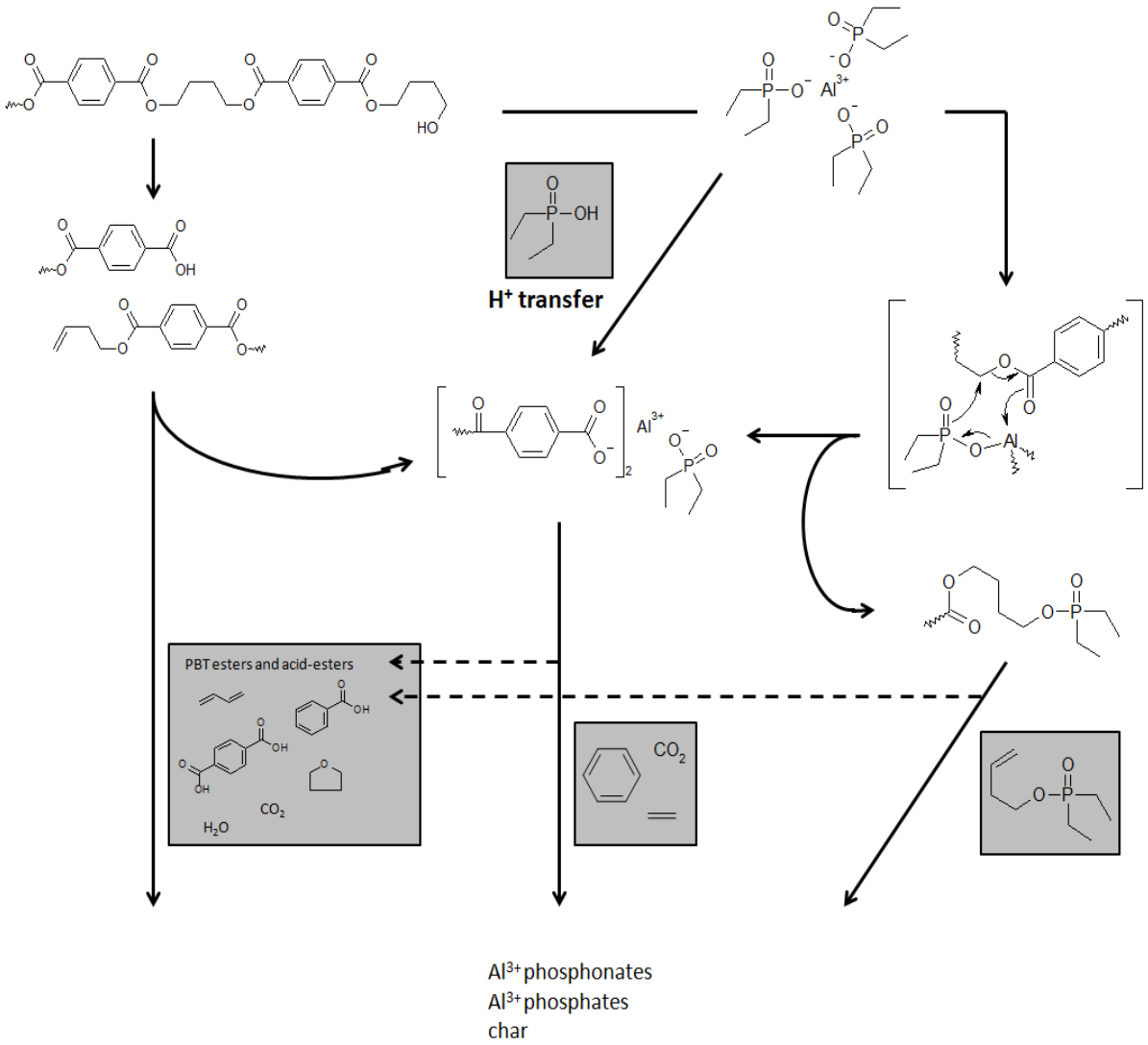

Figure 110 : PBT/GF/OP1240 degradation scheme (detected gaseous decomposition products in grey)

On the other hand, the pyrolysis GCMS analysis showed that a relatively significant proportion of diethylphosphinic acid butenyl ester (product 4) was liberated by the OP1240 containing material. This product possibly results from an addition reaction of diethyl phosphinic acid to butadiene[71]. Another mechanism, inspired by the Meerwein-Ponndorf-Verley (MPV) reduction[217], was envisaged to explain the formation of product 4 (see Figure 110). It consists in the substitution of PBT–COO^- by diethyl phosphinate. In this reaction, aluminum acts as a catalyst metal center by polarizing the carboxylic ester groups of PBT. Aluminum terephthalate salts as well as PBT with diethyl phosphinate end chain groups are

thus formed. Diethylphosphinic acid butenyl ester are released when β-elimination occur at the carbon-ester bonds.

This part showed that the decomposition modes of PBT/GF/OP1240 and PBT/GF/**C9** were noticeably different. Unlike the PBT/GF/C9 material, the thermal decomposition of PBT in PBT/GF/OP1240 plays a key role in the liberation of the phosphinic acid through proton transfer reactions and formation of aluminum terephthalate complexes. If such interaction did not occur, the aluminum phosphinate salt would be too stable compared to PBT and its fireproofing action would surely not be effective. Besides, the PBT chains undergo larger degradation in presence of OP1240 than in presence of **C9**. This would indicate that Exolit O1P240 itself catalyzes the β-elimination processes of PBT by allowing the carboxylic esters of the polymer to coordinate the aluminum. The coordination of carboxylic esters to aluminum eventually promote the polymer charring that is concomitant to the second step of THF liberation[39,141].

2.2.2.5 Conclusion

In this part, we have demonstrated that the thermal decomposition of PBT/GF/OP1240 occurred in a different way as for PBT/GF/**C9**. In the pure form, OP1240 exhibits a much higher thermal stability than PBT. Besides sublimating, the flame retardant degrades through mostly releasing ethene, phosphines (i.e. triethyl phosphine oxide) and diethyl phosphinic acid. Upon heat treatment of the PBT/GF/OP1240 material, the phosphinate salt and the polymer interact with each other via proton transfer reactions and formation of aluminum terephthalate salts. It results in the early release of diethyl phosphinic acid. Furthermore, the degradation of PBT appeared to be influenced by the presence of OP1240. This is likely due to the fact that aluminum accelerates the β-elimination processes of PBT through polarizing the carboxylic ester groups of PBT. As a result, PBT/GF/OP1240 releases a higher proportion of low boiling point PBT products than PBT/GF/**C9**. The coordination of carboxylic ester groups with aluminum is believed to promote the PBT charring and the release of THF during the decomposition. The pyrolysis-GCMS analysis demonstrated that the degradation of PBT/GF/OP1240 was also characterized by the formation of diethylphosphinic acid butenyl ester. The latter possibly results from addition reactions of the diethyl phosphinic acid to butadiene or else from the substitution of PBT-COO^- residues by the phosphinate via aluminum complexation.

As for PBT/GF/**C9**, the main flame retardant activity of PBT/GF/OP1240 occurs in gas phase. Exolit OP1240 releases phosphinic acid (also phosphinic ester derivatives) that inhibit the combustion chain reactions. However, charring of PBT is slightly promoted in presence of OP1240 while not in presence of **C9**. This charring presumably acts as a supplementary protection by limiting the fuel diffusion in the gas phase[141].

3. Conclusion

The thermal decomposition of PBT/GF/**C9** and PBT/GF/OP1240 was established and compared in this chapter. Both aluminum phosphinate salts exhibit a main gas phase mode of action through releasing phosphorus based species (in particular phosphinic acids). However, the mechanisms involved in the release of these species depend on the nature of the phosphinate.

The thermal decomposition of PBT is slightly influenced in presence of **C9**. Upon degrading, the latter liberates aniline which interacts with PBT by aminolysis of esters bonds. The polymer would also moderately influence the decomposition of **C9** by favoring the release of OP (Exolit PE110). The interaction between PBT and **C9** remains globally limited. The release of phosphorus based products (especially the aniline based phosphinic acid **C2**) is mostly triggered by chemical interactions occurring in the bulk of the phosphinate salt (i.e. polarization of carboxamide functions and proton transfer reactions). No additional char is produced when PBT is flame retarded with **C9**.

Unlike **C9**, pure Exolit OP1240 exhibits a much higher thermal stability compared to PBT. However, the incorporation of OP1240 in PBT modifies the thermal decomposition of both the polymer and the flame retardant. Upon heat treatment, the coordination of the carboxylic ester groups of PBT to aluminum would catalyze the degradation of PBT (especially the β-elimination processes) and trigger the early release of diethyl phosphinic acid as well as the formation of diethylphosphinic acid butenyl ester. Further, the char yield is increased when PBT is flame retarded with OP1240.

In chapter 4, it has been demonstrated that Exolit OP1240 exhibited a better flame retardant efficiency than **C9**. There could be two reasons for this. The first one is that a higher amount of phosphorus is released in the gas phase by OP1240. The higher phosphorus content of the diethyl phosphinic acid compared to the aniline based phosphinic acid **C2**, as well as the almost exclusive presence of alumino-phosphates in the final residue of PBT/GF/OP1240, would support this assumption. The other explanation is that the char induced by OP1240 would constitute a supplementary protection shield against the diffusion of fuel products[80].

GENERAL CONCLUSION - OUTLOOK

GENERAL CONCLUSION

This work was devoted to the development of a novel flame retarded glass fiber (25 wt%) reinforced PBT (PBT/GF) formulation for applications in the electrical/electronic industry. PBT/GF is indeed widely used in this domain to insulate electrical parts. Therefore, the polymer has to comply with severe requirements to limit flammability risks.

Two approaches have been chosen in this project. The first one consisted in improving the fire behavior of PBT/GF by combining the commercial aluminum diethylphosphinate (Exolit OP1240) or the mixture of aluminum diethylphosphinate and melamine cyanurate (Exolit OP1200) with nano-particles. The second approach aimed at synthesizing novel phosphinate salts to be used alone or in combination with traditional flame retardants or synergists.

In the first approach, various nano-particles, including organo-modified clays, POSS and graphene based additives were investigated in combination with the Exolit systems. A screening was performed based on the UL94 (0.8 mm) test which allowed defining a promising flame retardant combination: Exolit OP1240 + RDP bentonite. Finally, optimizing the combination allowed determining the most appropriate ratio of both additives, namely 18 wt% of the Exolit OP1240 + 2 wt% of the RDP bentonite. Better performances are achieved at the UL94 and cone calorimeter tests with the FR combination compared to 20 wt% OP1240 alone, while the LOI of the material is not significantly changed. The industrial challenge has therefore been fulfilled since an innovative flame retardant system was found which exhibits the highest performances through one of the most demanding fire test (UL94).

In the second approach, a variety of phosphinate salts were synthesized. These salts (except that containing the PEPA residue) were obtained in a two step process: first it involves the reaction of the oxaphospholane oxide (Exolit PE110) with nucleophilic reagents to afford carboxyethyl(methyl)phosphinic acid derivatives with different structural variations. Second the phosphinic acids are converted into aluminum phosphinate salts. Various nucleophilic reagents were reacted with Exolit PE110, including benzyl amine, aniline, piperazine, ethylene diamine and m-phenylene diamine. The synthesis of the PEPA based aluminum phosphinate required an additional step consisting in hydrolyzing Exolit PE110. The resulting product was then condensed with the nucleophilic reagent PEPA to afford the corresponding phosphinic acid. The latter was finally converted into aluminum salt. The fire performances of aluminum salts in PBT/GF were investigated through the UL94 (1.6 mm) and LOI tests. These tests globally highlighted that a too high thermal stability of salts compared to PBT/GF was not beneficial for improving the fire behavior of the polymer. Accordingly, the best performances were achieved with phosphinate salts degrading in the same range of temperature than PBT/GF, namely the benzyl amine and aniline based phosphinate salts (respectively **C8** and **C9**). **C9** proved to be particularly efficient at 17 wt% in PBT/GF, providing a high LOI value (50 Vol%) and a good UL94 classification (V-0 rating after a

2d.25°C aging). The zinc and calcium analogues of **C9** were also investigated but exhibited much lower performances. Several combinations of **C8** and **C9** with conventional flame retardants and synergists were tested. Only one FR combination, that is to say 16 wt% **C9** + 1 wt% RDP bentonite, has managed to provide higher FR properties than the pure phosphinate salts in the UL94 test. One may at last considered that the industrial challenge was also achieved through the second approach since the combination of **C9** and RDP bentonite nearly compete with FR performances of Exolit OP1240 at UL94 test while it significantly increases the fire behavior of the material according to the LOI. There is no doubt that the FR performances of **C9** could be further improved finding suitable synergists.

The understanding of flame retardant mechanisms was also an important concern of this work. The FR modes of action of Exolit O1P240 and **C9** were investigated and compared. Through performing thermogravimetric analyses (TGA), characterization of the condensed phase (solid state NMR) and gas phase (TGA-FTIR, pyrolysis-GCMS) analyses, it has been demonstrated that the thermal degradation of OP1240 and **C9** did not operate according to the same scheme in PBT/GF. OP1240 interacts with PBT during thermal decomposition processes, which allows the early evolution of diethylphosphinic acid in the gas phase. It is then evidenced that the degradation pathway of PBT is modified in presence of OP1240. This results in the release of PBT gaseous degradation products of relatively low molecular weights as well as an increase of the residue yield (carbonaceous char) of the material. On the contrary, **C9** degrades almost independently from PBT. The synthesized salt mostly releases aniline and the aniline based phosphinic acid in the gas phase whereas part of the aniline reacts with PBT (amminolysis of ester bonds). However, the degradation pathway of PBT is only slightly modified in presence of **C9**. It was finally assumed that the higher FR efficiency of OP1240 through the UL94 (in comparison to **C9**) would be due to the fact that the char promoted by the commercial product acts as an additional protection against the diffusion of combustible gases. Furthermore, the interaction between OP1240 and PBT would permit a simultaneous release of diethylphosphinic acid (flame inhibitor) and gaseous degradation products of PBT, resulting in a more effective inhibition of the flame.

OUTLOOKS

Many perspectives have emerged all along this dissertation. The FR modes of action of Exolit OP1240 and **C9** were fully described and compared, however the contribution of RDP bentonite as synergistic agent is still to be determined. Indeed, the organo-modified clay was found to improve the fire behavior of PBT/GF when combined to both commercial and synthesized phosphinates. Therefore, an interesting outlook would be to elucidate the synergistic effect between the flame retardants and the nano-particle. This new propect should allow answering the following questions:

- Are there chemical interactions between the additives?

- If there are some, are they responsible for the improvement of the apparent synergistic effect?

- If there is no chemical interaction between the phosphinate salts and RDP bentonite, does the nano-particle have a “physical role” in the fire retardancy mechanism, such as for example the formation of a surface barrier limiting the diffusion of combustible gases during the material degradation?

For this study, the same experiments as those implemented to investigate the FR mode of action of phosphinate salts in PBT/GF - including TGA-FTIR, pyrolysis-GCMS and solid state NMR - should be applied, especially to determine the degradation processes occurring in the phosphinate salt/RDP bentontie mixtures as well as those occurring in the PBT/GF/RDP bentonite and PBT/GF/phosphinate salt/RDP bentontie formulations. Thus, comparing these degradation processes with those already investigated in the present study would allow elucidating the influence of RDP bentonite on FR mechanisms. The use of X-ray scanning techniques (XRD) and microscopy (i.e. Transmission Electron Microscopy, TEM) would further be interesting to investigate the exfoliation or dispersion state of the bentonite clay in the PBT matrix.

On the other hand, other questions have been raised concerning the influence of the UL94 pre-conditioning on the flame retardant performances of the PBT/GF material. It was indeed observed that a 7d-70°C pre-conditioning of UL94 bar specimens damaged the FR performances of the materials. The evaluation of the FR performances of the PBT/GF/OP1200 formulation is particularly relevant to this issue since the material achieved a V-0 rating after a 2d-25°C aging while turning into a V-2 rating after a 7d-70°C aging due to the occurrence of flammable dripping (Table 30). Few experiments have already been performed to understand this phenomenom. They allowed providing some initial responses on the differences (in terms of chemical structure, physico-chemical or mechanical properties) between a PBT/GF/OP1200 material conditioned 2 days at 25°C and the same material conditioned 7 days at 70°C. In particular, solid state NMR analyses and capillary

viscosimetry experiments demonstrated that the conditioning did not affect the chemical structures in the material or the molecular weight of the PBT matrix.

Table 30 : UL94 results obtained for the OP1200 containing PBT/GF formulation

Composition (wt%)			UL-94, 0.8 mm bar			
PBT	**GF**	**OP1200**	**Conditioning**	**t1/t2[a] (s)**	**Dripping[b]**	Rating
55	25	20	2d.25°C	1.6/2.4	N	V-0
55	25	20	7d.70°C	1.9/1.8	N/D-Y	V-2

[a] *t1 and t2, average combustion times after the first and the second application of the flame*

[b] *dripping after the first and second application of the flame. N = no dripping, D-N = dripping without ignition of cotton, D-Y = dripping with ignition of cotton*

Electron Probe MicroAnalyses (EPMA) and contact angle measurements showed that OP1200 did not segregate or migrate at the surface of the material when the later was submitted to a 7d-70°C aging. Besides, a PBT/GF/OP1200 material conditioned at 70°C for 7 days in vacuum appeared to achieve the same UL94 performances as a sample conditioned under ambient atmosphere. It indicates that potential gas transfers between the atmosphere and the core of the material (i.e. diffusion of O_2 and H_2O) would not be involved in the modification of UL94 performances. Differences between a PBT/GF/OP1200 material submitted to a 2d-25°C aging and another submitted to a 7d-70°C aging were observed through Differential Scanning Calorimetry (DSC, Figure 111) and Dynamic Mechanical Analysis (DMA, Figure 112). Both methods showed that the conditioning leaded to a modification of the conformational structure of the material while no modification of the melting temperature or the enthalpy of melting of PBT was observed.

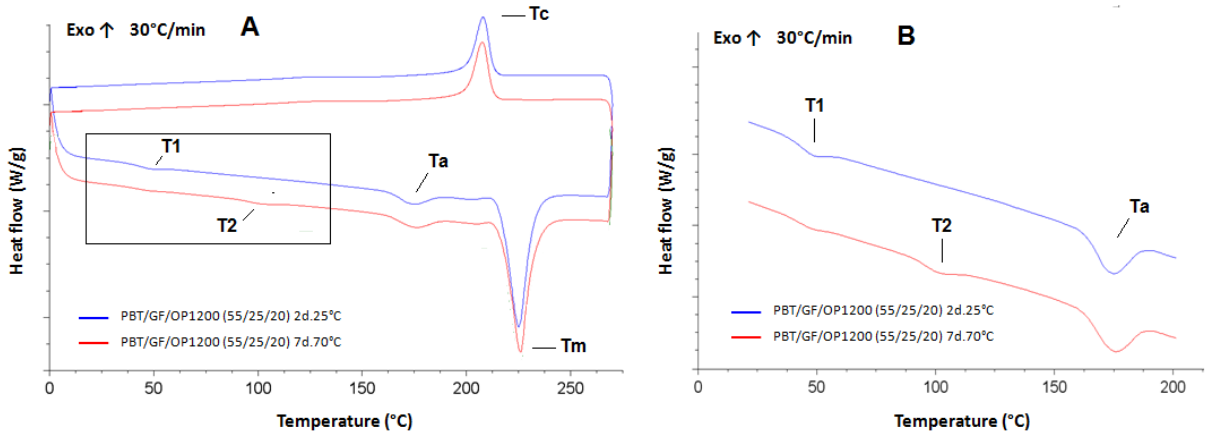

*With **T** = temperature; **T1**: relaxation of amorphous regions; **T2** : melting of imperfect crystallites, **Ta** : undefined transition occurring in Exolit OP1200, **Tm** : melting of PBT, **Tc**: crystallization of PBT.*

Figure 111 : DSC curve of PBT/GF/OP1200 after the 2d.25°C and 7d.70°C pre-conditioning. 1st heating-cooling cycle, 10°C/min under nitrogen flow. (A) full DSC curves, (B) zoom in the temperature range between 25°C and 200°C

Indeed, the DSC curve of the 2d.25°C aged sample exhibits an endotherm at around 43°C which was attributed to the structural relaxation of glassy amorphous regions under constraint in PBT[20,218,219]. These constrained amorphous domains are formed after cooling of the injected material from the melt. Their presence arises from the fast crystallization of PBT[23]. The DSC curve of the 7d.70°C aged sample does exhibit an additional endotherm at about 95°C while the endotherm at 43°C is hardly observed due to the relaxation of amorphous phases during the conditioning. This new endotherm was attributed to the melting of crystallites having a low degree of perfection[17]. Therefore, imperfect crystallites are formed in PBT during the 7d-70°C conditioning.

According to the DMA (Figure 112), these differences are reflected by a modification of the viscoelatic properties of the material in a temperature range between 40° and 120°C.

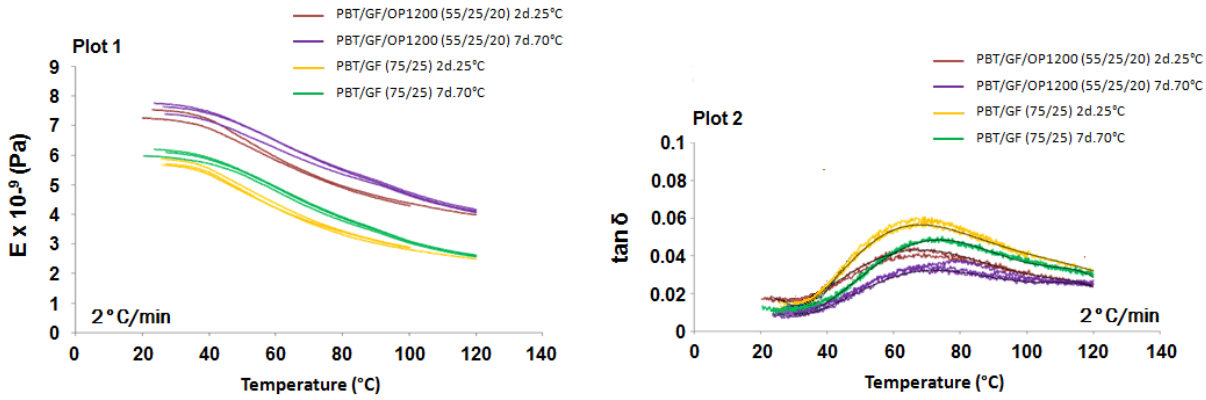

Figure 112 : Young's modulus (plot 1) and Phase angle (Plot 2) vs temperature obtained in DMA for the PBT/GF and PBT/GF/OP1200 samples. Temperature ramp: 2K/min, from 20°C to 120°C

Indeed, the 7d.70°C aged sample was found to present a higher stiffness than the 2d-25°C aged sample in this range of temperature which was explained by the presence of additional crystal phases (imperfect crystallites) in the 7d.70°C samples.

The correlation between these changes observed in DSC (physico-chemical properties) and DMA (mechanical properties) and the UL94 performances of the material still remains unclear. Future prospects should focus on determining whether the conformational changes in PBT caused by the pre-conditioning would be responsible for the decrease of the fire performances of the material. To this purpose, several experiments can be suggested among which a comparison of the expansion coefficients and the thermal diffusivity of the conditioned materials. Would the modification of the conformational structures in PBT induce a change of such parameters, resulting in a decrease of UL94 performances (i.e. increase of burning drops due to a change in the dilatation properties of the material or an increase of the thermal diffusivity of the material)? Otherwise, does the crystal structure of PBT influence the fire properties of the material? To investigate this issue, it should have been interesting to perform UL94 tests on samples exhibiting different crystallinity rates. The

latter could be obtained by specific quenching treatments. Finally, the solid state NMR analyses of burned residues could also be interesting to investigate potential modifications of the degradation mechanisms in the condensed phase.

Finally, the good FR performances of some of the synthesized phosphinates salts (especially **C8** and **C9**) provided us interesting insights and outlooks. Concerning **C8** and **C9**, further combinations with traditional fireproofing agents - for instance MDH, boehmite (AlOOH), melamine cyanurate, MPP…- should be investigate to go further in our research of high performing flame retarded PBT/GF materials. Evaluation of the FR performances of the synthesized salts in other polymeric matrix could also be an attractive perspective. Preliminary investigations of the FR performances of salts in a glass fiber (25 wt%) reinforced polyamide 6.6 (PA 6.6/GF) have already given promising results through the UL94 test. These results are summarized in Table 31.

Table 31 : UL94 results obtained for the synthesized phosphinate salts containing PA 6.6/GF formulations (results provided by BASF)

Aluminum salt (FR)	Composition (wt%)			UL94, 1.6 mm bar		
	PBT	GF	FR	Conditioning	t1+t2[a] (s)	Rating
-	75	25	-	2d.25°C	-	NC
C8	60	25	15	2d.25°C	22	V-2
C9	60	25	15	2d.25°C	-	NC
C12	60	25	15	2d.25°C	-	NC
C13	60	25	15	2d.25°C	12	V-1
C14-2	60	25	15	2d.25°C	-	NC

[a] *t1 and t2, average combustion times after the first and the second application of the flame*

It is observed that 15 wt% of the ethylene diamine based phosphinate aluminum salt (**C13**) in PA 6.6/GF provides a V-1 rating. It must be emphasized that the combination of 15 wt% **C13** with 5 wt% melamine polyphosphate (Melapur 200) allowed achieving the required V-0 rating. Besides, a promising V-2 rating is achieved with 15 wt% of the benzyl amine based phosphinate aluminum **C8** while no classification could be reached with the same amount of other salts in the polyamide.

REFERENCES

(1) Matières plastiques: faits et chiffres 2007, analyse de la production, de la consommation et de la valorisation des matières plastiques en Europe pour l'année 2007. PlasticsEurope, **2008**.

(2) Production mondiale de plastique. From http://www.planetoscope.com/petrole/989-production-mondiale-de-plastique.html.

(3) Karter, M. J.: "NFPA's Fire Loss in the United States During 2010", NFPA, **2011**.

(4) Hall, J. R.: "NFPA's The Total Cost of Fire in the United States During 2009", NFPA, **2012**.

(5) Alkhater, M. A.: Polybutylene terephthalate (PBT) project, **2006**.

(6) Handbook of thermoplastic polyesters. Fakirov, S., Ed.; **2002**; Vol. 1&2.

(7) Heitz, T.; Klatt, M.; Neuhaus, R.: US 6812321 B1, BASF Aktiengesellschaft, **2004**.

(8) Endert, E. S. V.; Hagen, R.; Hille, T.; Atlas, C.; Ulrich, T.: US patent 7115701 B2, Inventa-Fischer GMBH & Co KG, **2003**.

(9) Hoeschele, G. K.; McGirk, R. H.: EP patent 0472179 A2, E. I. Du pont de Nemours and Company, **1992**.

(10) Schmidt, W.; Thiele, U.; Griebler, W.-D.; Hirthe, B.; Hirschberg, E.: US patent 5656716, Zimmer Aktiengesellschaft, **1996**.

(11) Seidel, E.; Wilhelm, F.: US Patent 6967235, Zimmer Aktiengesellschaft, **2005**.

(12) Quentin, J. P.: Polycondensation des polyesters saturés. In *Techniques de l'ingénieur*, **2004**.

(13) PBT polybutylene Terephthalate Process. Lurgi Zimmer GmbH.

(14) Heinze, H.; Wilhelm, F.: US patent 4680376, Davy McKee A.G, **1987**.

(15) Heinze, H.; Wilhelm, F.; Mackensen, K.; Finkeldei, F.: US patent 4499261, Davy McKee AG, **1985**.

(16) Takahashi, Y.; Murakami, K.; Nishikawa, S.: Mechanism for the phase transition of poly(butylene terephthalate). *Journal of Polymer Science Part B: Polymer Physics* **2002**, *40*, 765-771.

(17) Konishi, T.; Miyamoto, Y.: Crystallization of Poly(butylene terephthalate) from the Glass. *Macromolecules* **2009**, *43*, 375-383.

(18) Gomez, M. A.; Cozine, M. H.; Tonelli, A. E.: High-resolution solid-state carbon-13 NMR study of the α and β crystalline forms of poly(butylene terephthalate). *Macromolecules* **1988**, *21*, 388.

(19) Perry, B. C.; Koenig, J. L.; Lando, J. B.: Relaxation behavior of the *p* phase of poly(butylene terephthalate). *Macromolecules* **1987**, *20*, 422.

(20) Tashiro, K.; Nakai, Y.; Kobayashi, M.; Tadokoro, H.: Solid-state transition of poly(butylene terephthalate) induced by mechanical deformation. *Macromolecules* **1980**, *13*, 137-45.

(21) Ludwig, H. J.; Eyerer, P.: Influence of the processing conditions on morphology and deformation behavior of poly(butylene terephthalate) (PBT). *Polymer Engineering & Science* **1988**, *28*, 143-146.

(22) Stein, R. S.; Misra, A.: Morphological studies on polybutylene terephthalate. *Journal of Polymer Science: Polymer Physics Edition* **1980**, *18*, 327-342.

(23) Pi Chang, E.; Kirsten, R. O.; Slagowski, E. L.: The effect of additives on the crystallization of poly (butylene terephthalate). *Polymer Engineering & Science* **1978**, *18*, 932-936.

(24) Cheng, S. Z. D.; Pan, R.; Wunderlich, B.: Thermal analysis of poly(butylene terephthalate) for heat capacity, rigid-amorphous content, and transition behavior. *Die Makromolekulare Chemie* **1988**, *189*, 2443-2458.

(25) Yeh, J. T.; Runt, J.: Multiple melting in annealed poly(butlene terephthalate). *Journal of Polymer Science Part B: Polymer Physics* **1989**, *27*, 1543-1550.

(26) Righetti, M. C.; Di Lorenzo, M. L.: Melting process of poly(butylene terephthalate) analyzed by temperature-modulated differential scanning calorimetry. *Journal of Polymer Science Part B: Polymer Physics* **2004**, *42*, 2191-2201.

(27) Pillin, I.; Pimbert, S.; Feller, J.-F.; Levesque, G.: Crystallization kinetics of poly(butylene terephthalate) (PBT): Influence of additives and free carboxylic acid chain ends. *Polymer Engineering & Science* **2001**, *41*, 178-191.

(28) Hobbs, S. Y.; Pratt, C. F.: Multiple melting in poly(butylene terephthalate). *Polymer* **1975**, *16*, 462-464.

(29) Kim, H. G.; Robertson, R. E.: Multiple melting endotherms in isothermally melt-crystallized poly(butylene terephthalate). *Journal of Polymer Science Part B: Polymer Physics* **1998**, *36*, 1757-1767.

(30) Nichols, M. E.; Robertson, R. E.: The origin of multiple melting endotherms in the thermal analysis of polymers. *Journal of Polymer Science Part B: Polymer Physics* **1992**, *30*, 305-307.

(31) Desbonnet, J.; Apchin, G.: Polyesters thermoplastiques PET et PBT pour injection. In *Techniques de l'ingénieur*, **2001**.

(32) Mohd Ishak, Z. A.; Ariffin, A.; Senawi, R.: Effects of hygrothermal aging and a silane coupling agent on the tensile properties of injection molded short glass fiber reinforced poly(butylene terephthalate) composites. *European Polymer Journal* **2001**, *37*, 1635-1647.

(33) Ishikawa, T.; Ueno, T.; Watanabe, Y.; Mizuno, K.; Takeda, K.: Flame retardancy of polybutylene terephthalate blended with various oxides. *Journal of Applied Polymer Science* **2008**, *109*, 910-917.

(34) Sato, H.; Kondo, K.; Tsuge, S.; Ohtani, H.; Sato, N.: Mechanisms of thermal degradation of a polyester flame-retarded with antimony oxide/brominated polycarbonate studied by temperature-programmed analytical pyrolysis. *Polymer Degradation and Stability* **1998**, *62*, 41-48.

(35) Ohtani, H.; Kimura, T.; Tsuge, S.: Analysis of thermal degradation of terephthalate polyesters by high-resolution pyrolysis-gas chromatography *Analytical Sciences* **1986**, *2*, 179-182.

(36) McNeill, I. C.; Bounekhel, M.: Thermal degradation studies of terephthalate polyesters: 1. Poly(alkylene terephthalates). *Polymer Degradation and Stability* **1991**, *34*, 187-204.

(37) Bounekhel, M.; McNeill, I. C.: Thermal degradation studies of terephthalate polyesters: 2. Poly(ether-esters). *Polymer Degradation and Stability* **1995**, *49*, 347-352.

(38) Balabanovich, A. I.; Engelmann, J.: Fire retardant and charring effect of poly(sulfonyldiphenylene phenylphosphonate) in poly(butylene terephthalate). *Polymer Degradation and Stability* **2003**, *79*, 85-92.

(39) Braun, U.; Schartel, B.: Flame Retardancy Mechanisms of Aluminium Phosphinate in Combination with Melamine Cyanurate in Glass-Fibre-Reinforced Poly(1,4-butylene terephthalate). *Macromolecular Materials and Engineering* **2008**, *293*, 206-217.

(40) Balabanovich, A. I.; Balabanovich, A. M.; Engelmann, J.: Intumescence in poly(butylene terephthalate): the effect of 2-methyl-1,2-oxaphospholan-5-one 2-oxide and ammonium polyphosphate. *Polymer International* **2003**, *52*, 1309-1314.

(41) Casu, A.; Camino, G.; De Giorgi, M.; Flath, D.; Laudi, A.; Morone, V.: Effect of glass fibres and fire retardant on the combustion behaviour of composites, glass fibres–poly(butylene terephthalate). *Fire and Materials* **1998**, *22*, 7-14.

(42) Hine, P. J.; Duckett, R. A.: Fiber orientation structures and mechanical properties of injection molded short glass fiber reinforced ribbed plates. *Polymer Composites* **2004**, *25*, 237-254.

(43) Joshi, M.; Maiti, S. N.; Misra, A.; Mittal, R. K.: Influence of fiber length, fiber orientation, and interfacial adhesion on poly (butylene terephthalate)/polyethylene alloys reinforced with short glass fibers. *Polymer Composites* **1994**, *15*, 349-358.

(44) Fung, C. P.: Fibre orientation of fibre-reinforced PBT composites in injection moulding. *Plastics, Rubber and Composites* **2004**, *33*, 170-176.

(45) Bergeret, A.; Bozec, M. P.; Quantin, J. C.; Crespy, A.; Gasca, J. P.; Arpin, M.: Study of interphase in glass fiber–reinforced poly(butylene terephthalate) composites. *Polymer Composites* **2004**, *25*, 12-25.

(46) Bergeret, A.; Krawczak, P.: Liaison renfort/matrice: définition et caractérisation. In *Techniques de l'ingénieur*, **2006**.

(47) Zhou, H.; Han, K.; Yu, M.: Preparation of Long Glass Fiber Reinforced Poly(butylene terephthalate) Composites with Chemical Bonding Interphase. *Journal of Macromolecular Science, Part A* **2006**, *43*, 1835-1851.

(48) Linak, E.; Yoneyama, M.: Thermoplastic polyester engineering resind. *Chemical Economics Handbook* **2009**, p. 580.1160 A.

(49) Weber, M.: Polymer blends: materials with versatile properties. *Macromolecular Symposia* **2001**, *163*, 235-250.

(50) Ambrósio, J. D.; Larocca, N. M.; Pessan, L. A.; Hage, E.: Influence of the process parameters of an intermeshing co-rotating twin screw extruder on the morphology and notched Izod impact strength of PBT/ABS/MGE blends. *Polymer Engineering & Science* **2010**, *50*, 2382-2391.

(51) Aravinthan, G.; Kale, D. D.: Blends of poly(ethylene terephthalate) and poly(butylene terephthalate). *Journal of Applied Polymer Science* **2005**, *98*, 75-82.

(52) Polybutylene terephthalate (PBT). Global Industry Analysts, Inc., **2011**.

(53) Brehme, S.; Schartel, B.; Goebbels, J.; Fischer, O.; Pospiech, D.; Bykov, Y.; Döring, M.: Phosphorus polyester versus aluminium phosphinate in poly(butylene terephthalate) (PBT): Flame retardancy performance and mechanisms. *Polymer Degradation and Stability* **2011**, *96*, 875-884.

(54) Laoutid, F.; Bonnaud, L.; Alexandre, M.; Lopez-Cuesta, J. M.; Dubois, P.: New prospects in flame retardant polymer materials: From fundamentals to nanocomposites. *Materials Science and Engineering: R: Reports* **2009**, *63*, 100-125.

(55) Papa, A. J.: Reactive Flame Retardants for Polyurethane Foams. *Product R&D* **1970**, *9*, 478-496.

(56) Levchik, S. V.; Weil, E. D.: Flame retardancy of thermoplastic polyesters—a review of the recent literature. *Polymer International* **2005**, *54*, 11-35.

(57) Cusack, P. A.; Heer, M. S.; Monk, A. W.: Zinc hydroxystannate as an alternative synergist to antimony trioxide in polyester resins containing halogenated flame retardants. *Polymer Degradation and Stability* **1997**, *58*, 229-237.

(58) Klein, J.; Dorge, S.; Trouvé, G.; Venditti, D.; Durécu, S.: Behaviour of antimony during thermal treatment of Sb-rich halogenated waste. *Journal of Hazardous Materials* **2009**, *166*, 585-593.

(59) Alaee, M.; Arias, P.; Sjödin, A.; Bergman, Å.: An overview of commercially used brominated flame retardants, their applications, their use patterns in different countries/regions and possible modes of release. *Environment International* **2003**, *29*, 683-689.

(60) Santillo, D.; Johnston, P.: Playing with fire: the global threat presented by brominated flame retardants justifies urgent substitution. *Environment International* **2003**, *29*, 725-734.

(61) Weber, R.; Kuch, B.: Relevance of BFRs and thermal conditions on the formation pathways of brominated and brominated–chlorinated dibenzodioxins and dibenzofurans. *Environment International* **2003**, *29*, 699-710.

(62) Innovative flame retardants in E&E applications. pinfa, **2009**.

(63) New ATH developments drive flame retardant cable compounding. *Plastics, Additives and Compounding* **2002**, *4*, 22-29.

(64) Zhang, S.; Horrocks, A. R.: A review of flame retardant polypropylene fibres. *Progress in Polymer Science* **2003**, *28*, 1517-1538.

(65) Haurie, L.; Fernández, A. I.; Velasco, J. I.; Chimenos, J. M.; Lopez Cuesta, J.-M.; Espiell, F.: Synthetic hydromagnesite as flame retardant. Evaluation of the flame behaviour in a polyethylene matrix. *Polymer Degradation and Stability* **2006**, *91*, 989-994.

(66) Hollingbery, L. A.; Hull, T. R.: The fire retardant behaviour of huntite and hydromagnesite – A review. *Polymer Degradation and Stability* **2010**, *95*, 2213-2225.

(67) Posner, S. "Survey and technical assessment of alternatives to TBBPA and HBCDD," Kemikalieinspektionen, **2006**.

(68) Tollbäck, J.; Crescenzi, C.; Dyremark, E.: Determination of the flame retardant tetrabromobisphenol A in air samples by liquid chromatography-mass spectrometry. *Journal of Chromatography A* **2006**, *1104*, 106-112.

(69) Kemmlein, S.; Herzke, D.; Law, R. J.: Brominated flame retardants in the European chemicals policy of REACH—Regulation and determination in materials. *Journal of Chromatography A* **2009**, *1216*, 320-333.

(70) De Schryver, D.; Landry, S. D.; Reed, J. S.: Latest developments on the flame retardancy of engineering thermoplastics – SAYTEX® HP-7010 (brominated polystyrene) in glass filled engineering thermoplastics. *Polymer Degradation and Stability* **1999**, *64*, 471-477.

(71) A.I, B.: The effect of melamine on the combustion and thermal decomposition behaviour of poly(butylene terephthalate). *Polymer Degradation and Stability* **2004**, *84*, 451-458.

(72) Yang, W.; Lu, H.; Tai, Q.; Qiao, Z.; Hu, Y.; Song, L.; Yuen, R. K. K.: Flame retardancy mechanisms of poly(1,4-butylene terephthalate) containing microencapsulated ammonium polyphosphate and melamine cyanurate. *Polymers for Advanced Technologies* **2011**, *22*, 2136-2144.

(73) Yanagimoto, A.; Kumazawa, I.; Takakuwa, F.: US Patent 4180496, Nissan Chemical Industries Ltd., **1979**.

(74) Penn, R. E.: US patent 5814690, E.I. du Pont de Nemours and Company, **1997**.

(75) Paul, C.: Novel coated fillers enhance flame-retardant properties. *Plastics, Additives and Compounding*, *9*, 26-29.

(76) In *Compounding world - december **2011***.

(77) Nass, B.; Wanzke, W.: US patent 6207736 B1, Clariant GmbH, **2001**.

(78) Jenewein, E.; Kleiner, H. J.; Wanzke, W.; Budzinsky, W.: US patent 6365071 B1, Clariant GmbH, **2002**.

(79) Schlosser, E.; Nass, B.; Wanzke, W.: US patent 6547992, Clariant GnbH, **2003**.

(80) Braun, U.; Bahr, H.; Sturm, H.; Schartel, B.: Flame retardancy mechanisms of metal phosphinates and metal phosphinates in combination with melamine cyanurate in glass fiber reinforced poly(1,4-butylene terephthalate): the influence of metal cation. *Polymer for Advancesand Technology* **2008**, *19*, 680-692.

(81) Schlosser, E.; Nass, B.; Wanzke, W.: US Patent 6255371, Clariant GmbH, **2001**.

(82) Yang, W.; Hu, Y.; Tai, Q.; Lu, H.; Song, L.; Yuen, R. K. K.: Fire and mechanical performance of nanoclay reinforced glass-fiber/PBT composites containing aluminum hypophosphite particles. *Composites Part A: Applied Science and Manufacturing* **2011**, *42*, 794-800.

(83) Yang, W.; Yuen, R. K. K.; Hu, Y.; Lu, H.; Song, L.: Development and Characterization of Fire Retarded Glass-Fiber Reinforced Poly(1,4-butylene terephthalate) Composites Based on a Novel Flame Retardant System. *Industrial & Engineering Chemistry Research* **2011**, *50*, 11975-11981.

(84) Richardson, J.; Dellar, R. J.: US patent 4972011 Ciba-Geigy corporation, **1990**.

(85) Kleiner, H. J.; Budzinsky, W.: US patent 6270560 B1, Ticona GmdH, **2001**.

(86) Dufton, P.: "Flame retardant for plastics", Smithers Rapra Technology Ltd, **2003**.

(87) Balabanovich, A. I.; Levchik, G. F.; Levchiky, S. V.; Engelmann, J.: Fire Retardant Synergism Between Cyclic Diphosphonate Ester and Melamine in Poly(Butylene Terephthalate). *Journal of Fire Sciences* **2002**, *20*, 71-83.

(88) Klatt, M.; Heitz, T.; Gareiss, B.: US patent 6306941 B1, BASF aktiengesellschaft, **2002**.

(89) Hastie, J. W.; McBee, C. L. "Mechanistic studies of TriPhenylPhosphine Oxide-Poly(Ethylne Terephthalate) and related flame retardant systems," Institute for material research - National bureau of standards, **1975**.

(90) Gareiss, B.; Deckers, A.; Klatt, M.; Weber, W.: US patent 6469095 B1, BASF Aktiengesellschaft, **2002**.

(91) Klatt, M.; Gareiss, B.; Yamamoto, M.: US patent 6103797, BASF Aktiengesellschaft, **2000**.

(92) Aufmuth, W.; Levchik, S. V.; Levchik, G. F.; Klatt, M.: Poly(butylene terephthalate) fire retarded by 1,4-diisobutylene-2,3,5,6-tetraxydroxy-1, 4-diphosphine oxide. I. Combustion and thermal decomposition. *Fire and Materials* **1999**, *23*, 1-6.

(93) A.I, B.: Poly(butylene terephthalate) fire retarded by bisphenol A bis(diphenyl phosphate). *Journal of Analytical and Applied Pyrolysis* **2004**, *72*, 229-233.

(94) Levchik, S. V.; Bright, D. A.; Alessio, G. R.; Dashevsky, S.: Synergistic action between aryl phosphates and phenolic resin in PBT. *Polymer Degradation and Stability* **2002**, *77*, 267-272.

(95) Klatt, M.; Gareiss, B.; Yamamoto, M.; Fisch, H.; Nam, M.; Heitz, T.; Leutner, B.: US patent 6538054 B1, BASF Aktiengesellschaft, **2003**.

(96) Levchik, G. F.; Grigoriev, Y. V.; Balabanovich, A. I.; Levchik, S. V.; Klatt, M.: Phosphorus–nitrogen containing fire retardants for poly(butylene terephthalate). *Polymer International* **2000**, *49*, 1095-1100.

(97) Levchik, S. V.; Levchik, G. F.; Balabanovich, A. I.; Weil, E. D.; Klatt, M.: Phosphorus oxynitride: a thermally stable fire retardant additive for polyamide 6 and poly(butylene terephthalate). *Die Angewandte Makromolekulare Chemie* **1999**, *264*, 48-55.

(98) Pecht, M.; Deng, Y.: Electronic device encapsulation using red phosphorus flame retardants. *Microelectronics Reliability* **2006**, *46*, 53-62.

(99) Salocks, C.; Kaley, K. B.: "Red Phosphorus". Office of Environmental Health Hazard Assessment.

(100) Anand, S. S.; Mehendale, H. M.: Red Phosphorus. In *Encyclopedia of Toxicology (Second Edition)*; Philip, W., Ed.; Elsevier: New York, **2005**; pp 624-626.

(101) Suzuki, M.; Saiki, N.: US patent 6133358, Teijin Ltd., **2000**.

(102) Weil, E. D.; Levchik, S. V.: *Flame retardants for plastics and textiles - Practical applications*. Hanser, **2009**.

(103) Laoutid, F.; Ferry, L.; Lopez-Cuesta, J. M.; Crespy, A.: Red phosphorus/aluminium oxide compositions as flame retardants in recycled poly(ethylene terephthalate). *Polymer Degradation and Stability* **2003**, *82*, 357-363.

(104) Kleiner, H.-J.; Finke, M.; Bollert, U.; Herwig, W.: US patent 3941752, Hoechst Aktiengesellschaft, **1976**.

(105) Bollert, U.; Lohmar, E.; Ohorodnik, A.: US patent 4033936, Hoechst Aktiengesellschaft, **1977**.

(106) Chajrullin, V. K.; Sobcuk, I. I.; Pudovik, A. N.: *Zurnal Obscej Chimii* **1967**, *37*, 710-714.

(107) Balabanovich, A. I.: Thermal decomposition study of 2-methyl-1,2-oxaphospholan-5-one 2-oxide. *Thermochimica Acta* **2004**, *409*, 33-39.

(108) Weissermel, K.; Kleiner, H.-J.; Finke, M.; Felcht, U.-H.: Advances in Organophosphorus chemistry based on dichloro(methyl)phosphane. *Angewandte Chemie International Edition,* **1981**, *20*, 223-233.

(109) Noetzel, s.; Herwig, W.; Kern, R.; Lotz, W.: US patent 3980614, Hoechst Aktiengesellschaft, **1976**.

(110) Noetzel, S.: US patent 3980615, Hoechst Aktiengesellschaft, **1976**.

(111) Blöcker, E.: US patent 5281637, Hoechst AG, **1994**.

(112) Bauer, H.; Hoerold, S.; Krause, W.: US patent 2008/0188598 A1, Clariant corporation, **2008**.

(113) Sinha Ray, S.; Okamoto, M.: Polymer/layered silicate nanocomposites: a review from preparation to processing. *Progress in Polymer Science* **2003**, *28*, 1539-1641.

(114) Lewin, M.: Some comments on the modes of action of nanocomposites in the flame retardancy of polymers. *Fire and Materials* **2003**, *27*, 1-7.

(115) Lewin, M.: Reflections on migration of clay and structural changes in nanocomposites. *Polymers for Advanced Technologies* **2006**, *17*, 758-763.

(116) Jeffrey W, G.: Flammability and thermal stability studies of polymer layered-silicate (clay) nanocomposites. *Applied Clay Science* **1999**, *15*, 31-49.

(117) Kiliaris, P.; Papaspyrides, C. D.: Polymer/layered silicate (clay) nanocomposites: An overview of flame retardancy. *Progress in Polymer Science* **2010**, *35*, 902-958.

(118) Hwang, S.-s.; Liu, S.-p.; Hsu, P. P.; Yeh, J.-m.; Chang, K.-c.; Lai, Y.-z.: Effect of organoclay on the mechanical/thermal properties of microcellular injection molded PBT–clay nanocomposites. *International Communications in Heat and Mass Transfer* **2010**, *37*, 1036-1043.

(119) Xiao, J.; Hu, Y.; Kong, Q.; Song, L.; Wang, Z.; Chen, Z.; Fan, W.: Poly(butylene terephthalate)/Clay Nanocomposites directly Prepared from Pristine Montmorillonite (MMT). *Polymer Bulletin* **2005**, *54*, 271-278.

(120) Samyn, F.; Bourbigot, S.; Jama, C.; Bellayer, S.; Nazare, S.; Hull, R.; Fina, A.; Castrovinci, A.; Camino, G.: Characterisation of the dispersion in polymer flame retarded nanocomposites. *European Polymer Journal* **2008**, *44*, 1631-1641.

(121) Schartel, B.; Pötschke, P.; Knoll, U.; Abdel-Goad, M.: Fire behaviour of polyamide 6/multiwall carbon nanotube nanocomposites. *European Polymer Journal* **2005**, *41*, 1061-1070.

(122) Hapuarachchi, T. D.; Peijs, T.: Multiwalled carbon nanotubes and sepiolite nanoclays as flame retardants for polylactide and its natural fibre reinforced composites. *Composites Part A: Applied Science and Manufacturing* **2010**, *41*, 954-963.

(123) Costache, M. C.; Heidecker, M. J.; Manias, E.; Camino, G.; Frache, A.; Beyer, G.; Gupta, R. K.; Wilkie, C. A.: The influence of carbon nanotubes, organically modified montmorillonites and layered double hydroxides on the thermal degradation and fire retardancy of polyethylene, ethylene–vinyl acetate copolymer and polystyrene. *Polymer* **2007**, *48*, 6532-6545.

(124) Modesti, M.; Lorenzetti, A.; Simioni, F.; Camino, G.: Expandable graphite as an intumescent flame retardant in polyisocyanurate–polyurethane foams. *Polymer Degradation and Stability* **2002**, *77*, 195-202.

(125) Wu, X.; Wang, L.; Wu, C.; Yu, J.; Xie, L.; Wang, G.; Jiang, P.: Influence of char residues on flammability of EVA/EG, EVA/NG and EVA/GO composites. *Polymer Degradation and Stability* **2012**, *97*, 54-63.

(126) Fina, A.; Abbenhuis, H. C. L.; Tabuani, D.; Camino, G.: Metal functionalized POSS as fire retardants in polypropylene. *Polymer Degradation and Stability* **2006**, *91*, 2275-2281.

(127) Gallo, E.; Braun, U.; Schartel, B.; Russo, P.; Acierno, D.: Halogen-free flame retarded poly(butylene terephthalate) (PBT) using metal oxides/PBT nanocomposites in combination with aluminium phosphinate. *Polymer Degradation and Stability* **2009**, *94*, 1245-1253.

(128) Gallo, E.; Schartel, B.; Braun, U.; Russo, P.; Acierno, D.: Fire retardant synergisms between nanometric Fe2O3 and aluminum phosphinate in poly(butylene terephthalate). *Polymers for Advanced Technologies* **2011**, *22*, 2382-2391.

(129) Vannier, A.; Duquesne, S.; Bourbigot, S.; Castrovinci, A.; Camino, G.; Delobel, R.: The use of POSS as synergist in intumescent recycled poly(ethylene terephthalate). *Polymer Degradation and Stability* **2008**, *93*, 818-826.

(130) Product information: Ultradur B 4520, PBT (PolyButylene Terephthalate). BASF.

(131) UnderwritersLaboratories UL94 standard for safety - test for flammibility of plastic materials for parts in devices and appliances, 1998.

(132) ISO 4589 Plastics - Determination of burning behavior by oxygen index, **1996**.

(133) ASTM E2102 - Standard test method for measurement of mass loss and ignitability for screening purposes using a conical radiant heater, **2009**.

(134) Ernst, R. R.; Bodenhausen G.; Wokaun, A.: *Principles of nuclear magnetic resonance in one and two dimensions*; Oxford Science Publications, **1987**.

(135) Gopalakrishnan, K.; Bodenhausen, G.: Cross polarization from spins I = 1/2 to spins S = 1 in nuclear magnetic resonance with magic angle sample spinning. *Journal of Chemical Physics* **2006**, *124*.

(136) Macomber, R. S.: *A complete introduction to modern NMR spectroscopy*; John Wiley & Sons, Ltd., **1998**.

(137) Hu, B.; Trébosc, J.; Amoureux, J. P.: Comparison of several hetero-nuclear dipolar recoupling NMR methods to be used in MAS HMQC/HSQC. *Journal of Magnetic Resonance* **2008**, *192*, 112-122.

(138) Fu, R.; Smith, S. A.; Bodenhausen, G.: Recoupling of heteronuclear dipolar interactions in solid state magic-angle spinning NMR by simultaneous frequency and amplitude modulation. *Chemical Physics Letters* **1997**, *272*, 361-369.

(139) Trebosc, J.; Amoureux, J.-P.; Gan, Z.: Comparison of high-resolution solid-state NMR MQMAS and STMAS methods for half-integer quadrupolar nuclei. *Solid State Nuclear Magnetic Resonance* **2007**, *31*, 1-9.

(140) Lee, S. K.; Stebbins, J. F.: The distribution of sodium ions in aluminosilicate glasses: a high-field Na-23 MAS and 3Q MAS NMR study. *Geochimica et Cosmochimica Acta* **2003**, *67*, 1699-1709.

(141) Braun, U.; Bahr, H.; Sturm, H.; Schartel, B.: Flame retardancy mechanisms of metal phosphinates and metal phosphinates in combination with melamine cyanurate in glass-fiber reinforced poly(1,4-butylene terephthalate): the influence of metal cation. *Polymers for Advanced Technologies* **2008**, *19*, 680-692.

(142) Koshiduka, T.; Ohkawa, T.; Takeda, K.: Computer simulation of thermal degradation of poly(butylene terephthalate) and analytical problems of terephthalic acid in scission products. *Polymer Degradation and Stability* **2003**, *79*, 1-11.

(143) Fujiwara, T.; Khandelwal, P.; Akutsu, H.: Compound Radiofrequency-Driven Recoupling Pulse Sequences for Efficient Magnetization Transfer by Homonuclear Dipolar Interaction under Magic-Angle Spinning Conditions. *Journal of Magnetic Resonance* **2000**, *145*, 73-83.

(144) Isitman, N. A.; Gunduz, H. O.; Kaynak, C.: Nanoclay synergy in flame retarded/glass fibre reinforced polyamide 6. *Polymer Degradation and Stability* **2009**, *94*, 2241-2250.

(145) Isitman, N. A.; Kaynak, C.: Nanoclay and carbon nanotubes as potential synergists of an organophosphorus flame-retardant in poly(methyl methacrylate). *Polymer Degradation and Stability* **2010**, *95*, 1523-1532.

(146) Feng, J.; Hao, J.; Du, J.; Yang, R.: Flame retardancy and thermal properties of solid bisphenol A bis(diphenyl phosphate) combined with montmorillonite in polycarbonate. *Polymer Degradation and Stability* **2010**, *95*, 2041-2048.

(147) Yang, W.; Kan, Y.; Song, L.; Hu, Y.; Lu, H.; Yuen, R. K. K.: Effect of organo-modified montmorillonite on flame retardant poly(1,4-butylene terephthalate) composites. *Polymers for Advanced Technologies* **2011**, *22*, 2564-2570.

(148) Laoutid, F.; Gaudon, P.; Taulemesse, J. M.; Lopez Cuesta, J. M.; Velasco, J. I.; Piechaczyk, A.: Study of hydromagnesite and magnesium hydroxide based fire retardant systems for ethylene–vinyl acetate containing organo-modified montmorillonite. *Polymer Degradation and Stability* **2006**, *91*, 3074-3082.

(149) Si, M.; Zaitsev, V.; Goldman, M.; Frenkel, A.; Peiffer, D. G.; Weil, E.; Sokolov, J. C.; Rafailovich, M. H.: Self-extinguishing polymer/organoclay nanocomposites. *Polymer Degradation and Stability* **2007**, *92*, 86-93.

(150) Song, L.; Hu, Y.; Lin, Z.; Xuan, S.; Wang, S.; Chen, Z.; Fan, W.: Preparation and properties of halogen-free flame-retarded polyamide 6/organoclay nanocomposite. *Polymer Degradation and Stability* **2004**, *86*, 535-540.

(151) Chang, Z.-H.; Guo, F.; Chen, J.-F.; Yu, J.-H.; Wang, G.-Q.: Synergistic flame retardant effects of nano-kaolin and nano-HAO on LDPE/EPDM composites. *Polymer Degradation and Stability* **2007**, *92*, 1204-1212.

(152) Zhang, B.; Li, Y.; Pan, X.; Jia, X.; Wang, X.: Intercalation of acrylic acid and sodium acrylate into kaolinite and their in situ polymerization. *Journal of Physics and Chemistry of Solids* **2007**, *68*, 135-142.

(153) Frost, R. L.; Locos, O. B.; Kristof, J.; Kloprogge, J. T.: Infrared spectroscopic study of potassium and cesium acetate-intercalated kaolinites. *Vibrational Spectroscopy* **2001**, *26*, 33-42.

(154) Sun, D.; Li, Y.; Zhang, B.; Pan, X.: Preparation and characterization of novel nanocomposites based on polyacrylonitrile/kaolinite. *Composites Science and Technology* **2010**, *70*, 981-988.

(155) Abecassis, D.; Wright, B.; Wiegel, E.; Glen Burnie Technologies, **2008**.

(156) Duquesne, S.; Le Bras, M.; Bourbigot, S.; Delobel, R.; Camino, G.; Eling, B.; Lindsay, C.; Roels, T.: Thermal degradation of polyurethane and polyurethane/expandable graphite coatings. *Polymer Degradation and Stability* **2001**, *74*, 493-499.

(157) Expandable graphite used as fire barrier in plastics. *Plastics, Additives and Compounding* **2000**, *2*, 12.

(158) Afanasov, I. M.; Shornikova, O. N.; Kirilenko, D. A.; Vlasov, I. I.; Zhang, L.; Verbeeck, J.; Avdeev, V. V.; Van Tendeloo, G.: Graphite structural transformations during intercalation by HNO3 and exfoliation. *Carbon* **2010**, *48*, 1862-1865.

(159) Uhl, F. M.; Yao, Q.; Nakajima, H.; Manias, E.; Wilkie, C. A.: Expandable graphite/polyamide-6 nanocomposites. *Polymer Degradation and Stability* **2005**, *89*, 70-84.

(160) Choi, S. Y.; Mamak, M.; Cordola, E.; Stadler, U.: Large scale production of high aspect ratio graphite nanoplatelets with tunable oxygen functionality. *Journal of Materials Chemistry* **2011**, *21*.

(161) Fukushima, K.; Murariu, M.; Camino, G.; Dubois, P.: Effect of expanded graphite/layered-silicate clay on thermal, mechanical and fire retardant properties of poly(lactic acid). *Polymer Degradation and Stability* **2010**, *95*, 1063-1076.

(162) UL-94 - Test for flammability of plastic materials for parts in devices an appliances Underwriters Laboratory Inc.

(163) Cheng, H.; Liu, Q.; Yang, J.; Zhang, Q.; Frost, R. L.: Thermal behavior and decomposition of kaolinite–potassium acetate intercalation composite. *Thermochimica Acta* **2010**, *503–504*, 16-20.

(164) Zhu, H.; Zhu, Q.; Li, J.; Tao, K.; Xue, L.; Yan, Q.: Synergistic effect between expandable graphite and ammonium polyphosphate on flame retarded polylactide. *Polymer Degradation and Stability* **2011**, *96*, 183-189.

(165) Wang, G.; Yang, J.: Influences of expandable graphite modified by polyethylene glycol on fire protection of waterborne intumescent fire resistive coating. *Surface and Coatings Technology* **2010**, *204*, 3599-3605.

(166) Köppl, T.; Brehme, S.; Wolff-Fabris, F.; Altstädt, V.; Schartel, B.; Döring, M.: Structure−property relationships of halogen-free flame-retarded poly(butylene terephthalate) and glass fiber reinforced PBT. *Journal of Applied Polymer Science* **2012**, *124*, 9-18.

(167) Samyn, F.: Compréhension des procédés d'ignifugation du polyamide 6: apport des nanocomposites aux systèmes retardateurs de flamme phosphorés. Université des sciences et technologies de Lille, **2007**.

(168) Wagener, R.; Budzinsky, W.; Hückstädt, H.: DE patent 10317487 A1, Ticona GmbH, **2004**.

(169) Svara, J.: US patent 5214178, Hoechst Aktiengesellshaft, **1993**.

(170) Peyman, A.; Budt, K.-H.; Spanig, J.; Li, J.-Q.; Stowasser, B.: US patent 5510504, Hoechst Aktiengesellshaft, **1996**.

(171) Maas, W.; Krause, W.; Bauer, H.: EP patent 1832596, Clariant, **2007**.

(172) Balabanovich, A. I.: Thermal decomposition study of intumescent additives: Pentaerythritol phosphate and its blend with melamine phosphate. *Thermochimica Acta* **2005**, 425, 188-196.

(173) Fontaine, G.; Bourbigot, S.; Duquesne, S.: Neutralized flame retardant phosphorus agent: Facile synthesis, reaction to fire in PP and synergy with zinc borate. *Polymer Degradation and Stability* **2008**, *93*, 68-76.

(174) Zhou, S.; Song, L.; Wang, Z.; Hu, Y.; Xing, W.: Flame retardation and char formation mechanism of intumescent flame retarded polypropylene composites containing melamine phosphate and pentaerythritol phosphate. *Polymer Degradation and Stability* **2008**, *93*, 1799-1806.

(175) Gao, F.; Tong, L.; Fang, Z.: Effect of a novel phosphorous–nitrogen containing intumescent flame retardant on the fire retardancy and the thermal behaviour of poly(butylene terephthalate). *Polymer Degradation and Stability* **2006**, *91*, 1295-1299.

(176) Gaw, K. G.; Smith, M. B.; Steed, J. W.: Facile syntheses of new multidentate (phosphino)amines: X-ray structure of 1,4-{(OC)4Mo(Ph2P)2NCH2}2C6H4. *Journal of Organometallic Chemistry* **2002**, *664*, 294-297.

(177) Bennani, Y. L.; Hanessian, S.: The asymmetric synthesis of α-substituted α-methyl and α-phenyl phosphonic acids: Design, carbanion geometry, reactivity and preparative aspects of chiral alkyl bicyclic phosphonamides. *Tetrahedron* **1996**, *52*, 13837-13866.

(178) Taylor, S. D.; Chen, M.-J.; Nicole Dinaut, A.; Batey, R. A.: A general method for the synthesis of O-alkyl N,O'-arylphosphoramidates and its application to the synthesis of a transition state analogue for carbamate hydrolysis. *Tetrahedron* **1998**, *54*, 4223-4242.

(179) Haggam, R.; Conrad, J.; Beifuss, U.: Practical and reliable synthesis of dialkyl N-arylphosphoramidates with nitroarenes as substrates. *Tetrahedron Letters* **2009**, *50*, 6627-6630.

(180) Keypour, H.; Rahpeyma, N.; Arzhangi, P.; Rezaeivala, M.; Elerman, Y.; Buyukgungor, O.; Valencia, L.: Synthesis and characterization of Co(II), Ni(II), Zn(II) and Cu(II) complexes with a new tetraazamacrocyclic Schiff base ligand containing a piperazine moiety: X-ray crystal structure determination of the Co(II) complex. *Polyhedron* **2010**, *29*, 1144-1148.

(181) Bararjanian, M.; Balalaie, S.; Movassagh, B.; Bijanzadeh, H. R.: Efficient synthesis of 1,4-disubstituted polyfunctional piperazines via a sequential one-pot Ugi/nucleophilic addition five-component reaction. *Tetrahedron Letters* **2010**, *51*, 3277-3279.

(182) Khan, S. A.; Nishat, N.; Parveen, S.; Rasool, R.: Preparation, spectral and biological investigation of formaldehyde-based ligand containing piperazine moiety and its various polymer metal complexes. *Spectrochimica Acta Part A: Molecular and Biomolecular Spectroscopy* **2011**, *81*, 290-295.

(183) Schildhauer, T. J.; Hoek, I.; Kapteijn, F.; Moulijn, J. A.: Zeolite BEA catalysed esterification of hexanoic acid with 1-octanol: Kinetics, side reactions and the role of water. *Applied Catalysis A: General* **2009**, *358*, 141-145.

(184) Seitz, T.: US patent 6096914, Ticona GmbH, **2000**.

(185) Lima, C. B. A.; Airoldi, C.: Layered crystalline calcium phenylphosphonate—synthesis, characterization and n-alkylmonoamine intercalation. *Solid State Sciences* **2002**, *4*, 1321-1329.

(186) Lima, C. B. A.; Airoldi, C.: Synthesis, characterization and thermodynamics of the reaction of calcium methylphosphonate with n-alkylmonoamines. *International Journal of Inorganic Materials* **2001**, *3*, 907-914.

(187) Costantino, F.; Midollini, S.; Orlandini, A.: Cobalt(II) and nickel(II) coordination polymers constructed from P,P'-diphenylmethylenediphosphinic acid (H2pcp) and 4,4'-bipyridine (bipy): Structural isomerism in [Co(pcp)(bipy)0.5(H2O)2]. *Inorganica Chimica Acta* **2008**, *361*, 327-334.

(188) Miyazaki, Y.; Hiramatsu, E.; Miura, Y.; Sakashita, H.: 27Al NMR studies on the complexation of aluminum(III) with phosphinate and phosphite ions. *Polyhedron* **1999**, *18*, 2041-2045.

(189) Mutin, P. H.; Guerrero, G.; Vioux, A.: Organic–inorganic hybrid materials based on organophosphorus coupling molecules: from metal phosphonates to surface modification of oxides. *Comptes Rendus Chimie* **2003**, *6*, 1153-1164.

(190) Silvestru, C.; Silvestru, A.; Haiduc, I.; Bryan Sowerby, D.; Ebert, K. H.; Breunig, H. J.: Triorganoantimony(V) diorganophosphinates. Crystal and molecular structure of (diphenylphosphinato)(hydroxo)trimethylantimony(V), exhibiting a polymeric chain supramolecular self-assembly through hydrogen bonds. *Polyhedron* **1997**, *16*, 2643-2649.

(191) Georgantas, V.; Kotsakis, N.; Raptopoulou, C. P.; Terzis, A.; Iordanidis, L.; Zervou, M.; Jakusch, T.; Kiss, T.; Salifoglou, A.: Synthetic, structural and solution speciation studies on binary Al(III)–(carboxy)phosphonate systems. Relevance to the neurotoxic potential of Al(III). *Journal of Inorganic Biochemistry* **2009**, *103*, 1530-1541.

(192) Cerin, O.: Development and characterization of a novel flame retardant EVM-based formulation: investigation and comprehension of the flame mechanisms. Université Lille 1, **2010**.

(193) Wiench, J. W.; Pruski, M.: Probing through bond connectivities with MQMAS NMR. *Solid State Nuclear Magnetic Resonance* **2004**, *26*, 51-55.

(194) Potrzebowski, M. J.; Gajda, J.; Ciesielski, W.; Montesinos, I. M.: Distance measurements in disodium ATP hydrates by means of 31P double quantum two-dimensional solid-state NMR spectroscopy. *Journal of Magnetic Resonance* **2006**, *179*, 173-181.

(195) Lookman, R.; Grobet, P.; Merckx, R.; Van Riemsdijk, W. H.: Application of 31P and 27Al MAS NMR for phosphate speciation studies in soil and aluminium hydroxides: promises and constraints. *Geoderma* **1997**, *80*, 369-388.

(196) Chen, Z.; Luan, Z.; Fan, J.; Zhang, Z.; Peng, X.; Fan, B.: Effect of thermal treatment on the formation and transformation of Keggin Al13 and Al30 species in hydrolytic polymeric aluminum solutions. *Colloids and Surfaces A: Physicochemical and Engineering Aspects* **2007**, *292*, 110-118.

(197) Andersen, M. D.; Jakobsen, H. J.; Skibsted, J.: A new aluminium-hydrate species in hydrated Portland cements characterized by 27Al and 29Si MAS NMR spectroscopy. *Cement and Concrete Research* **2006**, *36*, 3-17.

(198) Isobe, T.; Watanabe, T.; d'Espinose de la Caillerie, J. B.; Legrand, A. P.; Massiot, D.: Solid-state 1H and 27Al NMR studies of amorphous aluminum hydroxides. *Journal of Colloid and Interface Science* **2003**, *261*, 320-324.

(199) Jordan, P. A.; Clayden, N. J.; Heath, S. L.; Moore, G. R.; Powell, A. K.; Tapparo, A.: Defining speciation profiles of Al3+ complexed with small organic ligands: the A13+-heidi system. *Coordination Chemistry Reviews* **1996**, *149*, 281-309.

(200) Jones, M. R.; Macphee, D. E.; Chudek, J. A.; Hunter, G.; Lannegrand, R.; Talero, R.; Scrimgeour, S. N.: Studies using 27Al MAS NMR of AFm and AFt phases and the formation of Friedel's salt. *Cement and Concrete Research* **2003**, *33*, 177-182.

(201) Toplis, M. J.; Dingwell, D. B.: Shear viscosities of CaO-Al2O3-SiO2 and MgO-Al2O3-SiO2 liquids: Implications for the structural role of aluminium and the degree of polymerisation of synthetic and natural aluminosilicate melts. *Geochimica et Cosmochimica Acta* **2004**, *68*, 5169-5188.

(202) Bressel, A.; Frey, J.; Filek, U.; Sulikowski, B.; Freude, D.; Hunger, M.: Oxygen coordination of aluminum cations in dehydrated AlPW12O40 investigated by solid-state NMR spectroscopy. *Chemical Physics Letters* **2010**, *487*, 285-290.

(203) Pothiraja, R.; Shanmugan, S.; Walawalkar, M. G.; Nethaji, M.; Butcher, R. J.; Murugavel, R.: Structural Diversity in Zinc Phosphates and Phosphinates: Observation of a Lattice Water Dimer Sandwiched Between Phosphoryl Oxygen Atoms. *European Journal of Inorganic Chemistry* **2008**, *2008*, 1834-1845.

(204) Vannier, A.; Duquesne, S.; Bourbigot, S.; Alongi, J.; Camino, G.; Delobel, R.: Investigation of the thermal degradation of PET, zinc phosphinate, OMPOSS and their blends—Identification of the formed species. *Thermochimica Acta* **2009**, *495*, 155-166.

(205) Karrasch, A.; Wawrzyn, E.; Schartel, B.; Jäger, C.: Solid-state NMR on thermal and fire residues of bisphenol A polycarbonate/silicone acrylate rubber/bisphenol A Bis(diphenyl-phosphate) (PC/SiR/BDP) and PC/SiR/BDP/zinc borate (PC/SiR/BDP/ZnB) — Part II: The influence of SiR. *Polymer Degradation and Stability* **2010**, *95*, 2534-2540.

(206) Schartel, B.: Phosphorus-based flame retardancy Mechanisms - Old hat a starting point for future development? *Materials* **2010**, *3*, 4710-4745.

(207) Bourbigot, S.; Samyn, F.; Turf, T.; Duquesne, S.: Nanomorphology and reaction to fire of polyurethane and polyamide nanocomposites containing flame retardants. *Polymer Degradation and Stability* **2010**, *95*, 320-326.

(208) Kawai, K.; Kondo, H.; Ohtani, H.: Characterization of cross-linking structure in terephthalate polyesters formed through material recycling process by pyrolysis-gas chromatography in the presence of organic alkali. *Polymer Degradation and Stability* **2008**, *93*, 1781-1785.

(209) Jones, R. N.; Sandorfy, C.: *The application of Infrared and Raman spectrometry on the elucidation of molecular structure, In Weissberger's Technique of Organic Chemistry*. Interscience; New York, **1956**; Vol. 9.

(210) Devroede, J.: Study of the THF formation during the TPA-based synthesis of PBT. Eindhoven University of Technology, **2007**.

(211) Thomas, S.; Visakh, P. M.: *Handbook of Engineering and Speciality Thermoplastics, Volume 3: Polyethers and Polyesters*, **2011**.

(212) Palit, M.; Gupta, A. K.; Jain, R.; Raza, S. K.: Determination of pentafluorobenzyl derivatives of phosphonic and phosphonothioic acids by gas chromatography–mass spectrometry. *Journal of Chromatography A* **2004**, *1043*, 275-284.

(213) Srikanth, R.; Reddy, P. N.; Bhanuprakash, K.; Srinivas, R.; Chen, X.; Tureček, F.: Generation and Characterization of Ionic and Neutral [HS-P-OH]+/· and S=P(OH)2+/· in the Gas Phase by Tandem Mass Spectrometry and Computational Chemistry. *Journal of the American Society for Mass Spectrometry* **2005**, *16*, 1353-1366.

(214) Haake, P.; Ossip, P. S.: A mass spectrometric study of some dialkylphosphinic acids and their alkyl esters. *Tetrahedron* **1968**, *24*, 565-573.

(215) Braun, U.; Bahr, H.; schartel, B.: Fire retardancy effect of aluminium phosphinate and melamine polyphosphate in glass fibre reinforced polyamide 6. *e-polymers* **2010**.

(216) Edén, M.; Sundberg, P.; Stålhandske, C.: The split network analysis for exploring composition–structure correlations in multi-component glasses: II. Multinuclear NMR studies of alumino-borosilicates and glass-wool fibers. *Journal of Non-Crystalline Solids* **2011**, *357*, 1587-1594.

(217) Graves, C. R.; Joseph Campbell, E.; Nguyen, S. T.: Aluminum-based catalysts for the asymmetric Meerwein–Schmidt–Ponndorf–Verley–Oppenauer (MSPVO) reaction manifold. *Tetrahedron: Asymmetry* **2005**, *16*, 3460-3468.

(218) Cheng, Y. Y.; Brillhart, M. V.; Cebe, P.: Modulated differential scanning calorimetry study of blends of poly(butylene terephthalate) with polycarbonate. *Thermochimica Acta* **1997**, *304–305*, 369-378.

(219) Chung, H.-J.; Lee, E.-J.; Lim, S.-T.: Comparison in glass transition and enthalpy relaxation between native and gelatinized rice starches. *Carbohydrate Polymers* **2002**, *48*, 287-298.

APPENDICES

APPENDIX 1

NMR SPECTRA OF THE SYNTHESIZED PHOSPHINIC ACID AND PHOSPHINATE SALTS

● Benzyl amide of carboxyethyl(methyl)phosphinic acid (C1)

- Liquid NMR

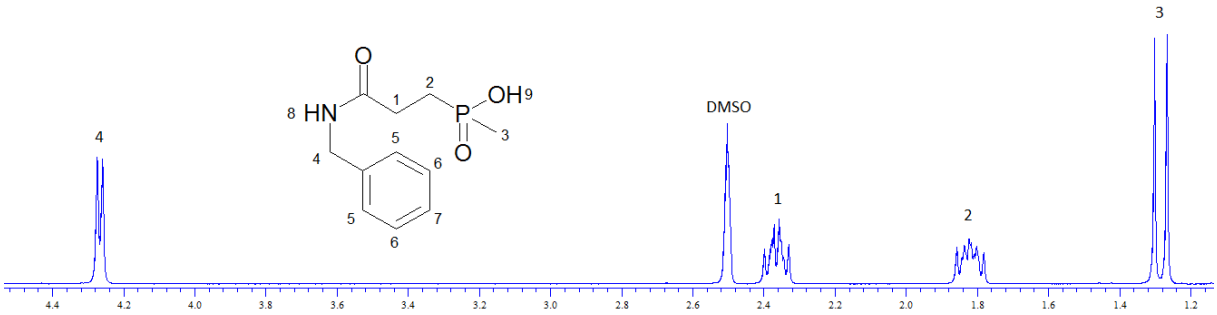

^{1}H NMR (DMSO)

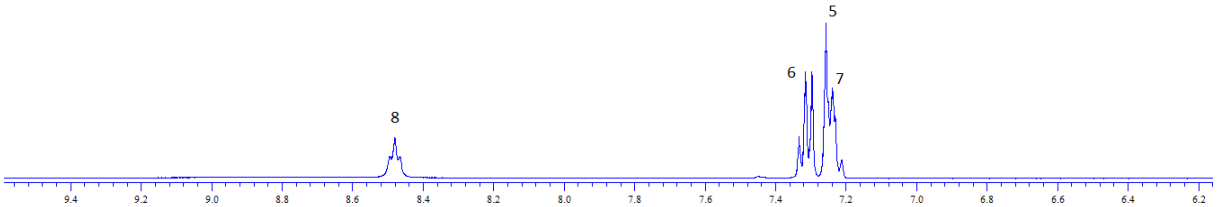

^{1}H NMR (DMSO)

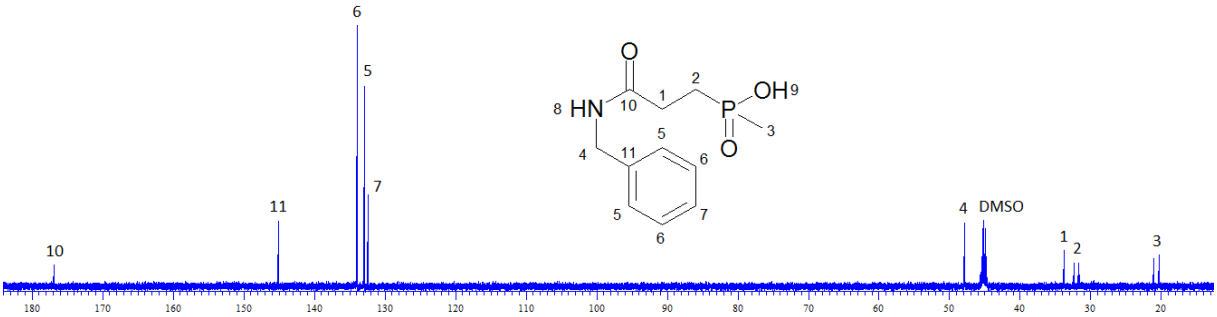

^{13}C NMR (DMSO)

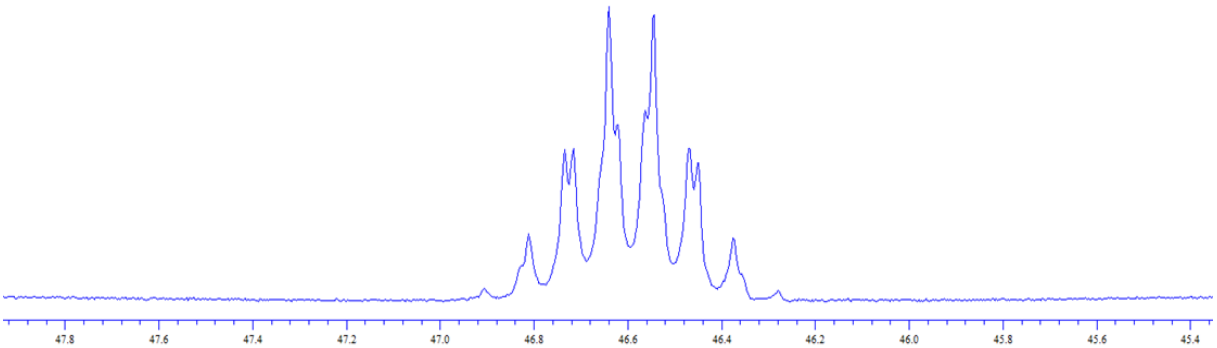

^{31}P (^{1}H coupling) (DMSO)

- Solid state NMR

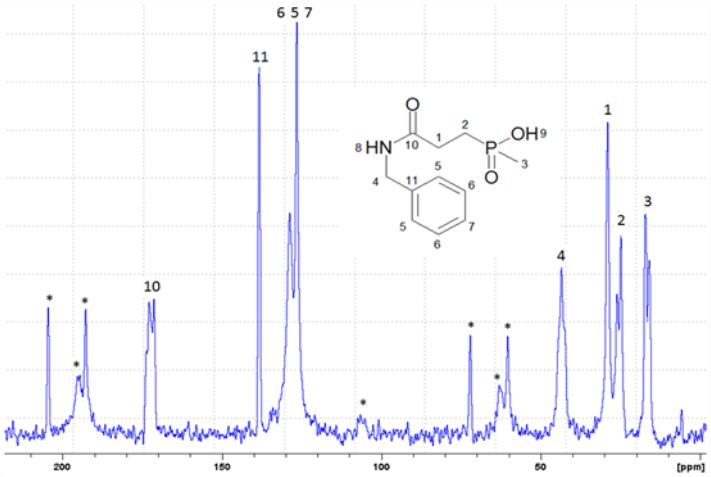

^{13}C CP/MAS NMR (Bo 300 Mhz); Probehead : 4 mm MAS; MAS: 5 kHz; CP ^{1}H–^{13}C: 3 ms; 10240 Scans (d1 = 2 s); High-power ^{1}H decoupling

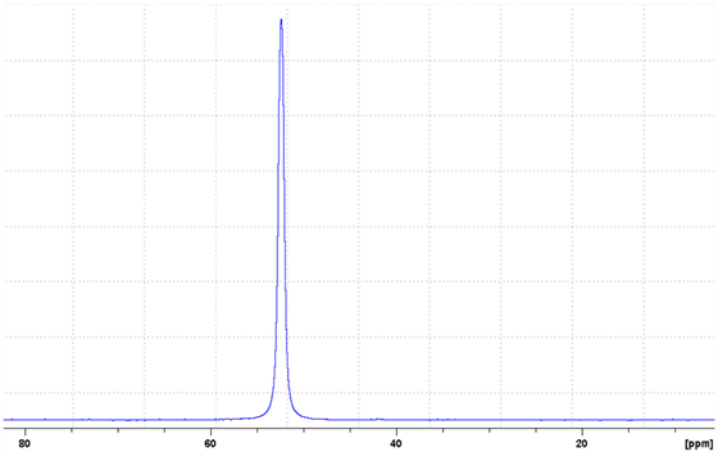

^{31}P CP/MAS NMR (Bo 300 Mhz); Probehead : 4 mm MAS; MAS: 10 kHz; CP ^{1}H–^{13}C: 3 ms; 1024 Scans (d1 = 2 s); High-power ^{1}H decoupling

● Phenyl amide of carboxyethyl(methyl)phosphinic acid (C2)

- Liquid NMR

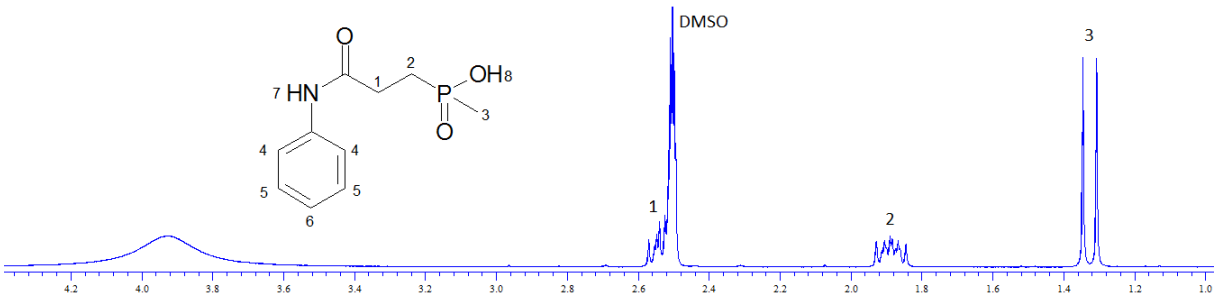

^{1}H NMR (DMSO)

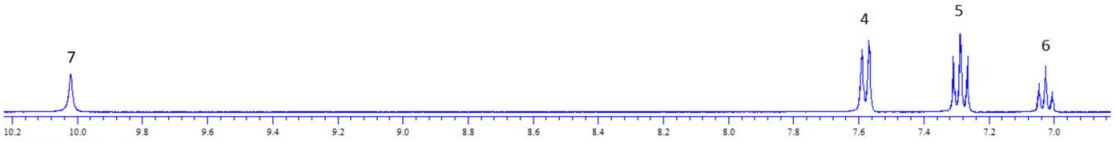

^{1}H NMR (DMSO)

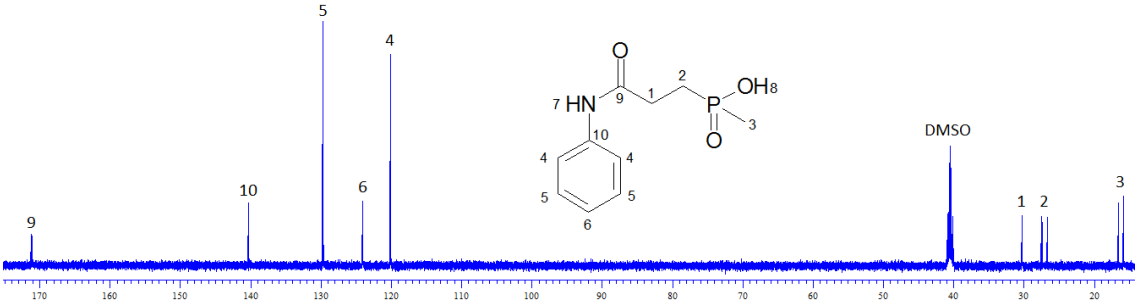

^{13}C NMR (DMSO)

- Solid state NMR

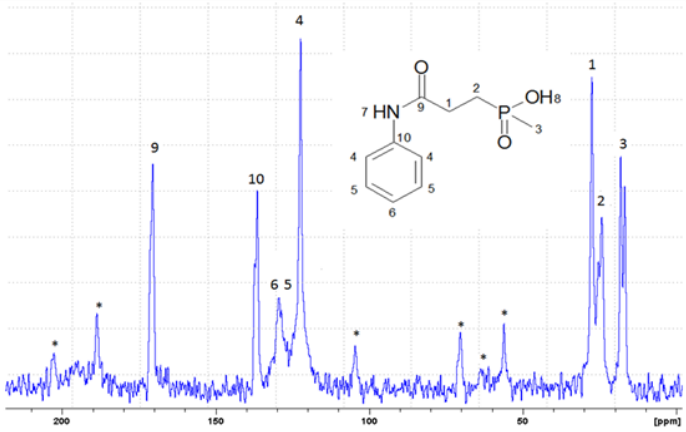

^{13}C CP/MAS NMR (Bo 300 Mhz); Probehead : 4 mm MAS; MAS: 5 kHz; CP ^{1}H–^{13}C: 3 ms; 10240 Scans (d1 = 2 s); High-power ^{1}H decoupling

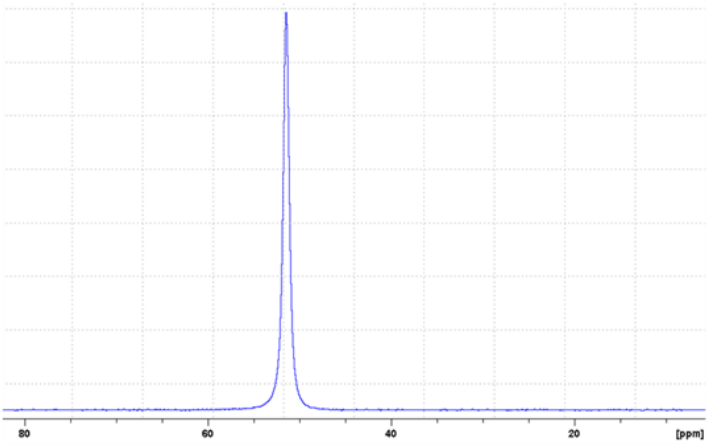

^{31}P CP/MAS NMR (Bo 300 Mhz); Probehead : 4 mm MAS; MAS: 10 kHz; CP ^{1}H–^{13}C: 3 ms; 1024 Scans (d1 = 2 s); High-power ^{1}H decoupling

● **piperazine diamide of carboxyethyl(methyl)phosphinic acid (C3)**

- Liquid NMR

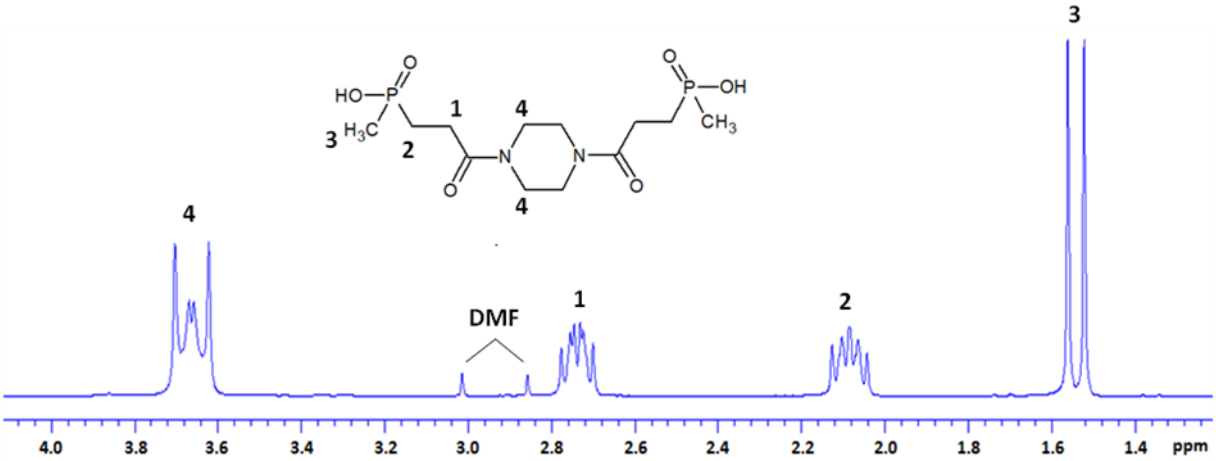

^{1}H NMR (D_2O)

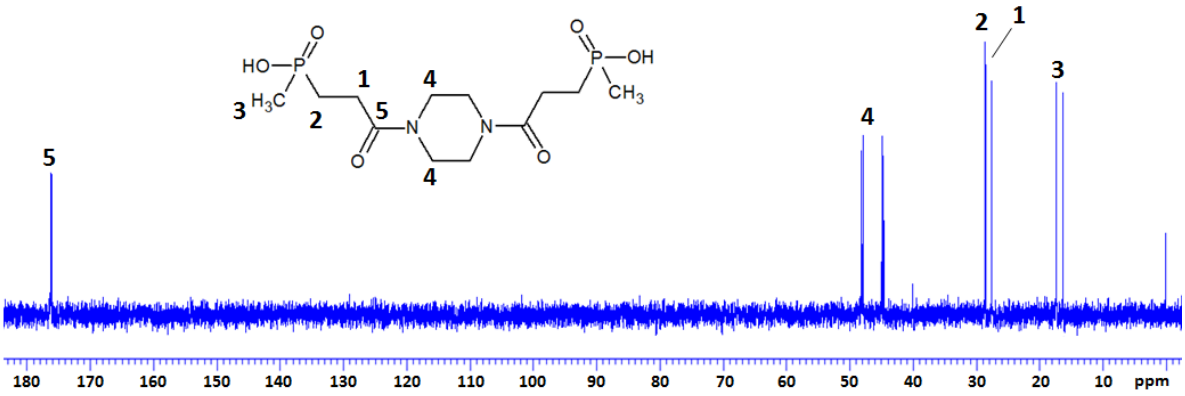

^{13}C NMR (D_2O)

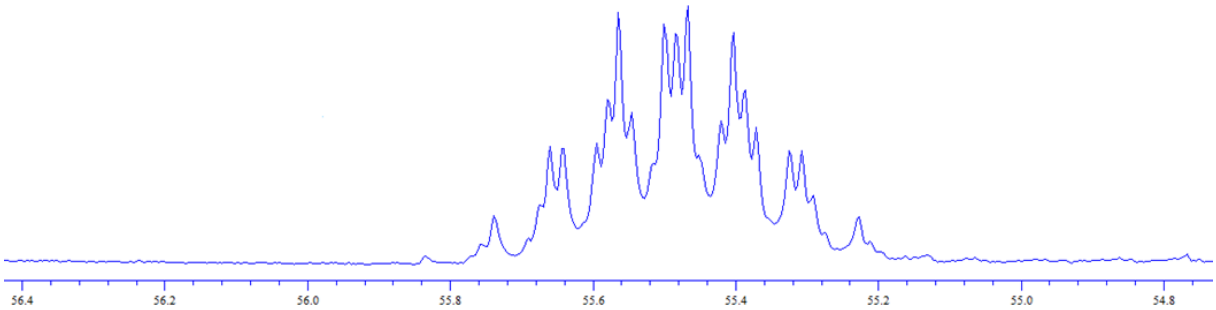

^{31}P (^{1}H coupling) (D_2O)

- Solid state NMR

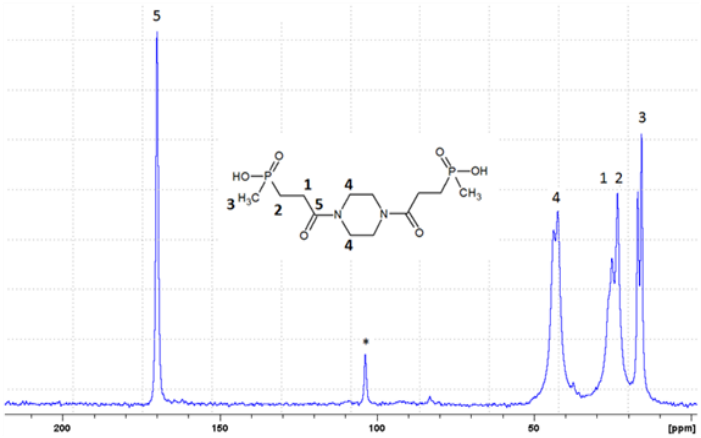

^{13}C CP/MAS NMR (Bo 300 Mhz); Probehead : 4 mm MAS; MAS: 5 kHz; CP ^{1}H–^{13}C: 3 ms; 10240 Scans (d1 = 2 s); High-power ^{1}H decoupling

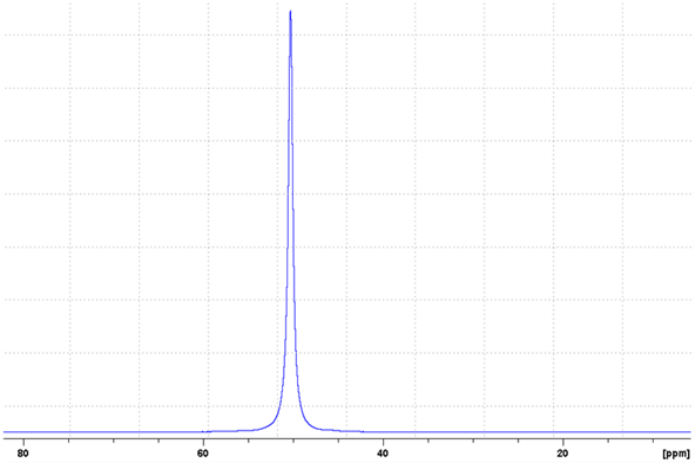

^{31}P CP/MAS NMR (Bo 300 Mhz); Probehead : 4 mm MAS; MAS: 10 kHz; CP ^{1}H–^{13}C: 3 ms; 1024 Scans (d1 = 2 s); High-power ^{1}H decoupling

● ethylene diamide of carboxyethyl(methyl)phosphinic acid (C4)

- Liquid NMR

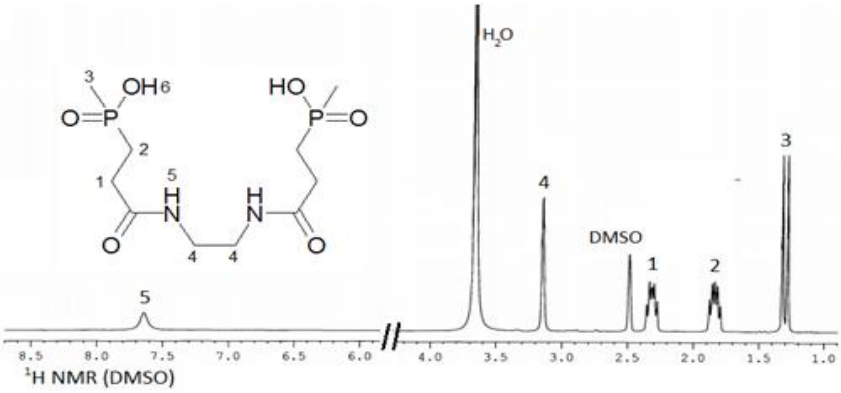

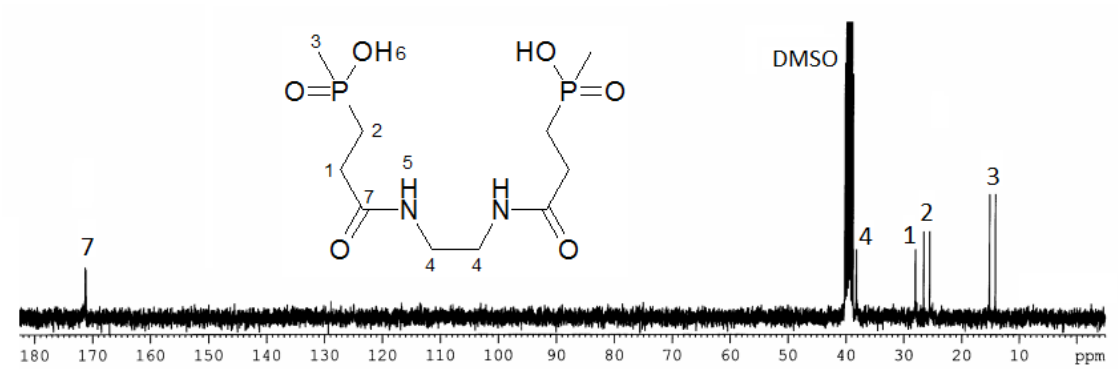

^{13}C NMR (DMSO)

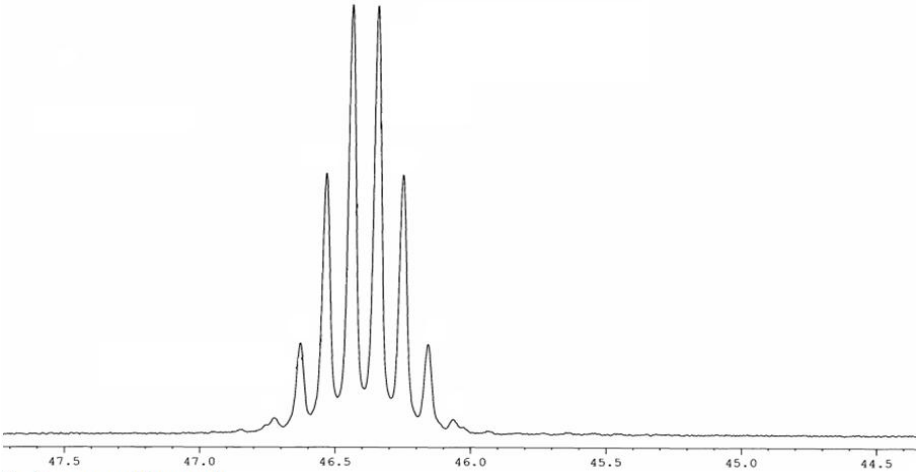

^{31}P (^{1}H coupling) (DMSO)

- Solid state NMR

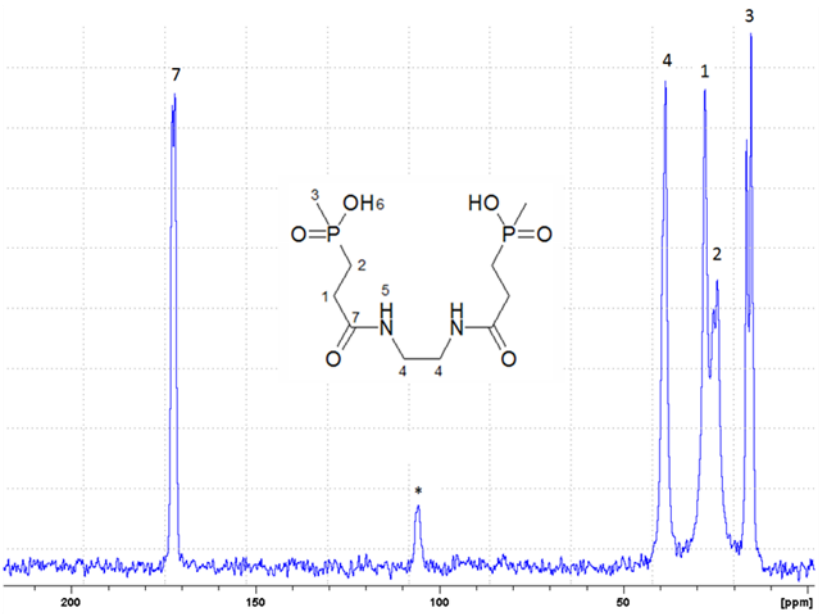

^{13}C CP/MAS NMR (Bo 300 Mhz); Probehead : 4 mm MAS; MAS: 5 kHz; CP ^{1}H–^{13}C: 3 ms; 10240 Scans (d1 = 2 s); High-power ^{1}H decoupling

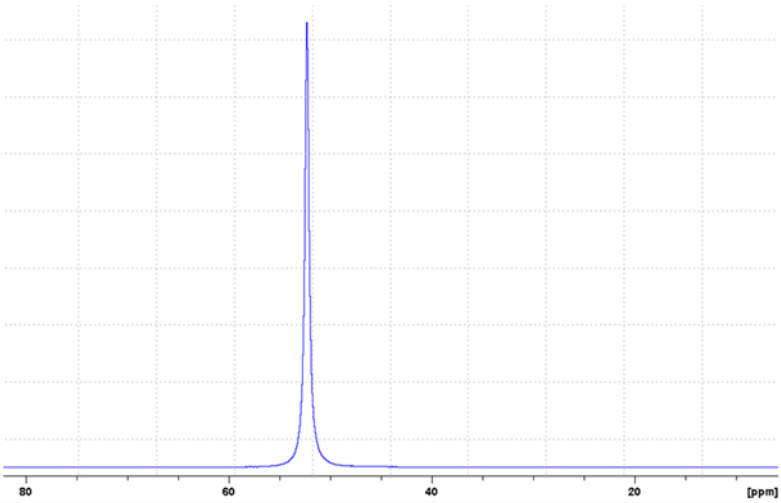

^{31}P CP/MAS NMR (Bo 300 Mhz); Probehead : 4 mm MAS; MAS: 10 kHz; CP ^{1}H–^{13}C: 3 ms; 1024 Scans (d1 = 2 s); High-power ^{1}H decoupling

● **m-phenylene diamide of carboxyethyl(methyl)phosphinic acid (C5)**

- Liquid NMR

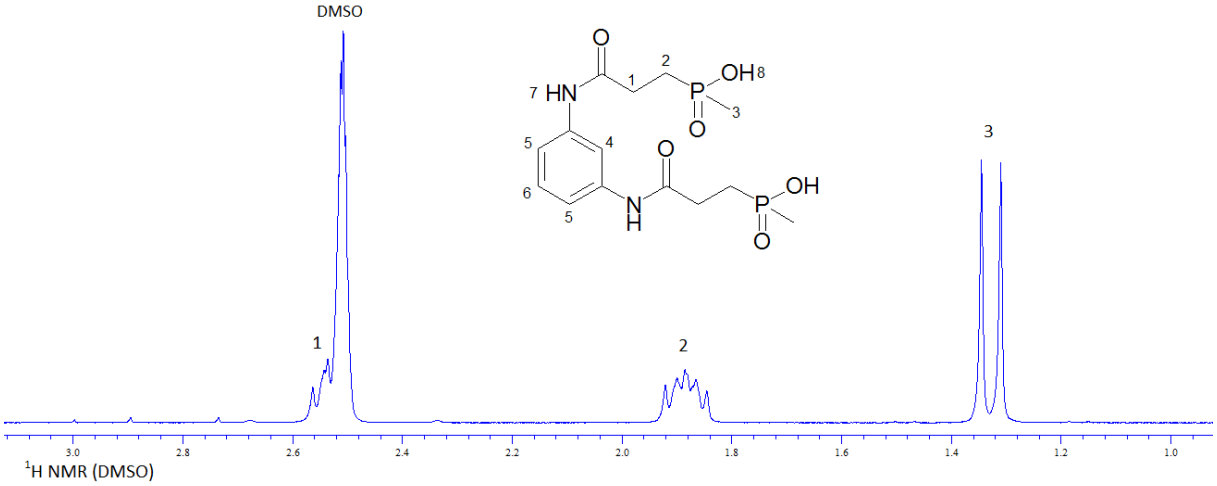

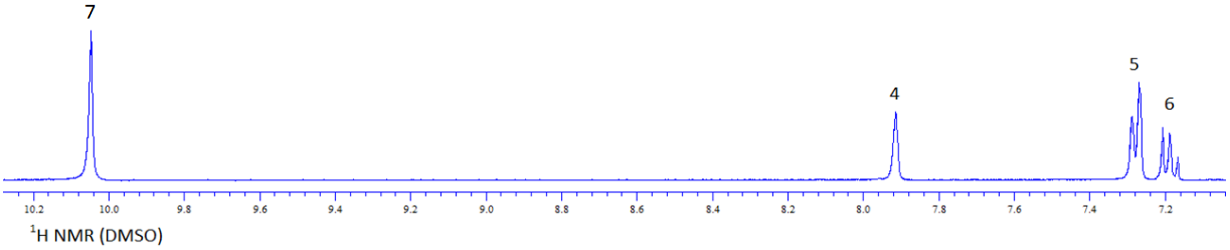

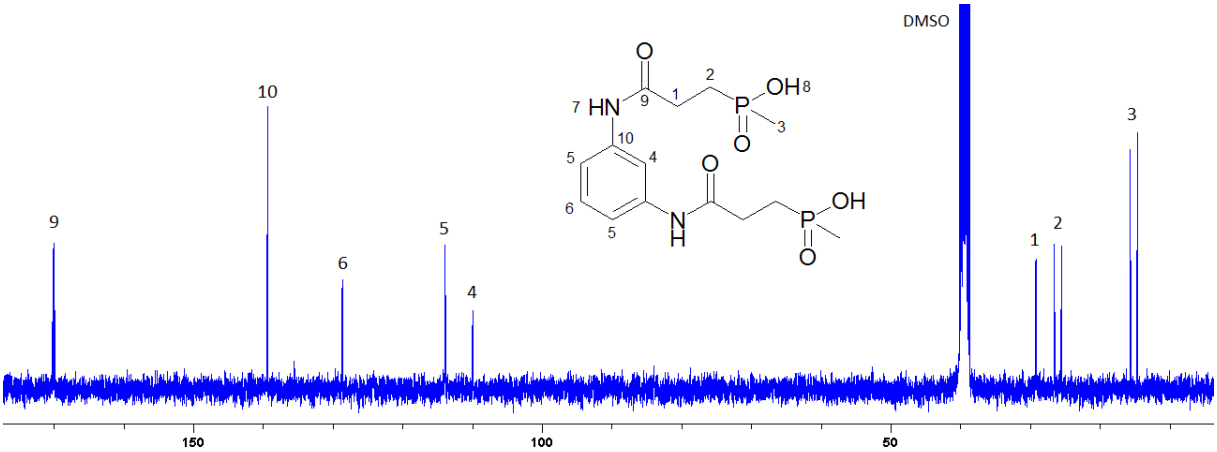

^{13}C NMR (DMSO)

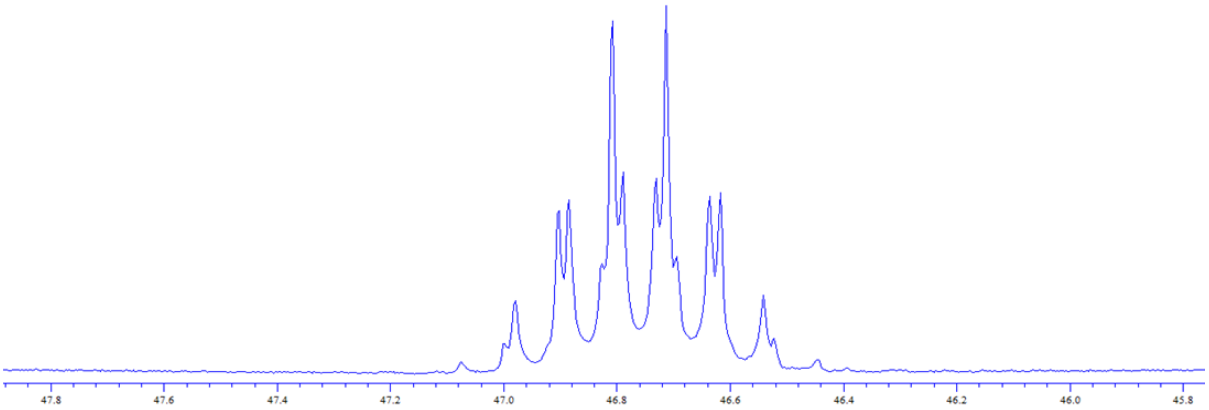

^{31}P (^{1}H coupling) (DMSO)

- Solid state NMR

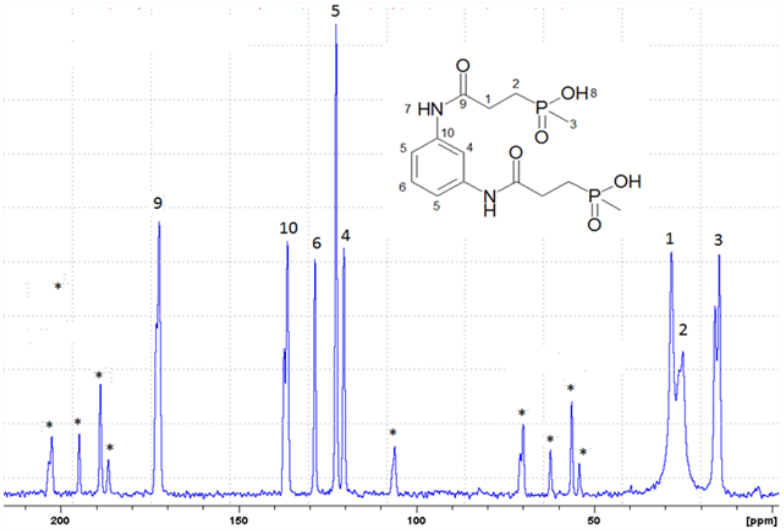

^{13}C CP/MAS NMR (Bo 300 Mhz); Probehead : 4 mm MAS; MAS: 5 kHz; CP ^{1}H–^{13}C: 3 ms; 10240 Scans (d1 = 2 s); High-power ^{1}H decoupling

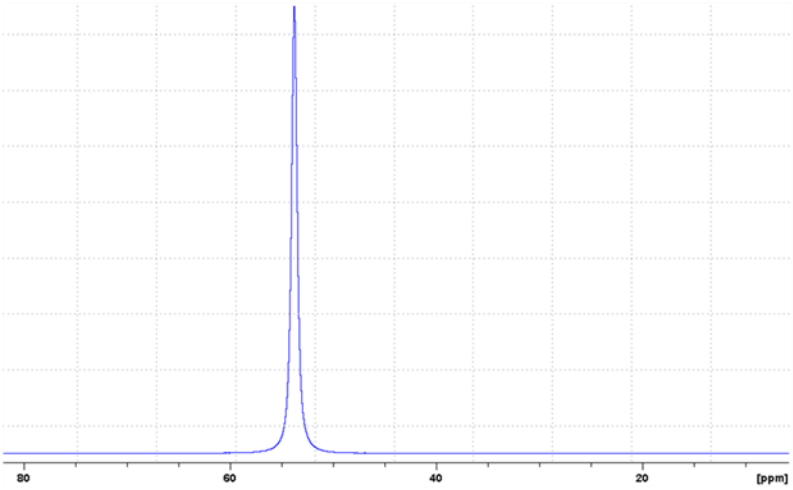

^{31}P CP/MAS NMR (Bo 300 Mhz); Probehead : 4 mm MAS; MAS: 10 kHz; CP ^{1}H–^{13}C: 3 ms; 1024 Scans (d1 = 2 s); High-power ^{1}H decoupling

● o-phenylene diamide of carboxyethyl(methyl)phosphinic acid (C6)

- Liquid NMR

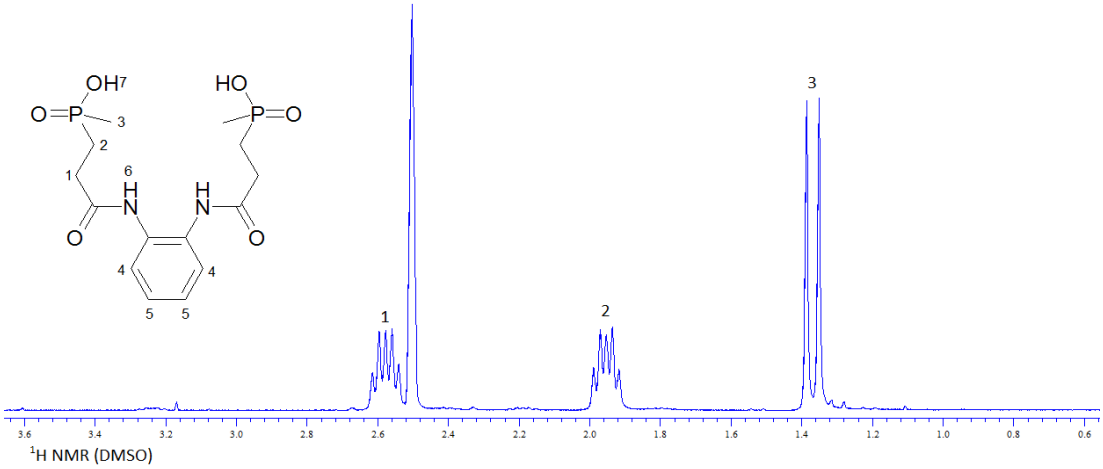

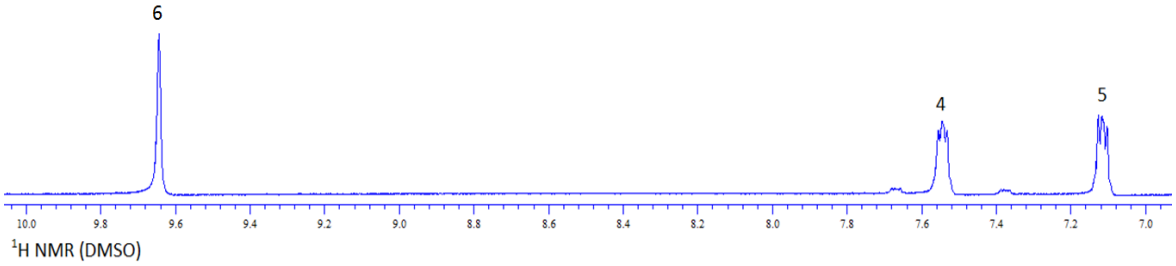

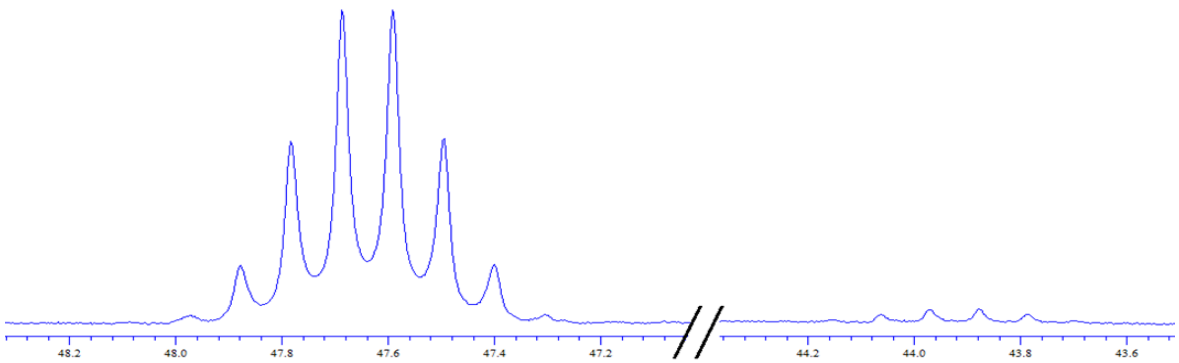

^{31}P (^{1}H coupling) (DMSO)

● **2-carboxyethyl(methyl)phosphinic acid (HydPE110)**

- ***Liquid NMR***

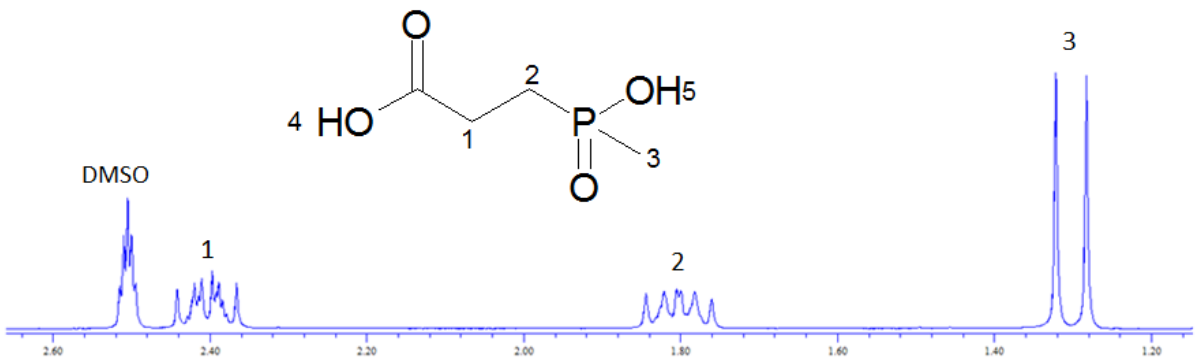

^{1}H NMR (DMSO)

● **PEPA ester of carboxyethyl(methyl)phosphinic acid (C7)**

- ***Liquid NMR***

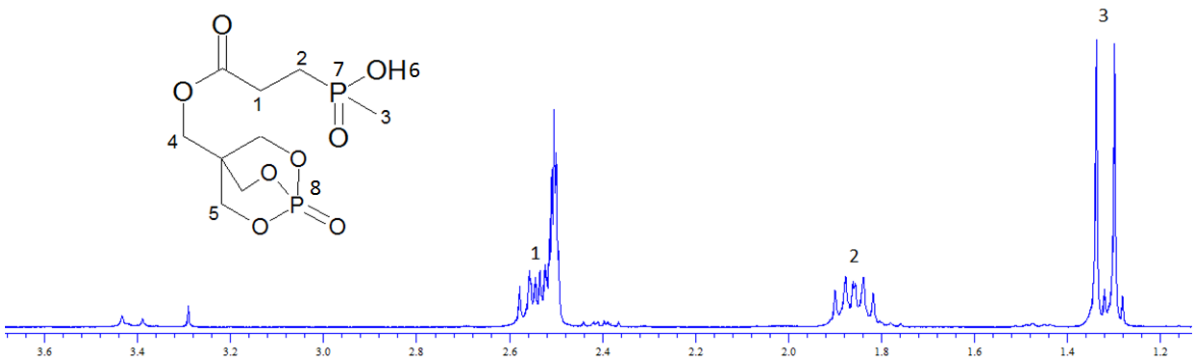

^{1}H NMR (DMSO)

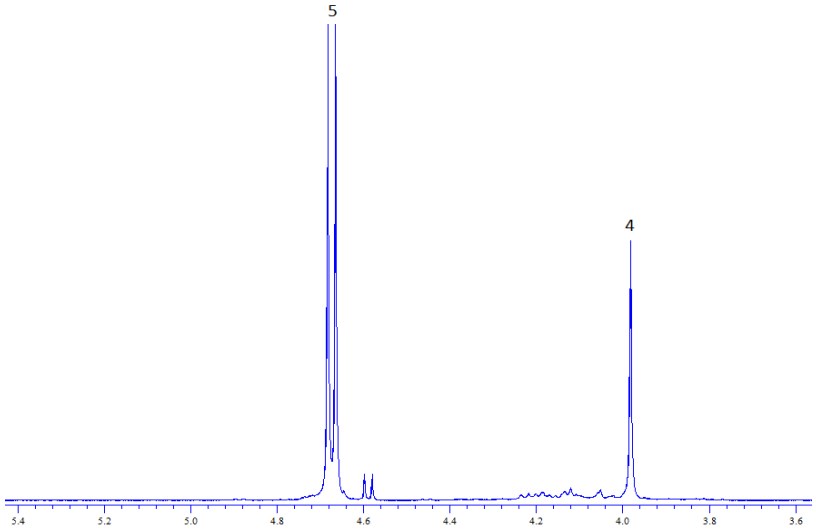

^{1}H NMR (DMSO)

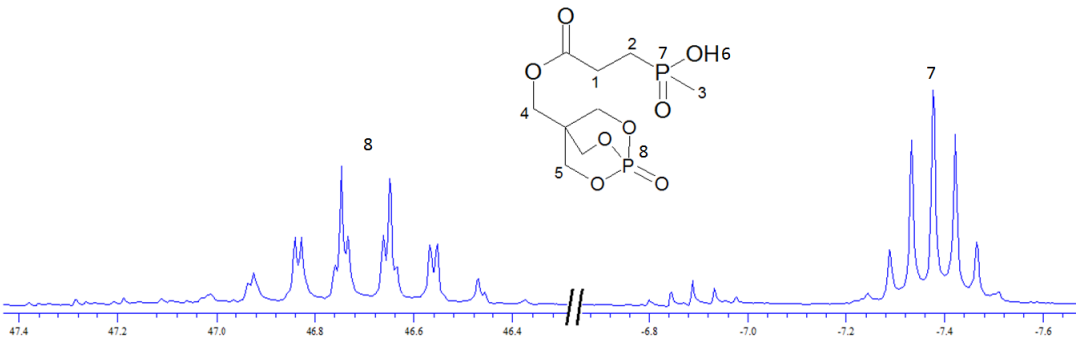

^{31}P (^{1}H coupling) (DMSO)

● **benzyl amide of carboxyethyl(methyl)phosphinate aluminum (C8)**

- Solid state NMR

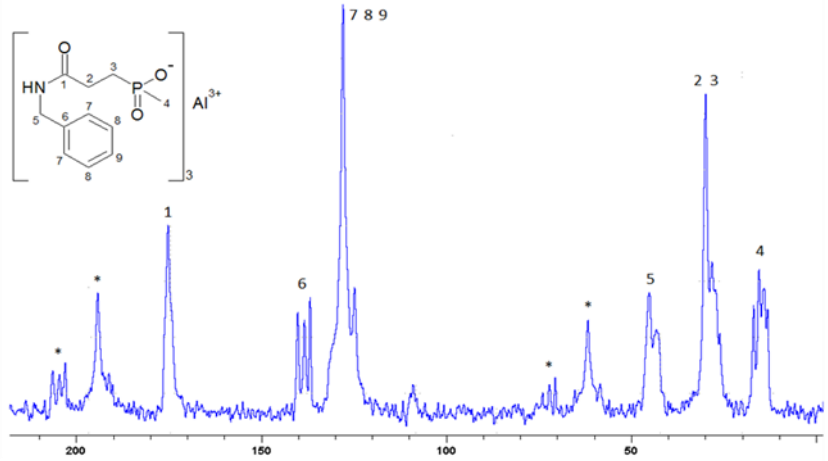

^{13}C CP/MAS NMR (Bo 300 Mhz); Probehead : 4 mm MAS; MAS: 5 kHz; CP ^{1}H–^{13}C: 3 ms; 10240 Scans (d1 = 2 s); High-power ^{1}H decoupling

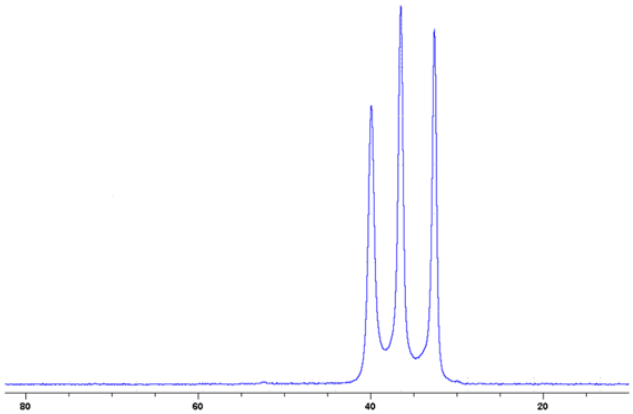

^{31}P CP/MAS NMR (Bo 300 Mhz); Probehead : 4 mm MAS; MAS: 10 kHz; CP ^{1}H–^{13}C: 3 ms; 1024 Scans (d1 = 2 s); High-power ^{1}H decoupling

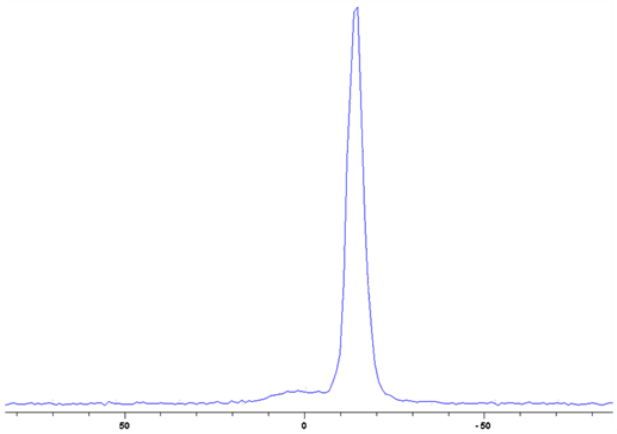

^{27}Al (Bo 300 Mhz); 15° pulse; Probehead : 4 mm MAS; MAS: 10 kHz; 122880 Scans (d1 = 0.25 s)

● **phenyl amide of carboxyethyl(methyl)phosphinate aluminum (C9)**

- Solid state NMR

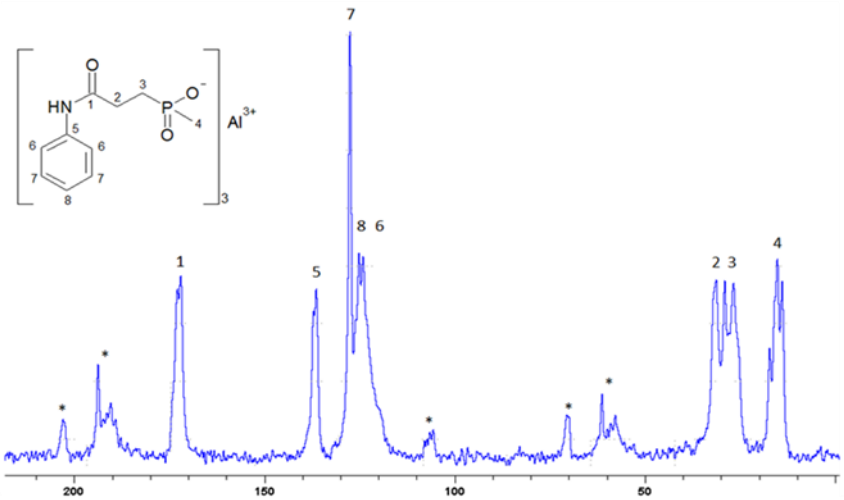

^{13}C CP/MAS NMR (Bo 300 Mhz); Probehead : 4 mm MAS; MAS: 5 kHz; CP ^{1}H–^{13}C: 3 ms; 10240 Scans (d1 = 2 s); High-power ^{1}H decoupling

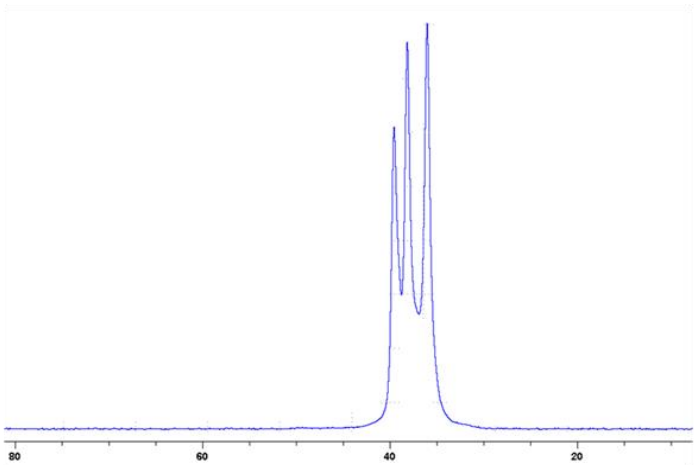

^{31}P CP/MAS NMR (Bo 300 Mhz); Probehead : 4 mm MAS; MAS: 10 kHz; CP ^{1}H–^{13}C: 3 ms; 1024 Scans (d1 = 2 s); High-power ^{1}H decoupling

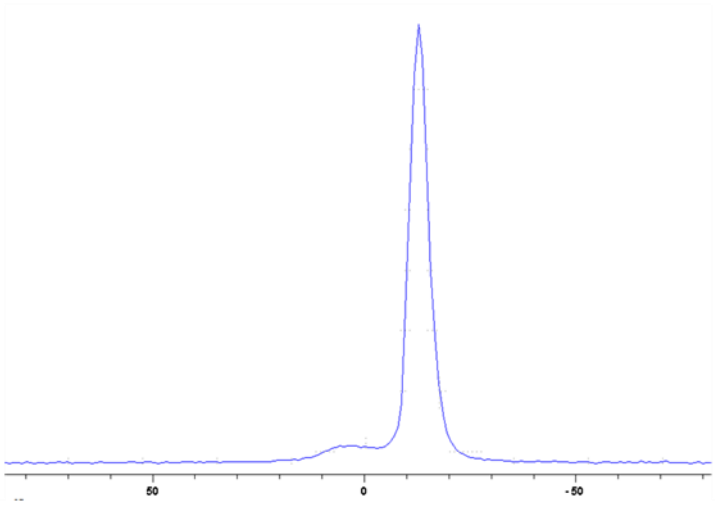

^{27}Al (Bo 300 Mhz); 15° pulse; Probehead : 4 mm MAS; MAS: 10 kHz; 122880 Scans (d1 = 0.25 s)

● **phenyl amide of carboxyethyl(methyl)phosphinate zinc (C10)**

- Solid state NMR

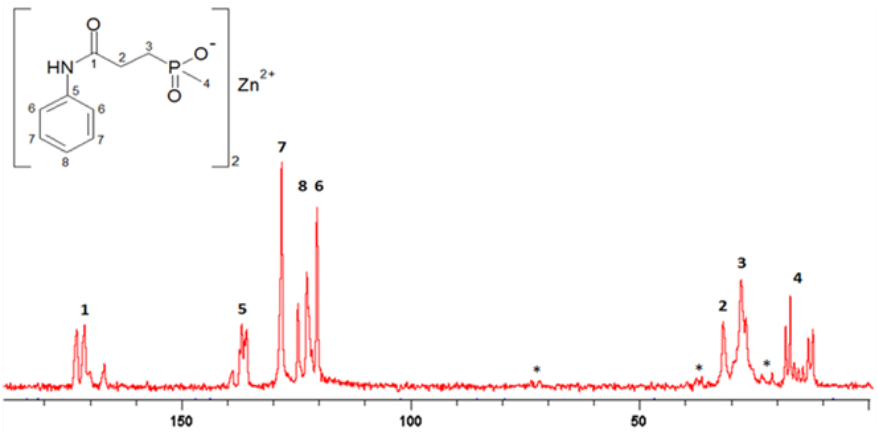

^{13}C CP/MAS NMR (Bo 400 Mhz); Probehead : 4 mm MAS; MAS:10 kHz; CP ^{1}H–^{13}C: 2 ms; 1024 Scans (d1 = 5 s); High-power ^{1}H decoupling

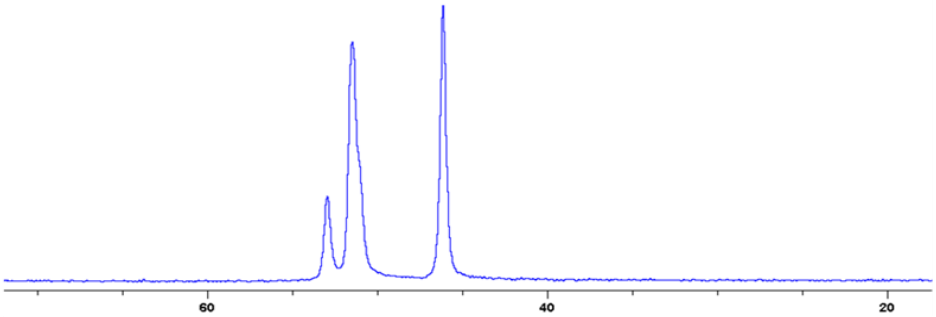

^{31}P NMR (Bo 400 Mhz); Probehead : 4 mm MAS; MAS: 13 kHz; 8 Scans (d1 = 120 s); High-power ^{1}H decoupling

● **phenyl amide of carboxyethyl(methyl)phosphinate calcium (C11)**

- Solid state NMR

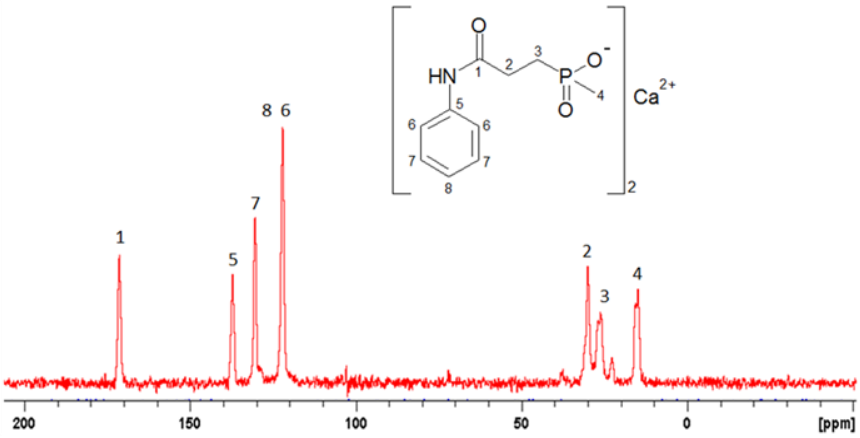

^{13}C CP/MAS NMR (Bo 400 Mhz); Probehead : 4 mm MAS; MAS:10 kHz; CP ^{1}H–^{13}C: 2 ms; 1024 Scans (d1 = 5 s); High-power ^{1}H decoupling

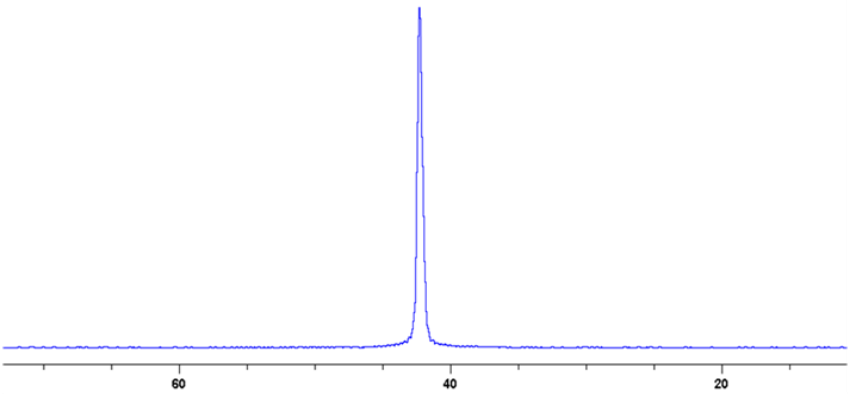

^{31}P NMR (Bo 400 Mhz); Probehead : 4 mm MAS; MAS: 13 kHz; 8 Scans (d1 = 120 s); High-power ^{1}H decoupling

● **piperazine diamide of methyl-β-(carboxamid)ethylphosphinate aluminum (C12)**

- Solid state NMR

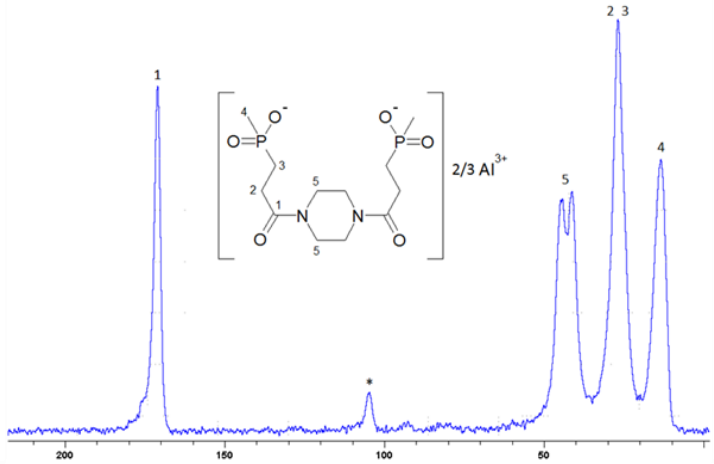

^{13}C CP/MAS NMR (Bo 300 Mhz); Probehead : 4 mm MAS; MAS: 5 kHz; CP ^{1}H–^{13}C: 3 ms; 10240 Scans (d1 = 2 s); High-power ^{1}H decoupling

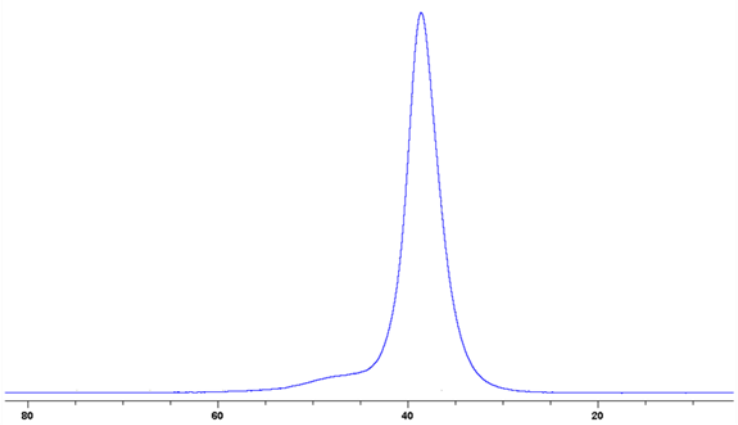

^{31}P CP/MAS NMR (Bo 300 Mhz); Probehead : 4 mm MAS; MAS: 10 kHz; CP ^{1}H–^{13}C: 3 ms; 1024 Scans (d1 = 2 s); High-power ^{1}H decoupling

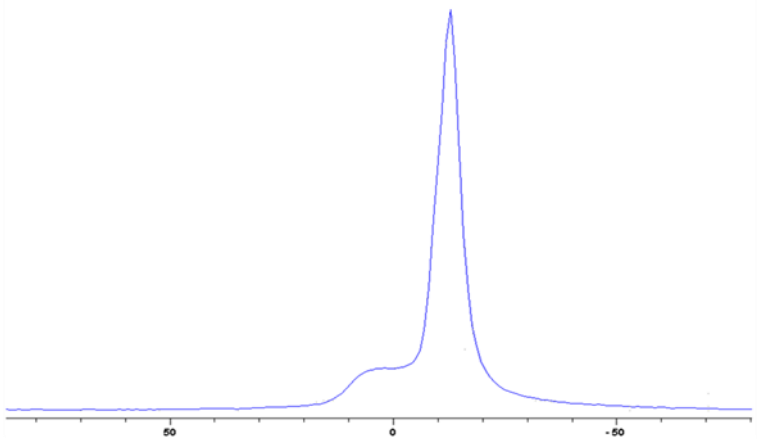

^{27}Al (Bo 300 Mhz); 15° pulse; Probehead : 4 mm MAS; MAS: 10 kHz; 122880 Scans (d1 = 0.25 s)

● **ethylene diamide of carboxyethyl(methyl)phosphinate aluminum (C13)**

- Solid state NMR

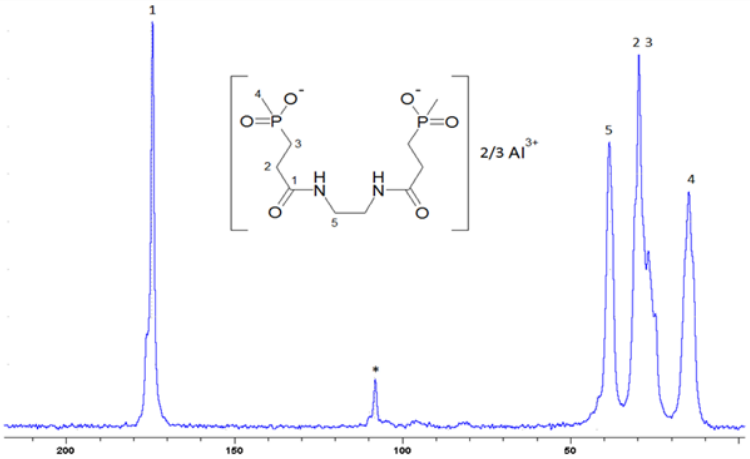

^{13}C CP/MAS NMR (Bo 300 Mhz); Probehead : 4 mm MAS; MAS: 5 kHz; CP ^{1}H–^{13}C: 3 ms; 10240 Scans (d1 = 2 s); High-power ^{1}H decoupling

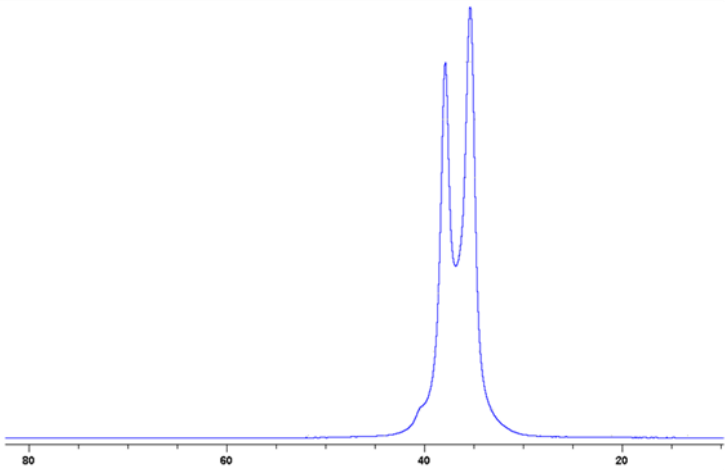

^{31}P CP/MAS NMR (Bo 300 Mhz); Probehead : 4 mm MAS; MAS: 10 kHz; CP ^{1}H–^{13}C: 3 ms; 1024 Scans (d1 = 2 s); High-power ^{1}H decoupling

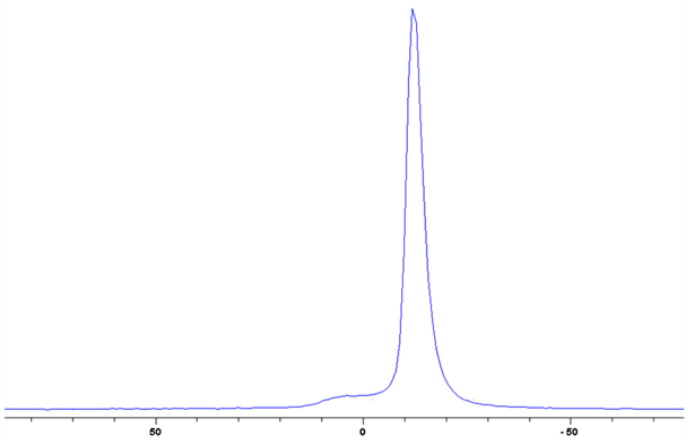

^{27}Al (Bo 300 Mhz); 15° pulse; Probehead : 4 mm MAS; MAS: 10 kHz; 122880 Scans (d1 = 0.25 s)

● **m-phenylene diamide of carboxyethyl(methyl)phosphinate aluminum (C14-1)**

*- **Solid state NMR***

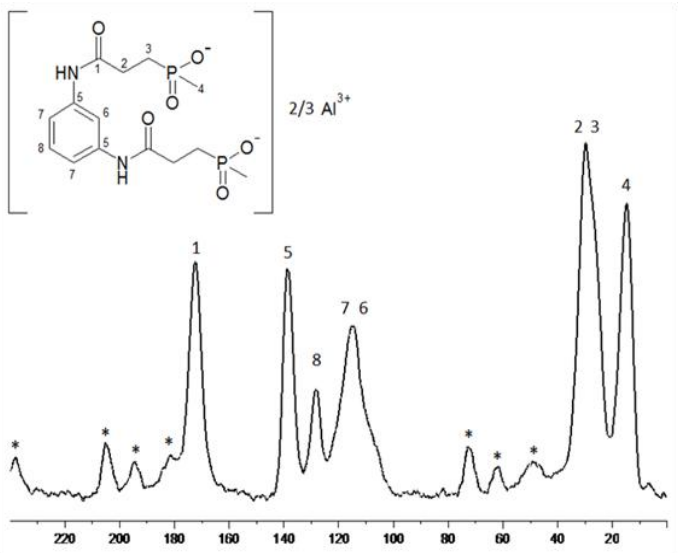

^{13}C CP/MAS NMR (Bo 300 Mhz); Probehead : 4 mm MAS; MAS: 5 kHz; CP ^{1}H–^{13}C: 3 ms; 10240 Scans (d1 = 2 s); High-power ^{1}H decoupling

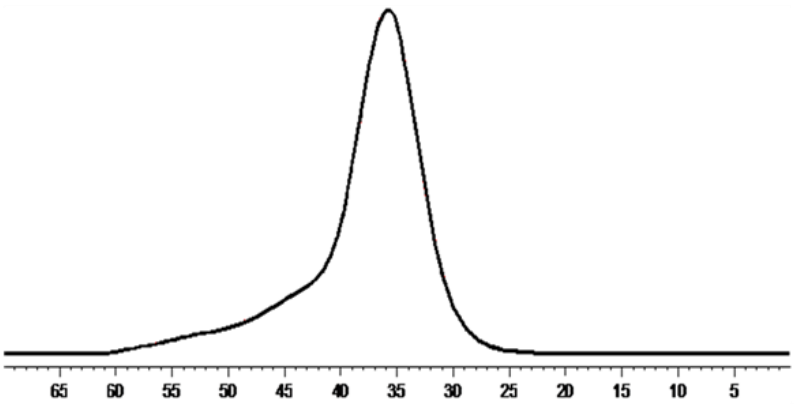

^{31}P CP/MAS NMR (Bo 300 Mhz); Probehead : 4 mm MAS; MAS: 10 kHz; CP ^{1}H–^{13}C: 3 ms; 1024 Scans (d1 = 2 s); High-power ^{1}H decoupling

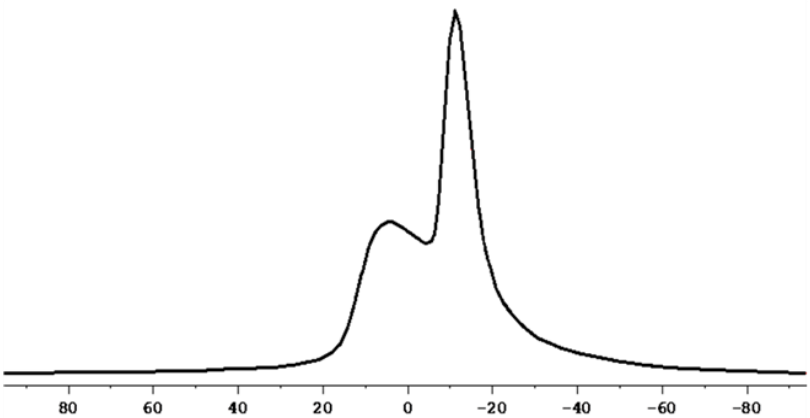

^{27}Al (Bo 300 Mhz); 15° pulse; Probehead : 4 mm MAS; MAS: 10 kHz; 122880 Scans (d1 = 0.25 s)

● **m-phenylene diamide of carboxyethyl(methyl)phosphinate aluminum (C14-2)**

- Solid state NMR

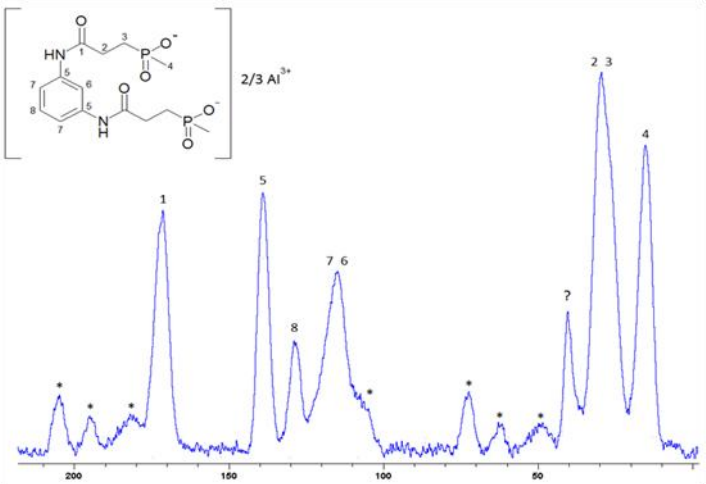

^{13}C CP/MAS NMR (Bo 300 Mhz); Probehead : 4 mm MAS; MAS: 5 kHz; CP ^{1}H–^{13}C: 3 ms; 10240 Scans (d1 = 2 s); High-power ^{1}H decoupling

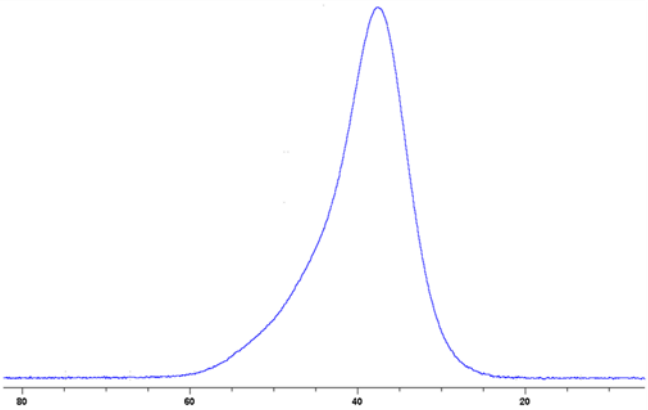

^{31}P CP/MAS NMR (Bo 300 Mhz); Probehead : 4 mm MAS; MAS: 10 kHz; CP ^{1}H–^{13}C: 3 ms; 1024 Scans (d1 = 2 s); High-power ^{1}H decoupling

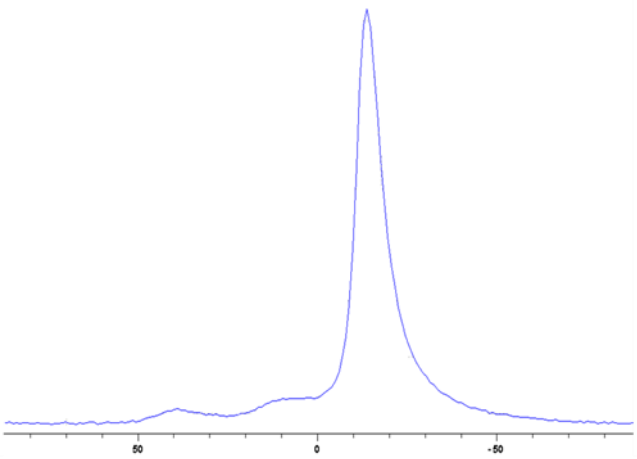

^{27}Al (Bo 300 Mhz); 15° pulse; Probehead : 4 mm MAS; MAS: 10 kHz; 122880 Scans (d1 = 0.25 s)

● **PEPA ester of carboxyethyl(methyl)phosphinate aluminum (15)**

- Solid state NMR

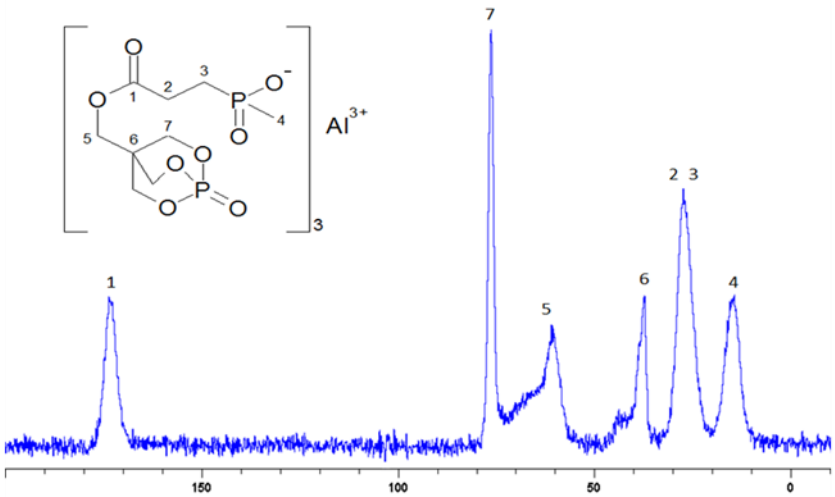

^{13}C CP/MAS NMR (Bo 400 Mhz); Probehead : 4 mm MAS; MAS:10 kHz; CP ^{1}H–^{13}C: 2 ms; 1024 Scans (d1 = 5 s); High-power ^{1}H decoupling

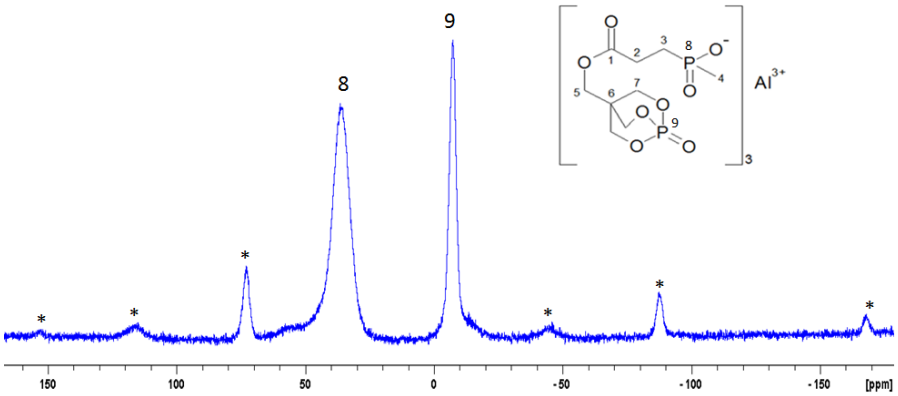

^{31}P NMR (Bo 400 Mhz); Probehead : 4 mm MAS; MAS: 13 kHz; 8 Scans (d1 = 120 s); High-power ^{1}H decoupling

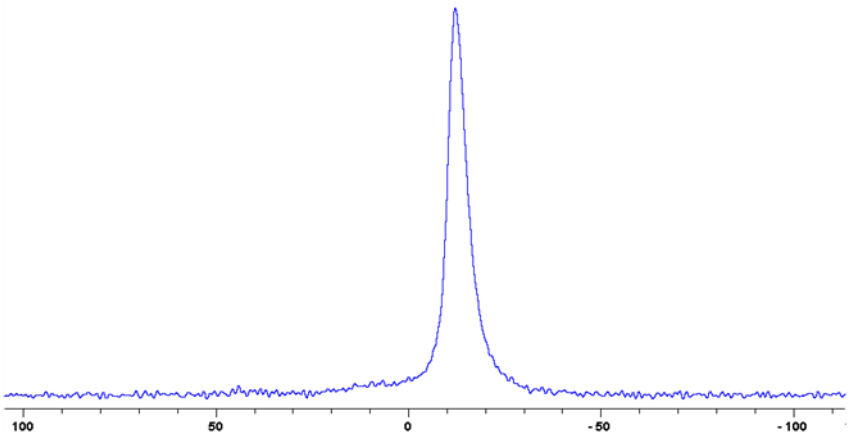

^{27}Al (Bo 400 Mhz); single pulse; Probehead : 3.2 mm MAS; MAS: 20 kHz; 512 Scans (d1 = 2 s)

APPENDIX 2:

COMPOSITION AND PROPERTIES OF THE FIRE RETARDANTS SYNERGISTS

Commercial name	Supplier	Composition / Structure	Specifications
Exolit© OP1240	Clariant	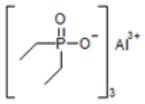 *Aluminium Diethyl-Phosphinate*	Particule size (d_{50}) : 25 - 50 µm Uses : flame retardant for polyester injection moulding applications
Exolit© OP1200	Clariant	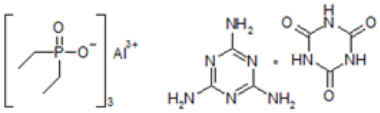 *2 Aluminium Diethyl-Phosphinate + 1 Melamine Cyanurate (w/w)*	Uses : flame retardant for polyester injection moulding applications
Cloisite 30B	Southern Clay Products	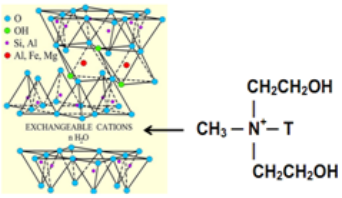 *Montmorillonite modified with methyl, tallow, bis-2-hydroxyethyl, quaternary ammonium*	Particule size (d_{50}) : 13 µm Specific surface : 750 m^2/g Modifier concentration : 90 meq / 100g clay Onset temperature of weight loss: 190°C (TGA analysis, N_2) Residual weight at 800°C: 76 % (TGA analysis, N_2) Uses: physical reinforcement for plastics and coatings
VP Cocoon 2125	Benefit	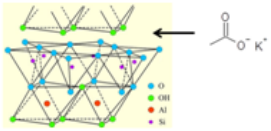 *Kaolinite modified with potassium acetate*	Particule size (d_{50}) : 10 µm Specific surface : 4 - 6 m^2/g Onset temperature of weight loss: 290°C (TGA analysis, N_2) Residual weight at 800°C: 83 % (TGA analysis, N_2) Uses : improve flame retarding properties of polymers
RDP bentonite	Glan Burnie Technologies (supplied by BASF)	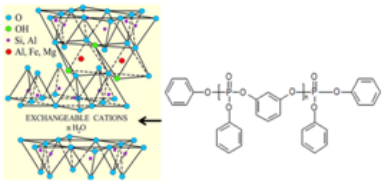 *Bentonite modified with Resorcinol bis(diphenyl phosphate*	Weight loss at 300°C: 2% (TGA analysis, N_2) Residual weight at 800°C: 83 % (TGA analysis, N_2) (Experimental product)
Octamethyl POSS	Hybrid Plastics	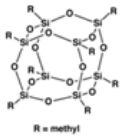 Octamethyl Polyhedral Oligomeric Silsesquioxane	Particule size : 0.7 - 30 Å Uses : improves hydrophobicity, printability, processing

Commercial name	Supplier	Composition / Structure	Specifications
Aminoehtyl Aminopropyl Isobutyl POSS	Hybrid Plastics	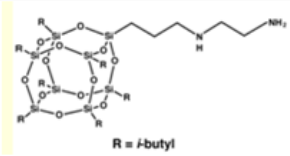 R = *i*-butyl Aminoethyl Aminopropyl Isobutyl Polyhedral Oligomeric Silsesquioxane	Uses : grafting agent, chain terminator to improve processing
Trisilanol Phenyl POSS	Hybrid Plastics	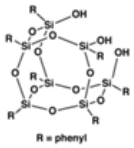 R = phenyl Trisilanol Phenyl Polyhedral Oligomeric Silsesquioxane	Uses : processing aid, surface modification, modulus retention, cure promotion in epoxy, BMI
ES 350 F5	Graphite Kropfmühl AG	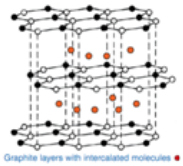 Expandable Graphite	Particule size (d_{50}) : 300 µm Start expansion temperature: 200°C (TGA analysis, N_2) Minimum expansion rate: 350 cm^3/g Uses : in metallurgical industries as a covering material for hot molten metal. Used in this application for thermal insulation and protection against oxidation
NordMin 503	Nordmann Rassmann GmbH	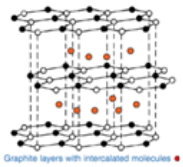 Expandable Graphite	Start expansion temperature: 300°C (TGA analysis, N_2)
GraphEx	Ciba (supplied by BASF)	Milled graphite nano-platelets	(Experimental product)
Fyrolflex RDP	Supresta (supplied by BASF)	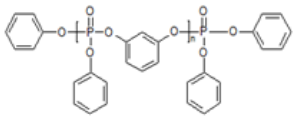 Resorcinol bis(Diphenyl phosphate)	Viscosity at 70°C: 600 CPS Boiling point: > 300°C Uses : Fire retarding agent
Bentonite	(supplied by BASF)	-	-

APPENDIX 3

ELEMENTAL ANALYSES (CALCULATION METHODS)

● **Theoretical mass fraction of elements (Theo.MF)**

Ex: Ethylene diamine based phosphinic acid (C13)

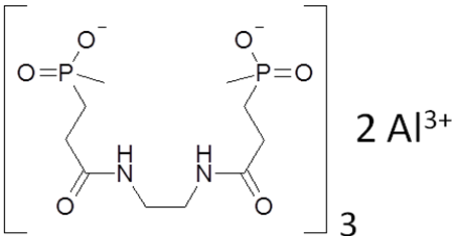

Element	M ($g.mol^{-1}$)	C_{theo}	Theo.M_{C13} ($g.mol^{-1}$)	Theo.MF (%)
C	12,011	30	360,33	34.9
O	15,999	18	287,982	27.9
N	14,007	6	84,042	8.1
H	1,008	60	60,48	5.9
Al	26,982	2	53,964	5.2
P	30,974	6	185,844	18.0
Total	-	-	1032,642	100

- C_{theo} : theoretical quantity of atom for 2 aluminums

- Theo.M_{C13} : theoretical mass of atom for 2 moles of aluminum

- Theo.MF : theoretical mass fraction of atom

Theo.M_{C13} (atom) = M (atom) x C_{theo} (atom)

Theo.MF (atom) = [M_{C13} (atom) X 100] / 1032.642; with 1032.642 the total Theo.M_{C13}

● **Elemental composition of the synthesized phosphinate salts**

Ex: Ethylene diamine based phosphinic acid (C13)

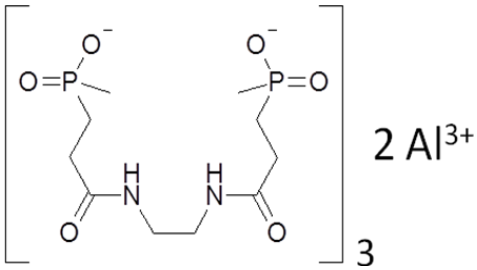

Element	M ($g.mol^{-1}$)	Exp.MF (%)	Exp.M_{C13} ($g.mol^{-1}$)	C_{Exp}	C_{Theo}	C_{Exp}/C_{Theo} (%)
C	12,011	32.5	313,184	26.1	30	87
O	15,999	29	279,456	17.5	18	97.2
N	14,007	7.6	73,237	5.2	6	86.6
H	1,008	5.8	55,891	55.4	60	92.3
Al	26,982	5.6	53,964	2	2	100
P	30,974	17.0	163,819	5.3	6	88.3
Total	-	97.5	-	-	-	-

- Exp.MF : experimental mass fraction of atom (determined by elemental analysis)

- Exp.M_{C13} : experimental mass of atom for 2 moles of aluminum

- C_{exp} : experimental quantity of atom for 2 aluminums

- C_{theo} : theoretical quantity of atom for 2 aluminums

Exp.M_{C13} (atom) = [Exp.MF (atom) x Exp.M_{C13} (aluminum)] / Exp.MF (aluminum)

C_{exp} (atom) = Exp.M_{C13} (atom) / M (atom)

C_{exp} / C_{theo} = [C_{exp} (atom) x 100] / C_{theo} (atom)

● **Determination of the empirical formula of the synthesized phosphinate salts**

Ex: Ethylene diamine based phosphinic acid (C13)

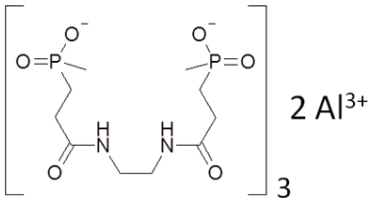

Element	C_{Exp}/C_{Theo} (%)	C_{Exp}	C_{Theo}	C_{exces}
C	87	26.1	30	-
O	97.2	17.5	18	1.84
N	86.6	5.2	6	-
H	92.3	55.4	60	3.2
Al	100	2	2	-
P	88.3	5.3	6	-
Total	-	-	-	-

- C_{exp} : experimental quantity of atom for 2 aluminums

- C_{theo} : theoretical quantity of atom for 2 aluminums

- C_{excess} : quantity of atom in excess of the actual quantity of atom contained in the phosphinate

Carbon is taken as reference (arbitrary) to determine the quantity of phosphinate (C_{C13}) associated to 2 atoms of aluminum:

***Notification**: no excess is determined for nitrogen and phosphorus as their C_{exp} / C_{theo} is considered to be equivalent to that of carbon*

C_{C13} = [3 x C_{exp} (carbon)] / C_{theo} = 2.6 ; with 3 the theoretical quantity of C13 for 2 aluminums

C_{excess} (atom) = C_{exp} (atom) - [(C_{theo} (atom) x C_{exp}/C_{theo} (carbon)) / 100]

→ Empirical formula (basic): 2 x Al + C_{excess} (O) + C_{excess} (H)

$Al_2(C4^{2-})_{C13}(O)_{1.8}(H)_{3.2}$

→ Empirical formula (obeying to the neutrality rule):

$Al_2(C4^{2-})_{2.6}(O^{2-})_{n/2}(OH^-)_{0.8-n/2}(H_2O)_{1.0+n/2}[H]_{0.4}$; where 0.8 < n < 0

APPENDIX 4:

PYROLYSIS-GCMS ANALYSES AND MASS SPECTRA OF PRODUCTS

● Pyrolysis GCMS analysis of PBT/GF (desorption: 390°C, 470°C)

- Chromatogram of the gases evolved during the thermal treatment of PBT/GF

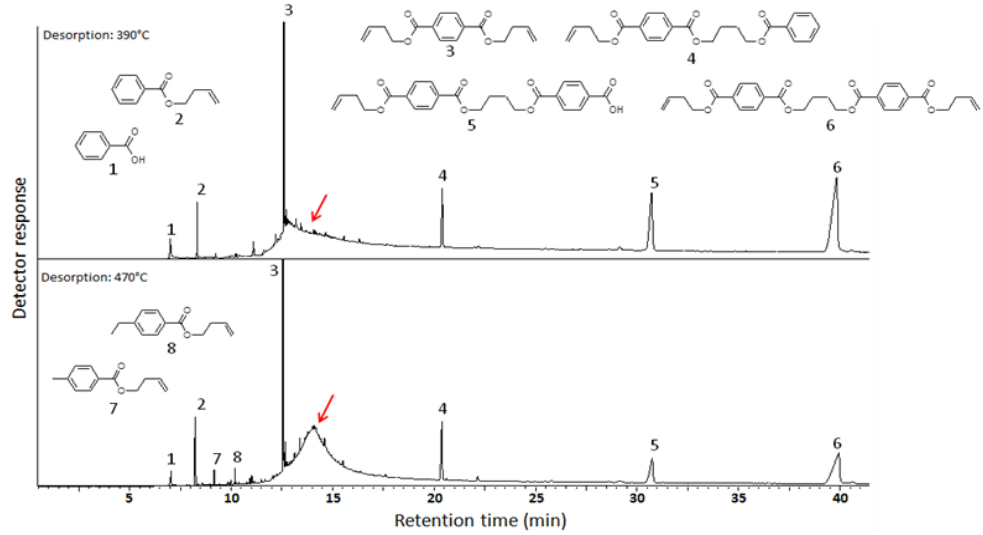

- Mass spectra

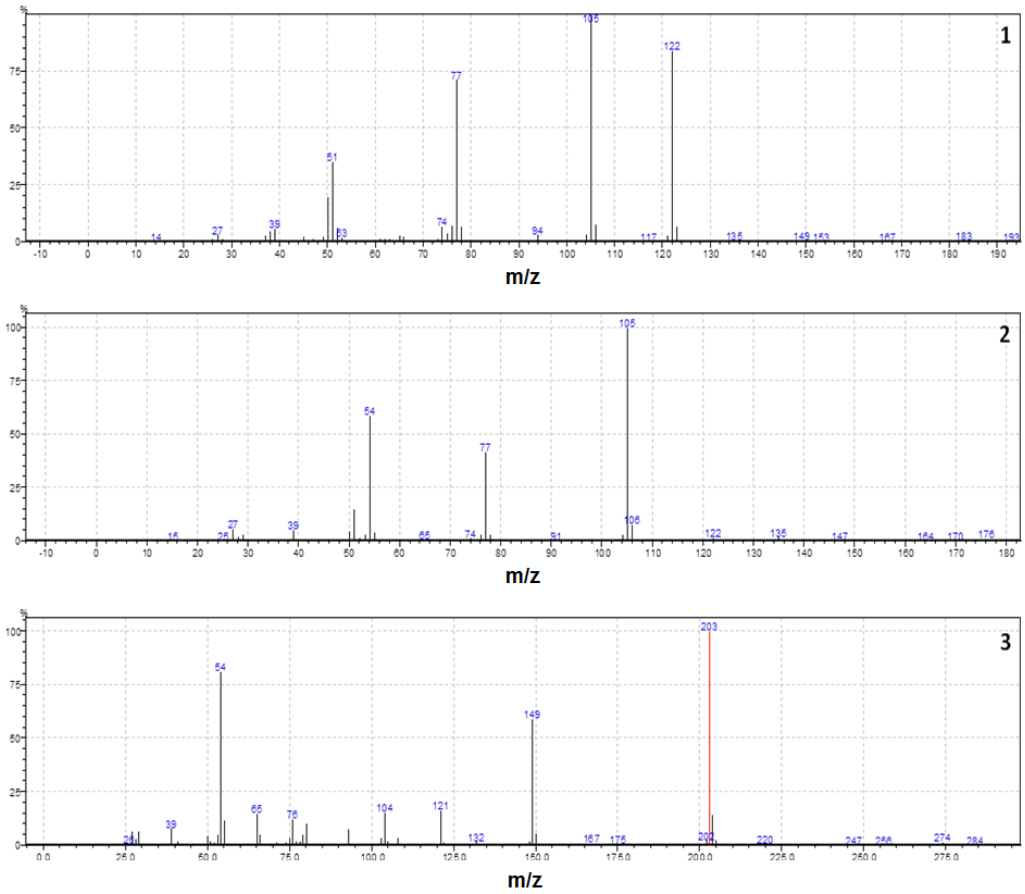

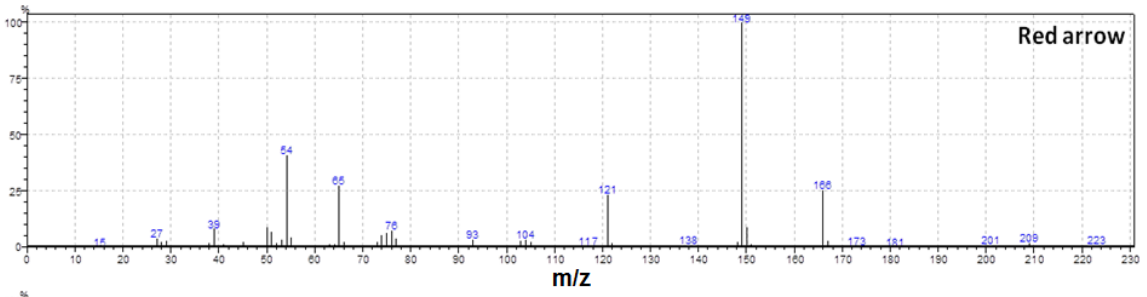
Red arrow
m/z

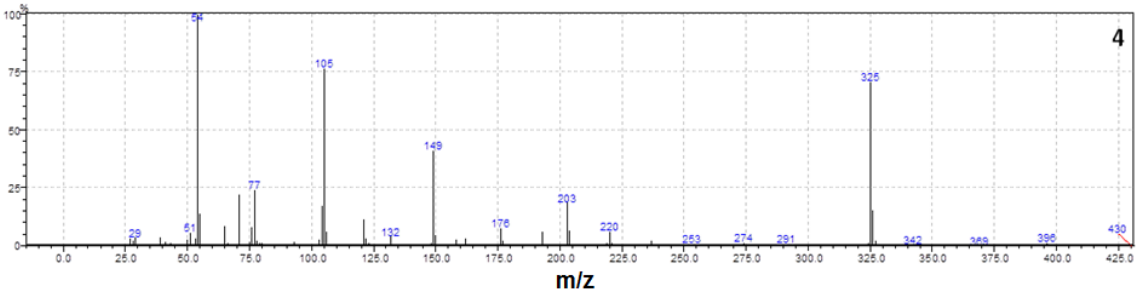
4
m/z

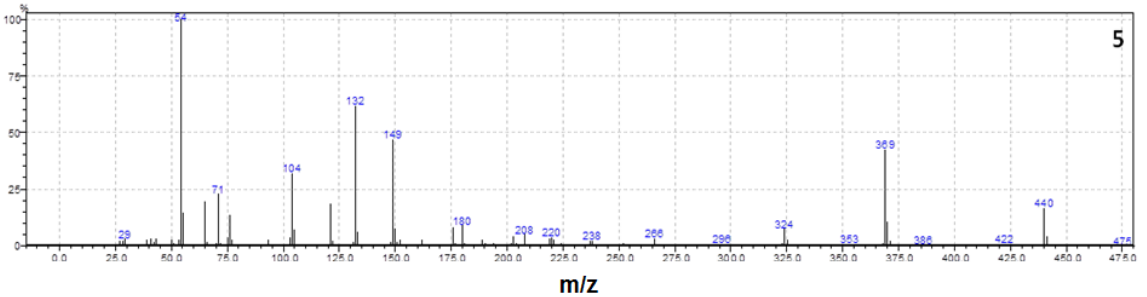
5
m/z

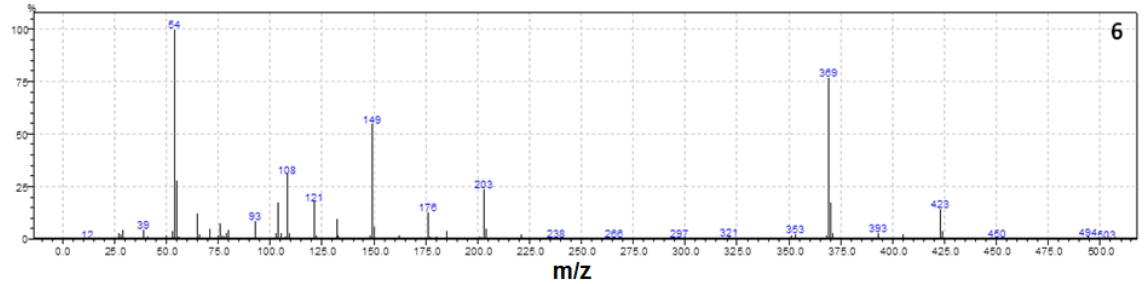
6
m/z

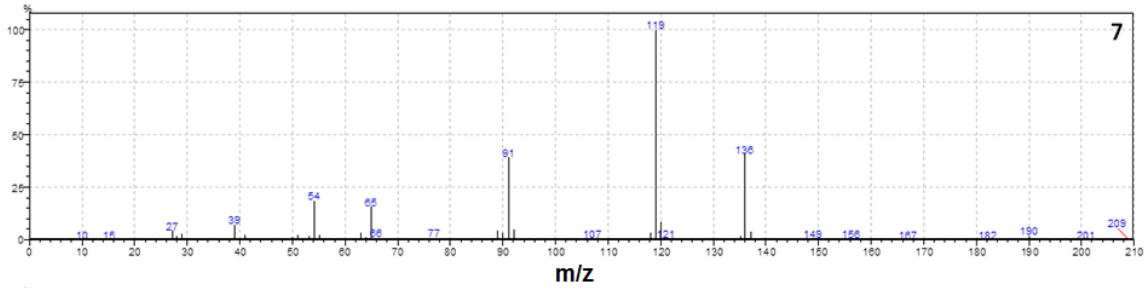
7
m/z

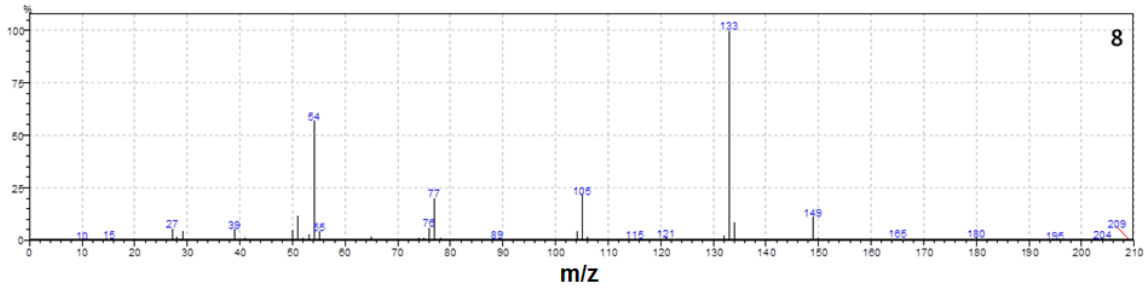
8
m/z

● **Pyrolysis GCMS analysis of C9 (desorption: 390°C, 600°C)**

- Chromatogram of the gases evolved during the thermal treatment of C9

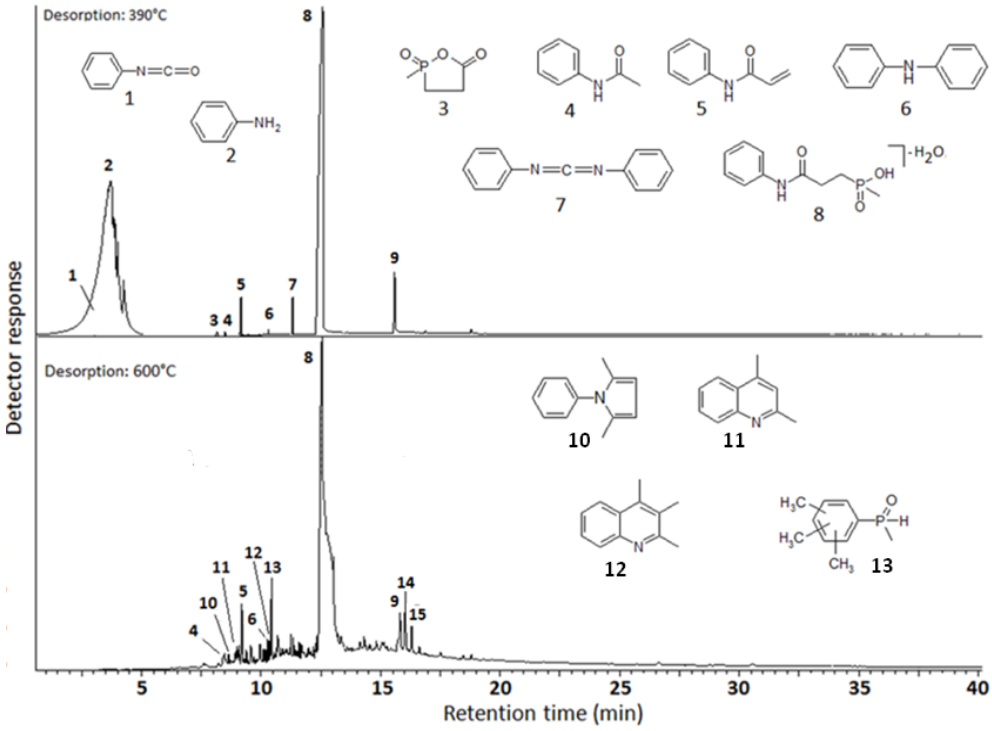

- Mass spectra

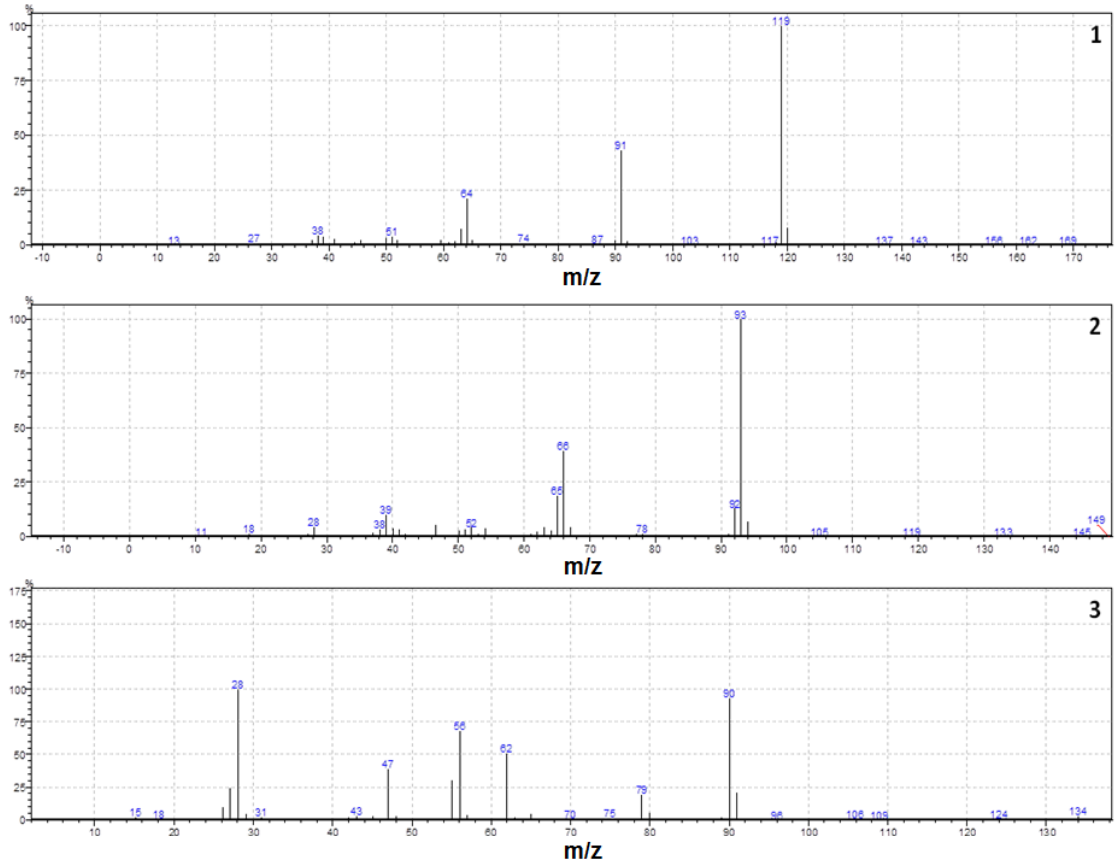

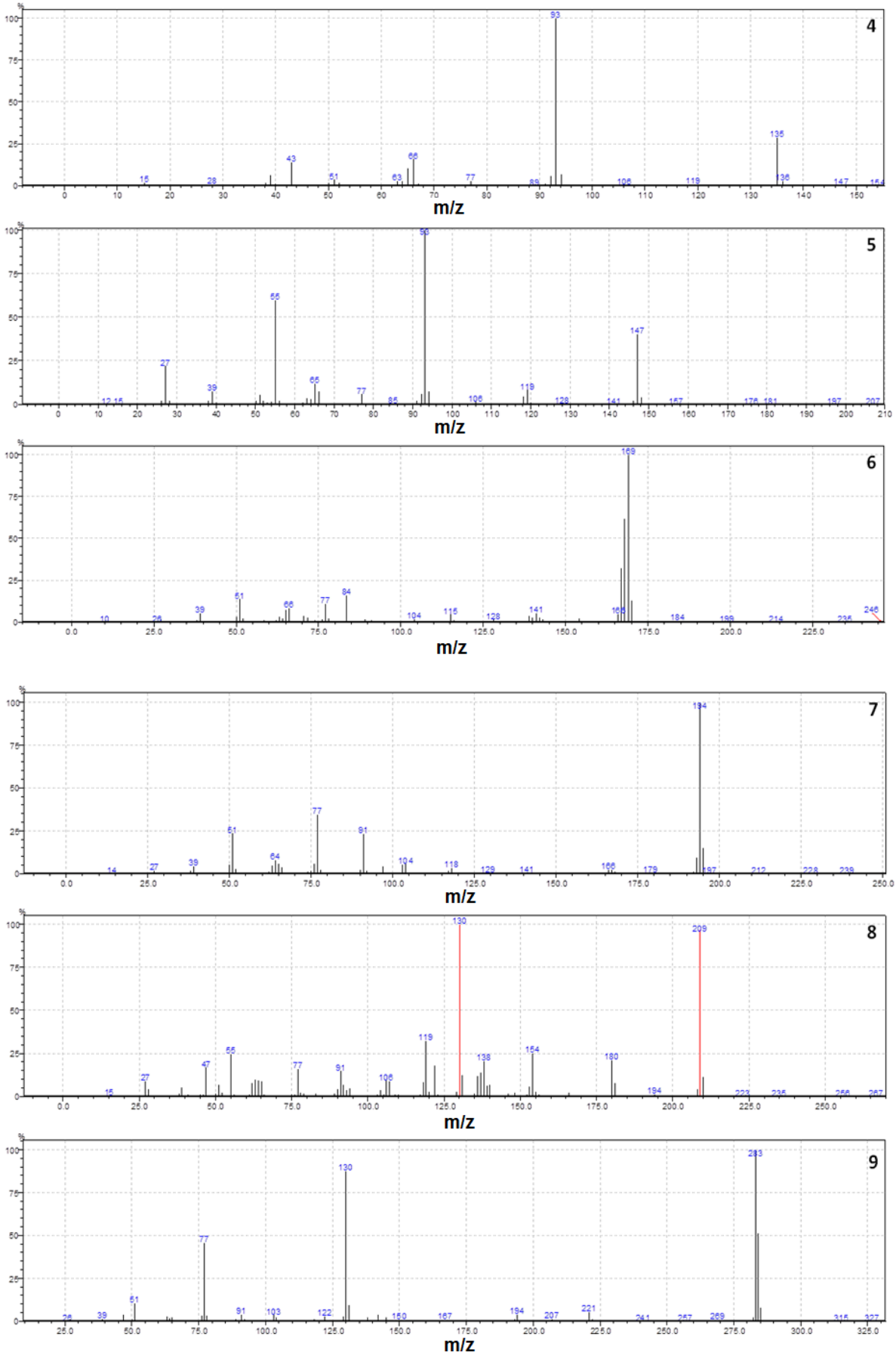
4
5
6
7
8
9
m/z

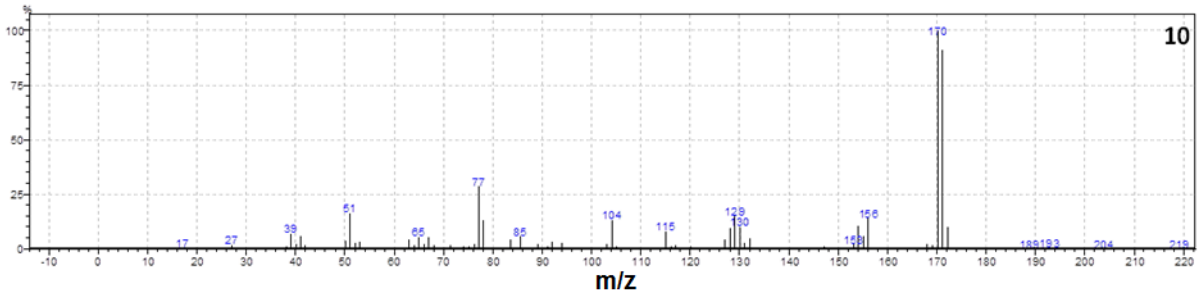
10
m/z

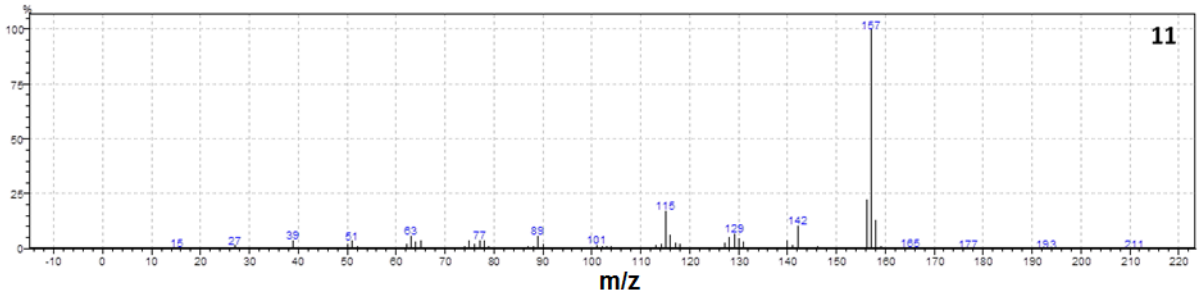
11
m/z

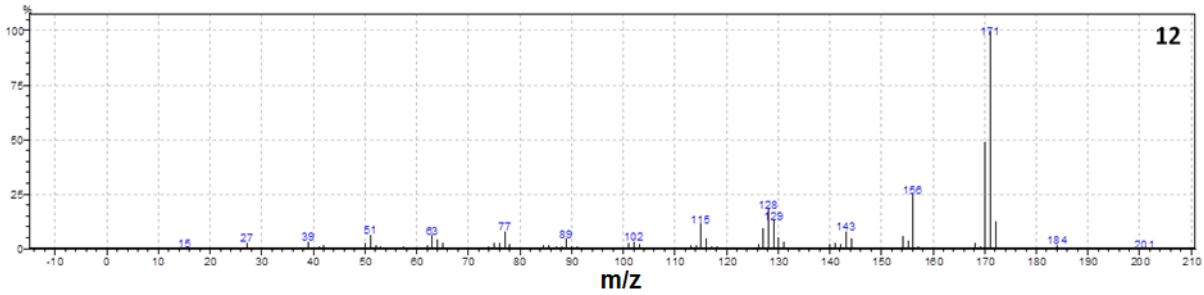
12
m/z

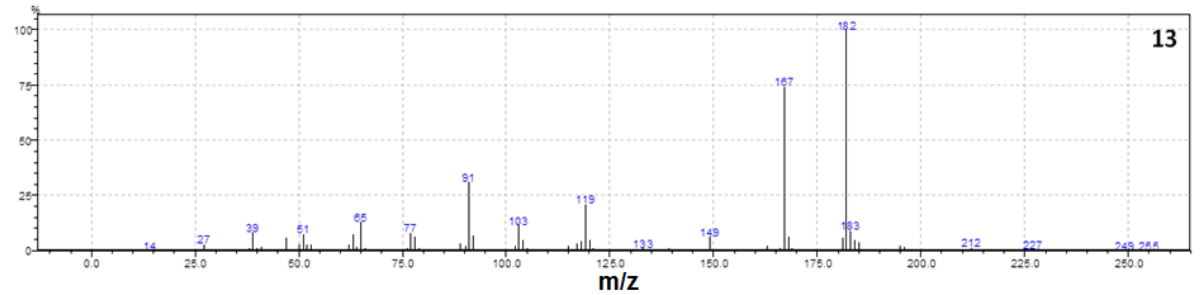
13
m/z

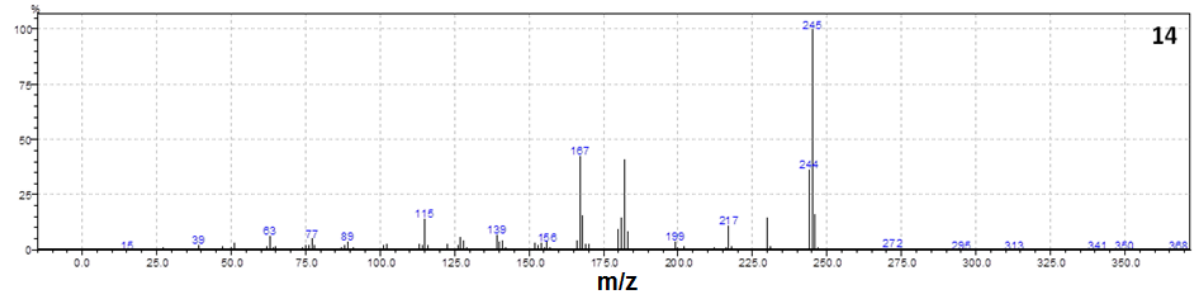
14
m/z

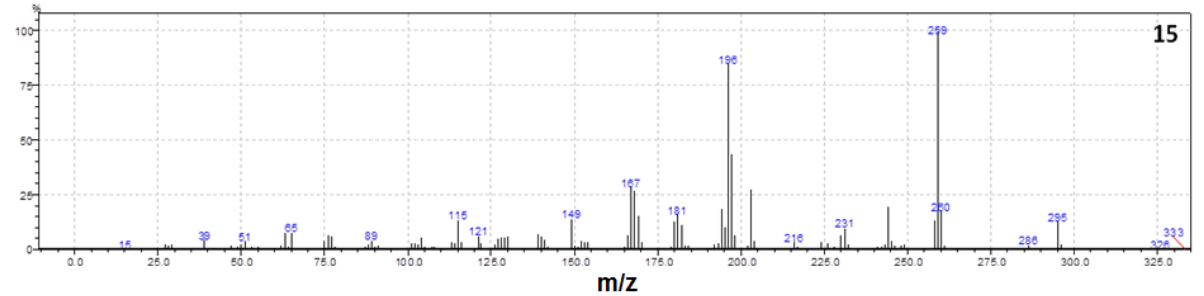
15
m/z

● **Pyrolysis GCMS analysis of PBT/GF/C9 (desorption: 390°C, 470°C)**

- Chromatogram of the gases evolved during the thermal treatment of PBT/GF/C9

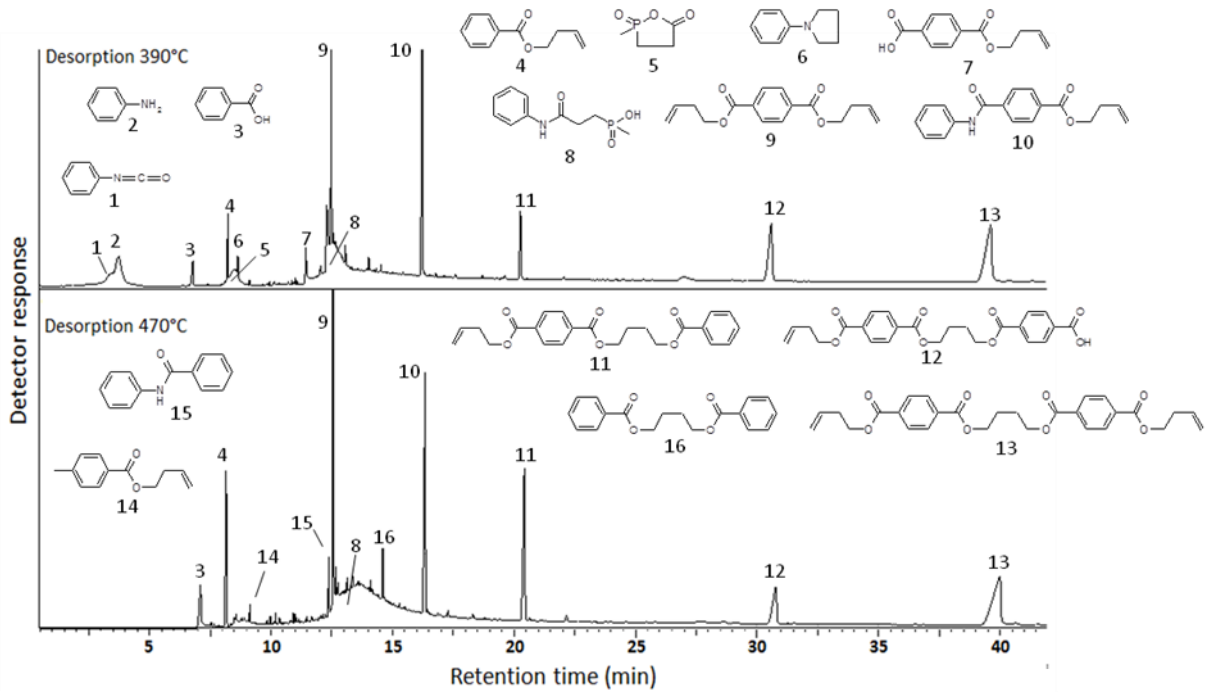

- Mass spectra

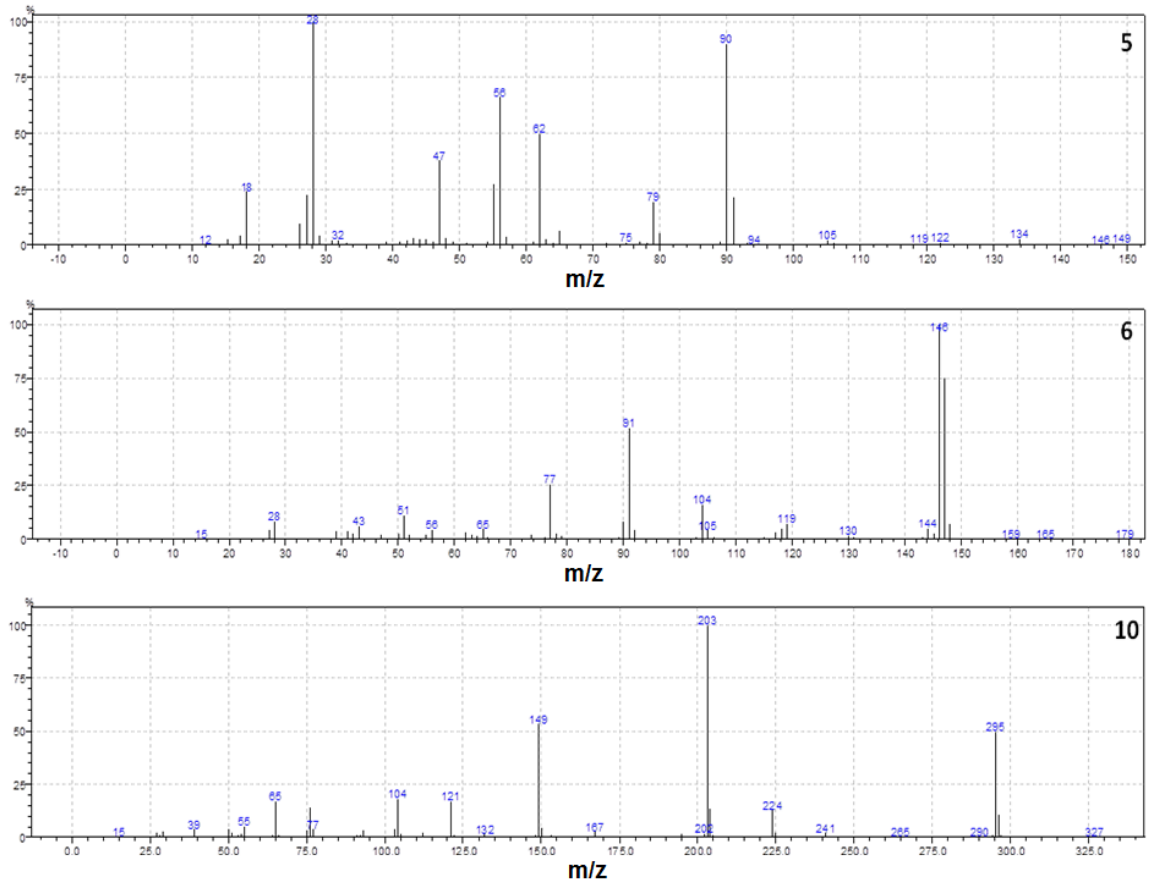

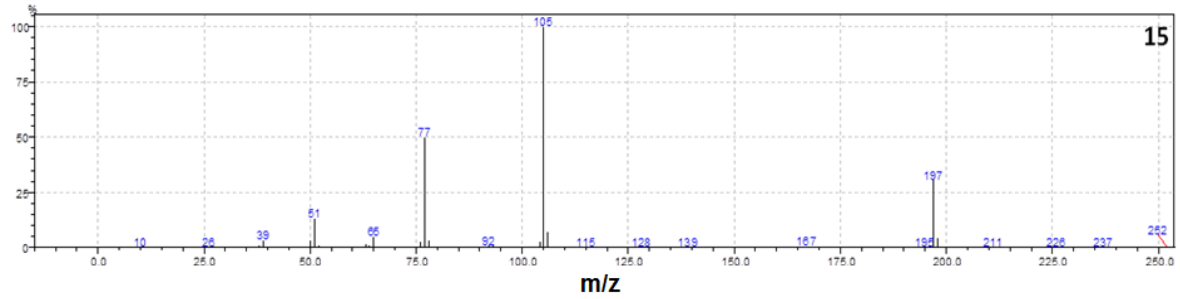

See previous parts for spectra of other products

● **Pyrolysis GCMS analysis of Exolit OP1240 (desorption: 475°C, 600°C)**

- Chromatogram of the gases evolved during the thermal treatment of Exolit OP1240

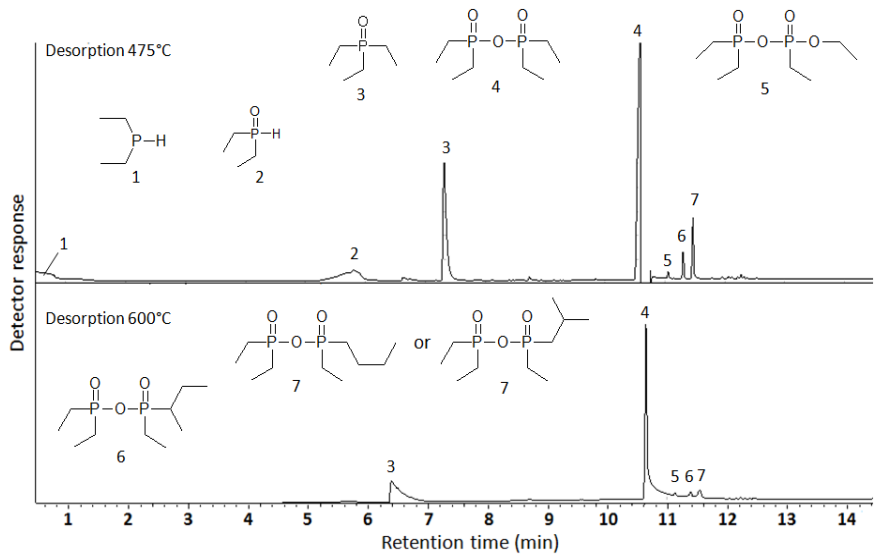

- Mass spectra

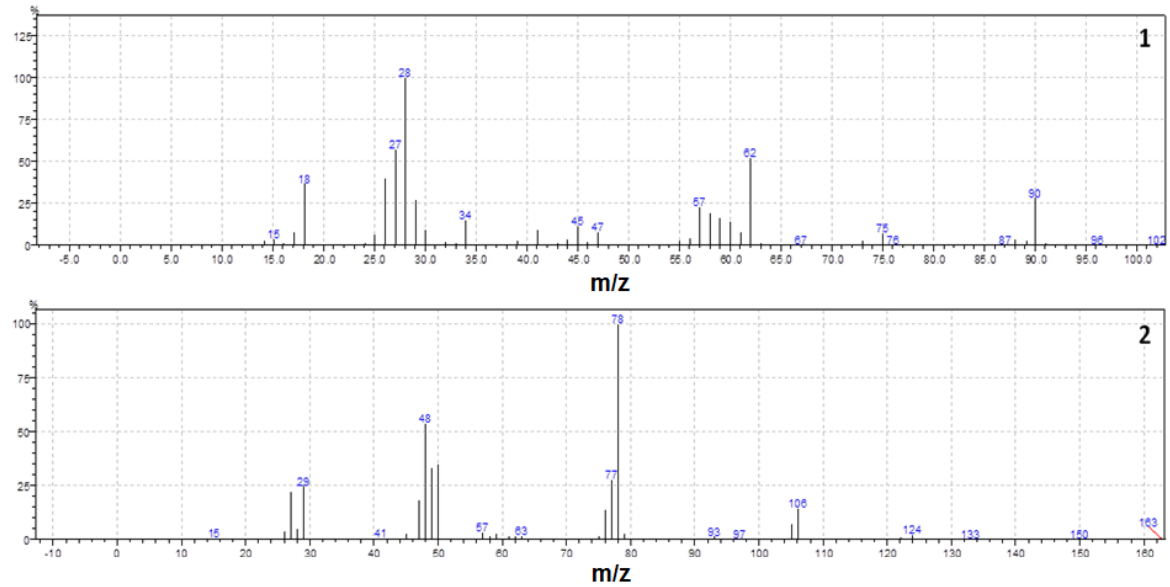

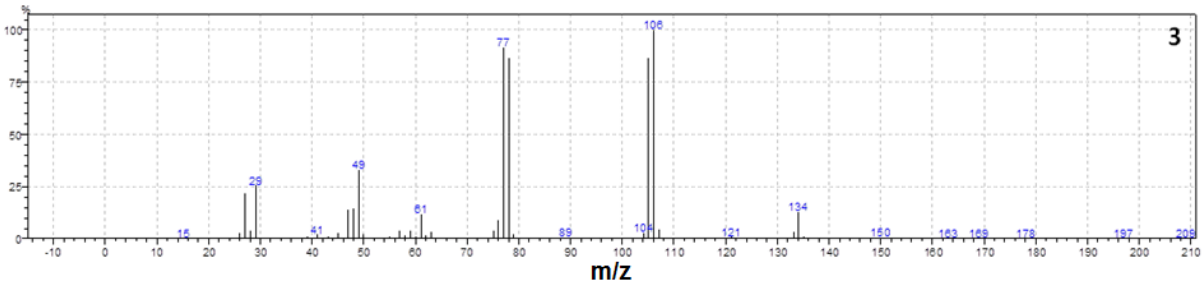
3
m/z

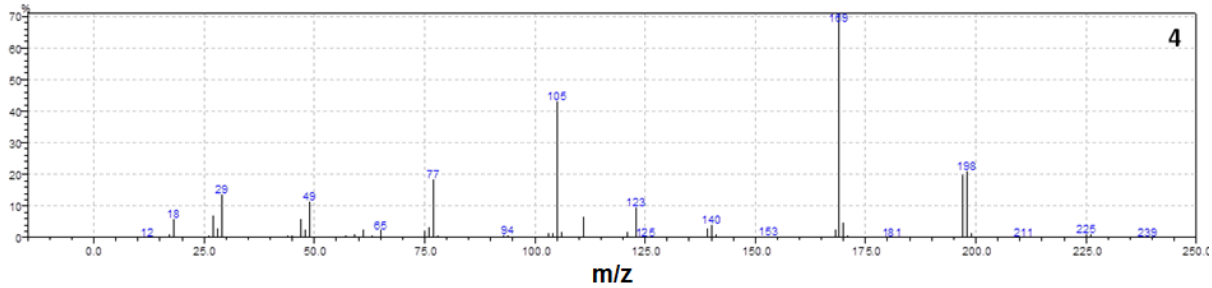
4
m/z

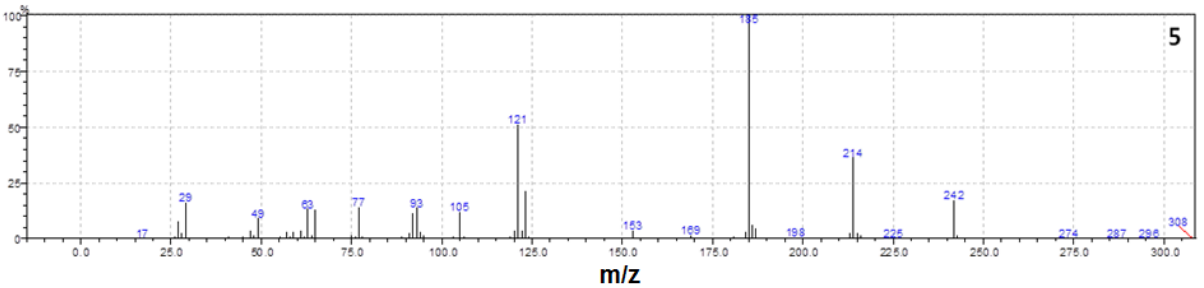
5
m/z

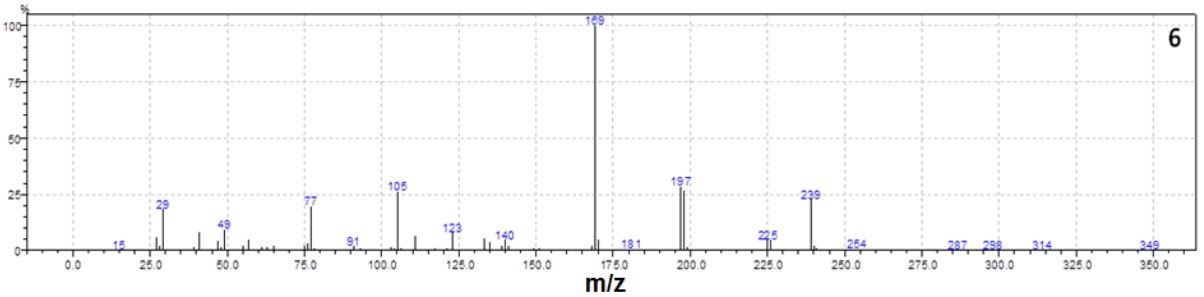
6
m/z

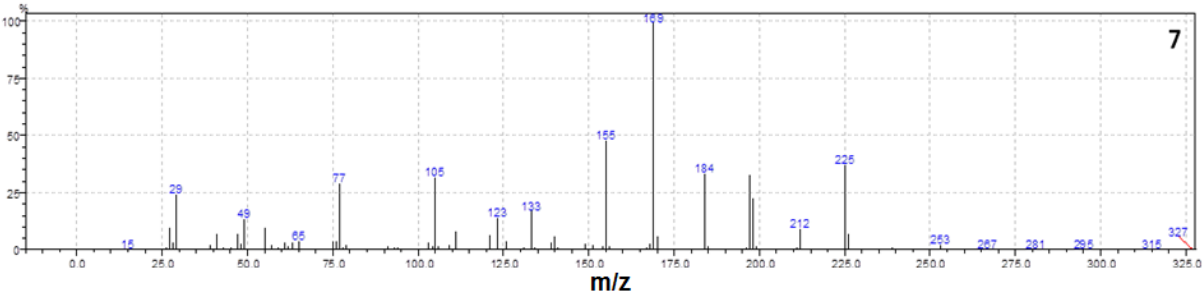
7
m/z

● **Pyrolysis GCMS analysis of PBT/GF/OP1240 (desorption: 390°C)**

- Chromatogram of the gases evolved during the thermal treatment of PBT/GF/OP1240

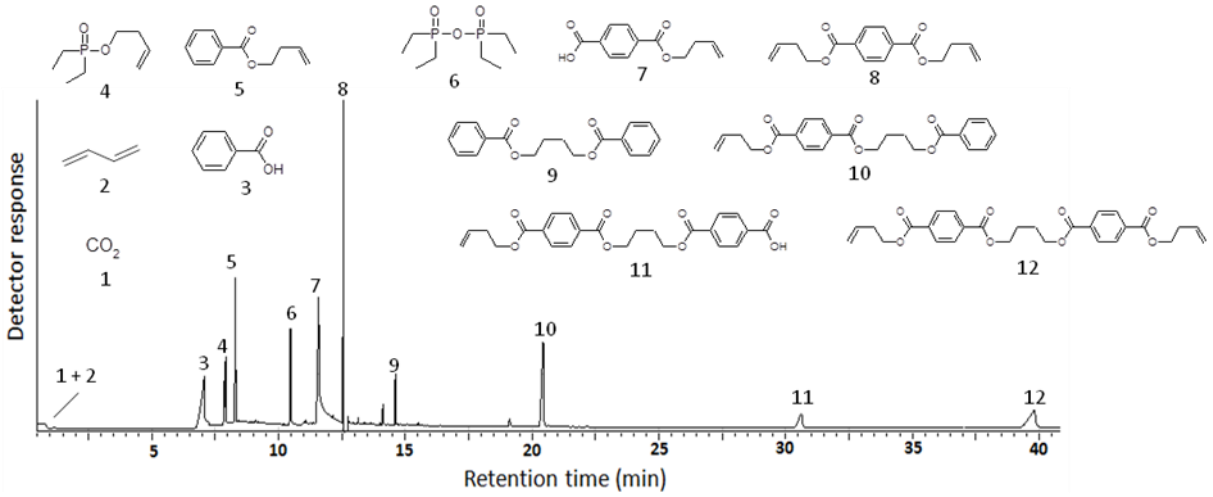

- Mass spectra

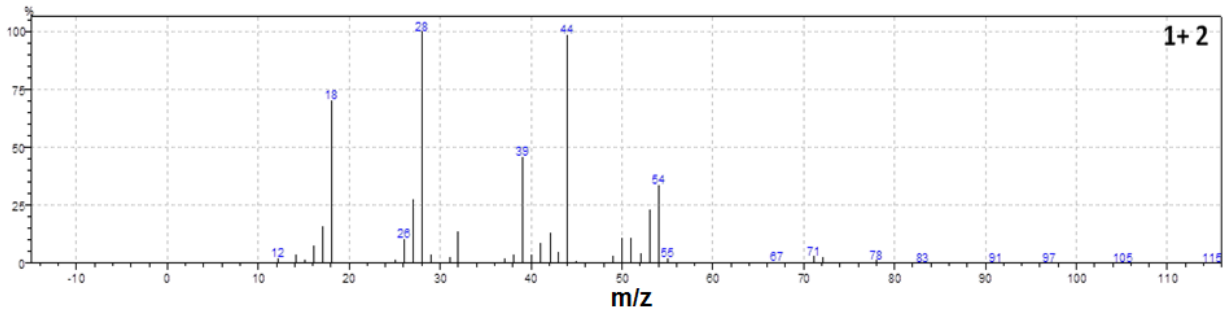

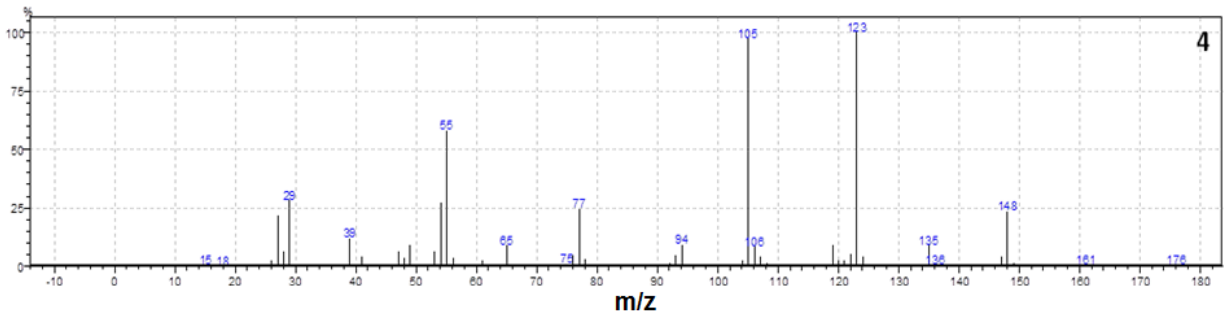

See previous parts for spectra of other products

APPENDIX 5:

TWO-DIMENSIONAL (2D) SOLID STATE NMR SPECTRA

● 2D ^{27}Al -^{31}P D-HMQC (Dipolar Heteronuclear Multiple Quantum Coherence) NMR spectrum of PBT/GF flame retarded with C9:

- Spectrum of PBT/GF/C9 heat treated at 425°C

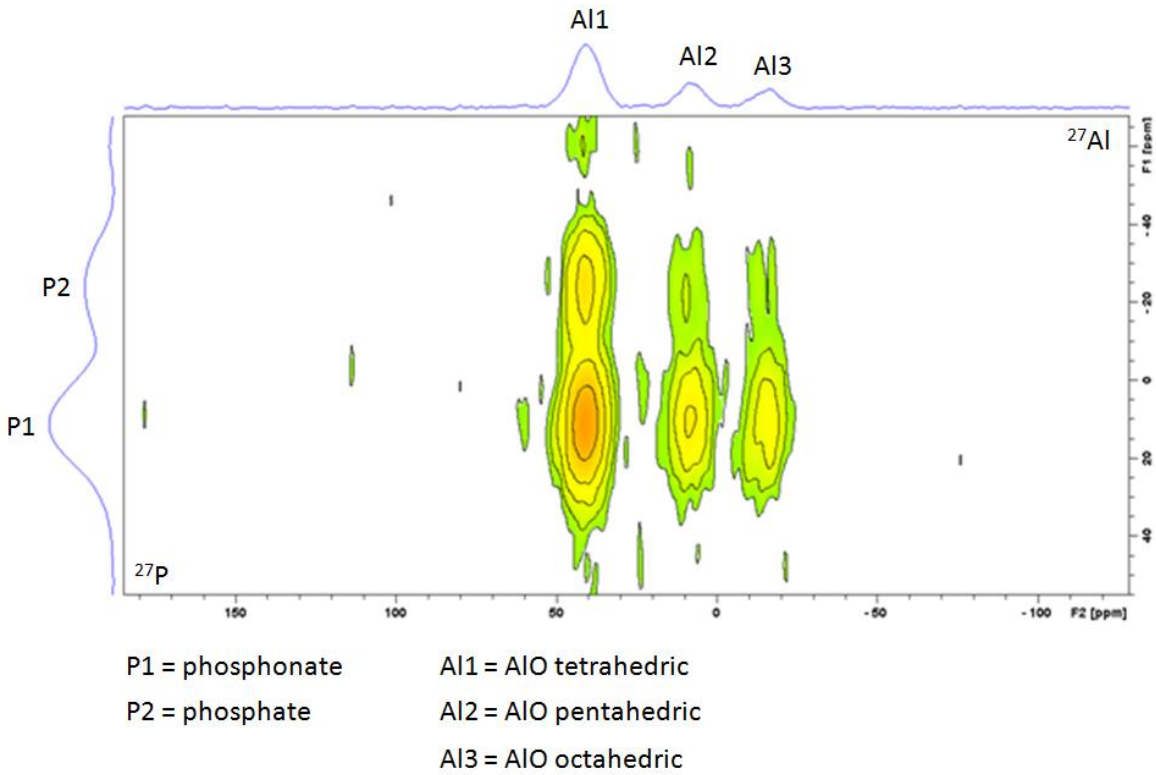

2D ^{27}Al-^{31}P NMR (Bo = 800 MHz); probehead: 3.2 mmMAS; MAS: 20 kHz; 1536 scans (d1 = 1s)

● ^{27}Al NMR spectrum of PBT/GF:

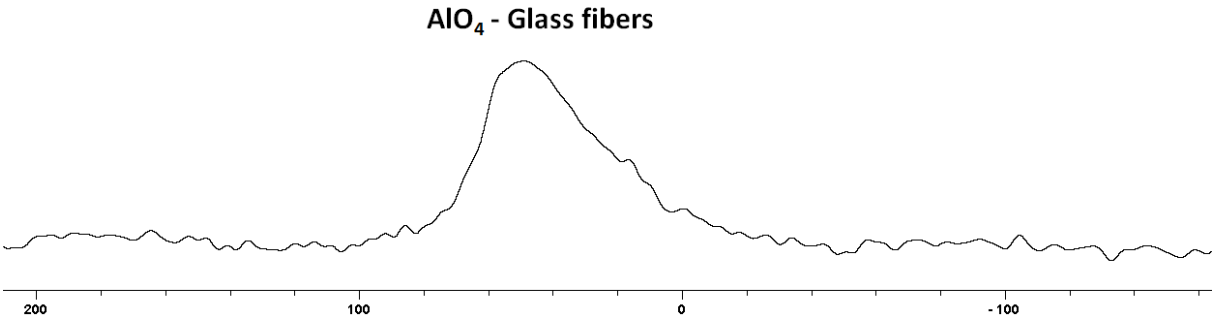

^{27}Al (Bo = 400 MHz); single pulse; probehead: 4 mmMAS; MAS: 12.5 kHz; 1024 scans (d1 = 2s)

Résumé - Cette étude s'intéresse aux procédés d'ignifugation d'un thermoplastique, le PolyButylène Téréphthalate (PBT), et plus particulièrement à l'ajout en masse de retardateurs de flamme à base de phosphore. L'objectif de ce projet consiste à mettre au point une formulation PBT renforcée avec des fibres de verre et ignifugée en vue d'application dans le domaine électrique et électronique. Dans un premier temps, les propriétés au feu de différents additifs combinés à un sel de diethylphosphinate d'aluminium commercial sont évaluées. Différents sels de phosphinate dérivés de l'acide carboxyethyl(methyl)phosphinique ont par ailleurs été synthétisés puis testés, soit seuls ou combinés à des additifs retardateurs de flamme. Deux systèmes retardateurs de flamme, l'un consistant en un mélange RDP bentonite - diethylphosphinate d'aluminium, l'autre en un mélange RDP bentonite - phenyl amide carboxyethyl(methyl)phosphinate d'aluminium, se sont avérés particulièrement efficaces en terme d'amélioration du comportement au feu du PBT renforcé. Les mécanismes d'ignifugation de ces systèmes ont été étudiés et comparés. Il a été démontré que les deux sels de phosphinate présentaient un mode d'action essentiellement en phase gaz, en libérant des espèces acides phosphiniques agissant comme inhibiteurs des réactions de combustion. Concernant le sel de phosphinate commercial, la libération d'acides phosphiniques s'effectue par interaction chimique entre l'additif et le PBT. A l'inverse, le sel de phosphinate synthétisé au laboratoire semble n'interagir que modérément avec le polymère.

Abstract - This study deals with the formulation of an innovative flame retardant material based on glass fiber reinforced PolyButylene Terephthalate (PBT/GF) used in Electronic and Electrical Equipments (EEE). In a first approach, the flame retardant properties of various additives in combination with the commercial aluminium diethylphosphinate are evaluated in PBT/GF. In a second approach, a variety of phosphinate salts derived from carboxyethyl(methyl)phosphinic acids are synthesized and then tested alone or in combination with FR additives. Two innovative flame retardant systems, namely the combination of Resorcinol bis-Diphenyl Phosphate (RDP) modified bentonite clay with either the aluminium diethylphosphinate or the aluminium phenyl amide of carboxyethyl(methyl)phosphinate, were found to greatly improve the fire behavior of PBT/GF. The FR mechanism of flame retardants were investigated and compared. Both phosphinate salts from the innovative systems mainly act through a gas phase mode of action by releasing phosphinic acids. Regarding the commercial product, the release of phosphinic acid occurs due to chemical interaction between the phosphinate salt and the PBT matrix while the synthesized product only moderately interacts with the polymer.